MONASH University

CTBP-1 regulation of axonal development in *C. elegans*

Tessa Sherry

BSc (Hons), University of Sydney

BSc/BA, University of Adelaide

A thesis submitted for the degree of Doctor of Philosophy at

Monash University in 2019

Monash Biomedicine Discovery Institute

Department of Anatomy and Developmental Biology

Copyright notice

Abstract

Correct development of the nervous system requires precise regulation of axon outgrowth, guidance and termination. However, little is known about how signalling and adhesion molecules that control axon development are transcriptionally regulated. In this thesis, I report that the *Caenorhabditis elegans* C-terminal binding protein CTBP-1, a conserved transcriptional repressor, is required for correct axonal development. Loss of *C. elegans* CTBP-1 causes defective outgrowth, guidance and termination of the SMD motor neurons. CTBP-1 regulates SMD axonal development by repressing the expression of the L1 cell adhesion molecule ortholog SAX-7. Repression of SAX-7 is crucial as dysregulated expression causes severe defects in SMD axon development. In a parallel pathway, the other *C. elegans* L1CAM ortholog LAD-2 regulates SMDD axon outgrowth and guidance. Collectively, my results reveal that harmonization of L1CAM expression is important for controlling SMD axonal development.

Declaration

This thesis is an original work of my research and contains no material which has been accepted for the award of any other degree or diploma at any university or equivalent institution and that, to the best of my knowledge and belief, this thesis contains no material previously published or written by another person, except where due reference is made in the text of the thesis.

Signature:

Print Name: Tessa Sherry

Date: 10/12/2019

Publications during enrolment

Micropublication

Sherry, T; Nicholas, HR; Pocock, R (2019). New deletion alleles for *Caenorhabditis elegans* Hedgehog pathway-related genes *wrt-6* and *wrt-10*. microPublication Biology. 10.17912/micropub.biology.000169

Acknowledgements

First of all, I would like to thank my supervisor Roger Pocock. Your endless encouragement, passion and knowledge inspires me daily. I am very thankful for all of the support and guidance you have given me over the last two years. In addition, thank you for making my transition as easy as possible.

I would like to also thank Hannah Nicholas for introducing me to the wonderful world of worms and for supporting me in the first two years of my candidature.

Thank you to all of the members of the Pocock lab for technical assistance, valuable discussions and friendship. Special thanks goes to my co-supervisor Ava Handley for being so welcoming and always willing to discuss results. Oguzhan Baltaci, thanks for encouraging me during the writing process.

I would also like to thank the Australian worm community, and particularly members of the Ashe and Neumann labs, for insight and advice. Rachel Woodhouse, thanks for being a great friend and inspiring colleague. Mallory Wood and Matthew Hoe, I will always fondly remember our tea-time chats.

Thanks to Monash University and University of Sydney for financial support. This research was supported by an Australian Government Research Training Program (RTP) Scholarship.

Thank you to my family and friends all across the country for being enthusiastic about my successes, even when you didn't understand what it is I do!

Finally, I would like to express my deep gratitude to Vinh. I couldn't have done it without your unconditional love and support.

Table of contents

List of Figures and Tables

Abbreviations

AFT	Acute functional tolerance
ANOVA	Analysis of variance
bp	Base pairs
cDNA	Complementary DNA
CtBP/CTBP	C-terminal binding protein
dCtBP	*Drosophila* C-terminal binding protein
DNA	Deoxyribonucleic acid
DIC	Differential interference contrast
DNC	Dorsal nerve cord
Ex	Extrachromosomal array
GFP	Green Fluorescent Protein
IPTG	Isopropyl β-D-1-thiogalactopyranoside
Is	Integrated array
LB	Luria-Bertani
NAD	Nicotinamide Adeninine Dinucleotide
NGM	Nematode Growth Medium
n.s	Not significant
p	p-value
PCR	Polymerase Chain Reaction
qRT-PCR	quantitative real-time polymerase chain reaction
RNA	Ribonucleic acid
RNAi	RNA interference
SD	Standard Deviation
SEM	Standard Error of Mean
SMDD	SMD Dorsal
SMDV	SMD Ventral
TAG	Triacylglycerol
THAP	Thanatos-associated protein
VNC	Ventral nerve cord

1. Introduction

1.1 The model organism *Caenorhabditis elegans*

Caenorhabditis elegans is a transparent nematode, approximately 1mm in length, that has been studied as a model organism since the 1970s [1]. *C. elegans* is a sexually dimorphic species comprised of self-fertilising hermaphrodites and a low frequency of males. Hermaphrodites produce approximately 300 progeny, making propagation of large genetically identical populations straightforward. *C. elegans* populations can be maintained between 15 and 25°C on nematode growth medium (NGM) agar plates seeded with a standard food source of *Escherichia coli* OP50 [2]. *C. elegans* has a short life cycle of 3 to 4 days depending on the temperature of cultivation [2]. In favourable conditions, hatched animals undergo four developmental larval stages (L1-L4) before reaching egg-laying adulthood (Figure 1.1) [2]. In harsh conditions, such as scarcity of food, high temperature and overcrowding, animals can enter a stress-resistant dauer arrest stage until favourable conditions are reached, upon which they resume development (Figure 1.1) [2].

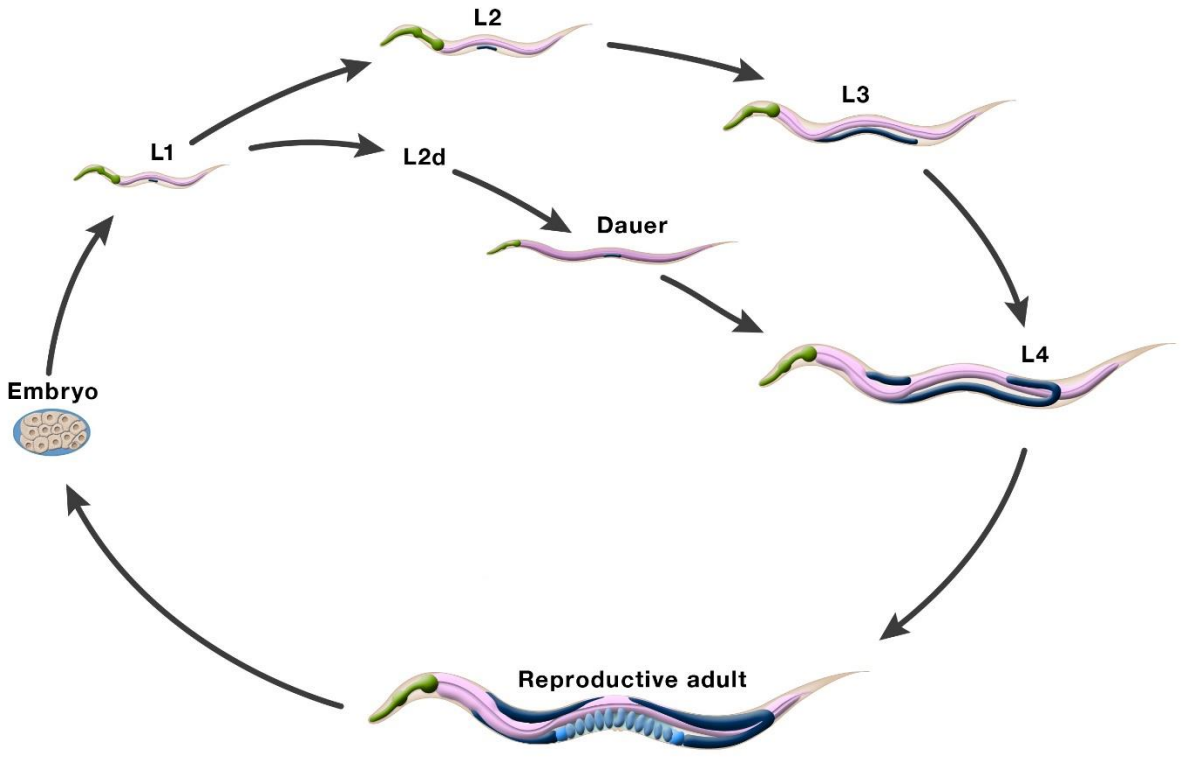

Figure 1.1 *C. elegans* life cycle.
Schematic of the hermaphrodite life cycle in favourable (outside arrows) or harsh conditions (inside arrows, dauer). Adapted from Wormatlas [3].

Hermaphrodites possess exactly 959 somatic cells and the entire invariant cell lineage has been mapped [4]. The adult animal is comprised of defined tissues, including muscle, nervous system, digestive system, reproductive system, and the hypodermis (epidermis) [2]. Because *C. elegans* is transparent, individual cells and tissues can be visualised in live animals using differential interference contrast (DIC) microscopy, transgenically-expressed fluorescent reporters, antibody staining and *in situ* hybridization. Of particular interest in this study is the nervous system, which comprises nearly a third of all somatic cells.

1.2 *C. elegans* nervous system

The *C. elegans* hermaphrodite nervous system comprises 302 neurons, which communicate through approximately 6400 chemical synapses, 900 gap junctions, and 1500 neuromuscular junctions [5, 6]. *C. elegans* neurons are categorised into 118 classes based on morphology, position and synaptic connectivity [6]. Neurons are broadly classified into four functional categories: sensory neurons, interneurons, motor neurons and polymodal neurons [7]. Sensory neurons receive sensory input from specific chemical and mechanical stimuli and directly communicate with interneurons. Interneurons subsequently transmit information to motor neurons, which synapse onto muscle cells to coordinate behavioural responses. Polymodal neurons perform more than one type of function, and can exhibit combinations of motor, sensory and interneuron functions. An example of this is the M3 neurons, which function as both motor and sensory neurons [7]. Neurons can also perform multiple functions within these categories. The ASH sensory neurons, for example, respond to both mechanical and chemical stimuli [8].

Neurons are generated during three developmental periods: proliferation phase of embryogenesis, late-L1 stage and L2 stage [4, 8]. The majority of *C. elegans* neuronal cell bodies are located in the head ganglia that form a nerve ring, which is the main integration centre (Figure 1.2) [6]. The second largest number of neuronal cell bodies are present in the tail ganglia, and few neuronal cell bodies are also present in the lateral or sublateral cords (Figure 1.2) [6]. The majority of neurons occur as bilateral pairs, positioned on the left and right sides of the animal, but there are also unpaired single neurons and nonsymmetric neurons of the same class [7].

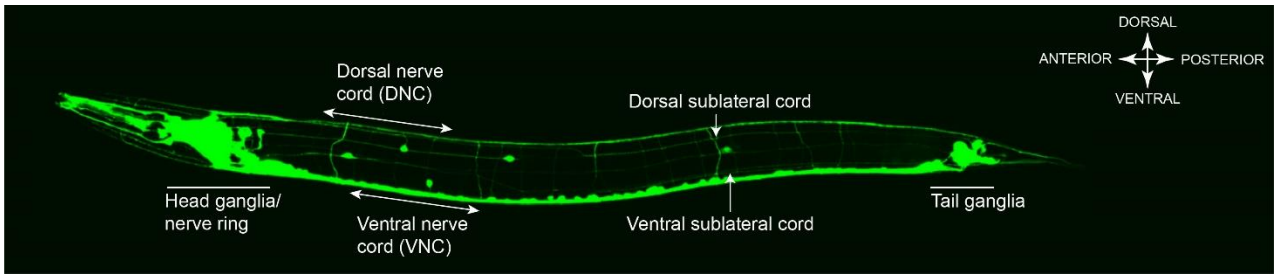

Figure 1.2 *C. elegans* nervous system.
All neurons (cell bodies and processes) are visible using GFP expressed under a pan-neuronal promoter (*prgef-1::GFP*). The majority of cell bodies are present in the head and tail ganglia. Fluorescent image supplied by Roger Pocock.

Almost all *C. elegans* neurons are monopolar or bipolar, which extend one or two processes (axons and dendrites) from the cell body, respectively. Exceptions to this are the PVD and FLP mechanosensory neurons that branch extensively by late larval development and envelop the whole animal body [9]. Neuronal processes are thin (~100-200 nm diameter), but vary greatly in length, with some axons extending along the entire body (~1 mm length in adults) [6]. Many of these processes follow stereotypical anterior-posterior or dorsal-ventral trajectories. The majority of processes are located in the ventral nerve cord (VNC) and dorsal nerve cord (DNC) that run along the hypodermis [7]. A small number of neuronal processes also develop in lateral cords along the hypodermis, and in sublateral cords between the hypodermis and body wall muscles (Figure 1.3) [7].

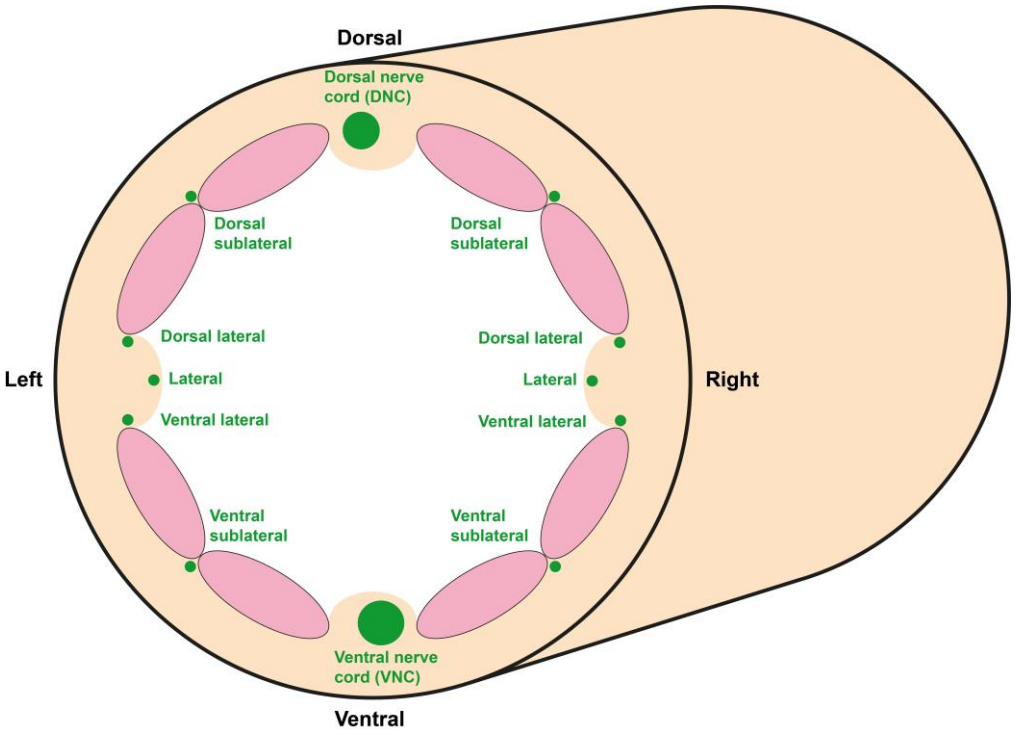

Figure 1.3 Axon tracts.

The majority of processes (green) are within the dorsal and ventral nerve cords, with only 1-4 present in the lateral and sublateral tracts. Cords lie within the hypodermis (tan) and sublateral cords lie between muscles (pink).

The *C. elegans* neuronal nomenclature consists of two or three letters and/or numbers, followed by their location [6]. For example, the SMD neurons are positioned on the ventral (SMDV) or dorsal (SMDD) side of the nerve ring, and are on either the left or right side of the body (SMDVL/R, SMDDL/R).

1.3 SMDD neurons

The SMD neurons are four sublateral cholinergic motor neurons that innervate dorsal muscle cells [6, 10]. The dorsal SMD (SMDD) neuron cell bodies are located in the ventral ganglion of the nerve ring and extend axons posteriorly along the dorsal sublateral tract (Figure 1.4) [6]. The pair of ventral SMD (SMDV) neurons are bilaterally symmetric to SMDD but their cell bodies are located in the dorsal ganglion (Figure 1.4) [6].

The SMDD neurons are embryonically born and extend dorsally-directed axons during the bean-embryo stage of embryogenesis (~350 min after fertilisation) [4, 11]. This embryonic SMDD axon outgrowth acts to pioneer the nerve ring [11]. During post-embryonic development,

the SMDD axons extend posteriorly from the nerve ring along the dorsal sublateral nerve cord before they terminate in the anterior half of the animal [6]. The SMDD axons are present within the dorsal sublateral cord between the body wall muscles and the hypodermis, and their main synaptic output is to the muscle [10]. The main synaptic inputs are from the RIA, RIM and RIC interneurons and OLL and URY sensory neurons [6].

Functional studies have revealed that the SMDs regulate key aspects of locomotion: head bending and omega turn amplitude [12-14]. The SMD neurons form an inhibitory feedback loop with the RME motor neurons through extrasynaptic cholinergic neurotransmission to regulate head bending [12]. Ablating SMD cell bodies at different developmental stages highlights the important roles of SMD motor neurons in exploratory behaviour. Ablation of all 4 SMD cell bodies at L1-L2 stage reduces head bending and omega turn frequency, and increases reversal frequency in young adults [12, 13]. Targeted SMDD or SMDV ablation in young adults leads to continuously ventral or circling movement, respectively [14]. Overall, these results indicate that SMD neurons are important for steering forward locomotion through regulation of head bending.

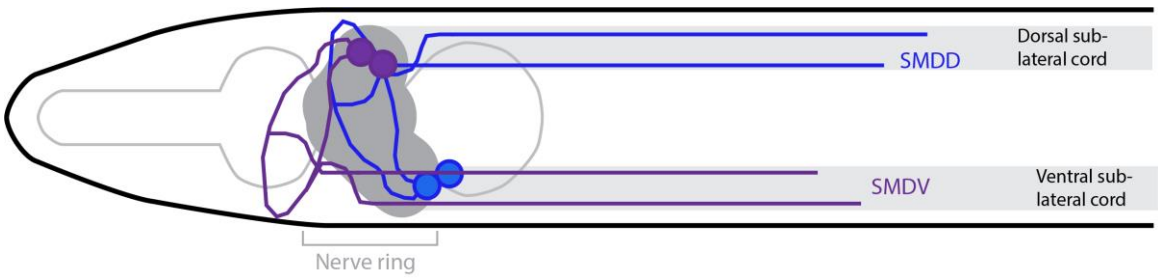

Figure 1.4 Position of SMDD and SMDV cell bodies and axons.
SMD cell bodies (blue or purple circles) reside in the nerve ring (grey), and processes extend along the sublateral cords (light grey). Faint grey line indicates the pharynx of the animal. Anterior/head of the animal is on the left, ventral is down. Schematic not to scale.

1.4 Axonal development

Axonal development is a highly regulated process that ensures correct connectivity and signal transduction between neurons and their synaptic partners (neurons-neurons and neurons-muscle). The ventral, dorsal, sublateral and lateral axon tracts are formed by the outgrowth of pioneer axons [15]. For example, the AVG axon pioneers the right VNC axon tract and is essential for organisation of the VNC [15]. Later in development, a neuronal cell body generates a process which begins outgrowth into a specific tract/cord (follower axons). The

axon extends and navigates along nerve cords, which can be across long distances and involve multiple guidance decisions. Finally, axon outgrowth terminates at specific, well-defined positions. Synapses between axons and other neurons or muscle cells occur *en passant* in reproducible positions all along the axon [6]. Because close proximity is required for these synaptic connections, defects in steps of axonal development can disrupt neuronal and circuit function and cause behavioural defects. Accordingly, many axonal development factors have been identified by screening mutants for behavioural defects, such as locomotion, or individual axon positioning defects [16].

Extensive research has been performed on dorsal-ventral axon guidance in *C. elegans*. Many axons extend circumferentially in a dorsal or ventral direction in *C. elegans* [6]. These axons have extensively been utilised to identify multiple conserved pathways, including UNC-6/Netrin and SLT-1/Slit signalling. The secreted protein UNC-6/Netrin is expressed in a ventral-dorsal gradient, with highest concentration at the ventral midline [17]. This expression attracts axons that express the UNC-40/DCC transmembrane receptor, causing them to grow ventrally [18]. Conversely, axons that express the UNC-5/UNC5 receptor are repelled by UNC-6 expression and grow dorsally [18]. The secreted protein SLT-1/Slit is expressed predominantly in dorsal muscle and acts through the SAX-3/Robo receptor to repel axon guidance [19]. These guidance cues act in parallel, and the correct balance of these signalling systems is essential for dorso-ventral axon guidance [19]. For example, the ventral outgrowth of the AVM touch receptor axons relies on both SLT-1 and UNC-6 expression [19]. The extensive current knowledge of dorsal-ventral axon guidance, including the conserved TGFβ signalling, has been recently reviewed [16], and will not be the focus of this thesis. Instead, I am interested in anterior-posterior, or longitudinal, axonal development.

1.4.1 Longitudinal axonal development

Longitudinal or anterior-posterior axonal development involves the outgrowth and guidance of axons along the ventral, dorsal, lateral or sublateral tracts. Axons extending in longitudinal tracts in *C. elegans* normally extend in a straight line across large distances. For example, the ALM sensory neurons have cell bodies on the lateral anterior body wall and extend axons anteriorly in the lateral cord before termination in the nerve ring [6]. The majority of longitudinal guidance mutations result in partially penetrant defects, where not all animals in a population are defective and/or neighbouring axons in a tract develop normally [20]. This incomplete penetrance in mutants suggest that several guidance cues may act redundantly [20].

Many axonal development defects previously identified involve incorrect axon guidance, where axons enter the wrong axon tract, or move between axon tracts (Figure 1.5) [20]. Defective longitudinal axons generally continue to extend in the anterior-posterior direction, but can enter and exit nearby longitudinal tracts [20]. These defects are not normally as severe as misguided dorsal-ventral axons, and this is likely due to longitudinal tracts being constrained by hypodermis and muscle [20]. An example of a factor involved in axon guidance is the ETS-domain transcription factor, AST-1. In *ast-1* mutants, interneuron axons in the VNC cross the ventral midline and extend in the left axon tract, or fail to reach the ventral cord and extend in incorrect lateral tracts [21]. A recent study demonstrated that the histone demethylase JMJD-1.2 regulates PVQ axon guidance through regulation of the Hedgehog-related genes *wrt-8* and *grl-16* [22]. When *jmjd1.2* is mutated or the hedgehog-related genes *wrt-8* and *grl-16* are overexpressed, the PVQ axons display guidance defects where they cross over the ventral midline [22]. Hedgehog genes are involved in neuronal development in mice and *Drosophila* [23, 24], and these results show a conserved role for Hedgehog-like signalling in *C. elegans* longitudinal axon guidance [22]. A final example of axon guidance defects is the cell adhesion molecule LAD-2. In *lad-2* mutants, the SDQ, PLN and SMD sublateral axons exhibit defective longitudinal axon guidance [25]. As L1CAMs are a focus of this thesis, this will be discussed later in more detail.

Very few genes have been identified that affect the termination of axon outgrowth [20]. Axon termination defects may result in premature axon termination, or overextension beyond their correct termination point (Figure 1.5). The PAM/Highwire/RPM-1 protein RPM-1 is involved in regulating axon termination and synapse organisation [26]. When *rpm-1* is mutated, mechanosensory and GABAergic motor neurons overextend [26, 27]. Normally, the mechanosensory PLM axon extends anteriorly from the tail and terminates near the vulva [6]. In *rpm-1* mutant animals, the PLM axon extends further along the longitudinal tract before extending ventrally [26]. Similarly, the GABAergic motor neurons of *rpm-1* mutants overextend in the dorsal cord [27]. Defects in dorsal-ventral guidance in *rpm-1* mutants were also identified, highlighting that genes involved in longitudinal axon guidance can also be involved in dorsal-ventral guidance [28].

Another protein that is involved in axon termination is the flamingo-type cadherin FMI-1. In *fmi-1* mutants, the DD and VD motor neuron axons navigate incorrectly to the wrong tracts and terminate prematurely, causing gaps in the VNC [29]. Although VD anterior growth prematurely terminates, the dorsal-ventral VD commissure growth occurs normally in *fmi-1* mutants, highlighting that only longitudinal axonal development is affected [30]. *fmi-1* mutants also display severe variable HSN axon defects, where the axons either incorrectly circle the vulva,

extend in the wrong direction along the VNC or prematurely terminate [31]. To regulate axonal development, FMI-1 acts in a parallel pathway to Wnt signalling. Other conserved pathways present in vertebrates are also important in *C. elegans* axonal development, including Semaphorin, Ephrin and Wnt signalling. These pathways have pleiotropic functions in nematode development, however I will focus on their roles in longitudinal axon guidance.

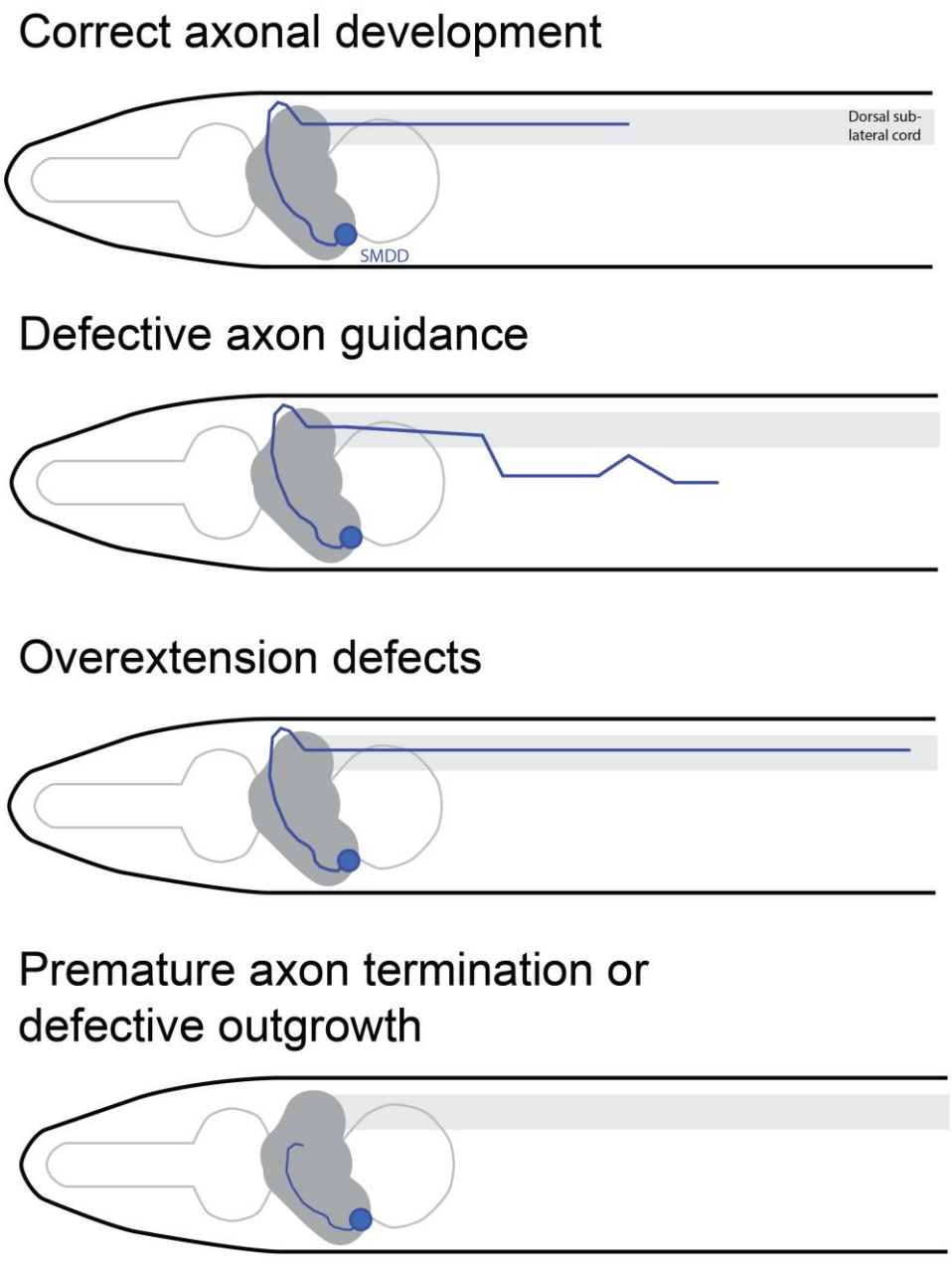

Figure 1.5 Types of axonal development defects.
SMDD axons (blue) as a model for axonal development. Defective axon guidance is where the axons leave the correct tract and extend in different tracts. Overextension defects are where the axon fails to terminate at the correct position. Premature axon termination and defective outgrowth are both evident by the lack of extension along the correct longitudinal tract.

1.4.2 Semaphorin signalling

The semaphorin family comprises transmembrane and secreted proteins that function as attractants and repellents in vertebrate axon guidance [32]. Semaphorins and their plexin receptors are conserved in *C. elegans*, but have limited known roles in axonal development. The transmembrane semaphorins, SMP-1 and SMP-2, function in PLM mechanosensory neuron axon guidance, with mutants displaying axons that extend dorsally instead of anteriorly [33]. The secreted Sema2A homolog MAB-20 has a limited known role in longitudinal axon guidance [25]. MAB-20 directs axon guidance of the SDQL, SDQR, SMD and PLN sublateral neurons, which all extend longitudinally in the sublateral cords [25]. By ectopically expressing *mab-20* in nearby neurons, Chen *et al.* demonstrated that secreted MAB-20 acts as a repulsive cue to guide the SDQL axons to extend towards and along the dorsal sublateral nerve cord [25]. MAB-20 function is mediated by the L1 cell adhesion molecule LAD-2 and the plexin receptor PLX-2 [25]. Accordingly, *lad-2* and *plx-2* mutants display axon guidance defects in these neurons [25].

1.4.3 Ephrin signalling

Ephrins act as membrane-bound axon guidance cues in vertebrates [34, 35]. The *C. elegans* genome encodes four ephrins, *efn-1/vab-2*, *efn-2*, *efn-3* and *efn-4*, and a single receptor, *vab-1* [36]. Correct ephrin signalling is required for axonal development of several classes of neurons, including the PVQ interneuron and HSN motor neurons. Both upregulation and loss-of-function of the VAB-1 ephrin receptor leads to defects in axon guidance, where PVQ and HSN axons aberrantly cross-over the ventral midline [37-39]. These axon cross-over defects are also present in *efn-1; efn-2; efn-3* triple mutants, but not single mutants, demonstrating that in this context, these ligands function redundantly to regulate axon guidance [38]. VAB-1 functionally interacts with the immunoglobulin molecule WRK-1, and VAB-1 function is also regulated by hypoxia and the HIF-1 transcription factor [38, 39].

Ephrin signalling is also involved in PLM mechanosensory axon outgrowth. Mutating *vab-1* causes PLM overextension, where they fail to terminate and extend too far anteriorly along the lateral cord [40]. Mutating the ephrin ligands (*efn-1* and triple *efn-2; efn-3; efn-4*) also causes these overextension phenotypes [40]. Overexpression of constitutively-active *vab-1* leads to severe PLM outgrowth defects, where the axon fails to extend or prematurely terminates, which is opposite to the loss-of-function overextension phenotype [40]. For both PVQ/HSN guidance and PLM termination, overexpression and loss-of-function of VAB-1 causes defects,

demonstrating that the correct level of ephrin signalling is required to regulate these developmental processes.

Ephrin signalling also occurs independently of the canonical VAB-1 receptor. The ephrin ligand EFN-4 directs axon guidance of the SDQL axons via the non-canonical L1CAM LAD-2 receptor [41]. This function is independent of VAB-1, and is in a separate pathway to the LAD-2-regulated Semaphorin pathway involving *mab-20* and *plx-2* described above [41]. EFN-4 likely functions as an attractive cue for SDQL axon extension, as EFN-4 can function non-cell-autonomously and engineered non-membrane-associated EFN-4 can rescue axon defects of *efn-4* null mutants [41]. EFN-4 is also involved in the outgrowth of DD motor neurons [42]. The six DD motor neurons extend axons that navigate dorsally before extending anteriorly in the dorsal nerve cord [6]. Mutating *efn-4* leads to gaps in the DNC, where axons fail to extend and reach their terminal position [42].

1.4.4 Wnt signalling

Members of the Wnt family are secreted glycoproteins that act as both attractants and repellents along the anterior-posterior axis in multiple developmental processes, including synaptogenesis and axon outgrowth [43]. In *C. elegans*, there are five Wnt ligands (CWN-1, CWN-2, MOM-2, EGL-20 and LIN-44), which are expressed in a series of partially overlapping regions along the anterior-posterior axis [44]. For example, *cwn-2* is expressed only in the anterior half of the animal, while *lin-44* is expressed only in the tail [44].

The Wnt signalling pathway has been implicated in multiple aspects of longitudinal axonal development. Defects in axon termination and extension have been observed in multiple Wnt and mutants. In double *cwn-1; egl-20* mutants, AVM and PVM mechanosensory axons terminate prematurely or extend axons along incorrect tracts [45]. Loss of Wnt ligands also causes the opposite defects, where axons fail to stop at their correct position and overextend into incorrect axon tracts. In *lin-44* and double *lin-44; egl-20* mutants, but not *egl-20* single mutants, D-type motor neuron axons overextend posteriorly into the tail [46]. Because these Wnt ligands are expressed in the posterior part of the animal, where D-type motor neuron axons direct their extension, this suggests that they normally function as a repellent of D-type motor neuron axons [46].

Furthermore, Wnt ligands are involved in initial axon outgrowth of RMED/V motor neurons. RMED/V motor neurons extend posterior processes from the nerve ring along the dorsal and ventral cords, respectively [6]. Axon extension occurs during late embryogenesis and larval

stages before they terminate near vulva [47]. In *cwn-2* mutants, RME motor neurons have shorter or non-existent axons [47]. In this context, CWN-2 acts a local attractive cue for RME axon outgrowth, as *cwn-2* expression posterior to the nerve ring rescues the mutant phenotype [47]. The *cwn-2* defects can also be rescued by driving other Wnts under the *cwn-2* promoter, demonstrating that Wnts can act redundantly if ectopically expressed in particularly locations along the anterior-posterior axis [47].

Correct Wnt signalling is also important for organizing neuronal polarity along the anterior-posterior axis. The PLM neurons are bipolar mechanosensory neurons which extend two processes from the cell body: a long anterior process that terminates near the vulva and a shorter posterior process that extends to the tail [6]. Most studies of PLM development, including those referenced thus far, focus on the longer anterior process which forms synapses. Loss-of-function of *lin-44* or the Frizzled receptor LIN-17 caused defective PLM process extension, where the long PLM process extends posteriorly instead of anteriorly, and vice versa for the short process [48, 49]. These defects are not caused by defective guidance, but are instead caused by reversed neuronal polarity. Similarly, *egl-20; cwn-1* double mutants display polarity defects in the ALM neurons, where the axons that normally extend anteriorly instead extend posteriorly from the cell body [48]. This highlights that Wnt signalling also functions in establishing neuron polarity early in development, so that later stages of axon outgrowth can occur.

1.4.5 Axon maintenance

Once axon guidance has completed, further mechanisms are in place to ensure that neuronal cell bodies and axons maintain their position. Axon maintenance pathways are in place to prevent mechanical stress-induced axon displacement. Axon maintenance defects can be suppressed by paralysis, caused pharmacologically with levamisole or genetically with mutations in muscle-structural or neuronal signalling pathways [50-52]. Defects in maintenance can only be observed once neuronal processes have completed development, which generally occurs during embryogenesis or early larval development [16]. In some specific cases, axons continue outgrowth during larval and adult stages, therefore examination of axon maintenance is dependent on when the neuron of interest develops [7]. For example, as previously detailed, the SMD axons continue to develop during larval stages and adulthood, therefore defects detected in adult animals could be due to errors in either axon guidance or maintenance.

Many identified axon maintenance factors are immunoglobulin domain proteins. An example of this is the sole *C. elegans* fibroblast growth factor receptor EGL-15, which has isoform-specific roles in both axon guidance and maintenance [50]. The *egl-15* locus encodes over 20 alternative transcripts and is expressed in the hypodermis [50, 53]. Null *egl-15* mutants display premature axon termination of PVP, PVQ, PVT and AVK interneuron axon guidance [50]. These defects occur in both posterior and anterior projections in the VNC [50]. In isoform-specific *egl-15(5A)* mutants, the PVQ and PVP axons displayed axon ventral midline flip-over defects [50]. These defects occur post-L1 stage and appear similar to axon midline cross-over defects, but only occur post-development once the neurons are being maintained in their correct positions [50]. Interestingly, resupplying only the EGL-15(5A) extracellular domain rescues the *egl-15(5A)* mutant maintenance defects, demonstrating a novel non-signalling function for the receptor [50].

Another immunoglobulin-containing protein involved in axon maintenance is the large secreted protein, DIG-1. Mutations in *dig-1* cause midline crossing defects in the PVQ, AVK, RMEV and HSN axons, all of which run longitudinally along the VNC [51]. These neurons (apart from HSN) have completed development during embryogenesis, and the axons appear normal in L1 stage animals, but become displaced across the ventral midline by adulthood [51]. DIG-1 is not expressed in neurons, and instead acts non-cell-autonomously from muscle to regulate axon maintenance [51]. A role for DIG-1 in axon guidance has also been identified. Defective fasciculation of head sensory neuron axons was identified in L1 stage *dig-1* mutants [54]. The OLL and OLQ sensory neurons normally extend a short process posteriorly towards the head, but in *dig-1* mutants these terminate prematurely or enter the wrong tracts [54]. These results demonstrate that DIG-1 functions to regulate both axon guidance and maintenance in different neuron classes.

The *zig* gene family of eight secreted immunoglobulin proteins are required for the maintenance of VNC axons. Mutating *zig-4* leads to defects in maintaining the AVK and PVQ axons within their VNC tract [55]. These flip-over defects occur in late-L1 stage, once these axons have finished axon outgrowth and extension, and can be rescued by immobilising mutants [55]. Because ZIG proteins are secreted, the *zig-4* mutant defects can be rescued by expressing *zig-4* from other VNC neurons [55]. Although ZIG-4 only acts in VNC axon maintenance, ectopically expressing *zig-4* during embryogenesis from muscle or neurons causes mispositioned PVQ axons [56]. These PVQ defects are visible in early L1-stage before the axons have finished growth, demonstrating that expressing *zig-4* earlier than it normally functions results in axon guidance defects [56]. Similar VNC axon maintenance defects are also seen in *zig-3* mutants [52]. ZIG-3 and ZIG-4 are most closely related by sequence analysis

and act in the same pathway to regulate axon maintenance [52]. Interestingly, the double *zig-5; zig-8* mutant, but not the single *zig-5* and *zig-8* mutants, also display similar VNC maintenance defects, where axons become displaced across the VNC midline during larval stages [57]. ZIG-5 and ZIG-8 function redundantly and within the same axon maintenance pathway as another immunoglobulin protein, the L1CAM SAX-7 [57]. SAX-7 is a major focus of this thesis so will be discussed in more detail later. It is possible that these genes all act in a common axon maintenance pathway. A *zig-3; zig-4* double mutant does not enhance the axon flip-over phenotype of *dig-1*, *sax-7* and *egl-15* single mutants [52].

1.5 C-terminal binding proteins

The conserved C-terminal binding proteins have been implicated in nervous system development in vertebrates and invertebrates, and are a major focus of this thesis. C-terminal binding proteins (CtBPs) function as transcriptional corepressors. CtBPs do not possess DNA-binding ability, and instead are recruited by DNA-binding transcription factors which contain a Pro-X-Asp-Leu-Ser (PXDLS) motif (where X is any amino acid) (Figure 1.6) [58]. These transcription factors include zinc-finger, basic helix-loop-helix and homeodomain proteins [58]. CtBPs subsequently physically associate with co-regulatory proteins to mediate repression of target genes (Figure 1.6) [59, 60]. Proteins in the core CtBP-containing repressor complex include histone deacetylases HDAC-1 and HDAC-2, and the chromatin-modifying enzyme coREST (corepressor with RE1 Silencing Transcription Factor) [59, 60]. CtBP corepressor complexes regulate diverse biological processes, including development and oncogenesis [61, 62].

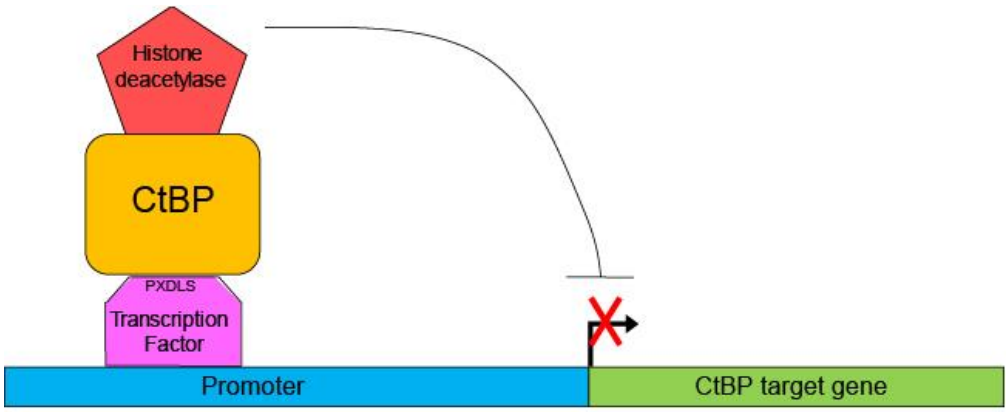

Figure 1.6 CtBP mechanism of action.
CtBP is recruited by PXDLS-motif containing transcription factors, and in turn recruits histone modifying enzymes, such as histone deacetylases, to mediate repression of target genes.

CtBPs contain three key characteristic regions: the PXDLS-binding clefts, a nucleotide-binding dehydrogenase-like domain, and an unstructured C-terminal region (Figure 1.7) [63]. The dehydrogenase-like domain, which shares homology to D-hydroxyacid dehydrogenases, can bind the dinucleotide molecule NADH [64, 65]. This NADH binding is required for CtBP dimerization, which is essential for corepressor activity [66, 67]. The conserved dehydrogenase-like domain also contains hydrophobic PXDLS-binding clefts, which contact with CtBP-interacting proteins. Mutations in CtBP clefts, or PXDLS motifs in partner proteins, prevents interaction [60, 68, 69]. Although the C-terminal region is largely unstructured [70], it contains key post-translational modification sites for regulation of CtBP function and colocalisation, including SUMOylation [71, 72] and phosphorylation [73, 74]. The general structure and function of CtBPs is highly conserved from invertebrates to vertebrates.

Figure 1.7 Schematic of CtBP protein structure.
The PXDLS-binding cleft and NADH-binding sites are in the dehydrogenase-like domain. The C-terminal region is largely unstructured. N-terminus on left, not to scale.

1.6 Vertebrate CtBPs

Vertebrate genomes contain two Ctbp genes, *Ctbp1* and *Ctbp2.* The two genes encode multiple protein isoforms, however the two major splice forms are CtBP1 and CtBP2 [61]. Both Ctbp1 and Ctbp2 are widely expressed in mouse embryos, with strong expression detected in the nervous system [75]. In the adult mouse, Ctbp1 is uniformly expressed throughout the brain, whereas Ctbp2 is highly expressed in specific brain regions, including the cerebellum and olfactory bulbs [76].

Mutant analysis of CtBP1 and CtBP2 revealed overlapping developmental functions. Ctbp1 knockout mice are small but viable and fertile [75]. Knocking out CtBP2, however, is embryonic lethal due to severe defects in early embryonic development, including aberrant heart formation [75]. Ctbp2 mutant embryos also display delayed development of the forebrain and midbrain, and degeneration of the neural epithelium [75]. Null mutations of CtBP1 and CtBP2

leads to the most severe phenotype, where the embryos arrest at the head fold stage, highlighting that Ctbp1 and Ctbp2 function redundantly during embryogenesis [75].

Recent studies have also revealed a role for CtBP in human neurodevelopment [77-79]. Whole-exome sequencing revealed that 12 patients with similar phenotypes, including developmental delay, intellectual disability and ataxia (lack of muscle control or coordination), possessed a deleterious mutation in CTBP1 [77-79]. All patients carried the same Arg331Trp variant in the PXDLS-binding cleft, which is required for recruitment of proteins in the CtBP corepressor complex [77-79]. Consistent with this predicted role in recruitment, the Arg331Trp mutation was shown to cause reduced interaction with known members of the CtBP corepressor complex, including HDAC1, HDAC2 and coREST, in cell culture modelling systems [79]. RNA-sequencing analysis also revealed changes in expression levels of genes involved in key biological processes, including transcriptional regulation and brain development [79]. This Arg331 residue is highly conserved across species, including *C. elegans* [78]. This is to date the only human disease associated with mutations in CtBP.

1.7 Invertebrate CtBP

Invertebrate genomes contain a single CtBP gene. Studies have found that *Drosophila* CtBP (dCtBP) functions as a corepressor for the known repressors, Knirps, Krüppel, Hairy and Snail, which function in embryo development [80, 81]. Consistent with these functions in development, mutations in dCtBP lead to severe segmentation and dorsoventral patterning defects [80, 81]. dCtBP is also essential for the patterning of the peripheral nervous system [81-83]. Null dCtBP mutants are homozygous lethal at adult stage and display extra mechanosensory bristles, which are key sensory organs [81, 83]. In contrast, overexpression of dCtBP leads to loss of mechanosensory bristles [82]. dCtBP plays additional roles in sensory organ development by binding and forming complexes with several known transcription factors, including Pax6 homolog Eyeless and Dachshund, to regulate eye and antennal development [84].

The *C. elegans* CtBP, CTBP-1, has also been implicated in nervous system development, and will be discussed in further detail.

1.8 *C. elegans* CtBP, CTBP-1

The *C. elegans* genome contains a single CtBP gene, *ctbp-1*. The *ctbp-1* locus generates two isoforms: *ctbp-1a* (F49E10.5a) and *ctbp-1b* (F49E10.5b). The translated proteins, called

CTBP-1a and CTBP-1b respectively, contain the conserved dehydrogenase-like domain, PXLDS-binding motifs and unstructured C-terminal region found in all CtBPs (Figure 1.8) [68]. *C. elegans* CTBP-1 displays a high degree of sequence homology to the vertebrate CtBPs, including all of the essential residues for binding PXDLS-containing proteins and dehydrogenase activity [68]. However, unlike the vertebrate CtBP family members, the *C. elegans* CTBP-1a isoform contains an additional N-terminal Thanatos-associated protein (THAP) domain (Figure 1.8) [68, 85]. This THAP domain is not present in the shorter CTBP-1b isoform (Figure 1.8). THAP domains are zinc-dependent sequence-specific DNA-binding motifs approximately 90 amino acid residues in length [86, 87]. THAP domains are characterised by their N-terminal location, a C2CH zinc-coordination site and additional highly conserved residues required for DNA binding [86]. THAP domains are present in >100 distinct proteins in vertebrates and invertebrates involved in many different biological processes, including cell proliferation, apoptosis and chromatin modification [87]. Although mammalian CtBPs do not contain THAP domains, THAP-CtBPs are present in diverse invertebrate lineages [68]. The THAP protein sequence in three *Caenorhabditis* species, *C. elegans, C. remanei* and *C. briggsae,* is 100% conserved [68]. The distribution of THAP-CtBPs in a phylogenetic tree suggests that THAP was present in ancestral animal CtBPs but has been lost in vertebrate lineages [68].

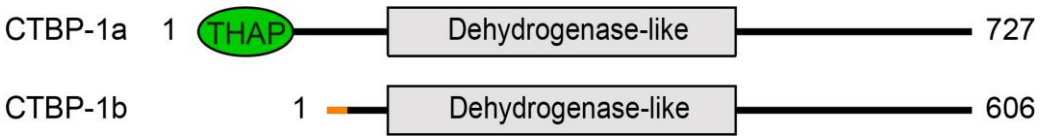

Figure 1.8 *C. elegans* CTBP-1a contains an additional THAP domain.
Predicted domain structure of CTBP-1a and CTBP-1b, where different amino acids in CTBP-1b are in orange. Unstructured C-terminal domain indicated by black line. Length of proteins on the right, N-terminus is on the left.

Like other CtBPs, *C. elegans* CTBP-1 mediates repression of gene expression by binding proteins containing a PXDLS motif [68]. Disrupting the PXDLS motif in a partner zinc-finger protein PAG-3 or the PXDLS-binding cleft in CTBP-1 results in loss of interaction in yeast-two-hybrid experiments [68]. CTBP-1 also has a conversed repressor function, but the THAP domain is not required for repression [68]. This suggests that there is another function for the CTBP-1 THAP domain. Because THAP domains directly bind DNA, it is possible that nematode CtBPs may be able to directly bind to promoter regions of DNA. The Nicholas laboratory (University of Sydney) found that the *C. elegans* CTBP-1 THAP domain contains a large, positively charged surface patch that could bind to the 11-bp consensus sequence recognised

by hTHAP1 [85], but this was later determined to be non-specific binding [88]. This is unsurprising, as THAP domains even within the same species bind to different DNA consensus sequences [88]. Therefore, we predict that *C. elegans* CTBP-1 can bind directly to DNA, but the DNA-binding recognition sequence has not been determined.

1.9 Known roles for *C. elegans* CTBP-1

Studies in *C. elegans* have identified that CTBP-1 regulates diverse physiological functions. Loss of *ctbp-1* expression results in increased lifespan and increased resistance to oxidative and heat stress [89, 90]. Tissue-specific rescue experiments demonstrate that CTBP-1 functions solely in the nervous system to regulate lifespan [89]. To identify genes involved in CTBP-1-regulated longevity, Chen *et al.* performed a genome-wide microarray analysis that compared wild-type and *ctbp-1* hypomorph mutant populations [90]. They identified over 200 putative CTBP-1 target genes, including genes involved in metabolism, stress response and cell signalling [90]. Chen *et al.* focussed on the putative triacylglycerol (TAG) lipase, LIPS-7, that was upregulated in a *ctbp-1* mutant background [90]. TAG lipases hydrolyse ester bonds of lipids and regulate TAG uptake and distribution. RNAi inhibition of *lips-7* suppressed the lifespan extension caused by CTBP-1 [90]. Therefore, they proposed that CTBP-1 controls lifespan through regulation of TAG levels.

A role for CTBP-1 in acute functional tolerance to ethanol (AFT) has also been demonstrated [91]. After exposure to ethanol, wild-type animals are sensitive to the intoxicating effects of ethanol, causing a decrease in locomotory speed. When animals are continually exposed to ethanol (meaning there is no decrease in internal ethanol concentration) they develop AFT and recover their ability to move [92]. Animals with decreased *ctbp-1* expression have reduced AFT, suggesting that CTBP-1 is a regulator of AFT [91].

Analysis of translational reporter constructs revealed that *C. elegans* CTBP-1 is predominantly expressed in the nervous system nuclei throughout embryonic development, larval stages and adulthood [89]. Weaker expression levels were also detected in hypodermal nuclei along the body [89]. The endogenous individual expression patterns of CTBP-1a or CTBP-1b have not been elucidated.

In this project, I was interested in the recently identified role for *C. elegans* CTBP-1 in nervous system development.

1.10 CTBP-1 in neuronal development

Recently, the Nicholas laboratory (University of Sydney) demonstrated that CTBP-1 regulates the development of the SMDD axons [93]. In wild-type animals, SMDD axons extend posteriorly along the dorsal sublateral cord (Figure 1.9, Figure 1.4). In *ctbp-1* mutants, the SMDD axons leave the dorsal sublateral cord and extend in different directions (Figure 1.9) [93]. SMDD axons were defective at the fourth larval stage (L4 stage), and the severity and penetrance of the SMDD axonal morphology defect increased throughout adulthood [93]. This study was the first to identify a role for *C. elegans* CTBP-1 in neuronal development, but we were unable to determine the cells/tissues that CTBP-1 acts in to regulate SMDD morphology [93].

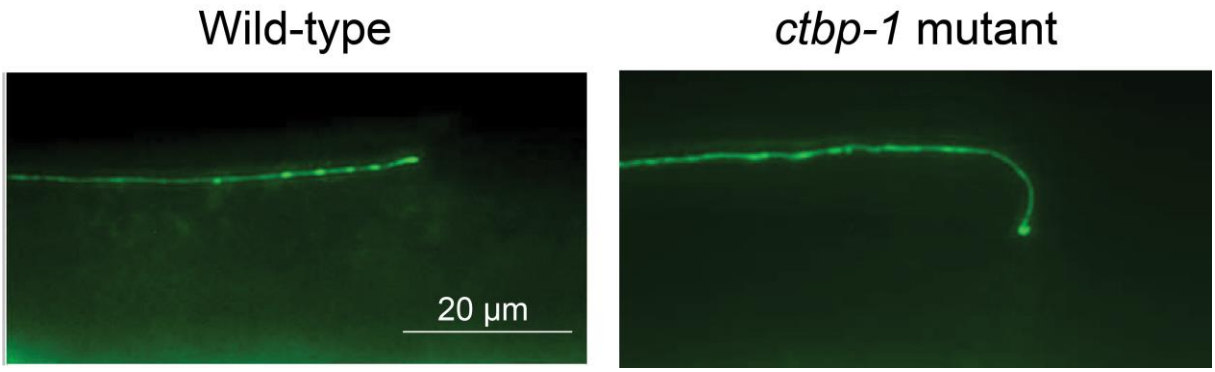

Figure 1.9 Reduced *ctbp-1* results in defective SMDD axons that leave the dorsal sublateral cord. Representative image of SMDD axons at L4 stage *ctbp-1(tm5512)* mutant animals. Scale bar= 20 µm. Adapted from [93].

We also found that *ctbp-1* mutant animals displayed reduced exploration behaviour across a uniformly seeded bacterial plate [93]. Reduction-of-function *ctbp-1* mutant animals explored less than wild type, and this is possibly due to defects in the SMDD neurons that have known functions in locomotion (see section 1.3) [93]. Furthermore, Yeon *et al.* identified that *ctbp-1* reduction-of-function mutant animals exhibit defective locomotion, where they display continuous ventral circular movement [14]. The authors attribute this inability to properly induce forward locomotion to the defective SMDD axons present in mutant animals due to the similarity of phenotypes present in SMDD-ablated animals [14].

1.11 L1CAM family

Another major focus of this thesis is the role of L1 cell adhesion molecules in neuronal development. The L1 cell adhesion molecule (L1CAM) gene family is a highly conserved group of transmembrane cell adhesion receptor molecules. L1CAMs are characterised by 6 immunoglobulin-like (Ig-like) domains, 4-5 fibronectin-III (FNIII) repeats, a single transmembrane domain and a conserved cytoplasmic tail (Figure 1.10) [94]. There are four members in vertebrates: L1, NrCAM (NgCAM-related cell adhesion molecule), Neurofascin and CHL1 (close homolog of L1) [94]. Vertebrate L1CAMs are all predominantly expressed in the nervous system [94]. In the highly conserved cytoplasmic tail, vertebrate L1CAMs possess binding sequences for membrane-cytoskeletal linker proteins (FERM, PDZ and ankyrin proteins) [94]. Ankyrin proteins reversibly bind and stabilise the L1CAM family members at the actin cytoskeleton, which is essential for cell-cell adhesion and axon outgrowth [95]. The ankyrin-binding ability of L1CAMs is regulated by tyrosine (Y) phosphorylation in the highly conserved FIGQY motif [96]. Unlike the other mammalian L1CAMs, Neurofascin also contains a Proline/Alanine/Thymine (PAT) domain that is rich for these amino acids and is predicted to be a target of O-linked glycosylation [97].

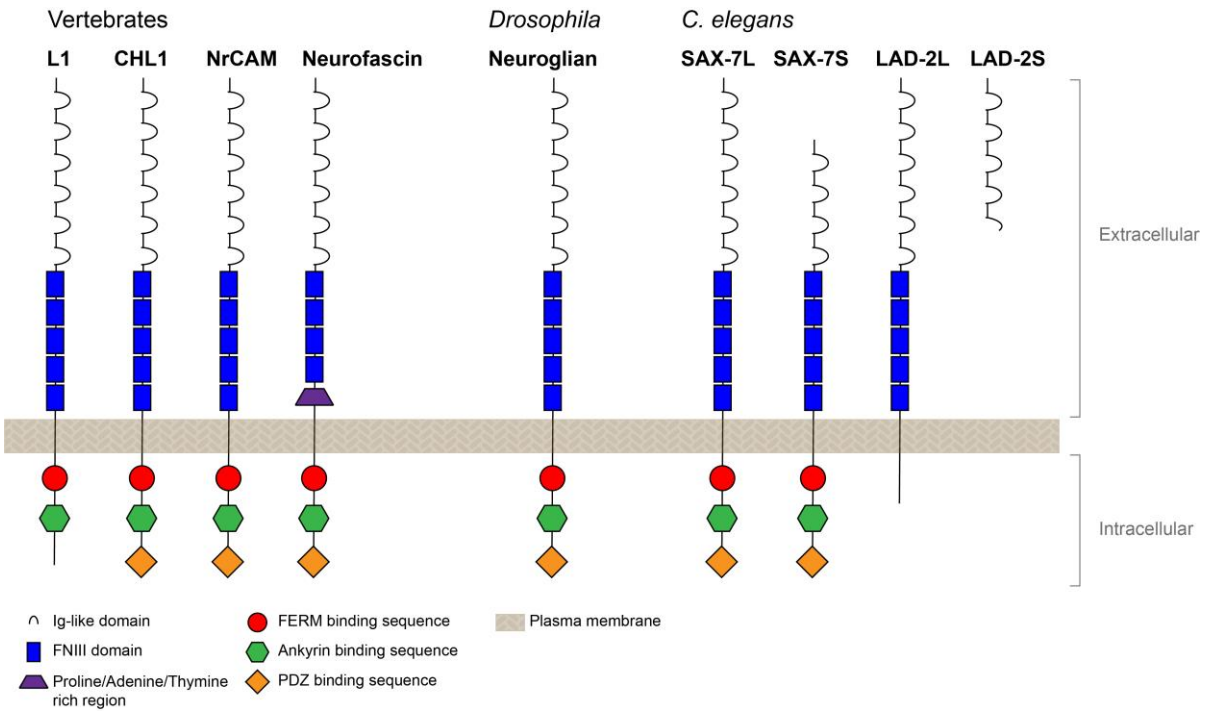

Figure 1.10 Protein structure of the L1CAM family in vertebrates and invertebrates.
Long (L) and short (S) isoforms are represented for the *C. elegans* L1CAM members. Key for the different domains is in the bottom-left corner.

L1, also known as L1CAM, regulates many aspects of nervous system development and function, including axon guidance, outgrowth and fasciculation (reviewed in [94]). L1 has been extensively studied because mutations in the L1 gene cause an X-linked recessive disorder known as L1 syndrome (previously known as CRASH syndrome for the symptoms corpus callosum hypoplasia, retardation, adducted thumbs, spastic paraplegia and hydrocephalus. For a comprehensive list of clinical phenotypes, see [98]). Diagnosis of L1 syndrome occurs after mutations are found in the L1 gene through sequence analysis [98]. Over 250 distinct L1 mutations causing L1 syndrome have been identified in over 90 publications, and are collated in the 'L1CAM Mutation Database' at http://www.l1cammutationdatabase.info/ (last updated in 2012) [99]. Pathogenic point mutations or deletions have been identified in all domains and are predicted to cause a variety of protein effects, including missense amino acid changes, truncation and aberrant splicing [94, 100]. The severity of phenotypes in patients with L1 syndrome is highly variable, and this has been linked to the location of the pathogenic mutation. Deletions causing absent or truncated L1 protein are linked to more severe phenotypes [101, 102]. Point mutations in key residues for the Ig-like and FNIII extracellular domains lead to more severe neurological problems than mutations in the cytoplasmic domains [102].

Mouse models of L1 syndrome mirror the phenotypes of humans with the disorder. Mice with L1 mutations display many neuronal phenotypes, including defective axon guidance, abnormal dendrite and ventricle architecture, hydrocephalus and corpus callosum dysgenesis [103-107]. L1-null lines independently generated by different groups demonstrate high phenotypic diversity, which suggests that other factors influence the severity. Analysis of L1 mutant lines that differ in severity of hydrocephalus revealed a genetic L1 modifier region on chromosome 5 [108], but further analysis is necessary to determine what genes in this locus may be involved.

Like L1, the other mammalian L1CAMs have roles in nervous system function and are linked to human neurological diseases. In mouse models, CHL1 and NrCAM both have roles in axon guidance and dendrite outgrowth [109-111]. Although they have overlapping functions, CHL1 and NrCAM are linked to different human diseases. A missense mutation in human CHL1 was linked to schizophrenia in two separate studies [112, 113]. It was later demonstrated that CHL1 interacts with DISC1 (disrupted-in-schizophrenia-1) to regulate neurite outgrowth [114]. NrCAM mutations are strongly associated with autism [115, 116]. Neurofascin is important for the assembly and maintenance of the nodes of Ranvier in the CNS, and Neurofascin-deficient or Neurofascin-null mice display severe motor coordination defects and early death [117-120]. Recent studies have also proposed that novel Neurofascin mutations are the cause of severe neurodevelopmental disorders in multiple families [121-123]. There is evidence for functional

redundancy between the mammalian L1CAMs. Single L1 and NrCAM knockout mice are viable and display mild neurodevelopmental defects, but a double L1/NrCAM knockout results in severe cerebellar development defects and postnatal lethality [124].

The severe axon guidance phenotypes in mammalian L1CAM mouse models are attributed to disruptions in semaphorin signalling [125]. With neuropilin-1, L1 functions as a co-receptor for the repulsive guidance cue semaphorin Sema3A [125]. L1 mutations disrupt correct semaphorin signalling, leading to cortical axon guidance errors [125]. Other mammalian L1CAMs also associate with neuropilins in receptor complexes to regulate semaphorin signalling: NrCAM and neuropilin-2 regulate anterior commissure axon guidance [126], and CHL1 and neuropilin-1 regulate thalamocortical axon guidance [127].

L1CAMs are also present in invertebrate species, including *Drosophila* and *C. elegans.* The singular *Drosophila* L1CAM, Neuroglian, possesses the canonical 6 Ig-like domains, 5 FNIII domains and cytoplasmic tail (Figure 1.10) [128]. Like mammalian L1CAMs, Neuroglian interacts with ankyrins (Dank1 and Dank2) [129, 130]. Differential splicing of Neuroglian results in two protein isoforms: Nrg^{180} and Nrg^{167}. The long isoform Nrg^{180} is expressed exclusively in neurons, while the shorter isoform Nrg^{167} is expressed ubiquitously, including epithelia [131]. Loss-of-function Nrg mutations are late embryonic lethal and cause defective axon pathfinding of multiple types of neurons, including motor and sensory neurons [132-137]. Neuroglian also functions in synapse development and stability [138], and dendritic pruning [139]. The role of Neuroglian in nervous system development is similar to the roles seen for mammalian L1CAMs, and suggests functional conservation between vertebrate and invertebrate L1CAM family members. Strikingly, expressing human L1 in Nrg mutants can rescue axon guidance and synaptic formation defects [134, 140].

1.12 *C. elegans* L1CAM, LAD-2

LAD-2 is one of the two *C. elegans* members of the L1CAM family and is most closely related to the *Drosophila* L1CAM Neuroglian [25]. There are two protein isoforms of LAD-2, called LAD-2S and LAD-2L, respectively. The secreted isoform LAD-2S is 496 amino acids long and contains the first four and a partial fifth Ig-like domain (Figure 1.10). LAD-2L is 1187 amino acids long and contains six immunoglobulin domains, five fibronectin type III repeats and a short cytoplasmic tail (Figure 1.10). The cytoplasmic tail of LAD-2L differs from other L1CAMs due to its length and absence of canonical motifs, including the ankyrin-binding domain [25]. This divergence has led to the classification of LAD-2 as a non-canonical L1CAM.

LAD-2 is expressed on the plasma membrane of axons and cell bodies of 14 neurons, including the SMD neurons [25]. LAD-2 expression is observed from the embryonic or post-embryonic birth of neurons and persists during axon extension in larval stages and maintenance during adulthood [25]. Chen *et al.* reported that the long isoform of LAD-2 (LAD-2L) is required for the guidance of SDQL, SDQR, SMD and PLN axons [25]. These *lad-2*-expressing neurons all extend axons along the sublateral cords [6]. Chen *et al.* focussed on the SDQL axons, which normally extend anteriorly along the lateral and then dorsal sublateral cord towards the nerve ring [25]. In *lad-2* mutants, the SDQL axons extend ventrally along the VNC [25]. LAD-2L regulates SDQL axon guidance by acting as a receptor for members of well-known axon guidance pathways: the *C. elegans* secreted semaphorin-2A ortholog MAB-20 and ephrin EFN-4 [25, 41].

1.13 *C. elegans* L1CAM, SAX-7

SAX-7 (formerly known as LAD-1) is the canonical *C. elegans* L1CAM and is most closely related to *Drosophila* Neuroglian [141, 142]. The long isoform SAX-7L contains six Ig-like domains, five FNIII domains and a cytoplasmic tail containing an ankyrin-binding sequence (Figure 1.10) [142]. The shorter isoform SAX-7S lacks the first two Ig-like domains (Figure 1.10) [142]. SAX-7 is expressed widely across tissues and life stages, and is highly expressed in the nerve cords and hypodermal cells [142-144].

SAX-7 is required to maintain the positions of neuronal cell bodies and processes. *sax-7* mutant animals do not display defects in axon guidance, but their axons and cell bodies become displaced as they age. Specifically, defects in VNC axon and cell body maintenance have been observed in *sax-7* mutants [145, 146]. Displacement of cell bodies of sensory, motor and interneurons is evident in the head ganglia [37, 141, 145, 147]. SAX-7 function in maintaining correct neuronal positioning is regulated by its interaction with the ankyrin UNC-44 and γ-syntrophin STN-2 [146]. UNC-44 and STN-2 bind the cytoplasmic ankyrin-binding and PDZ-binding motifs, respectively, and these complexes are predicted to link SAX-7 to the actin cytoskeleton [146]. Defective axon and cell positioning can be partially suppressed by paralysing *sax-7* mutants by treating with levamisole or crossing with locomotion-defective genetic mutants [141, 145]. This highlights SAX-7's important role in countering the mechanical forces exerted by locomotion.

SAX-7 is also necessary for correct morphogenesis of dendrites in the highly branched PVD sensory neurons [143, 144, 148], and axon branching of AIY interneurons and HSN motor neurons [149]. In the hypodermis, SAX-7 forms a complex with MNR-1/menorin and directs

dendrite patterning through interaction with the neuronal receptor DMA-1 in the PVD neurons [143, 144]. Furthermore, SAX-7 is involved in synaptic regulation [150]. SAX-7 also has non-neuronal roles in gastrulation and pharyngeal morphogenesis [151, 152].

For different roles, SAX-7 functions within neurons or from neighbouring tissues. For example, SAX-7 acts in the hypodermis to pattern PVD dendrites [144]. Conversely, VNC axon maintenance defects of *sax-7* mutant animals can be rescued with neuronal *sax-7* expression [145]. SAX-7 can also function simultaneously in multiple tissues. The defective position of GABA neuron axons and soma in *sax-7* mutants can be rescued only when SAX-7 was expressed in the neurons, muscle and hypodermis [147]. Overlapping and differential roles for the two SAX-7 isoforms (SAX-7S and SAX-7L) have also been identified. For example, only the SAX-7S isoform is involved in AIY and PVD branching [144, 149]. Both isoforms can rescue VNC maintenance defects [146].

Overall, the *C. elegans* L1CAMs LAD-2 and SAX-7 have distinct roles in the nervous system. SAX-7 is more widely studied and is primarily involved in maintaining nervous system integrity. Conversely, LAD-2 is only involved in axon guidance during development. No overlapping roles for SAX-7 and LAD-2 have been identified [153].

1.14 Thesis overview

The highly conserved C-terminal binding proteins regulate gene expression and play important roles in mammalian and invertebrate nervous system development. We recently identified a novel role for the *C. elegans* C-terminal binding protein CTBP-1 in the development of the SMDD motor neurons. In this thesis, I investigate how CTBP-1 regulates axonal development. In the first chapter, I characterise the role of the different CTBP-1 isoforms in the guidance and termination of the SMD neurons. In the second chapter, I investigate the mechanism by which CTBP-1 influences SMDD development using epistasis experiments with putative CTBP-1 target genes and known regulators of axon guidance and maintenance. In the third chapter, I focus on the role of the *C. elegans* L1 cell adhesion molecules (L1CAMs) in axonal development. I demonstrate that CTBP-1 controls SMDD development by repressing SAX-7/L1CAM, and this function acts in parallel to the LAD-2/L1CAM function.

2. Materials and Methods

2.1 Materials

2.1.1 Chemicals and reagents

- 6x Loading Dye Solution (Fermentas, Glen Burnie, MD, USA)
- Acetic acid, glacial (Ajax Finechem Pty. Ltd., Taren Point, NSW, Australia)
- Agar (Merck, Darmstadt, Germany)
- Ampicillin sodium salt (Astral Scientific Pty. Ltd., Gymea, NSW, Australia)
- Calcium chloride dehydrate (Merck)
- Carbenicillin (AG Scientific, San Diego, CA, USA)
- Cholesterol (Sigma-Aldrich Corporation, St. Louis, MO, USA)
- Chloroform - isoamyl alcohol mixture (Fluka Analytical, now Sigma-Aldrich)
- CutSmart® Buffer (New England Biolabs (NEB), Ipswich, USA)
- Deoxynucleotide triphosphates (dNTPs) (Fisher Biotec, Wembley, WA, Australia)
- Di-potassium hydrogen orthophosphate (Ajax Finechem Pty. Ltd.)
- Ethidium bromide solution (Sigma-Aldrich)
- Ethylenediaminetetraacetic acid (EDTA) (Ajax Finechem Pty. Ltd.)
- Gelatine (Davis Gelatine, Botany, NSW, Australia)
- Generuler™ DNA ladder mix (Progen Industries, Darra, QLD, Australia)
- Isopropyl β-D-1-thiogalactopyranoside (IPTG) (Biochemicals, Gymea, NSW, Australia)
- Levamisole hydrochloride (Sigma-Aldrich)
- Magnesium sulfate heptahydrate (Merck)
- Methanol (Sigma-Aldrich)
- Nonyl phenoxypolyethoxyethanol (NP-40 (Igepal)) (Sigma-Aldrich)
- Peptone (Merck)
- Potassium chloride (BDH Chemicals, Port Fairy, VIC, Australia)
- Potassium dihydrogen phosphate (Sigma-Aldrich)
- Sodium chloride (Merck)
- Sodium hydroxide (Ajax Finechem Pty. Ltd.)
- Sodium hypochlorite 12.5% w/v solution (Nuplex Industries (Australia) Pty. Ltd., Seven Hills, Australia)
- Tetramisole hydrochloride (Sigma-Aldrich)
- Tris-hydroxymethyl-methylamine (Tris) (Ajax Finechem Pty. Ltd.)

- TRIzol™ Reagent (Invitrogen™, Carlsbad, CA, United States)
- Tween 20 (AMRESCO LLC, Solon, OH, USA)
- UltraPure™ Agarose (Invitrogen™)
- Yeast extract powder (Affymetrix Inc., Santa Clara, CA, United States

2.1.2 Enzymes

- ClaI (NEB)
- FastAP Thermosensitive Alkaline Phosphatase (Thermo Scientific™)
- FastDigest BamHI (Thermo Scientific™)
- FastDigest HindIII (Thermo Scientific™)
- FastDigest KpnI (Thermo Scientific™)
- FastDigest DpnI (Thermo Scientific™)
- FastDigest EcoRI (Thermo Scientific™)
- HindIII-HF® (NEB)
- ImProm-II™ Reverse Transcriptase (Promega Corporation, Madison, WI, USA)
- KLD Enzyme Mix (NEB)
- MangoTaq™ DNA Polymerase (Bioline (Aust) Pty. Ltd., Alexandria, NSW, Australia)
- NotI-HF® (NEB)
- Phusion® High-Fidelity DNA Polymerase (NEB)
- Proteinase K (Boehringer Ingelheim Pty. Ltd., North Ryde, NSW, Australia)
- Q5® High-Fidelity DNA Polymerase (NEB)
- RNAse-Free DNase (Qiagen, Hilden, Germany)
- RNasin® Ribonuclease Inhibitor (Promega)
- SpeI-HF® (NEB)
- LightCycler® 480 SYBR Green I Master (Roche Molecular Systems, Inc, Pleasanton, CA, USA)
- T4 DNA ligase (NEB)
- T4 Polynucleotide Kinase (NEB)

2.1.3 Plasmids

Table 2.1 Plasmids used in this project.

TS indicates that I generated this plasmid during this project and construction details are present in the Methods section.

Purpose	Plasmid	Source
CRISPR-Cas9	*peft-3::cas9::tbb-2 3'UTR*	Mario de Bono (Addgene plasmid 48960) [154]
	pU6::klp-12 sgRNA expression vector	John Calarco (Addgene plasmid 46170) [155]
	mCherry-pmyo-2::GFP neoR loxP	John Calarco [155]
	pDD104 (*peft-3::Cre*)	Bob Goldstein (Addgene plasmid 47551)
	ctbp-1 sgRNA 1	TS
	ctbp-1 sgRNA 2	TS
	wrt-10 sgRNA	TS
	wrt-6 sgRNA	TS
	pTS1 mCherry::CTBP-1b repair template	TS
	pTS2 mutated mCherry::CTBP-1b repair template	TS
Co-injection markers	pCFJ90 (*pmyo-2::mCherry::unc-54 3'UTR*)	Erik Jorgensen (Addgene plasmid 19327) [156]
	pCFJ104 (*pmyo-3::mCherry::unc-54 3'UTR*)	Erik Jorgensen (Addgene plasmid 19328) [156]
	coel::GFP (*punc-122::GFP*)	Piali Sengupta (Addgene plasmid 8937) [157]
	pttx-3::dsRed2	Pocock lab
Expression and rescue	pPD95.75	Andrew Fire
	pPD95.75 *mCherry*	Andrew Fire
	pTB80 (*pdpy-7::GFP*)	Oliver Hobert [50]
	RJP383 (*pctbp-1a::GFP*)	TS
	RJP414 (*pctbp-1a::sax-7S cDNA*)	TS
	RJP420 (*ctbp-1a long cDNA::mCherry*)	TS
	RJP421 (*ctbp-1b short cDNA::mCherry*)	TS
	RJP422 (*pctbp-1a::ctbp-1a::mCherry*)	TS
	RJP423 (*pctbp-1a::ctbp-1b::mCherry*)	TS
	RJP424 (*plad-2::ctbp-1a::mCherry*)	TS
	RJP425 (*pdpy-7::ctbp-1a::mCherry*)	TS
	RJP515 (*plad-2::sax-7S cDNA*)	TS
	pRP13 (*pdpy-7::sax-7S cDNA*)	Roger Pocock [145]
RNAi	L4440 (empty backbone)	Andrew Fire (Addgene plasmid 1654)
	L4440-*ctbp-1*	Marc Vidal [158]

2.1.4 Commercial Kits

- Gibson Assembly Master Mix (NEB)
- In-Fusion® HD Cloning Kit (Takara Bio USA, Inc., Mountain View, CA, USA)
- Q5® Site-Directed Mutagenesis Kit (NEB)
- QIAprep Spin Miniprep Kit (Qiagen)
- QIAquick Gel Extraction Kit (Qiagen)
- QIAquick PCR Purification Kit (Qiagen)
- RNeasy® Mini Kit (Qiagen Pty. Ltd.)

2.1.5 Equipment

- CyberScan510 pH meter (Eutech Instruments Pty Ltd., Singapore)
- Eppendorf MasterCycler EP S Thermal Cycler (Eppendorf AG, Hamburg, Germany)
- Gel Doc™ XR Gel Documentation System (Bio-Rad Laboratories)
- LightCycler® 480 Instrument II (Roche)
- P-97 Flaming/Brown micropipette puller (Sutter Instrument Co., Novato, CA, USA)
- Nanodrop1000 Spectrophotometer (Thermo Fisher Scientific, Waltham, MA, USA)
- Olympus MVX10 fluorescence microscope with X-Cite® 120Q lamp (formerly Lumen Dynamics, now Excilitas Technologies, Waltham, MA, USA)
- Olympus BX51 microscope fitted with an Olympus F-View II camera (Olympus)
- Olympus SZ51 stereo microscope (Olympus Corporation, Shinjuku-ku, Tokyo, Japan)
- Zeiss Axio Imager M2 microscope fitted with Zeiss Axiocam 506 mono camera (Zeiss, Oberkochen, Germany)
- Zeiss Axio Vert A1 microscope fitted with Eppendorf FemtoJet 4X and Eppendorf InjectMan 4 (Eppendorf)

2.1.6 Software

- Adobe Photoshop (Adobe Inc., San Jose, CA, USA)
- Excel 2016 (Microsoft Corporation, Redmond, WA, USA)
- Fiji (ImageJ) [159]
- Graphpad Prism® (GraphPad Software, San Diego, CA, USA)
- Zen 2 pro (Zeiss)

2.1.7 Bacterial strains

- OP50 *Escherichia coli* (*E. coli*)
- HT115(DE3) *E. coli* [F-, mcrA, mcrB, IN(rrnD-rrnE)1, rnc14::Tn10(DE3 lysogen: lavUV5 promoter -T7 polymerase]
- α-Select Silver Efficiency Chemically Competent Cells (Bioline)
- NEB® 5-alpha Competent *E. coli* (High Efficiency) (NEB)

2.1.8 *C. elegans* strains

In nematode strains, promoters are represented as *p*. For example, *p*xxx::yyy represents expression of gene yyy being driven by the promoter of gene xxx. Gene names are in lower-case italics, with mutant alleles in parentheses, and protein names are in upper-case. Chromosomes are represented by roman numerals I-V and X, with X chromosome as the sex chromosome. Transgenic strain details are indicated in the genotype name. *Is* indicates that transgenes have been integrated into a chromosome location and *Ex* indicates transmissible extrachromosomal arrays.

Table 2.2 External strains.

Strain	Genotype	Source
N2	Wild-type, Bristol strain	*Caenorhabditis* Genetics Centre (CGC), University of Minnesota
LH247	*lad-2(tm3056) IV; otEx331*	CGC
PHX601	*ctbp-1(syb601) X*	Sunybiotech, Fujian, China

Table 2.3 Strains generated in Nicholas and Pocock labs.

Strain	Genotype
HRN169	*rhIs4 III*
HRN173	*ctbp-1(tm5512) X*
HRN226	*rhIs4 III; ctbp-1(tm5512) X*
HRN498	*rhIs4 III; cwn-2(ok895) IV*
HRN499	*rhIs4 III; cwn-2(ok895) IV; ctbp-1(tm5512) X*
HRN508	*rhIs4 III; rpm-1(ju41) V*
HRN509	*rhIs4 III; rpm-1(ju41) V; ctbp-1(tm5512) X*
HRN539	*ctbp-1(aus24[mCherry::ctbp-1b + loxP myo-2::gfp loxP)]*
HRN541	*ctbp-1(aus15) X*
HRN543	*ctbp-1(aus14) X*

Strain	Genotype
HRN551	*rhIs4; ctbp-1(aus14) X*
HRN552	*rhIs4; ctbp-1(aus15) X*
HRN553	*ctbp-1(aus26[mCherry::ctbp-1b + loxP]) X*
HRN556	*rhIs4 III; ctbp-1(aus23) X*
HRN575	*otEx331[lad-2p::GFP + pha-1(+)]*
HRN585	*rhIs4 III; lad-2(tm3056) IV; ctbp-1(tm5512) X*
HRN586	*rhIs4 III; lad-2(tm3056) IV*
HRN587	*otEx331; lad-2(tm3056) IV; ctbp-1(tm5512) X*
HRN588	*otEx331; ctbp-1(tm5512) X*
HRN666	*wrt-10(aus36) II*
HRN667	*wrt-10(aus37) II*
HRN680	*wrt-6(aus41) X*
HRN495	*ast-1(rh300) II; rhIs4 III*
HRN496	*ast-1(rh300) II; rhIs4 III; ctbp-1(tm5512) X*
HRN508	*rhIs4 III; rpm-1(ju41) V*
HRN509	*rhIs4 III; rpm-1(ju41) V; ctbp-1(tm5512) X*
HRN539	*ctbp-1(aus24[mCherry::ctbp-1b + loxP myo-2::gfp loxP)] X*
HRN554	*ctbp-1(aus23) X*
HRN623	*lips-7(ok3110) II; rhIs4 III; ctbp-1(tm5512) X*
HRN626	*rhIs4 III; fsn-1(gk429) II*
HRN627	*rhIs4 III; fsn-1(gk429) III; ctbp-1(tm5512) X*
HRN629	*lips-7(ok3110) II; rhIs4 III*
HRN638	*rhIs4 III; grl-5(ok2671) V*
HRN639	*rhIs4 III; grl-5(ok2671) V; ctbp-1(tm5512) X*
HRN643	*rhIs4 III; nas-38(ok3407) X*
HRN644	*rhIs4 III; nas-38(ok3407) X; ctbp-1(tm5512) X*
HRN645	*rhIs4 III; grl-5(ok2700) V*
HRN646	*rhIs4 III; grl-5(ok2700) V; ctbp-1(tm5512) X*
HRN685	*rhIs4 III; acs-2(ok2457) V*
HRN686	*rhIs4 III; acs-2(ok2457) V; ctbp-1(tm5512) X*
HRN687	*grl-16(ok2959) I; rhIs4 III*
HRN688	*grl-16(ok2959) I; rhIs4 III; ctbp-1(tm5512) X*
HRN689	*ins-4(ok3534) II; rhIs4 III*
HRN690	*ins-4(ok3534) II; rhIs4 III; ctbp-1(tm5512) X*
HRN696	*wrt-10(aus36) II; rhIs4 III*
HRN697	*wrt-10(aus36) II; rhIs4 III; ctbp-1(tm5512) X*
HRN698	*wrt-10(aus37) II; rhIs4 III*
HRN699	*wrt-10(aus37) II; rhIs4 III; ctbp-1(tm5512) X*

Strain	Genotype
HRN711	*rhIs4 III; wrt-6(aus41) X*
HRN712	*rhIs4 III; wrt-6(aus41) X; ctbp-1(tm5512) X*
RJP3981	*ctbp-1(aus26[mCherry::ctbp-1b + loxP]) X*
RJP3994	*ctbp-1(syb601) X*
RJP3995	*rhIs4 III; ctbp-1(aus26[mCherry::ctbp-1b + loxP]) X*
RJP4005	*rhIs4 III; sax-7(nj48) IV*
RJP4006	*rhIs4 III; sax-7(nj48) IV; ctbp-1(tm5512) X*
RJP4012	*rhIs4 III; ctbp-1(syb601) X*
RJP4072	*ctbp-1(tm5512) X*
RJP4076	*rpEx1739 (pctbp-1a::GFP + pttx-3::dsRed2)*
RJP4077	*rpEx1740 (pctbp-1a::GFP + pttx-3::dsRed2)*
RJP4078	*rpEx1741 (pctbp-1a::GFP + pttx-3::dsRed2)*
RJP4079	*rpEx1742 (pctbp-1a::GFP + pttx-3::dsRed2)*
RJP4080	*rhIs4 III; sax-7(eq1) IV*
RJP4081	*rhIs4 III; sax-7(eq1) IV; ctbp-1(tm5512) X*
RJP4082	*rhIs4 III; sax-7(nj53) IV*
RJP4083	*rhIs4 III; sax-7(nj53) IV; ctbp-1(tm5512) X*
RJP4144	*rhIs4 III; ast-1(hd1) II; rol-6(e187) II*
RJP4145	*rhIs4 III; ast-1(hd1) II; rol-6(e187) II; ctbp-1(tm5512) X*
RJP4164	*ctbp-1(tm5512) X; rpEx1739 (pctbp-1a::GFP)*
RJP4234	*ast-1(hd1) II ; rol-6(e187) II; rpEx1739 (pctbp-1a::GFP)*
RJP4235	*ast-1(hd1) II; rol-6(e187) II; ctbp-1(tm5512) X; rpEx1739 (pctbp-1a::GFP)*
RJP4250	*rhIs4 III; sax-7(eq1) IV; lad-2(tm3056) IV*
RJP4251	*rhIs4 III; sax-7(eq1) IV; lad-2(tm3056) IV; ctbp-1(tm5512) X*
RJP4270	*rhIs4 III; ctbp-1(tm5512) X; rpEx1812 (pctbp-1a::ctbp-1a cDNA::mCherry + coel::GFP)*
RJP4271	*rhIs4 III; ctbp-1(tm5512) X; rpEx1813 (pctbp-1a::ctbp-1a cDNA::mCherry + coel::GFP)*
RJP4272	*rhIs4 III; ctbp-1(tm5512) X; rpEx1814 (pctbp-1a::ctbp-1a cDNA::mCherry + coel::GFP)*
RJP4278	*rhIs4 III; ctbp-1(tm5512) X; rpEx1815 (pctbp-1a::ctbp-1b cDNA::mCherry + coel::GFP)*
RJP4279	*rhIs4 III; ctbp-1(tm5512) X; rpEx1816 (pctbp-1a::ctbp-1b cDNA::mCherry + coel::GFP)*
RJP4280	*rhIs4 III; ctbp-1(tm5512) X; rpEx1817 (pctbp-1a::ctbp-1b cDNA::mCherry + coel::GFP)*
RJP4286	*rhIs4 III; rpEx1823 (pctbp-1a::sax-7s cDNA + coel::GFP)*
RJP4287	*rhIs4 III; rpEx1824 (pctbp-1a::sax-7s cDNA + coel::GFP)*
RJP4288	*rhIs4 III; rpEx1825 (pctbp-1a::sax-7s cDNA + coel::GFP)*
RJP4315	*sax-7(ot820) IV*
RJP4316	*ast-1(rh300) II; rhIs4 III; lad-2(tm3056) IV*
RJP4322	*rhIs4 III; ctbp-1(tm5512) X; rpEx1842 (pctbp-1a::ctbp-1a THAP only cDNA::mCherry + coel::GFP)*

Strain	Genotype
RJP4323	*rhIs4 III; ctbp-1(tm5512) X; rpEx1843 (pctbp-1a::ctbp-1a THAP only cDNA::mCherry + coel::GFP)*
RJP4327	*rhIs4 III; rpEx1847 (pdpy-7::sax-7s cDNA + coel::GFP)*
RJP4328	*rhIs4 III; rpEx1848 (pdpy-7::sax-7s cDNA + coel::GFP)*
RJP4334	*rhIs4 III; ctbp-1(tm5512) X; rpEx1851 (pdpy-7::ctbp-1a cDNA::mCherry + coel::GFP)*
RJP4335	*rhIs4 III; ctbp-1(tm5512) X; rpEx1852 (pdpy-7::ctbp-1a cDNA::mCherry + coel::GFP)*
RJP4336	*rhIs4 III; ctbp-1(tm5512) X; rpEx1853 (pdpy-7::ctbp-1a cDNA::mCherry + coel::GFP)*
RJP4339	*rhIs4 III; ctbp-1(tm5512) X; rpEx1855 (pctbp-1a::ctbp-1a cDNA (C5A,C10A)::mCherry + coel::GFP)*
RJP4340	*rhIs4 III; ctbp-1(tm5512) X; rpEx1856 (pctbp-1a::ctbp-1a cDNA (C5A,C10A)::mCherry + coel::GFP)*
RJP4341	*rhIs4 III; ctbp-1(tm5512) X; rpEx1857 (pctbp-1a::ctbp-1a cDNA (C5A,C10A)::mCherry + coel::GFP)*
RJP4349	*rhIs4 III; sax-7(ot820) IV; ctbp-1(tm5512) X*
RJP4360	*rhIs4 III; sax-7(ot820) IV*
RJP4401	*rhIs4 III; ctbp-1(tm5512) X; rpEx1881 (pctbp-1a::ctbp-1a cDNA (A203E)::mCherry + coel::GFP)*
RJP4402	*rhIs4 III; ctbp-1(tm5512) X; rpEx1882 (pctbp-1a::ctbp-1a cDNA (A203E)::mCherry + coel::GFP)*
RJP4403	*rhIs4 III; ctbp-1(tm5512) X; rpEx1883 (pctbp-1a::ctbp-1a cDNA (A203E)::mCherry + coel::GFP)*
RJP4418	*rhIs4 III; rpEx1891 (plad-2::sax-7s cDNA + coel::GFP)*
RJP4419	*rhIs4 III; rpEx1892 (plad-2::sax-7s cDNA + coel::GFP)*
RJP4420	*rhIs4 III; rpEx1893 (plad-2::sax-7s cDNA + coel::GFP)*
RJP4421	*rhIs4 III; rpEx1894 (plad-2::sax-7s cDNA + coel::GFP)*
RJP4483	*rhIs4 III; lad-2(tm3056); rpEx1891 (plad-2::sax-7s cDNA + coel::GFP)*
RJP4384	*rhIs4 III; ctbp-1(tm5512) X; rpEx1874 (plad-2::ctbp-1a cDNA::mCherry + coel::GFP)*
RJP4385	*rhIs4 III; ctbp-1(tm5512) X; rpEx1875 (plad-2::ctbp-1a cDNA::mCherry + coel::GFP)*
RJP4386	*rhIs4 III; ctbp-1(tm5512) X; rpEx1876 (plad-2::ctbp-1a cDNA::mCherry + coel::GFP)*

2.1.9 External procedures

- Sanger sequencing was performed by Australian Genome Research Facility (AGRF, Melbourne, Australia) and Micromon (Melbourne, Australia).
- Oligonucleotides were generated by Integrated DNA Technologies (Baulkham Hills, Australia) and Sigma-Aldrich (Castle Hill, Australia).
- The CRISPR-tagged strain PHX601 *ctbp-1(syb601)* was generated by Sunybiotech (Fujian, China).

2.2 Methods

2.2.1 Nematode stocks and maintenance

C. elegans strains were cultured according to standard protocols [1]. Strains were cultured on Nematode Growth Medium (NGM) [2% w/v agar, 50 mM NaCl, 0.25% w/v peptone, 1 mM $CaCl_2$, 5 µg/ml cholesterol, 25 mM KH_2PO_4 and 1 mM $MgSO_4$ in H2O] plates seeded with *E. coli* strain OP50, unless stated otherwise. Nematode stocks were cultured at 20 or 25°C.

2.2.2 Crosses

Homozygous males were generated by heat shocking L4 stage hermaphrodites in a 37°C incubator for 1 hour before placing them at 20°C to lay eggs. Heat shocking increases the incidence of males in the next generation.

To cross a mutant allele and/or integrated transgene into a strain, three hermaphrodites and ten males were placed on an NGM plate seeded with OP50 and incubated at 20°C. Successful crosses were identified by the presence of ~50% male progeny 3 days later. L4 stage hermaphrodite progeny were then transferred to individual plates and allowed to self-fertilise to return the mutations and/or integrated transgenes to homozygosity. Genotypes were confirmed using genotyping PCR methods (section 2.2.2) and/or screening for fluorescence markers using a dissecting microscope. Crosses that involve extrachromosomal transgenes were performed as above while ensuring that animals containing the fluorescent transgene were isolated at each generation.

2.2.3 Synchronisation of animals

Two different temperatures were used throughout this project, depending on the sensitivity of strains: 20°C and 25°C. The majority of assays were performed at 25°C, using populations of specific developmental stages. To obtain synchronous populations, gravid adult hermaphrodites were placed onto *E. coli* OP50-seeded NGM plates and allowed to lay eggs for 4 hours. The gravid parent hermaphrodites were then removed and eggs allowed to hatch and grow to the desired developmental stage.

Table 2.4 Developmental stages at 25°C.

Developmental stage	Hours after egg-lay
L2	27
L3	39
L4	48
Day 1 adult	72
Day 3 adult	120
Day 5 adult	168

Assays were also performed on Day 2 adults at 20°C. These were synchronised by selecting only mid-L4 stage animals with Christmas-tree-like vulval morphology and leaving on a plate for 48 hours before using for assays.

2.2.4 Microscopy

Animals were mounted in 0.2% tetramisole hydrochloride for microscopy. Fluorescent and DIC images were captured with a Zeiss AXIO Imager M2 fitted with an Axiocam 506 mono camera using the Zen 2 pro software (Zeiss).

2.2.5 Genotyping mutant alleles

For determining the strain genotype, individual animals were picked into 16 µL of lysis solution [50 mM KCl, 10 mM Tris pH 8.3, 2.5 mM $MgCl_2$, 0.45% NP-40, 0.45% Tween 20, 0.01% gelatine and 0.5 mg/mL Proteinase K] in a PCR tube and frozen at -80°C for at least 15 minutes. These were then placed at 65°C for 60 minutes followed by 95°C for 15 minutes in a thermocycler.

For deletion alleles, each PCR reaction was carried out in a total volume of 25 µL containing 4 µL of the above lysis mixture, 0.25 mM dNTPs, 4mM $MgCl_2$, 0.4-0.8 µM of primers, 1.25 U Mango*Taq*™ and adequate Mango*Taq*™ Coloured Reaction Buffer. The PCR mix was then incubated at 94°C for 2 minutes, followed by 30 cycles of 15 seconds denaturation at 94°C, 15 seconds annealing at 56°C and varying extension time at 72°C, and an additional 5 minutes extension at 72°C after the 30 cycles (Table 2.5).

The resulting products were run on 1% agarose gels in TAE buffer [40 mM Tris, 20 mM acetic acid, 1 mM EDTA]. GeneRuler™ DNA Ladder was used to estimate band sizes. Gels contained

ethidium bromide (0.1 µg/mL) for visualisation under ultraviolet light. Products that are expected in wild-type and/or mutant alleles are detailed in Table 2.5.

Table 2.5 PCR reactions for genotyping.

For primer sequences, see Appendix Table 8.1.

Gene	Allele	Deletion length (bp)	Primers used	Extension time (min)	Product size (bp)
ctbp-1	*tm5512*	632	1354 1355	0:45	Wild-type: 698 Mutant: 267
ctbp-1	*aus15*	4	1330 1351 1330 1328	0:30	Wild-type: 704, 474 Mutant: 700
ctbp-1	*aus14*	39 (exon 1b)	1330 1351 1330 1328	0:30	Wild-type: 704, 474 Mutant: 665
		5 (exon 4b)	1325 1326 1327	0:30	Wild-type: 341, 173 Mutant: 341
wrt-6	*aus41*	49	1555 1556	0:20	Wild-type: 213 Mutant: 49
wrt-10	*aus36*	5	1558 1559 1560	0:45	Wild-type: 539, 241 Mutant: 534
wrt-10	*aus37*	2	1558 1559 1560	0:45	Wild-type: 539, 241 Mutant: 537
acs-2	*ok2547*	1868	1535 1536 1537	0:30	Wild-type: 850 Mutant: 433
grl-5	*ok2671*	365	1540 1541 1542	0:30	Wild-type: 628 Mutant: 259
	ok2700	623	1540 1541 1542	0:30	Wild-type: 628 Mutant: 517
grl-16	*ok2959*	473	1545 1546 1547	0:30	Wild-type: 332 Mutant: 440
nas-38	*ok3407*	378	1543 1544	0:45	Wild-type: 1327 Mutant: 949
ins-4	*ok3534*	415	1538 1539	0:45	Wild-type: 1426 Mutant: 1011
fsn-1	*gk429*	1001	1250 1251 1252	0:30	Wild-type: 938 Mutant: 438

Gene	Allele	Deletion length (bp)	Primers used	Extension time (min)	Product size (bp)
lips-7	*ok3110*	300	1082 1083 1084	0:30	Wild-type: 242 Mutant: 388
lad-2	*tm3056*	1064	1427 1428 1429	0:30	Wild-type: 469 Mutant: 295
sax-7	*nj48*	568	TS31 TS32	0:45	Wild-type: 883 Mutant: 315
	eq1	2020	TS43 TS45	1:00	Wild-type: 1025 Mutant: no band
	eq1		TS43 TS46	1:00	Wild-type: no band Mutant: 650
	nj53	724	TS40 TS42	1:00	Wild-type: 1387 Mutant: 663
	ot820	8	TS142 TS143	0:15	Wild-type: 192 Mutant: no band

For single nucleotide polymorphism (SNP) alleles, each PCR reaction was carried out in a total volume of 50 µL containing 4 µL of worm lysis mixture, 200 µM dNTPs, 0.5 µM of primers, 1 U/µL Phusion® High-Fidelity DNA polymerase and 1X HF Phusion® buffer (Table 2.6). Target sequences were amplified using the following parameters: 98°C for 30 seconds, followed by 30 cycles of 10 seconds denaturation at 98°C, 30 seconds annealing at 56°C and 30 seconds extension at 72°C, and an additional 10 minutes extension at 72°C after the 30 cycles.

Table 2.6 PCR reactions for genotyping single nucleotide polymorphisms.
For primer sequences, see Appendix Table 8.1.

Gene	Allele	Primers used	Product size (bp)
ast-1	*rh300*	TS73 TS74	523
	hd1		
rpm-1	*ju41*	TS181 TS182	660

The PCR products were prepared for sequencing using the QIAquick PCR Purification Kit (Qiagen) and were sequenced in both directions using the primers used for amplification (Table 2.6) (AGRF).

2.2.6 Worm microinjections

Plasmids for injection were prepared using the QIAprep Spin Miniprep Kit (Qiagen) and injection mixes were prepared in milliQ water and stored at -20°C. Injection mixes were prepared as detailed in Table 2.8 before centrifuging for 10 minutes to sediment any debris. Glass microinjection needles were prepared using a micropipette puller (Sutter Instrument Co). 1 µL of the spun-down injection mix was loaded into the needle via capillary action. Loaded needles were attached to the pressurised injection system (Eppendorf FemtoJet 4X and InjectMan 4). Before injecting animals, the loaded needle was broken to a fine tip on a glass needle adhered to an agarose pad (1% agarose in water) on a glass cover slip.

An agarose pad (1% agarose in water) on a glass cover slip was covered with a layer of mineral oil. A single young adult worm was lightly pressed down onto the agarose pad to prevent locomotion. The cover slip was placed under the Zeiss Axio Vert A1 inverted microscope and manoeuvred until the germline of the animal was in line with the needle. The loaded needle was pierced into the germline and pressure was applied to release injection mix. The animal was recovered by being picked from the slide onto an NGM plate and placing a drop of M9 (22 mM KH2PO4, 50 mM Na2HPO4, 86 mM NaCl, 1 mM MgSO4 in H2O) on top of the animal. 2-4 injected animals were placed on each plate and incubated at 20°C for 4 days.

2.2.7 Cloning of CRISPR-Cas9 sgRNAs

sgRNA templates were designed using the online tool ‘CRISPR design’ (http://crispr.mit.edu/) (Table 2.7). sgRNA-specific forward primers were designed as 5′-G(N_{20}) GTTTTAGAGCTAGAAATAGCAAG-3′, where N represents a 20 base target sequence from the genome, adjacent to a PAM site [155]. If a G was not present at the front of the $N_{20,}$ a G was added [155].

sgRNA target sequences were incorporated into a *pU6::klp-12* sgRNA expression vector by PCR [155]. The sgRNA-specific forward primer was used with the universal reverse primer (AA149) to amplify the whole plasmid by PCR. The reaction was carried out in a total volume of 50 µL containing 20 pg/µL *klp-12* sgRNA vector (as a template), 0.5 mM dNTPs, 0.5 µM of appropriate primers and AA149 2 U/µL Phusion® High-Fidelity DNA polymerase and 1X HF Phusion® buffer (primer details are in Appendix Table 8.2). The reaction was then incubated at 98°C for 30 seconds, followed by 10 cycles of 30 seconds denaturation at 98°C, 1 minute annealing at 60°C and 1 minute 45 seconds extension at 72°C, 15 cycles of 30 seconds denaturation at 98°C, 30 seconds annealing at 65°C 1 minute, 45 seconds extension at 72°C

and an additional 5 minutes extension at 72°C after the 15 cycles. The PCR product was purified before 5 U T4 Polynucleotide Kinase and 1X T4 DNA Ligase buffer were added (NEB). The reaction was incubated at 37°C for 20 minutes. 400 U T4 DNA Ligase (NEB) was then added and the reaction was incubated for 60 minutes at room temperature. The mix was transformed into α-Select Silver Competent Cells (Bioline) and transformants were selected on Luria-Bertani (LB) agar plates [10 g/L peptone, 5 g/L yeast extract, 10 g/L NaCl, 15 g/L agar] supplemented with ampicillin (50 µg/mL). Successfully assembled sgRNA plasmids were verified by sequencing (AGRF).

Table 2.7 sgRNA targeting sequences.

sgRNA name	Target sequence location	Target sequence
ctbp-1 sgRNA 1	*ctbp-1*b exon 4	GGTGTTAAATGAAGCTGTGG
ctbp-1 sgRNA 2	*ctbp-1*b exon 1	GCCAATGGTACTAAACCGACG
wrt-10 sgRNA 1	*wrt-10* exon 1	GATGCTGTTACACCTCGTGT
wrt-6 sgRNA 2	*wrt-6* exon 1	GCGGATTCCATTCATGATGG

2.2.8 CRISPR-Cas9 microinjections to produce putative null mutants

Microinjections were performed on young adult animals, as in section 2.2.6. The injection mixes consisted of Cas9, sgRNAs and co-injection markers (see Table 2.8). The F1 progeny were screened for the appearance of a red fluorescent pharyngeal marker (pCFJ90 *pmyo2::mCherry*) and/or red fluorescent body wall marker (pCFJ104 *pmyo-3::mCherry*) using the Olympus fluorescence dissecting microscope. These animals were isolated onto individual NGM plates and allowed to lay (F2) progeny for 2-3 days before being picked off to detect any possible deletions using PCR.

Table 2.8 CRISPR-Cas9 injection mixes to generate random mutations.

Purpose	Strain injected	Plasmid	Concentration (ng/µL)
Targeting both *ctbp-1* exons 1 and 4 to generate *aus14*	HRN173	*peft-3::cas9::tbb-2* 3′UTR	50
		ctbp-1 sgRNA 1	125
		ctbp-1 sgRNA 2	125
		pCFJ90 *pmyo2::mCherry*	2.5
		pCFJ104 *pmyo-3::mCherry*	5
Targeting *ctbp-1* exon 1 to generate *aus15*	N2	*peft-3::cas9::tbb-2* 3′UTR	50
		ctbp-1 sgRNA 2	125
		pCFJ90	2.5
		pCFJ104	5
Targeting *wrt-10* exon 1 to generate *aus36* and *aus37*	N2	*peft-3::cas9::tbb-2* 3′UTR	50
		wrt-10 sgRNA	250
		pCFJ90	2.5
		pCFJ104	5
Targeting *wrt-6* exon 1 to generate *aus41*, *aus42* and *aus43*	N2	*peft-3::cas9::tbb-2* 3′UTR	50
		wrt-6 sgRNA	250
		pCFJ90	2.5
		pCFJ104	5

2.2.9 Detecting CRISPR-Cas9 indels

Polymerase chain reaction (PCR) screening for insertions and deletions (indels) at CRISPR-Cas9 targeted sites was performed as previously described [160]. Individual animals were lysed before PCR reactions were set up (for details on genotyping, see 2.2.3). PCR reactions contained 3 primers: external forward (EF), internal forward (IF) directly upstream of the PAM site, and reverse (R). Two products are expected from the wild-type allele and CRISPR-Cas9-mediated indels can be detected by loss of the internal band. Primer details are provided in Table 2.9 and Appendix Table 8.1.

Table 2.9 PCR reactions for detecting CRISPR-Cas9 mutations.

For primer sequences, see Appendix Table 8.1.

Gene and exon being targeted	Primers used	Extension time (min)	Wild-type band sizes
ctbp-1b exon 1	EF 1351 IF 1328 R 1330	0:30	External: 704 Internal: 474
ctbp-1b exon 4	EF 1326 IF 1325 R 1327	0:30	External: 341 Internal: 173
wrt-6 exon 1	EF 1554 IF 1556 R 1557	0:45	External: 578 Internal: 308
wrt-10 exon 1	EF 1558 IF 1559 R 1560	0:45	External: 539 Internal: 241

The resulting products were run on 2% agarose gels in TAE buffer. GeneRuler™ DNA Ladder was used to estimate band sizes. Gels contained ethidium bromide (0.1 µg/mL) for visualisation under ultraviolet light.

PCR products that contained putative indels were prepared for sequencing using the Zymo Research DNA Clean and Concentrator™-5 kit after PCR reactions containing only the external forward and external reverse primers.

2.2.10 Cloning of CRISPR-Cas9 tagging constructs

Cloning of the mCherry::CTBP-1b repair template plasmid (pTS1) was performed using a Gibson Assembly® approach as described by Norris et al. [155]. The homology arms were amplified by PCR using Phusion® High-Fidelity DNA Polymerase (NEB). The reaction was carried out in a total volume of 50 µL containing 5 ng WRM0622cG05 p*ctbp-1*::*ctbp-1*::mCherry + unc-119(+) [89], 0.5 mM dNTPs, 0.4 µM of primers 1342 and 1343 (for the upstream homology arm) or 1344 and 1345 (for the downstream homology arm), 2 U/µL Phusion® High-Fidelity DNA polymerase and 1X HF Phusion® buffer. Target sequences were amplified using the following parameters: 98°C for 30 seconds, followed by 30 cycles of 10 seconds denaturation at 98°C, 30 seconds annealing at 52°C (for the upstream homology arm) or 57°C (for the downstream homology arm) and 1 minute 15 seconds extension at 72°C, and an additional 10 minutes extension at 72°C after the 30 cycles.

A two-fold molar excess of homology arms was used in the subsequent Gibson Assembly® reaction. The *mCherry-Pmyo-2::GFP neoR loxP* vector (a gift from John Calarco, University of Toronto) was digested with SpeI-HF and NotI-HF restriction enzymes (NEB) and treated with FastAP Thermosensitive Alkaline Phosphatase (Thermo Scientific™) at 37°C for 30 minutes. The digested plasmid was added to a two-fold molar excess of both homology arms and 1X Master Assembly mix. The mix was incubated at 50°C for 1 hour before transformation into α-Select Silver Competent Cells (Bioline). Transformants were selected on LB agar plates supplemented with ampicillin (50 µg/mL). The successfully assembled plasmid was screened for by restriction digest with HindIII and ClaI and verified by sequencing with primers 1329, 1330, M13F-pUC(-40) and M13-rev (AGRF).

To prevent cleavage of the mCherry::CTBP-1b repair vector when performing CRISPR-Cas9, Q5 directed mutagenesis was performed. NEBaseChanger (http://nebasechanger.neb.com/) was used to design primers to generate a silent mutation in the PAM site in the mCherry::CTBP-1b repair vector (G to C at base 36 of exon 1b). The reaction was carried out in a total volume of 25 µL containing 25 ng/µL of the repair vector, 0.5 µM of primers 1363 and 1364 (Appendix Table 8.4) and 1X Q5 Hot Start High-Fidelity Master Mix (NEB). The mutated plasmid was amplified using the following parameters: 98°C for 30 seconds, followed by 25 cycles of 10 seconds denaturation at 98°C, 30 seconds annealing at 63°C and 9 minute extension at 72°C, and an additional 2 minutes extension at 72°C after the 25 cycles. 1µL of the PCR product was then used in a total reaction volume of 10 µl with 1x KLD reaction buffer and 1x KLD enzyme mix and incubated at room temperature for 5 minutes before transformation into α-Select Silver Competent Cells (Bioline). The Q5-mutated plasmid (pTS2) was screened for by restriction digest with HindIII and verified by sequencing with primers 1309, 1329, 1330, 1368, 1369, 1380, 1381 and 1382 (Appendix Table 8.5).

2.2.11 CRISPR-Cas9 microinjections to produce tagged CTBP-1b::mCherry

Microinjections were performed as described in section 2.2.8. Animals were injected with Cas9, the *ctbp-1b* targeting sgRNA, the Q5-mutated repair vector and co-injection markers (Table 2.10). The F1 progeny were screened for the appearance of a faint green fluorescent pharyngeal marker (repair vector pTS2) and red fluorescent pharyngeal marker (*pmyo2::mCherry*) and/or red fluorescent body wall marker (*pmyo-3::mCherry*) using the Olympus fluorescent microscope. These animals were isolated onto individual NGM plates and allowed to lay (F2) progeny for 2-3 days. The F2 progeny was then scored for the proportion

of animals with the green fluorescent marker. Populations with 100% GFP-positive worms were monitored for multiple generations to ensure that the repair vector was integrated into the genome, and not present as an extrachromosomal array. The presence of the mCherry::CTBP-1b repair vector was confirmed by PCR using primers 1353 and 1330 (Appendix Table 8.1). If animals did not have the mCherry insert, the product size was predicted to be 659 bp. Strain HRN539 *ctbp-1(aus24[mCherry::ctbp-1b + loxP myo-2::GFP loxP)]* was created.

The integrated tagged HRN539 animals were subsequently injected with Cre recombinase (*peft-3::Cre)* to excise the *loxP Pmyo-2::GFP + neoR loxP* section of the transgene (Table 2.10). The F1 progeny were screened for the loss of the excised green fluorescent pharyngeal marker and the appearance of a red fluorescent pharyngeal marker (*pmyo2::mCherry*). Subsequent generations were then isolated for the complete loss of the green pharyngeal marker and red pharyngeal marker. The successful Cre-mediated excision of the *loxP*-flanked segment was confirmed via sequencing (primers AA86, AA89, 1222, 1330, 1353 and 1386, Appendix Table 8.5). The strain created was HRN553 *ctbp-1(aus26[mCherry::ctbp-1b + loxP]).* This strain was outcrossed 3 times to create RJP3981 before being crossed into the *pglr-1::GFP* (*rhIs4*) reporter for analysis (RJP3995).

Table 2.10 Injection mixes for tagging CTBP-1b

Purpose	Strain injected	Plasmid or construct	Concentration (ng/µL)
Tagging N-terminus of CTBP-1b with mCherry	N2	*peft-3::cas9::tbb-2* 3′UTR	50
		ctbp-1 sgRNA 2	125
		pTS2 *ctbp-1*b mCherry repair vector	70
		pCFJ90	2.5
		pCFJ104	5
For removing the selection cassette flanked by loxP sites with Cre recombinase	HRN539	*peft-3::Cre*	50
		pCFJ90	2.5

2.2.12 Generation of novel plasmids for genetic rescue and gene expression

For cloning of expression and rescue constructs, the In-Fusion® HD Cloning Kit was used according to the manufacturer's protocol (Takara Bio USA). The original vector was linearised by restriction enzyme digestion or PCR, and purified using QIAquick PCR Purification Kit

(Qiagen) after DpnI digest for 15 min to digest the original/uncut vector (Thermo Scientific™). The online In-Fusion Cloning Primer Design Tool was used to design primers that amplify the desired insert with 15 bp complementary to the ends of the linearised vector. The insert was amplified by PCR using Phusion® High-Fidelity DNA Polymerase (NEB). The reaction was carried out in a total volume of 50 µL containing 5 ng of plasmid or 50 ng of genomic DNA/ cDNA, 200 µM dNTPs, 0.5 µM of appropriate primers, 1 U/µL Phusion® High-Fidelity DNA polymerase and 1X HF Phusion® buffer. The inserts were amplified using the following parameters: 98°C for 30 seconds, followed by 30 cycles of 10 seconds denaturation at 98°C, 30 seconds annealing at varying temperatures, and varying extension at 72°C, and an additional 10 minutes extension at 72°C after the 30 cycles. Recommended annealing temperatures by the online In-Fusion Cloning Primer Design Tool were followed. The extension times varied based on length (recommended Phusion protocol of 30 seconds per kb was followed). The insert products were purified using using QIAquick PCR or Gel Purification Kit (Qiagen). The In-Fusion cloning reaction was incubated for 15 min at 50°C (2 µL 5X In-Fusion HD Enzyme Premix, 100 ng linearised vector, 100 ng insert). The reaction was then transformed into NEB® 5-alpha competent cells. Transformants were selected on LB agar plates supplemented with ampicillin (50 µg/mL). The successfully assembled plasmid was screened for by restriction digest with appropriate restriction enzymes and verified by sequencing with primers pPD49.26 F, pPD49.26 R, pPD95.75 F, pPD95.75 R and pPD95.75 mCherry (Appendix Table 8.5).

RJP383 *pctbp-1a::GFP* expression construct

RJP383 was generated by cloning the 5008 bp *ctbp-1a* promoter from genomic DNA (primers TS1 and TS2) into the pPD95.75 vector (linearised by HindIII and XbaI).

RJP414 *pctbp-1a::sax-7S* overexpression construct

RJP414 was generated by amplifying the pRP13 *pdpy-7::sax-7* vector minus the *pdpy-7* sequence (primers TS102 and TS103) [145] and amplifying the 5008 bp *ctbp-1a* promoter from RJP383 (primers TS100 and TS101).

RJP422 *pctbp-1a::ctbp-1a cDNA::mCherry* rescue construct

First, the RJP420 *ctbp-1a cDNA::mCherry* vector was generated by amplifying the pPD95.75 mCherry vector (primers TS122 and TS123) and amplifying the 2181 bp *ctbp-1a* cDNA from pAER019 *pglr-1::ctbp-1a::V5::ctbp-1* 3' UTR (primers TS124 and TS125) [93, 161]. RJP422

was then generated by cloning the 5008 bp *ctbp-1a* promoter from RJP383 (primers TS128 and TS129) into the RJP420 vector (linearised by BamHI).

RJP423 *pctbp-1a::ctbp-1b cDNA::mCherry* rescue construct

First, the RJP421 *ctbp-1b cDNA::mCherry* vector was generated by amplifying the pPD95.75 mCherry vector (primers TS122 and TS123) and amplifying the 1818 bp *ctbp-1b* cDNA from wild-type DNA (primers TS125 and TS126). RJP422 was then generated by cloning the 5008 bp *ctbp-1a* promoter from RJP383 (primers TS128 and TS129) into the RJP421 vector (linearised by BamHI).

RJP424 *plad-2::ctbp-1a cDNA::mCherry* rescue construct

RJP424 was generated by cloning the 4063 bp *lad-2* promoter from genomic DNA (primers TS130 and TS131) into the RJP420 vector (linearised by BamHI).

RJP424 *pdpy-7::ctbp-1a cDNA::mCherry* rescue construct

RJP424 was generated by cloning the 249 bp *dpy-7* promoter from pTB80 (primers TS140 and TS141) into the RJP420 vector (linearised by BamHI).

RJP515 *plad-2::sax-7S* overexpression construct

RJP515 was generated by amplifying the sax-7s cDNA sequence from RJP414 (primers TS136 and TS137) and amplifying the *lad-2* promoter from RJP424 (primers TS138 and TS139).

2.2.13 Mutagenesis of the rescuing construct

In-Fusion cloning was used to mutate specific domains in the *pctbp-1a::ctbp-1a cDNA::mCherry* rescue construct (RJP422) to create the RJP426, RJP427 and RJP514 (details in Table 2.11). The online In-Fusion Cloning Primer Design Tool was used to design two primers that incorporated the desired substitution or deletion and overlapped each other at their 5' ends. The insert was amplified using Phusion® Polymerase: 200 µM dNTPs, 0.5 µM of primers, 1 U/µL Phusion® High-Fidelity DNA polymerase and 1X HF Phusion® buffer (Table 2.11). Target sequences were amplified using the following parameters: 98°C for 30 seconds, followed by 30 cycles of 10 seconds denaturation at 98°C, 30 seconds annealing at 56°C and

5:30 min extension at 72°C, and an additional 10 minutes extension at 72°C after the 30 cycles. PCR reactions were purified using QIAquick PCR Purification Kit (Qiagen). The In-Fusion cloning reaction and transformation were performed as described in section **Error! Reference source not found.**. The successfully assembled plasmid were verified by sequencing with primer pPD49.26 F (Micromon, Appendix Table 8.5). Details for each construct are below, with mutations made, and primer sequences are in Appendix Table 8.4.

Table 2.11 Rescue plasmid mutagenesis.
All mutagenesis performed on RJP422 *pctbp-1a::ctbp-1a cDNA::mCherry*. For primer sequences, see Appendix Table 8.4.

Plasmid	Primers
RJP426 *pctbp-1a::THAP only cDNA::mCherry*	TS148 TS149
RJP427 *pctbp-1a::ctbp-1a cDNA(C5A,C10A)::mCherry*	TS150 TS151
RJP514 *pctbp-1a::ctbp-1a cDNA(A203E)::mCherry*	TS152 TS153

2.2.14 Generation of transgenic strains carrying extrachromosomal arrays

N2 animals were injected with the below injection mixes (Table 2.12) and placed on NGM plates and allowed to recover at 20°C. Total concentrations were made up to 150 ng/µl by addition of bacterial DNA. Progeny of the injected worms were screened for the appearance of a red neuron in the head (*pttx-3::dsRed2)* or green fluorescent coelomycytes (*coel::GFP*), which were used as transformation markers. Animals with visible markers were isolated onto individual NGM plates and allowed to lay progeny for 3-4 days. The presence of the fluorescent marker in the next generation suggests that the transgene has been incorporated as an extrachromosomal array. These extrachromosomal strains were maintained by continuing to isolate animals with the markers each generation.

Table 2.12 Injection mixes for transgenic extrachromosomal rescue and expression lines.
All mixes made up to a final concentration of 150 ng/µL with digested bacterial DNA.

Purpose	Strain injected	Resulting Ex arrays	Plasmid or construct	Conc (ng/µL)
Transcriptional reporter	N2	*rpEx1739-1742*	RJP383 *pctbp-1a::GFP*	50
			pttx-3::dsRed2	50
Endogenous rescue	HRN226	*rpEx1812-1817*	RJP422 *pctbp-1a::ctbp-1a cDNA::mCherry*	2
			coel::GFP	20
pctbp-1a::sax-7S overexpression	HRN169	*rpEx1823-1828*	RJP414 *pctbp-1a::sax-7s cDNA*	20
			coel::GFP	20
THAP only rescue	HRN226	*rpEx1842-1846*	RJP426 *pctbp-1::ctbp-1a(THAP only)::mCherry*	2
			coel::GFP	20
Hypodermal *sax-7S* overexpression	HRN169	*rpEx1847-1848*	*pdpy-7::sax-7s cDNA*	5
			coel::GFP	20
Hypodermal rescue	HRN226	*rpEx1851-1854*	RJP425 *pdpy-7::ctbp-1a cDNA::mCherry*	2
			coel::GFP	20
Mutated THAP rescue	HRN226	*rpEx1855-1859*	RJP427 *pctbp-1a::ctbp-1a cDNA (C5A, C10A)::mCherry*	2
			coel::GFP	20
Mutated PXDLS cleft rescue	HRN226	*rpEx1881-1882*	RJP514 *pctbp-1a::ctbp-1a cDNA (A203E)::mCherry*	2
			coel::GFP	20
SMDD *sax-7s* overexpression	HRN169	*rpEx1891-1894*	RJP515 *plad-2::sax-7s cDNA*	20
			coel::GFP	20
SMDD rescue	HRN226	*rpEx1874-1876*	RJP424 *plad-2::ctbp-1a cDNA::mCherry*	2
			coel::GFP	20

2.2.15 Body length quantification

Animals were synchronised and mounted for microscopy at the relevant life stages (section 2.2.3). DIC images were captured using the 20x objective. For animals that spanned more than one image, overlapping images were captured and overlaid using Adobe Photoshop. Animals were measured along the middle of the animal from the anterior tip to the tail.

Two biological replicates were performed and each length measurement was plotted as a single data point. Unpaired t-tests between wild-type and mutant at each life stage was used to determine statistical significance.

2.2.16 SMDD axon assays

Animals carrying the *pglr-1::GFP* (*rhIs4*) transgenes were grown at the appropriate temperature for two generations and synchronized by egg-laying (section 2.2.3). Animals were picked for microscopy at the relevant life stages.

For genetic mutant analysis, SMDD curls (%) indicates the percentage of SMDD axons that leave the dorsal sublateral path along which the SMDD axons extend. One or two SMDD neurons were scored per animal and pooled within each replicate for statistical analysis. Scoring was performed by a single scorer who was blind to the genotypes of all strains, to ensure consistent scoring between experiments. Experiments were performed three times, unless otherwise specified, and a one-way ANOVA followed by Tukey's correction was used to determine statistical significance.

For overexpression assays, SMDD axonal phenotype (%) measures the proportion of axons exhibiting the three possible phenotypes: 'Straight', 'Curly' and 'Not visible'. 'Straight' SMDD axons (wild-type) extend along the dorsal sublateral cord, 'Curly' SMDD axons leave the dorsal sublateral cord, and 'Not visible' means that there is no axon visible at any position along the dorsal sublateral cord. For each genotype, the total percentages of 'Straight', 'Curly' and 'Not visible' phenotypes add up to 100%. Assays were performed three times. To determine statistical significance, a one-way ANOVA followed by Dunnett's multiple comparisons test was performed, comparing each overexpression line to the wild-type control.

2.2.17 SMDD axon length quantification

Animals carrying the *pglr-1::GFP* (*rhIs4*) transgenes were grown at 25°C for two generations and synchronized by egg-laying (section 2.2.3). Animals were picked for microscopy at the relevant life stages.

The area containing the distal tip of the axons was found on the 40x objective and images of the distal tip of 1 or 2 SMDD axons was taken under the GFP fluorescent and DIC modes. If the axons were defective, the entire area in which the axon leaves the dorsal sublateral path was captured in the image. If the posterior bulb of the pharynx was not visible in the image,

the field of view was then moved to the anterior of the worm to capture the posterior bulb of the pharynx, ensuring sufficient overlap with the previous image.

All of the above micrographs for each worm were processed using Adobe Photoshop. The images of each animal's body were aligned and the fluorescent image containing the SMDD neuron(s) was overlayed. These aligned files are saved as JPEG or TIFF images of 2000 by 2000 pixels. On ImageJ, a segmented line was traced from the posterior bulb of the pharynx to the distal tip of the SMDD axon and the Measure tool calculated the length. The inbuilt scale bar from the Zen 2 pro software was used as a reference to measure the length in µm.

For SMDD length assays, the SMDD length (µm) is the length of the SMDD axon from the posterior bulb of the pharynx to the distal tip of the SMDD axon. The length of one or two SMDD neurons was scored per animal. Two biological replicates were performed and each length measurement was plotted as a single data point. A one-way ANOVA followed by Tukey's correction was used to determine statistical significance.

For SMDD curl length, the SMDD curl length (µm) is the length of only the curled portion of the SMDD axon. This is the length of the axon after it has extended away from the dorsal sublateral cord in any direction. The same animals that were measured in the SMDD length assays were used for this analysis. A one-way ANOVA followed by Tukey's correction was used to determine statistical significance.

2.2.18 SDQ and PLN axon guidance assays

SDQR, SDQL and PLN axon guidance assays were performed as previously described, using the extrachromosomal *plad-2::GFP* transgene *otEx331* [25]. The SDQR axon was scored as defective if the axon extended ventrally. The SDQL axon was scored as defective if the axon extended ventrally. The PLN axon was scored as defective if the axon extended posteriorly. One or two PLN axons were scored per animal. Animals were grown for at least two generations at 25°C and synchronized by egg-laying (section 2.2.3). Animals containing the *otEx331* transgene were picked for microscopy at day 1 of adulthood. Scoring was performed by a single scorer who was blind to the genotypes of all strains. Experiments were performed three times, and a one-way ANOVA followed by Tukey's correction was used to determine statistical significance.

2.2.19 RNA interference (RNAi)

RNAi was performed by feeding as described [162]. HT115(DE3) bacteria carrying either L4440 (empty vector), L4440-*ctbp-1* or L4440-*lad-2* plasmids from the Vidal lab RNAi library [158] were grown overnight at 37°C in LB media with 100 µg/ml ampicillin. Expression of dsRNA was induced by adding Isopropyl β-D-1-thiogalactopyranoside (IPTG) to a final concentration of 3 mM followed by an additional three hours of growth at 37°C. HT115(DE3) bacteria carrying plasmid constructs were seeded on NGM plates containing 25 µg/ml carbenicillin and 3 mM IPTG. Nematode strains were grown at 25°C for at least two generations on NGM plates before the RNAi experiments, which were conducted at 25°C. Eggs were obtained by treatment of gravid adults with bleaching solution (1.7 M NaOH, 2.1% v/v NaOCl). The eggs were placed next to the bacterial lawn and allowed to hatch. The gravid adults which developed on the lawn were used to synchronize a second generation by egg-laying for 4 hours on a plate covered completely with the plasmid carrying bacteria. These animals were assayed at the L4 stage and day 1 of adulthood using the SMDD axon assay (section 2.2.16).

2.2.20 Exploration behaviour

Exploration behaviour was quantified as described previously [163] with modifications. Animals were grown at 25°C for two generations and synchronized by egg-laying (section 2.2.3). Young adult animals were picked ~54 hours later to the centre of 50 mm NGM plates uniformly seeded with *E. coli* OP50 and were incubated at 25°C for 16 hours. Animals were removed from plates and the plates were positioned over a grid containing 177 3.5 mm squares. The number of squares entered by the worm tracks was manually counted under a dissecting microscope. Animal tracks could enter a maximum of 177 squares. If the animal was not on the lawn after 16 hours, its plate was disqualified. Scoring was performed by a single scorer who was blind to the genotypes of all strains. Exploration behaviour assays were performed three times, and a one-way ANOVA followed by Tukey's correction was used to determine statistical significance.

2.2.21 Analysis of microarray datasets

Two microarray datasets were obtained: wild-type vs *ctbp-1(eg613)* [90], and wild-type vs *ctbp-1(ok498)* (PhD thesis [164]). The datasets were processed with Microsoft Excel to determine the genes were upregulated >2 fold and present in both datasets. These overlapping genes

were analysed for known expression patterns and key description terms using the Wormmine tool on Wormbase (http://intermine.WormBase.org/tools/wormmine/begin.do). Genes expressed in the nervous system and/or hypodermis were selected for further analysis.

2.2.22 Quantification of fluorescence using ImageJ

L4 stage animals with the *rpEx1739* (*pctbp-1a::GFP*) transgene were selected and were mounted for microscopy as described in section 2.2.3, and DIC and fluorescent images were captured using the 40x objective. The head region was captured, focusing on the pharynx of the worm with identical exposure times (10 ms GFP). The GFP fluorescence was quantified from the anterior tip of the head to the posterior bulb of the pharynx. The area of fluorescence and a background region were selected in the free image processing program Fiji, and the area, integrated density and mean grey value were measured. The calculated total fluorescence (CTCF) was calculated in Microsoft Excel by: integrated density – (area of selection × mean fluorescence of background reading). Scoring was performed by a single scorer who was blind to the genotypes of strains. This assay was performed three times, and an unpaired t-test was used to determine statistical significance.

2.2.23 qRT-PCR

Animals were grown at 25°C for two generations. L4 stage animals were synchronized by egg-lay (section 2.2.3). Mixed stage populations contained all different developmental stages. Worm populations were homogenized with TRIzol™ by freezing in liquid nitrogen and thawing at 37°C. The RNA was extracted by phase separation with chloroform and the RNeasy® Mini Kit (Qiagen Pty. Ltd.). RNA samples was treated with RNAse-Free DNase to remove DNA. Total RNA concentration was measured using the Nanodrop1000 Spectrophotometer (Thermo Fisher Scientific). cDNA synthesis was carried out in 20 µL reactions containing 500 ng total RNA, 5 µg oligoDT/ random hexamer primers, 2.5 mM MgCl2, 0.5 mM dNTPs, 20 U RNasin® Ribonuclease Inhibitor, ImProm-II™ Reverse Transcriptase and 1x ImProm-II™ Reaction Buffer (Promega). Reactions were incubated at 25°C for 5 minutes, then 42°C for 60 minutes, before heat inactivation at 70°C for 15 minutes.

qRT-PCR (quantitative real-time polymerase chain reaction) was carried out in 20 µL reactions on cDNA samples with 1 mM of relevant forward and reverse primers (Appendix Table 8.7) and LightCycler® 480 SYBR Green I Master mix (Roche). Reactions were performed using the

LightCycler® 480 Instrument II (Roche). cDNA samples from three biological replicates were run in triplicate. Relative transcript levels were normalised to the gene Y45F10D.4 or *pmp-3*.

2.2.24 Statistical analysis

Quantification and statistical parameters are indicated in each figure legend, including error bars (SEM or SD as indicated), numbers (n), and p values. All statistical analysis was performed using GraphPad Prism® software (GraphPad Software Inc.). One-way ANOVA with Tukey's or Dunnett's multiple comparisons test, or unpaired t-tests were performed. p values <0.05 were considered significant.

3. Characterisation of the role of CTBP-1 in SMD axonal development

3.1 Introduction

CtBPs are transcriptional corepressors that downregulate gene expression. In both mammalian and invertebrate model systems, CtBPs have been implicated in nervous system development [75, 81-83]. *C. elegans* CTBP-1 is expressed in the nervous system and hypodermis [89], and the Nicholas laboratory (University of Sydney) recently identified a role for CTBP-1 in regulating the development of the SMDD motor neuron axons and exploration behaviour [93]. In this chapter, I investigated the role of the distinct CTBP-1 isoforms in regulating SMDD axon guidance and termination. In addition, I performed rescue experiments to determine the cells in which CTBP-1 functions to regulate SMDD axonal development.

3.2 Generation of CTBP-1 mutants using CRISPR-Cas9

In order to better understand the roles of CTBP-1 in SMDD development, I aimed to generate mutations that removed the function of one or both CTBP-1 isoforms. From the *ctbp-1* locus, two isoforms are transcribed: *ctbp-1a* and *ctbp-1b.* The longer *ctbp-1a* transcript consists of 13 exons (Figure 3.1A) [68, 85]. In contrast, the shorter *ctbp-1b* isoform has an alternative start site, which encodes a distinct first exon followed by the final 9 exons shared with *ctbp-1a* (Figure 3.1A) [89]. Translation of *ctbp-1a* and *ctbp-1b* results in two protein isoforms CTBP-1a and CTBP-1b, which are 727 and 606 amino acids in length, respectively (Figure 3.2A) [68]. Both CTBP-1 proteins contain the dehydrogenase-like domain, PXDLS-binding motifs and unstructured C-terminal region, however, the CTBP-1a isoform contains an additional N-terminal THAP domain that is predicted to have DNA-binding ability [68, 85].

Previously, only mutants that removed CTBP-1a or disrupted the C-terminus of both isoforms were published and publicly available. The CTBP-1a isoform-specific allele, *tm5512*, was available from the National BioResource Project in Japan. The *tm5512* allele contains a 634 bp deletion over the *ctbp-1a* promoter region, transcriptional start site and first exon, which contains the CTBP-1a THAP domain (Figure 3.2A) [89]. As this deletion removes the translational start site, no full-length CTBP-1a is predicted to be produced, but the shorter CTBP-1b isoform is unaffected at the genomic level (Figure 3.2B). Hereafter, the *ctbp-1(tm5512)* mutant is used as a CTBP-1a isoform-specific allele and is referred to as *ctbp-1a(tm5512)*.

To generate a CTBP-1b isoform-specific mutation, I generated a deletion using CRISPR-Cas9-induced non-homologous end joining. The Cas9 nuclease is targeted to a specific protospacer

adjacent motif (PAM) using a sequence-specific single-guide RNA (sgRNA), creating double stranded breaks [165]. These double-stranded breaks can be repaired by accident-prone non-homologous end joining, which generates insertions and/or deletions near the Cas9 cleavage site (PAM site) [165]. The shorter CTBP-1b has a unique first exon that is not shared with the longer CTBP-1a isoform, therefore I designed a sgRNA to target *ctbp-1b* exon 1 (exon 1b) (sgRNA 1, Figure 3.1A). I injected young adult wild-type animals with the exon 1b sgRNA, Cas9 and co-injection markers, and selected F1 progeny expressing the co-injection marker(s) [166, 167]. I used PCR genotyping to isolate a 4 bp deletion early in exon 1b (*aus15*, Figure 3.1B). The *aus15* deletion results in a predicted premature stop codon (Figure 3.1B), thereby leading to a severely truncated protein of 37 amino acids long, compared to the wild-type length of 606 amino acids. Therefore, c*tbp-1(aus15)* mutant animals are not predicted to encode a functional CTBP-1b protein. This deletion does not affect the CTBP-1a isoform at the genomic level, and is hence a *ctbp-1b*-specific deletion.

Next, I designed CRISPR-Cas9 experiments to generate putative null *ctbp-1* mutant animals. I wanted to disrupt the two *ctbp-1* isoforms from being translated, but did not want to remove the whole genomic region due to 8 non-coding RNAs (ncRNAs) that are present within the intronic regions (WormBase, Figure 3.1A). Because these ncRNAs may have important unidentified functions, I decided to generate random mutations in each *ctbp-1* isoform. To generate *ctbp-1a/b* null mutants, I simultaneously targeted CTBP-1b exons 1 and 4 in *ctbp-1a(tm5512)* mutant animals. I used the same exon 1b sgRNA used to generate the *ctbp-1b*-specific allele *aus15*, and another sgRNA in exon 4b, to increase likelihood of generating a deletion (Figure 3.1A). I generated two separate alleles: *aus14* and *aus23*. The *aus14* deletion contains two deletions: a 39 bp deletion over the end of exon 1b and continues into the next intron, and a 5 bp deletion in exon 4b/exon 7a (Figure 3.1B). As the *ctbp-1b* exon-intron boundary is deleted, I predict that splicing is affected and no full-length CTBP-1b is generated. The *aus23* deletion is a 74 bp deletion over the translational start site and majority of exon 1b (Figure 3.1B). Because the *aus23* deletion removes the translational start site, I predict no full-length CTBP-1b protein will be produced. Both of these deletions were generated in the *ctbp-1a(tm5512)* background, therefore they are predicted null mutants because they affect correct translation of both CTBP-1a and CTBP-1b isoforms. These predicted null mutants will be henceforth referred to as *ctbp-1a/b(tm5512aus14)* and *ctbp-1a/b(tm5512aus23)*. Before being used for any assays, these new lines were outcrossed 6 times to a wild-type strain to ensure any background mutations were removed.

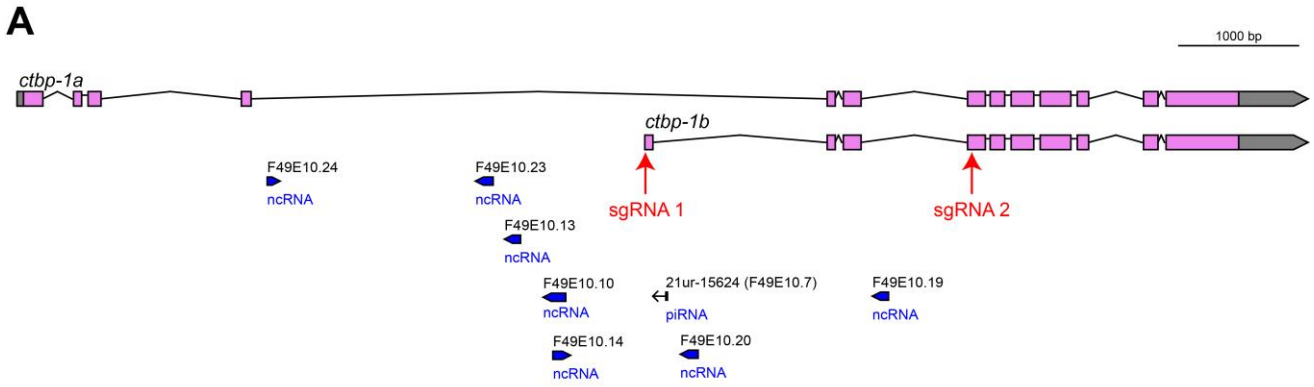

B **Mutations in *ctbp-1b* Exon 1b**

	Exon 1b start site; sgRNA 1; PAM
Wild-type	5′ cttcgttatcagctgatagcaATGGGTGGCGAAGCCAATGGTACTAAACCGACGGGGTCGCAAAAGCGGAAACGAAgtgagttataac
aus15	5′ cttcgttatcagctgatagcaATGGGTGGCGAAGCCAATGGTACTAA----ACGGGGTCGCAAAAGCGGAAACGAAgtgagttataac
aus14	5′ cttcgttatcagctgatagcaATGGGTGGCGAAGCCAATGGTACTAAAC----------
aus23	5′ ----------AAgtgagttataac

	Mutations in *ctbp-1b* Exon 4b	Deletion	Effect	Injected into
	sgRNA 2; PAM			
Wild-type	GTGTTAAATGAAGCTGTGGCGGCACTCATGTATCACTCT			
aus15	GTGTTAAATGAAGCTGTGGCGGCACTCATGTATCACTCT	4 bp in Exon 1b	Premature stop codon after 37 aa	Wild-type
aus14	GTGTTAAATGAA-----GGCGGCACTCATGTATCACTCT	39 bp over Exon 1b 5 bp in Exon 4b	Removes end of Exon 1b and exon-intron boundary	*ctbp-1a(tm5512)*
aus23	GTGTTAAATGAAGCTGTGGCGGCACTCATGTATCACTCT	74 bp over Exon 1b	Removes start site of *ctbp-1b*	*ctbp-1a(tm5512)*

Figure 3.1 CRISPR-Cas9-generated mutations of CTBP-1b using two sgRNAs.

(A) Schematic of *ctbp-1* gene locus, where sgRNAs (red arrows) target *ctbp-1b* first and fourth exons. The position of ncRNAs in *ctbp-1* intronic regions are indicated (blue boxes and black arrows). Exons (pink boxes), introns (solid lines) and untranslated regions (grey box) are indicated; 5' is on the left. (B) Mutations made in wild-type sequence of *ctbp-1b*. sgRNA targets (red) with respective PAM (black) in *ctbp-1b* exon 1 and *ctbp-1b* exon 4b/ *ctbp-1a* exon 7a. Dashes indicate deleted bases in mutant alleles: *aus15* is a 4 bp deletion, *aus14* is a 39 bp deletion in exon 1b and 5 bp deletion in exon 4b, and *aus23* is a 74 bp deletion. Predicted effects on amino acid sequence and genotype of injected animals. 5' is on the left, *ctbp-1b* transcriptional start site indicated in blue.

In summary, I used CRISPR-Cas9 to generate a *ctbp-1b*-specific mutation allele (*aus15*) and 2 *ctbp-1a/b* predicted null alleles (*aus14* and *aus23*). In addition, a *ctbp-1a* specific allele (*tm5512)* was available, of which no full-length CTBP-1a protein is predicted to be produced, but CTBP-1b is unaffected [89]. These deletions and their predicted effects on the protein isoforms are detailed in Figure 3.2.

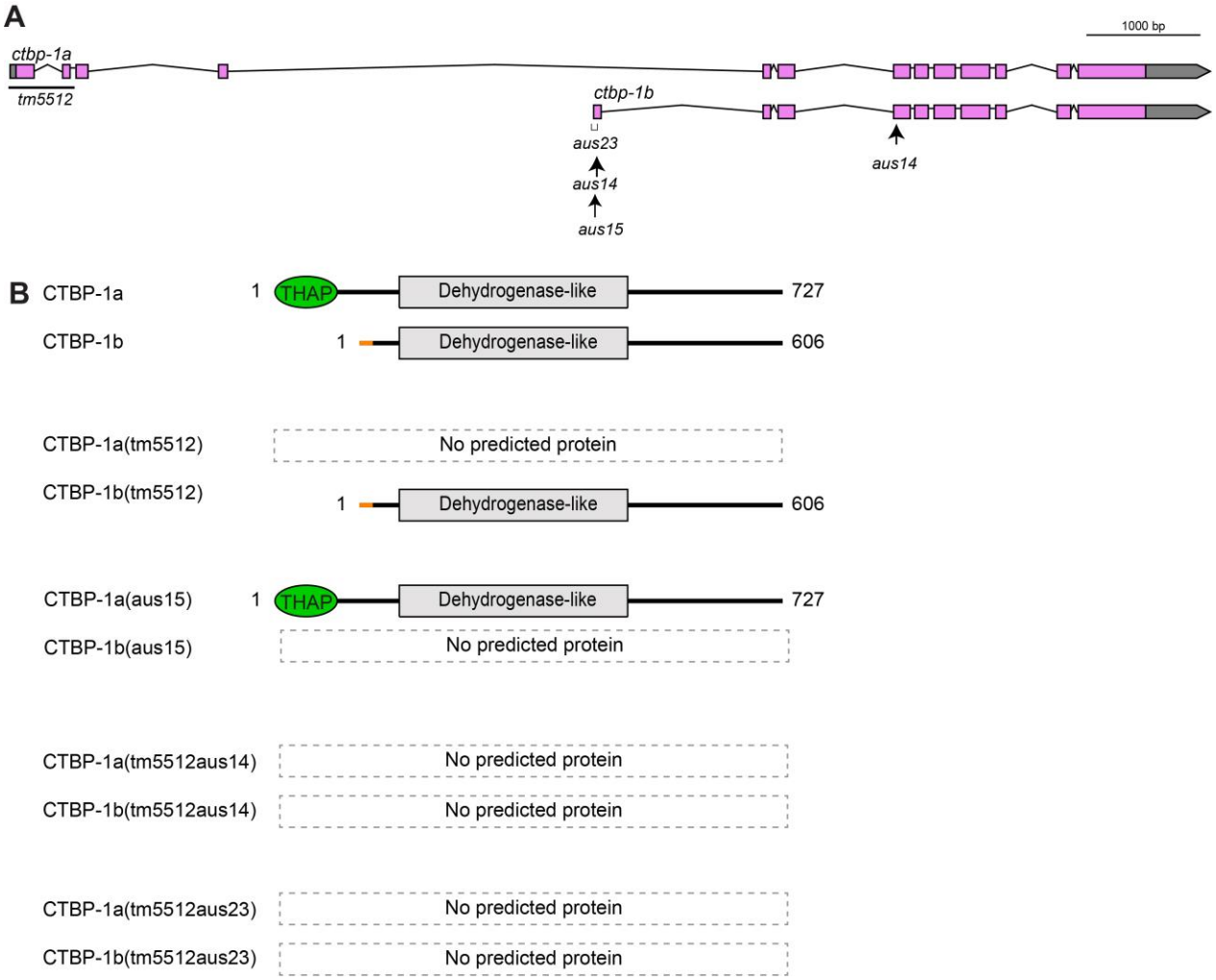

Figure 3.2 CRISPR-Cas9 generated *ctbp-1* mutations.
(A) Schematic of *ctbp-1* transcripts: *ctbp-1a* and *ctbp-1b*. The position of *ctbp-1* mutant alleles *tm5512*, *aus15*, *aus14* and *aus23* are indicated (arrowheads and horizontal lines). Exons (pink boxes), introns (lines) and UTRs (grey box) are indicated; 5' is on the left. (B) Predicted isoforms of wild-type and *ctbp-1* mutant alleles. The *tm5512* allele generated by National BioResource Project (Tokyo, Japan).

To determine if mutating one isoform of CTBP-1 causes transcriptional changes in the other isoform, I performed quantitative real-time PCR (qRT-PCR) to determine the relative expression levels of the *ctbp-1a* and *ctbp-1b* isoforms in isoform-specific *ctbp-1* mutants. In

ctbp-1a(tm5512) mutants, expression of the *ctbp-1b* transcript is not significantly changed relative to wild-type (~1.3 fold change, p>0.05) (Figure 3.3A). This demonstrates that mutating the CTBP-1a isoform does not alter the transcript levels of the shorter CTBP-1b isoform. Interestingly, expression of the *ctbp-1a* transcript increased ~2.9 fold in *ctbp-1a(tm5512)* mutant animals relative to wild-type (p<0.05) (Figure 3.3A). These data suggest that when *ctbp-1a* is lost, there is an induction of *ctbp-1a* expression. CTBP-1 is known to repress transcription [68], and these results suggest that CTBP-1a normally functions to repress itself.

In *ctbp-1b(aus15)* mutants, the *ctbp-1a* and *ctbp-1b* expression levels do not significantly differ relative to wild-type (p>0.05) (Figure 3.3B). This demonstrates that loss of CTBP-1b does not alter the transcript levels of the longer CTBP-1a isoform.

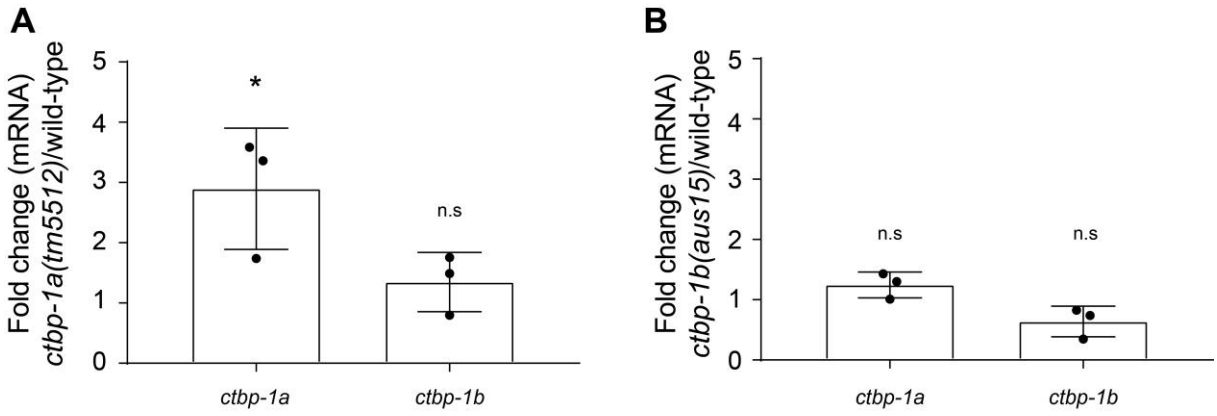

Figure 3.3 The *ctbp-1a(tm5512)* mutation causes upregulation of *ctbp-1a* mRNA.
qRT-PCR data demonstrating the mRNA expression level of *ctbp-1a* and *ctbp-1b* transcripts in *ctbp-1a(tm5512)* mutants (A) and *ctbp-1b(aus15)* mutants (B) relative to the same isoform in wild-type animals. Data presented as 3 biological replicates (points) with mean ± SEM (bar). Statistical significance was determined relative to the corresponding transcript in wild-type animals, *p<0.05, n.s – not significant (one-way ANOVA with Dunnett's multiple comparisons test).

3.3 CTBP-1a regulates SMDD axonal development

The SMDD motor neuron axons extend from the nerve ring posteriorly along the dorsal sublateral cord before terminating anterior to the vulva [6]. We previously found that *ctbp-1a* hypomorphic mutants display defective SMDD morphology at the L4 stage, where the axons 'curl' away from the dorsal sublateral cord [93]. I analysed the SMDD axons of the newly generated isoform-specific CRISPR-Cas9 mutants to examine whether the SMDD axons displayed the 'curl' phenotype. Consistent with our previously published results, *ctbp-1a(tm5512)* mutants displayed ~23% SMDD curls at L4 stage and this increased to ~48% at

day 1 of adulthood at 25°C (Figure 3.4A). Heterozygous *ctbp-1a(tm5512)*/+ animals do not display SMDD axon guidance defects, demonstrating that this mutation is recessive (1 biological replicate of 20 animals, data not shown). In contrast, the *ctbp-1b(aus15)* mutants displayed the same low levels of defective SMDD axons as wild-type animals at both L4 stage and day 1 stages (both ~1% at L4 stage; ~4% and ~1%, respectively at day 1) (Figure 3.4A). This demonstrates that CTBP-1b does not play a role in SMDD axonal development.

The *ctbp-1a/b(tm5512aus14)* predicted null mutants displayed ~19% SMDD curls at L4 stage and ~47% at day 1 of adulthood (Figure 3.4A). The *ctbp-1a(tm5512)* and *ctbp-1a/b(tm5512aus14)* mutants did not significantly differ in SMDD curl penetrance at either stage (Figure 3.4A). These data indicate that removal of both CTBP-1 isoforms does not increase the SMDD curl defects seen in *ctbp-1a(tm5512)* mutants.

The *ctbp-1a/b(tm5512aus23)* strain appeared sick and had delayed development when grown for multiple generations at 25°C. Therefore, I performed the SMDD curl assay at 20°C on Day 2 adults. The *ctbp-1a(tm5512)* mutants exhibited a similar penetrance at day 2 of adulthood at 20°C and day 1 of adulthood at 25°C (~56% and ~47%, respectively, Figure 3.4A-B), indicating that the SMDD axons can be assayed at this life stage and temperature if the organism is sensitive to higher temperatures. At day 2 of adulthood at 20°C, the SMDD curl percentage of *ctbp-1a/b(tm5512aus23)* mutants did not significantly differ from *ctbp-1a(tm5512)* mutants (~56% and ~60%, respectively, Figure 3.4B). These data demonstrate that predicted null alleles do not increase the SMDD curls observed in *ctbp-1a* mutant animals, and *ctbp-1a(tm5512)* is acting as a null in this context.

The *ctbp-1a/b(tm5512aus23)* strain was outcrossed 6 times before crossing into the *pglr-1::GFP* (*rhIs4*) reporter for SMDD analysis, so it is unclear whether this mutant has a tightly linked background mutation(s) that would cause sensitivity to higher temperatures. As seen in Figure 3.4A, the other predicted null mutant *ctbp-1a/b(tm5512aus14)* was assayed at 25°C, and displayed wild-type body morphology and growth after multiple generations at this higher temperature.

Figure 3.4 CTBP-1a, but not CTBP-1b, regulates SMDD axonal morphology.
(A-B) Quantification of SMDD curls (%) of (A) L4 and day 1 adults at 25°C or (B) Day 2 adults at 20°C. Data presented as mean ± SEM (bar) of 3 biological replicates, n>80 axons. *p<0.05, **p<0.01, ****p<0.0001, n.s – not significant (one-way ANOVA with Tukey's correction).

Because the SMDD curl phenotype of *ctbp-1a(tm5512)* mutants increased in penetrance between L4 stage and day 1 of adulthood, I was interested to determine whether defects occurred earlier than L4 stage and/or continued to increase in penetrance after early adulthood. Wild-type animals have straight SMDD axons that extended along the dorsal sublateral cord throughout all life stages analysed (L2 stage- day 5 of adulthood, Figure 3.5A). In contrast, *ctbp-1a(tm5512)* mutant animals displayed axons that curled away from the dorsal sublateral cord and extended in varying directions (Figure 3.5A). These curls increased in severity as the mutant animals aged (Figure 3.5A). The morphology of the defects varies greatly across individual animals, and even between the two SMDD axons of the same animal. I found that the SMDD axons extend in all directions (dorsal, ventral, anterior, posterior, left, right) once they leave the dorsal sub-lateral cord. These defective axons do not appear to follow or join any specific axon tracts after they leave the dorsal sublateral cord, instead they wander randomly. This suggests once the SMDD axons have left the sublateral tract, they are not misguided by a specific guidance cue to a particular location.

I quantified the penetrance of SMDD curls at defined larval and adulthood stages at 25°C. At both L2 and L3 stage, *ctbp-1a(tm5512)* mutants exhibited wild-type axons (Figure 3.5B). In *ctbp-1a(tm5512)* mutants, SMDD curls were evident at the L4 stage (~17%) and increased in penetrance between the L4 stage and day 1 of adulthood (~49%, Figure 3.5B). There was a further increase in SMDD curl penetrance in day 3 adults (~64%) compared to day 1 adults (Figure 3.4B). However, there was no significant difference in SMDD curl penetrance of *ctbp-1a(tm5512)* mutant animals between day 3 and day 5 (both ~64%, Figure 3.5B). The *ctbp-1a* mutant animals exhibit SMDD curls beginning at L4 stage, and the SMDD curls increase in penetrance until day 3 of adulthood. These data demonstrate that the *ctbp-1a* mutant SMDD

axons are unable to correctly guide their extension along the dorsal sublateral cord in late larval development and during adulthood.

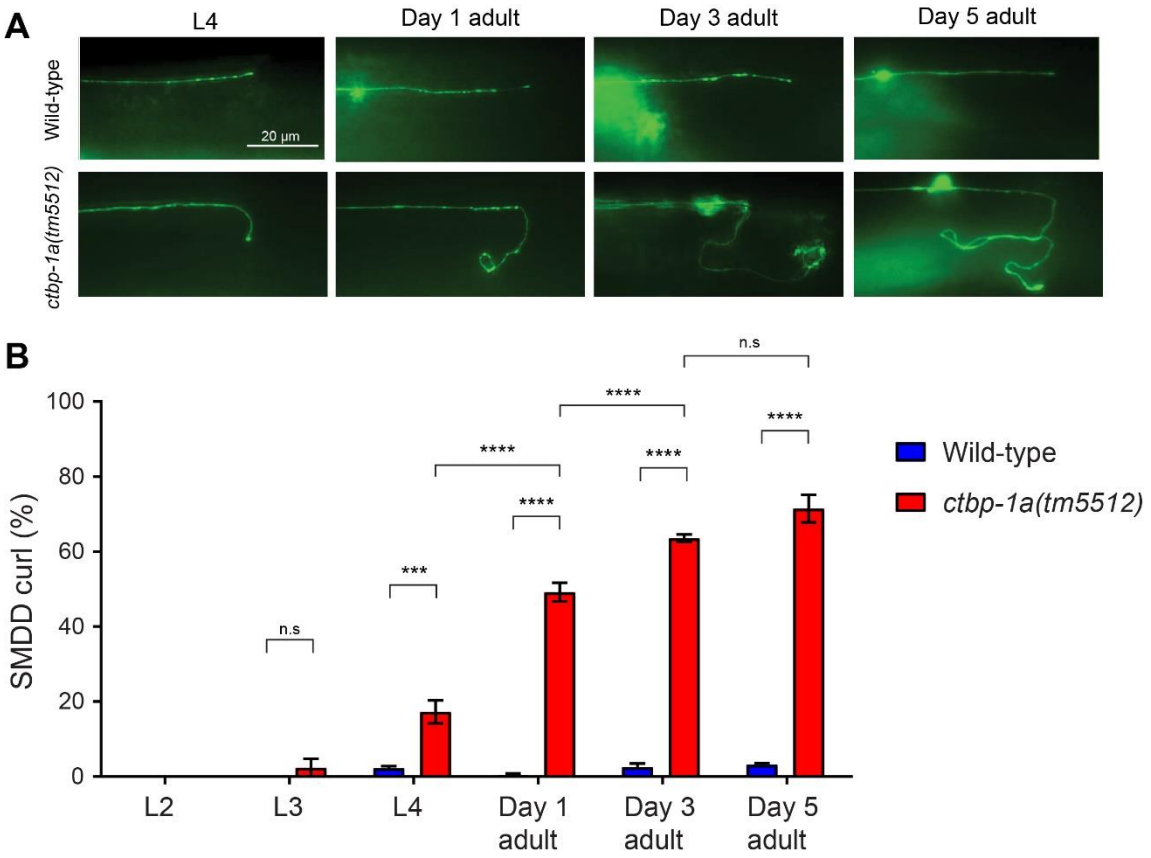

Figure 3.5 CTBP-1a is required for SMDD axon guidance from late larval stages.
(A) Representative SMDD axons of L4 to Day 5 adult. Scale bar= 20 µm. (B) Quantification of SMDD curls (%) of wild-type and *ctbp-1a* mutants at 25°C. Data presented as mean ± SEM (bar) of 3 biological replicates, n>100 axons. ***p<0.001, ****p<0.0001, n.s – not significant (one-way ANOVA with Tukey's correction). L4-Day 5 adult in (A) and (B) modified from [93].

When measuring the penetrance of SMDD curls, I observed that the length of the SMDD axons in *ctbp-1a(tm5512)* mutants appeared longer than in wild-type animals. I quantified the length of the SMDD axons from the anterior bulb of the pharynx, where the axon is not obscured by the bright fluorescence in the nerve ring, to the distal tip of the axon (Figure 3.6A). The SMDD axon length measures the total length of the axon, including the curled off portion of SMDD curls if they leave the dorsal sublateral cord. At the L2 stage, where *ctbp-1a(tm5512)* mutants do not display SMDD curls (Figure 3.5B), the length of SMDD axons does not differ from wild-type (~45 µm and ~44 µm, respectively, Figure 3.6B). At the L3 stage, however, *ctbp-1a(tm5512)* mutants display significantly longer axons than wild-type (~88 µm and ~68 µm respectively, Figure 3.6B). These L3 stage axons of the *ctbp-1a(tm5512)* mutant do not curl

away from the dorsal sublateral cord but overextend beyond the wild-type position (Figure 3.6B, Figure 3.5B). This demonstrates that the overextension defects caused by loss of CTBP-1a occur earlier than the curl phenotype.

L4 stage *ctbp-1a(tm5512)* animals display a significant increase in SMDD axon length compared to wild-type (~137 and ~137 µm, respectively, Figure 3.6B). The *ctbp-1a(tm5512)* mutant animals displayed longer axons than wild-type at all analysed adulthood stages (days 1, 3 and 5 of adulthood, Figure 3.6B). The length of the *ctbp-1a(tm5512)* mutant axons increased significantly between L4 stage and day 1 of adulthood (~137 to ~213 µm, Figure 3.6B). There was a further increase in *ctbp-1a(tm5512)* SMDD axon length from day 1 adults to day 3 adults (~213 µm to ~250 µm, Figure 3.6B). There was no significant difference in axon length between day 3 and day 5 mutant animals (~250 and ~249 µm, Figure 3.6B). These results demonstrate that *ctbp-1a(tm5512)* mutant animals exhibit longer SMDD axons beginning at the L3 stage and curly SMDD axons beginning at the L4 stage. The SMDD axons of *ctbp-1a* mutant animals continued to increase in length and curl penetrance until day 3 of adulthood. Overall, these results demonstrate that in *ctbp-1a* mutants, the SMDD axons display aberrant axon extension and do not terminate their growth at the correct position.

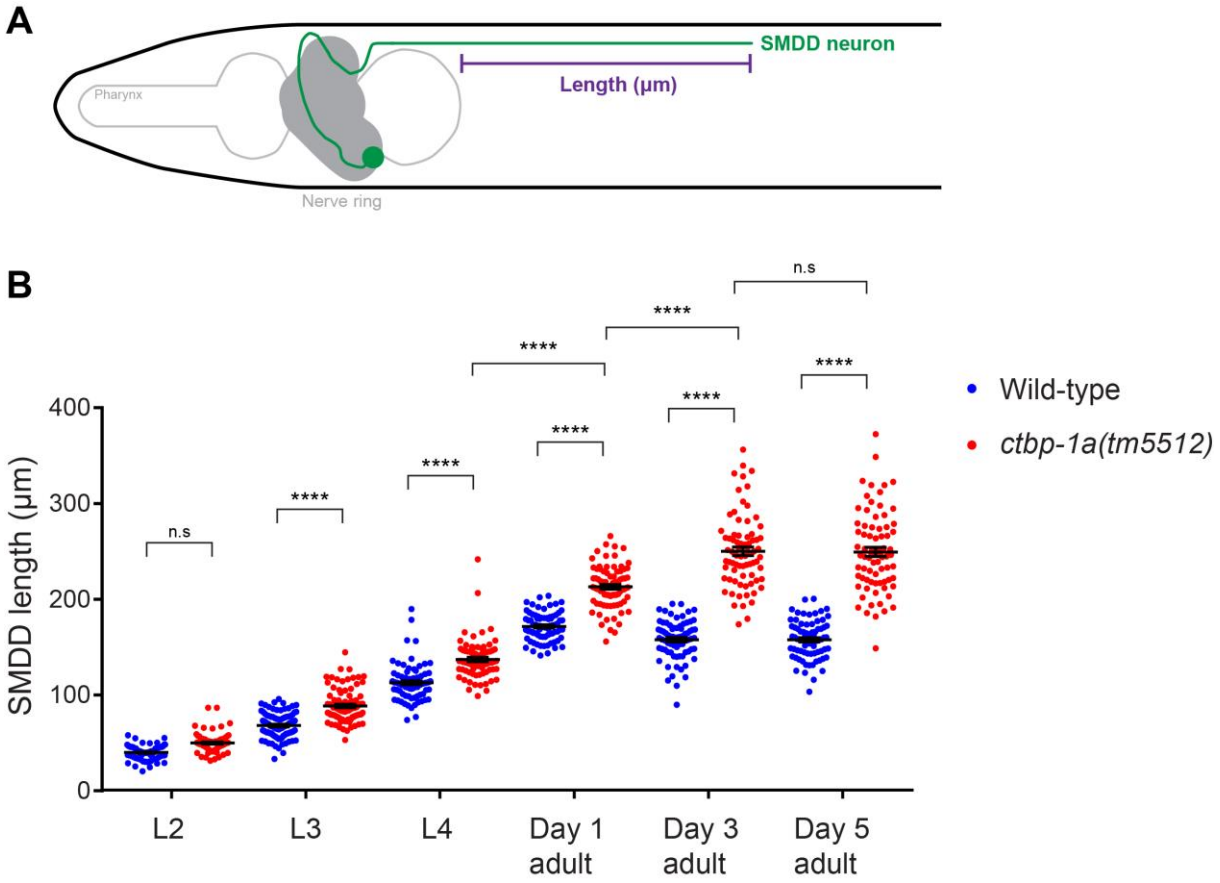

Figure 3.6 CTBP-1a is required for SMDD axon termination from the L3 stage.

(A) Schematic of SMDD length measurement methodology. SMDD length (µm) measures the length of the SMDD axon from the posterior bulb of the pharynx (light grey line) to the distal tip of the SMDD axon (purple line). The SMDD neuron cell body is obscured by GFP expression in the nerve ring (dark grey). (B) Quantification of SMDD length (µm) of wild-type and mutant animals at 25°C . Data presented as individual axon lengths (points) with mean ± SEM (bar) of 2 biological replicates, n>70 axons. ****p<0.0001, n.s – not significant (one-way ANOVA with Tukey's correction).

I further analysed the length of the SMDD axons to determine whether the increased axon length of *ctbp-1a(tm5512)* mutants is due to the increased curl penetrance (for penetrance scoring, see Figure 3.5B). I plotted the lengths of the whole SMDD axon of *ctbp-1a(tm5512)* mutant animals, distinguishing whether they extend wild-type axons ("straight" along the dorsal sublateral cord) or display the curl phenotype ("curly", extending away from the dorsal sublateral cord). Because wild-type animals do not display the curl phenotype (Figure 3.5B), these were excluded from analysis. There was no significant difference between the length of straight and curly *ctbp-1a(tm5512)* mutant axons at the L4 stage and day 1 of adulthood (Figure 3.7A). At day 3 and day 5 of adulthood, there is a significant increase in the length of curly axons compared to straight axons (Figure 3.7A). At these late stages of adulthood, the majority of *ctbp-1a(tm5512)* mutant axons curl away from the sublateral cord (Figure 3.5B).

These data demonstrate that axons that either leave or remain in the dorsal sublateral cord all extend further than their correct termination length. However, the increased length of SMDD axons of *ctbp-1a(tm5512)* mutant animals is independent of the curl phenotype, except in late adulthood when axons wander in a random manner.

I also plotted the length of the SMDD curl of *ctbp-1a(tm5512)* mutant animals. This measures the length of only the portion of the SMDD axon that curls away from the dorsal sublateral cord (Figure 3.7B). There was no significant increase in curl length between L4 stage and day 1 of adulthood (Figure 3.7B). The curl length increased between day 1 and day 3 of adulthood, but there was no significant difference between day 3 and day 5 of adulthood (Figure 3.7B). Interestingly, the penetrance of curls and overall length of SMDD axons does not increase between day 3 and day 5 of adulthood (Figure 3.5, Figure 3.6), suggesting that CTBP-1 no longer influences SMDD axon morphology at these later stages of adulthood. Alternatively, these axons have reached positions in the body of the worm, where growth is no longer possible or that axon-promoting mechanisms are no longer present.

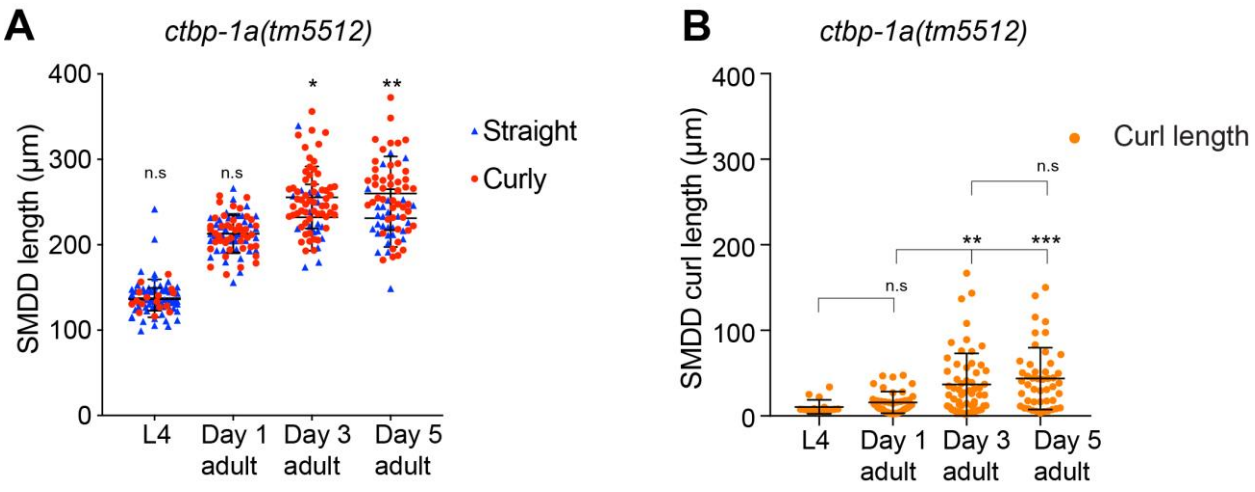

Figure 3.7 The length of SMDD axons increases in *ctbp-1a* mutant animals, whether they curl away from or remain in the dorsal sublateral cord.

(A) Quantification of SMDD length (in µm) of straight (blue triangle) and curly (red circle) axons in *ctbp-1a(tm5512)* mutant animals. Data presented as individual axon lengths (straight: blue triangle, curly: red dot) with mean ± SD (bar) of 2 biological replicates, n>70 axons. *p<0.05, **p<0.01, n.s – not significant (unpaired t-test for each developmental stage). (B) Quantification of SMDD curl length (in µm) of *ctbp-1a(tm5512)* mutant curly axons. Data presented as individual axon curl lengths (points) with mean ± SD (bar), n-17-60 axons. **p<0.01, ***p<0.001, n.s – not significant (one-way ANOVA with Tukey's correction). All performed at 25°C.

To rule out the possibility that the axons were longer simply because the length of the whole animal was increased, I quantified the length of wild-type and *ctbp-1a(tm5512)* mutant animals at all developmental stages where the length was assayed: L2-L4 stages, days 1, 3 and 5 of adulthood (Appendix Figure 8.1). The body length of *ctbp-1a(tm5512)* mutant animals is shorter than wild-type at all larval stages and day 3 of adulthood, whereas there is no significant difference in length at day 1 and 5 of adulthood (Appendix Figure 8.1). This demonstrates that overgrowth of SMDD axons caused by loss of CTBP-1 is not due to an overall scaling of axons with increased length of the animal.

Overall, these results demonstrate that multiple aspects of axon outgrowth are impacted when CTBP-1a is lost: guidance, outgrowth and termination. In *ctbp-1a* mutants, the axons display guidance defects, where they extend within incorrect regions of the body. Furthermore, the mutant axons extend beyond their correct termination length, demonstrating that termination cues may be lost or misinterpreted when CTBP-1 is mutated. Due to the occurrence of both of these outgrowth defects in *ctbp-1a* mutants, which first occur at different developmental stages, I summarise these as defects in axonal development.

3.4 CTBP-1b is not involved in SMDD development

So far, I have demonstrated distinct roles for the two CTBP-1 isoforms: CTBP-1a and CTBP-1b. The CTBP-1a isoform, which contains an additional DNA-binding THAP domain, regulates both SMDD axon guidance and termination. In contrast, I demonstrated that removing *ctbp-1b* does not cause SMDD axon guidance defects (Figure 3.4). This shorter CTBP-1b isoform lacks the THAP domain but contains the other domains necessary for binding proteins in a co-repressor complex [89]. I was therefore interested in whether the shorter CTBP-1b isoform is involved in the termination of the SMDD axons. As previously quantified in Figure 3.4, the *ctbp-1b(aus15)* mutants display straight axons that extend along the dorsal sublateral cord (Figure 3.8A). I further found that the length of *ctbp-1b(aus15)* SMDD axons does not significantly differ from wild-type at all stages (L4 stage to day 5 of adulthood, Figure 3.8B). These data demonstrate that CTBP-1b is not involved in any stage of SMDD development, and suggests that domains only present in CTBP-1a may regulate SMDD axonal development.

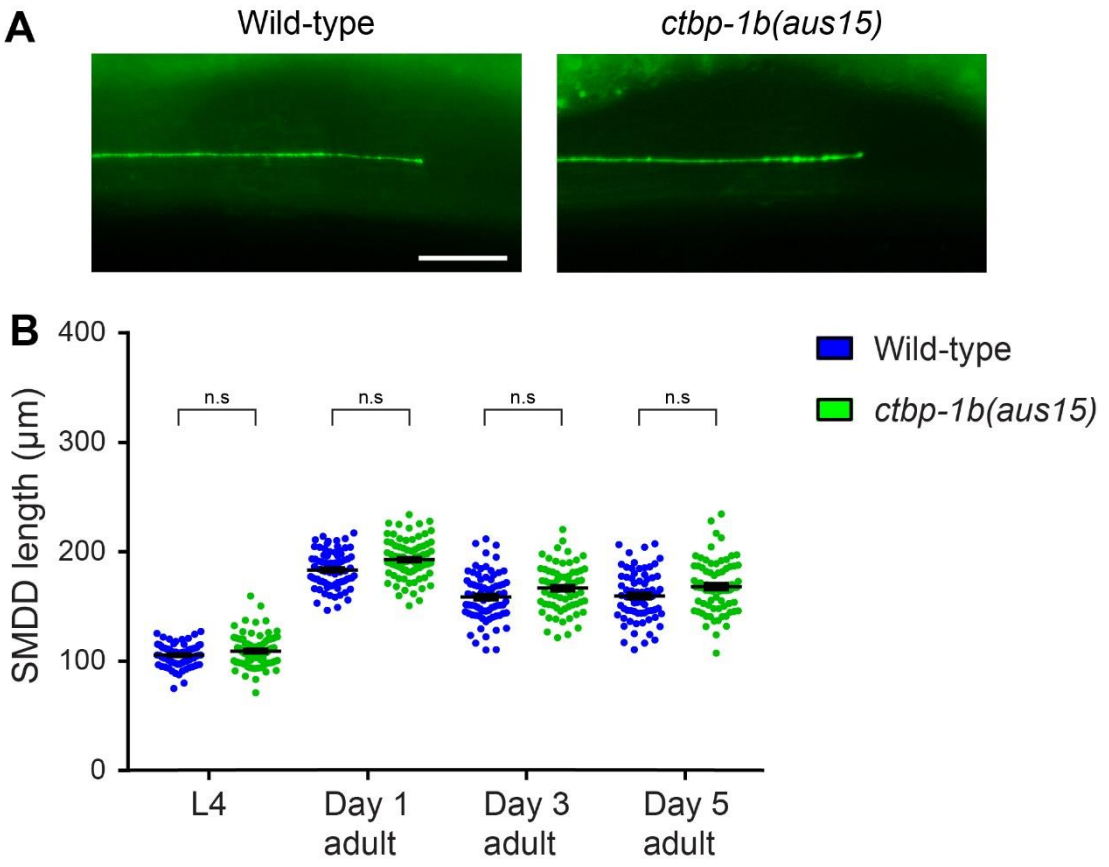

Figure 3.8 The length of *ctbp-1b* mutant animals does not differ from wild-type.

(A) Representative fluorescence micrographs of day 1 adult SMDD axons. Scale bar = 20 µm. (B) Quantification of SMDD length (in µm) of wild-type and *ctbp-1b* mutant axons. Data presented as individual axon lengths (points) with mean ± SEM (bar) of 2 biological replicates, n= 70-80 axons. n.s – not significant (one-way ANOVA with Tukey's correction).

3.5 Tagging CTBP-1a or CTBP-1b with mCherry causes defective SMDD axons

The results I have reported thus far demonstrate differential roles for CTBP-1a and CTBP-1b in the control of SMDD axonal development. I was interested in whether this could be due to different temporal or spatial expression of the two isoforms. I therefore designed CRISPR-Cas9 experiments to insert an mCherry tag at the unique N-terminus of each isoform to observe the endogenous expression of CTBP-1a or CTBP-1b. The method I used for tagging was adapted from the Calarco lab [155]. Briefly, I injected young adult wild-type animals with Cas9, sgRNA, co-injection markers and a repair template. The repair template contained the mCherry sequence, homology arms flanking the desired tagging site, and a reporter expressing both pharyngeal GFP and a neomycin resistance transgene flanked by LoxP sites

[155]. I screened multiple generations of animals with the GFP pharyngeal marker to ensure integration of the repair cassette. To remove the dual-marker cassette from the repaired region, I subsequently injected the successfully integrated homozygous animals with Cre recombinase to remove the regions between the loxP sites. Finally, I sequenced the locus with Sanger sequencing to ensure the mCherry tag was in frame with the respective *ctbp-1* gene. For details, see Methods 2.2.10-2.2.11.

Using the sgRNA I used previously to generate random mutations in CTBP-1b (Figure 3.1), I successfully tagged CTBP-1b with worm-optimised mCherry. This resulted in an in-frame insertion of mCherry at the N-terminus of CTBP-1b (Figure 3.9A).

Because I had not previously used CRISPR-Cas9 on *ctbp-1a*, I first designed and tested the ability of multiple sgRNAs to generate random mutations in the first 2 exons of *ctbp-1a*. These sgRNAs had very low efficiency in generating random mutations, suggesting that double-stranded breaks were not occurring, and hence could not be used for integration. To avoid more delays, I outsourced the CRISPR-Cas9 experiments to SunyBiotech (Fujian, China). SunyBiotech successfully generated the CTBP-1a tag allele *syb601* (Figure 3.9B).

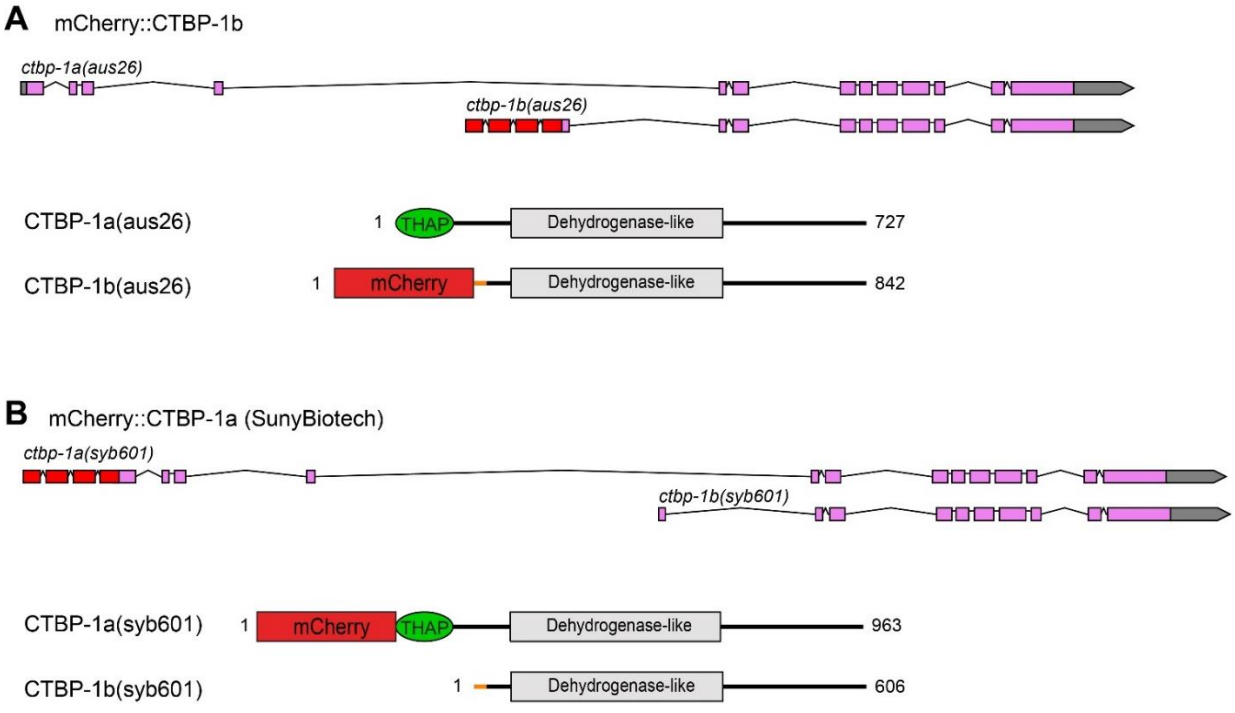

Figure 3.9 N-terminal mCherry tags of CTBP-1a or CTBP-1b.

(A) mCherry-tagged CTBP-1b, where isoform CTBP-1a is not affected. Generated in this project. (B) mCherry-tagged CTBP-1a, where isoform CTBP-1b is not affected. Generated by SunyBiotech. (A-B) The *ctbp-1* gene locus, showing where mCherry exons (red) were inserted for each isoform. Exons (pink

or red boxes), introns (solid lines) and untranslated regions (grey box) are indicated; 5' mCherry (red) is on the left. CTBP-1 protein isoforms, with the mCherry tag at the N-terminus. N-terminus is on the left.

I outcrossed these endogenous tagged strains 6 times before beginning any assays. To ensure the tagged strains were functional, I crossed the tagged alleles into the *pglr-1::GFP* (*rhIs4*) strain to determine if the SMDD axons develop normally. For both tagged strains, mCherry expression was visible in the nuclei of head neurons, however both N-terminal tags (*aus26* and *syb601*) caused SMDD curls similar to those seen in *ctbp-1a(tm5512)* mutant worms (n>50 mixed stage worms). This demonstrates that the N-terminal mCherry tags caused the proteins to be nonfunctional. This was surprising for the CTBP-1b isoform because mutating CTBP-1b does not cause SMDD defects (Figure 3.4), therefore a disruption to CTBP-1b was not expected to cause curly SMDD axons. The appearance of SMDD curls indicates that CTBP-1a expression and/or function must be disrupted. I confirmed with sequencing that the CTBP-1b tag does not disrupt any coding sequence or splice junctions of CTBP-1a, but the mCherry tag is present in *ctbp-1a* intron 4. I hypothesise that the long mCherry tag (861 bp long) disrupts the intron spacing of *ctbp-1a*, hence disrupting important regulatory sequences and/or causing incorrect splicing [168]. To determine if there were any conserved sequences within this intron sequence, I aligned the genomic sequence of *C. elegans ctbp-1a* intron 4 with the *C. briggsae ctbp-1a* intron 4 (*Cbr-ctbp-1*, WormBase) and found that they had high sequence similarity, including long stretches of conserved nucleotides. *C. elegans* and *C. briggsae* diverged 80-110 million years ago, and intronic sequences are rarely conserved between these species [169]. Therefore, this large conserved intronic region could be important for regulation of transcription and splicing [168, 170].

In summary, due to the interference of CTBP-1 function by mCherry tags, I was unable to use these strains for expression analysis.

3.6 CTBP-1a is expressed in neurons, including the SMD axons

So far, I have demonstrated that CTBP-1a regulates SMDD axonal development, but we have not determined in which cells or tissues CTBP-1a functions to regulate this process. Because I was unable to determine the expression of CTBP-1a using endogenous tags, I generated a *pctbp-1a::GFP* transcriptional reporter. This construct contained a 5 kb sequence upstream of the transcriptional start site of *ctbp-1a* fused to GFP coding sequence and *unc-54* 3' UTR (Figure 3.10A). I injected *pctbp-1a::GFP* into wild-type animals and generated 4

extrachromosomal transgenic lines (*rpEx1739-1742*). All extrachromosomal lines exhibited similar expression patterns, therefore I used *rpEx1739* for further analysis. I found that the *ctbp-1a* promoter drives expression in a subset of neurons (Figure 3.10B-D). The *pctbp-1a::GFP* expression is first visible in the comma stage of embryogenesis (Figure 3.10B). GFP expression is visible in the cell body (1 cell body shown in Figure 3.10B, the other is in different plane). Based on the cell body position and axon morphology, I predict these are the SMDD neurons. The SMDD axons function as pioneer axons for nerve ring development, and are therefore one of the only axons extending at this stage of embryogenesis [11]. Later in larval development, the *ctbp-1a* promoter drives expression in a subset of neuronal cell bodies in the head (Figure 3.10C). GFP expression is also visible in 4 axons that extend along the dorsal and ventral sublateral tracts (2 in each) (Figure 3.10D, Figure 3.11A). These are the SMDD and SMDV axons. Further analysis is required to determine the identity of the other neurons.

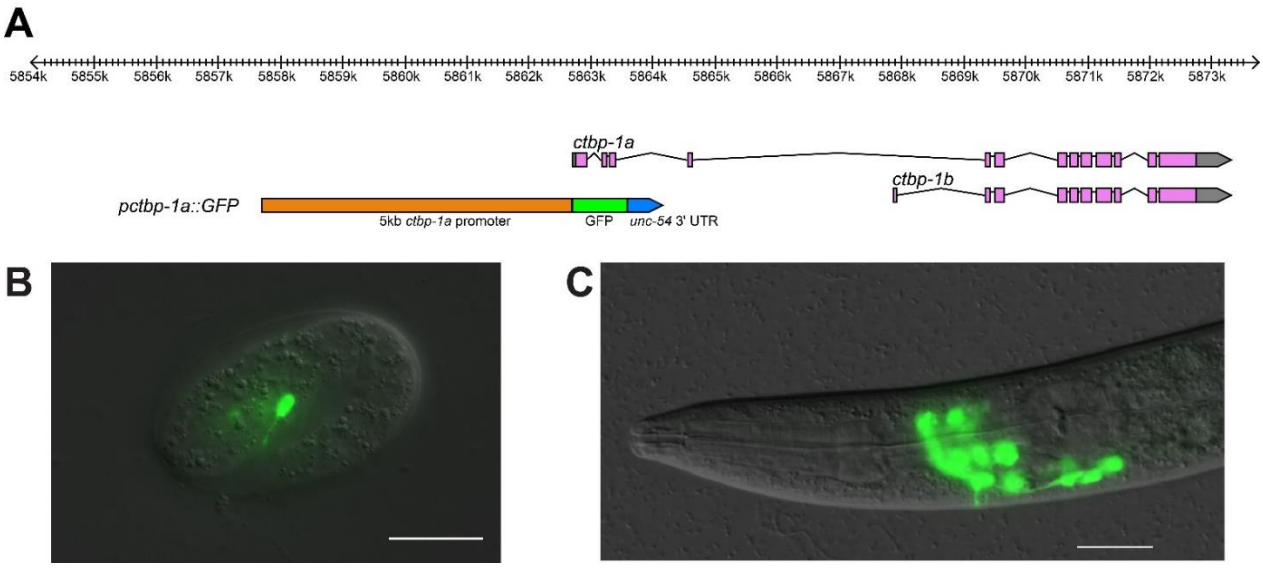

Figure 3.10 *pctbp-1a::GFP* is expressed in head neurons, including the SMDDs.
(A) Schematic of the *pctbp-1a::GFP* construct: 5 kb *ctbp-1a* promoter region (orange box) fused to GFP (green box) and *unc-54* 3' UTR (blue box). Figure modified from WormBase. (B-C) Expression of a *pctbp-1a::GFP* transcriptional reporter during different developmental stages. (B) SMDD cell body and axon projection visible in a comma stage embryo. (C) Neuronal cell bodies in head visible in a L4 stage animal. Corresponding DIC images are overlaid. Anterior is to the left, ventral is down. Scale bars = 20 µm.

The *pctbp-1a::GFP* expression persists in adulthood stages, including in the SMDD and SMDV axons (Figure 3.11A). This is the first time that I was able to observe all 4 SMD axons, as

SMDV axons are obscured by VNC neurons in the *pglr-1::GFP* (*rhIs4*) reporter strain. To my knowledge, this *pctbp-1a::GFP* transcriptional reporter is the first marker in which only the SMDD and SMDV axons are detectable. Although other cell bodies are expressed in the head, the SMD axons can be easily visualized leaving the nerve ring and extending along sublateral cords. Therefore, with this new transcriptional reporter, I was able to quantify whether the SMDV axons are also defective in *ctbp-1a* mutants. Wild-type animals displayed straight SMDD and SMDV axons, but *ctbp-1a(tm5512)* mutant animals displayed both SMDD and SMDV curls (Figure 3.11A). The *ctbp-1a(tm5512)* mutants exhibited ~43% SMDV curls and ~40% SMDD curls, compared to ~1% for both in wild-type (Figure 3.11B). These results demonstrate that CTBP-1 regulates both SMDD and SMDV axonal development, which occur in the dorsal sublateral and ventral sublateral cords, respectively.

In *ctbp-1a(tm5512)* mutant animals, SMDD and/or SMDV curls occurred independently of each other i.e. the appearance of SMDD curls did not affect the penetrance of SMDV curls, and vice versa. This is likely due to compensatory axon development mechanisms, as axon guidance defects are not completely penetrant [16, 20]. These defects occur randomly in each of the 4 sublateral cords, which are similarly constrained by muscle and hypodermis but contain different associated neuron processes (Figure 1.3), suggesting that CTBP-1-regulated axonal development is not dependent on other neurons in the cords.

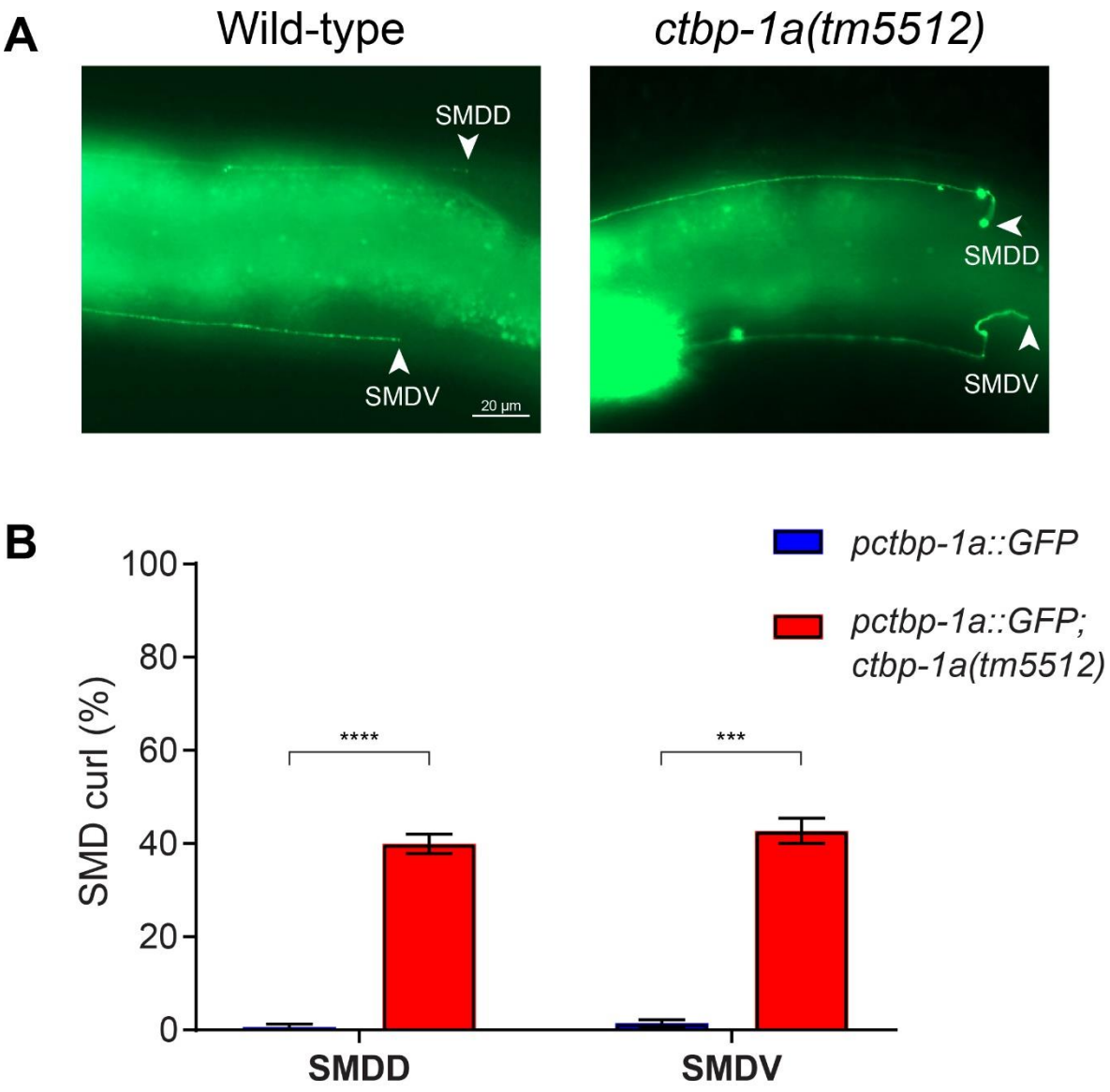

Figure 3.11 *ctbp-1a* mutants display defects in SMDV axonal development.

(A) Expression of the *pctbp-1a::GFP* transcriptional reporter, highlighting SMDD and SMDV axons (arrowhead) in wild-type and *ctbp-1a(tm5512)* mutant animals. Anterior is to the left, ventral is down. Scale bar = 20 µm. (B) Quantification of SMDD or SMDV curls (%) in wild-type and mutant animals using *pctbp-1a::GFP*. Data presented as mean ± SEM (bar) of 3 biological replicates, n>100 axons, day 1 adults at 25°C. ***p<0.001, ****p<0.0001 (unpaired t-test).

3.7 CTBP-1a regulates its own expression

When quantifying the SMDV and SMDD curls, I observed that the GFP intensity of the *pctbp-1a::GFP* marker was brighter in *ctbp-1a(tm5512)* mutants. I therefore quantified the *pctbp-1a::GFP* expression of the head region of L4 stage animals and determined that *ctbp-1a* promoter activity increased ~2 fold in *ctbp-1a(tm5512)* mutants (Figure 3.12A-B). CTBP-1 is a

known transcriptional repressor [68], and indeed I found that the longer CTBP-1a isoform is capable of repressing its own expression at the transcriptional level.

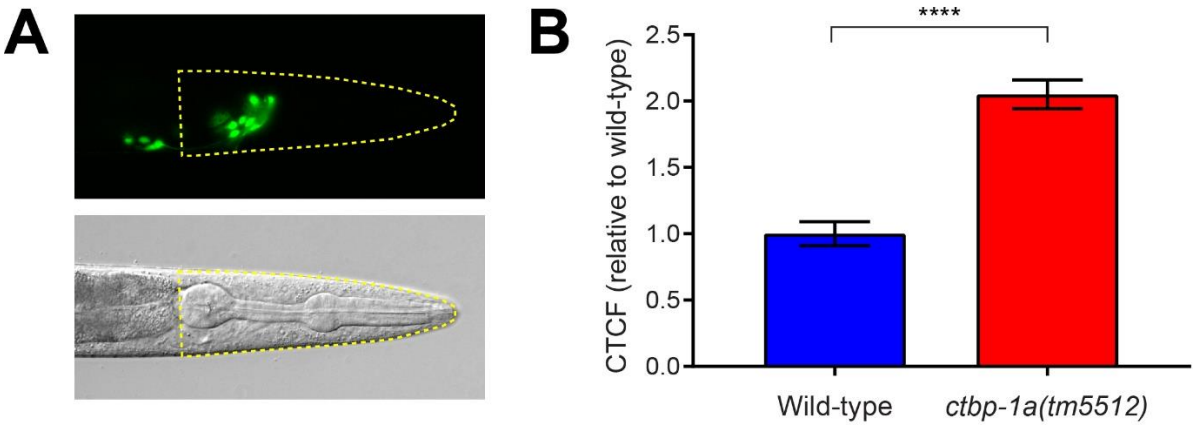

Figure 3.12 CTBP-1a regulates its own expression.
(A) Representative GFP and DIC images of region of quantified head fluorescence from anterior bulb of pharynx to tip of head (inside dotted yellow line). (B) Quantification of GFP intensity (CTCF= calculated total fluorescence) of *pctbp-1a::GFP (rpEx1739)* in the head. Data presented as mean ± SEM (bar) of 3 biological replicates, n>30 L4 stage animals at 20°C. ****p<0.0001 (unpaired t-test).

3.8 CTBP-1a, but not CTBP-1b, can rescue SMDD curl defects

Thus far, I have demonstrated that *ctbp-1a* mutant animals display SMDD axon outgrowth defects. To verify that the axonal developmental defects were specifically caused by loss of *ctbp-1a*, I resupplied the *ctbp-1a* cDNA driven under the endogenous *ctbp-1*a 5kb promoter. This 5 kb promoter was used to generate the *pctbp-1a::GFP* construct, and drives expression in a subset of neurons, including the 4 SMD neurons (Figure 3.10). Expressing *ctbp-1*a cDNA under its own promoter in *ctbp-1a(tm5512)* mutants fully rescued the SMDD defects back to wild-type levels (Figure 3.13A). This *ctbp-1a* rescue construct also contained mCherry at the C-terminus, and mCherry was visible in neurons (Appendix Figure 8.2). This indicates that unlike tagging the N-terminus, tagging the C-terminus does not disrupt the function of CTBP-1a.

Next, I wanted to determine whether expressing the shorter *ctbp-1b* isoform could rescue the SMDD defect. I drove *ctbp-1b* cDNA under the endogenous *ctbp-1a* 5kb promoter and found that this failed to rescue the SMDD curl phenotype of *ctbp-1a(tm5512)* mutant animals (Figure 3.13B). mCherry expression was visible in neurons in all transgenic extrachromosomal lines,

indicating that the inability to rescue defective SMDD axons was not due to incomplete/inconsistent expression. These data therefore suggest that the longer isoform contains important domains for CTBP-1 function in SMDD development. Hence, from here on all rescue constructs will contain *ctbp-1a* cDNA.

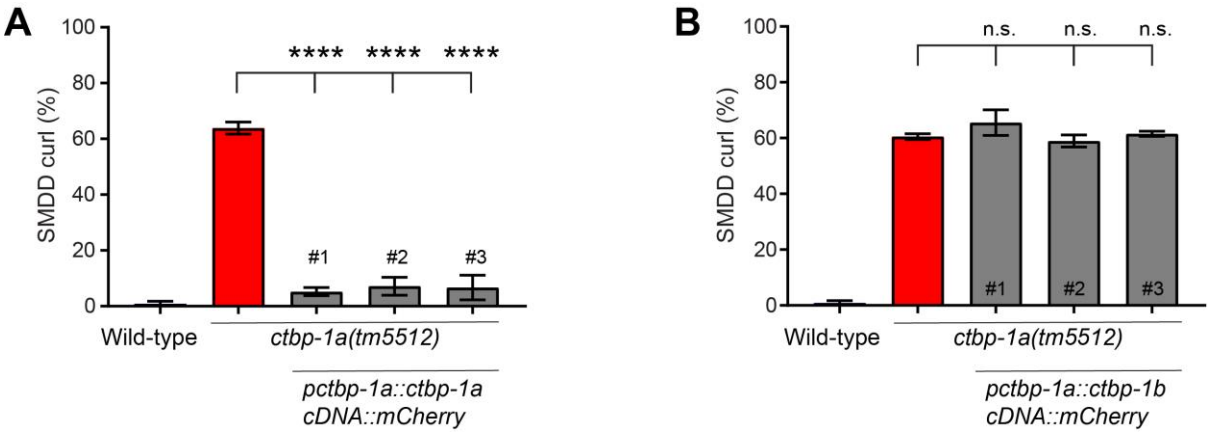

Figure 3.13 Endogenously expressed *ctbp-1a* cDNA rescues SMDD curls.
(A-B) Quantification of SMDD curl phenotype (%) when driving *ctbp-1a* cDNA (A) or *ctbp-1b* cDNA (B) with the 5 kb *pctbp-1a* promoter. Data presented as mean ± SEM (bar) of 3 biological replicates, n>100 axons, Day 2 adults at 20°C. ****p<0.0001, n.s – not significant (one-way ANOVA with Tukey's correction).

3.9 CTBP-1 regulates SMDD development cell- and non-cell-autonomously

Next, I was interested in whether CTBP-1a functions cell-autonomously from the SMDD neurons to regulate axonal development. I first drove *ctbp-1a* cDNA in a subset of neurons (SMD, SAA, SDQ, ALN and PLN neurons) under the 4kb *lad-2* promoter [55]. Driving *ctbp-1a* cDNA under the neuronal *lad-2* promoter in *ctbp-1a(tm5512)* mutants completely rescued the SMDD curl phenotype in two out of three extrachromosomal lines (Figure 3.14A). The third line partially rescued the SMDD curl penetrance (line #3, Figure 3.14A). Therefore, expressing CTBP-1a solely from a subset of neurons, including SMD, is sufficient to restore correct SMDD axon morphology. Together with the endogenous rescue data, these results suggest that CTBP-1a regulates SMDD development cell-autonomously due to the spatial overlap between the *ctbp-1a* and *lad-2* promoters in the SMD neurons.

The SMDD axons grow in the dorsal sublateral cord between the muscle and hypodermis [6]. Hypodermal cells can act as a growth substrate surface for axon growth [15]. CTBP-1 was

previously shown to be expressed in both the nervous system and hypodermis [93], and recently, single cell sequencing analysis also reported that *ctbp-1* is expressed in the neurons and at a lower level in the hypodermis [171]. Therefore, I was interested in whether CTBP-1 expressed in the hypodermal tissue can regulate SMDD axonal development. I expressed *ctbp-1a* cDNA under the 249 bp hypodermal-specific *dpy-7* promoter. Driving *ctbp-1*a cDNA under the hypodermal *dpy-7* promoter partially rescued the SMDD curl penetrance of *ctbp-1a(tm5512)* mutants (Figure 3.14B). This suggests that CTBP-1a can also function non-cell-autonomously from the hypodermis to control SMDD development.

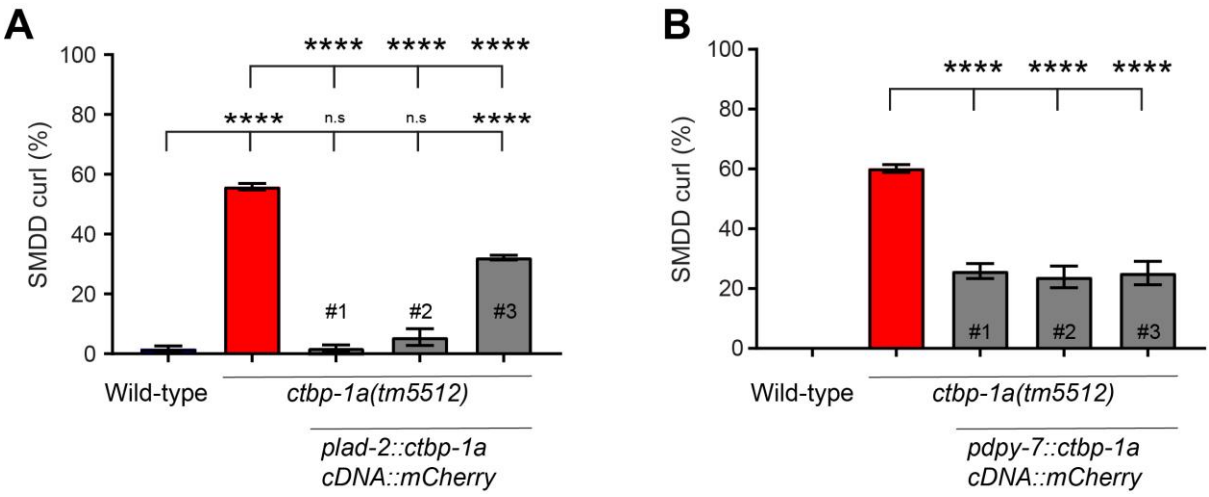

Figure 3.14 Resupplying *ctbp-1* cDNA in the SMDD neurons or hypodermis can rescue the c*tbp-1a* mutant SMDD axon guidance defects.

(A-B) Quantification of SMDD curl phenotype (%) when driving *ctbp-1a* cDNA expression in neurons (A) or hypodermis (B). Data presented as mean ± SEM (bar) of 3 biological replicates, n>100 axons, Day 2 adults at 20°C. ****p<0.0001, n.s – not significant (one-way ANOVA with Tukey's correction).

3.10 The THAP domain of CTBP-1a is important for regulation of SMDD development

Results from genetic mutant and tissue-specific rescue analysis demonstrate that the longer CTBP-1a, but not the shorter CTBP-1b isoform, is involved in SMDD axonal development. I hypothesised that the specific domains that are present in the longer isoform CTBP-1a, and absent in CTBP-1b, are important for the function of CTBP-1a in SMDD development. Present at the N-terminus of only CTBP-1a is a THAP domain that is predicted to have DNA binding properties [86, 87]. THAP domains contain a C2CH signature of metal-coordinating residues

(three cysteines and a single histidine). Mutagenesis of each cysteine or histidine residue to a smaller, hydrophobic alanine residue results in loss of DNA-binding activity [87]. These mutations do not affect the protein translation or stability [87]. To determine if the THAP domain is required in CTBP-1-regulated SMDD development, I mutated the first two cysteines of the endogenously expressed *ctbp-1a* cDNA rescue construct to alanines (C5A and C10A) using site-directed mutagenesis. The *ctbp-1a cDNA(C5A,C10A)* rescue construct did not rescue the SMDD curl phenotype of *ctbp-1a(tm5512)* mutant animals (Figure 3.15A). These data suggest that the THAP domain may be vital for CTBP-1 control of SMDD development. To explore this further, I made a construct that solely contains the THAP domain driven by the endogenous *ctbp-1a* promoter. This construct contains the 140 amino acids found in CTBP-1a but not CTBP-1b: amino acids 1-89 comprise the THAP domain and amino acids 90-140 consist of part of the linking domain to the dehydrogenase domain [68]. Two out of five transgenic lines containing *pctbp-1a::THAP only cDNA::mCherry* partially rescued the defective SMDD axons in *ctbp-1a(tm5512)* mutants (Figure 3.15B). These data suggest that the THAP domain may be solely responsible for CTBP-1a's function in regulating SMDD development.

CTBP-1a also contains a PXDLS-binding cleft that is essential for interaction with PXDLS-containing proteins [60, 69]. Mutating a small, hydrophobic alanine (A) residue to a larger, negatively charged glutamic acid (E) residue within the PXDLS-binding cleft disrupts the ability of mammalian CtBP to bind the partner protein, viral E1A protein [65]. The analogous mutation in *C. elegans* CTBP-1 (A203E) was also shown to disrupt the interaction with the zinc-finger protein PAG-3 [68]. To determine whether the PXDLS-binding function of CTBP-1 is necessary for regulating SMDD development, I generated the A203E mutation in the endogenous *ctbp-1a* cDNA rescue construct and analysed SMDD axon morphology. The *ctbp-1a cDNA(A203E)* rescue construct was able to completely rescue the defective SMDD axon phenotype of *ctbp-1a(tm5512)* mutants (3 independent lines, Figure 3.15C). This demonstrates that the PXDLS-binding domain is not essential for the function of CTBP-1 in regulating SMDD development.

Together, this structure-functional analysis suggests that the DNA-binding capacity of the CTBP-1a THAP domain, and not interactions with corepressor proteins, is important for the function of CTBP-1a in controlling SMDD axonal development.

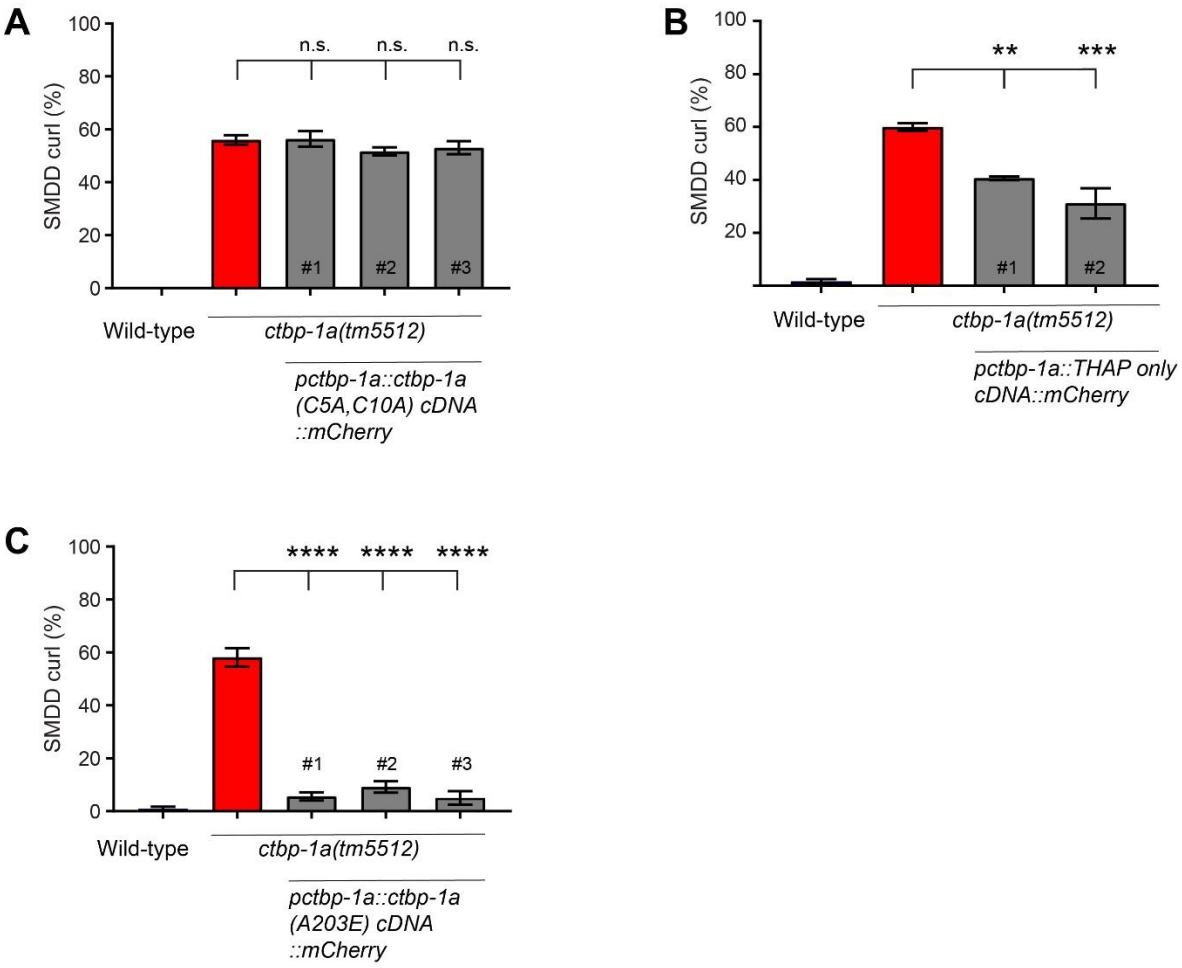

Figure 3.15 The THAP domain of CTBP-1a is sufficient to rescue SMDD curls.
(A-C) Quantification of SMDD curl phenotype (%) in wild-type, mutant and transgenic animals containing *ctbp-1a* cDNA with mutated cysteines of the THAP domain (A), THAP domain only (B), or *ctbp-1a* cDNA with mutated PXDLS binding motif (C). Data presented as mean ± SEM (bar) of 3 biological replicates, n>100 axons, Day 2 adults at 20°C. *p<0.05, ***p<0.001,****p<0.0001, n.s – not significant (one-way ANOVA with Tukey's correction).

3.11 CTBP-1a, but not CTBP-1b, is involved in exploration behaviour

We previously observed that *ctbp-1* reduction-of-function mutants are defective in exploration behaviour [93]. These experiments were performed using a well-established exploration behaviour assay [163]. In this assay, a single young adult animal was allowed to explore a uniformly seeded bacterial lawn for 16 hours overnight. The next day, the animal was removed and I recorded the number of squares the animal tracks entered (a maximum of 177 squares can be entered) (Figure 3.16A). Because the previous study exhibited that *ctbp-1* hypomorph mutants displayed reduced exploration behaviour, I wanted to determine whether the different

isoforms of CTBP-1 have independent roles in exploration behaviour. I performed exploration behaviour assays on the CRISPR-Cas9 isoform-specific and null mutants (for details of mutation alleles, see Section 3.2). The *ctbp-1a(tm5512)* mutants exhibited decreased exploration behaviour compared to wild-type (~28 and ~82 squares, respectively) (Figure 3.16B). The *ctbp-1a/b(tm5512aus14)* mutants also exhibited decreased exploration behaviour (~35 squares), and this was not significantly different to the *ctbp-1a(tm5512)* mutants (Figure 3.16B). The *ctbp-1b(aus15)* mutants explored to a similar extent as wild-type animals (~80 and ~84 squares, respectively) (Figure 3.16C). Therefore, CTBP-1a, but not CTBP-1b, is involved in regulating exploration behaviour.

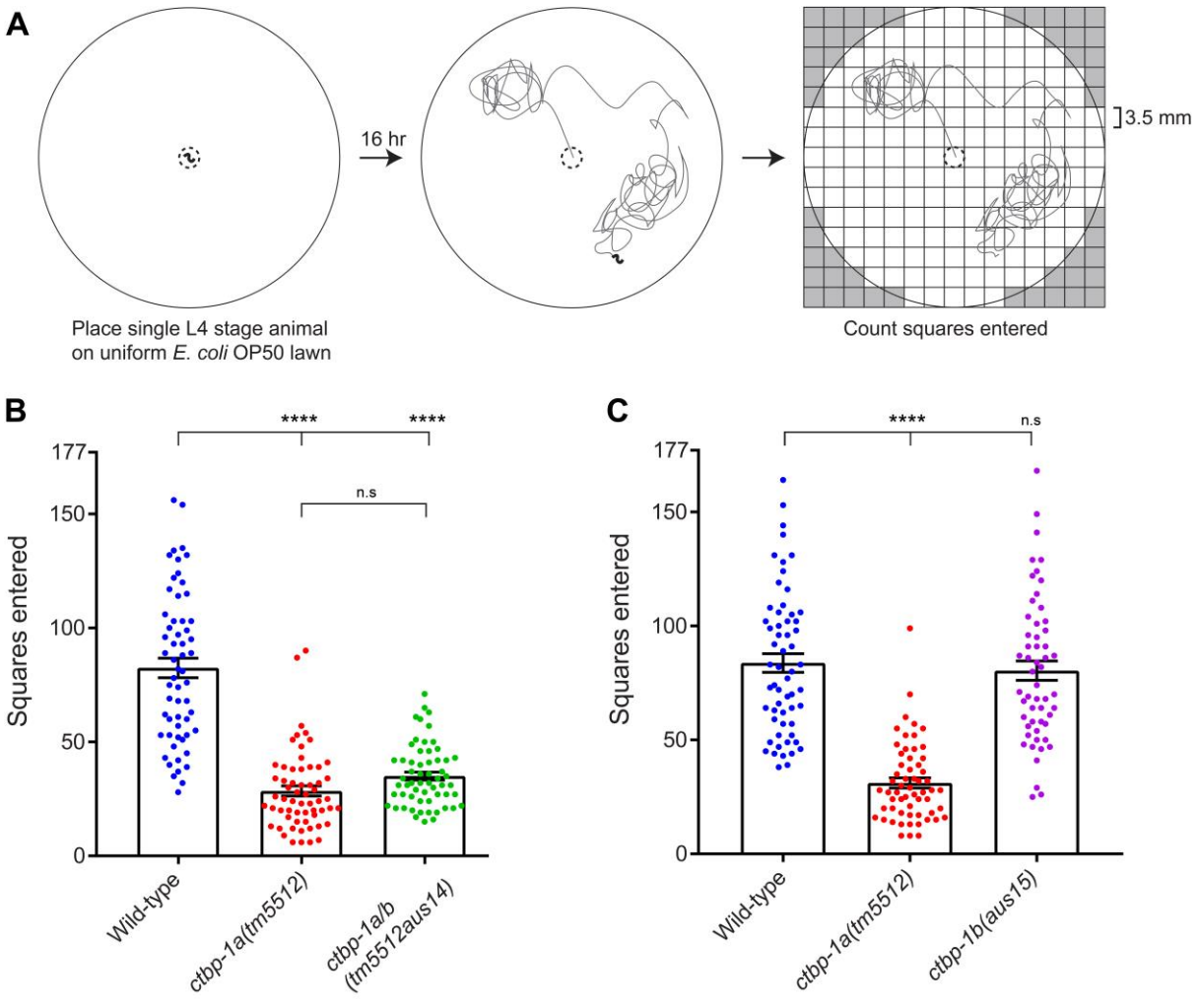

Figure 3.16 CTBP-1a controls exploration behaviour.

(A) Schematic of the exploration behaviour assay. Animals can enter a maximum of 177 squares. (B-C) Exploration assay data of *ctbp-1* mutants. Data presented as individual animal (points) with mean ± SEM (bar) of 3 biological replicates, n>55 young adult animals at 25°C. ****p<0.0001, n.s– not significant (one-way ANOVA with Tukey's correction). (A) and (B) performed separately; the number of squares entered can vary from day to day, so all mutants are compared with controls tested in parallel.

3.12 Discussion

We recently identified a novel role for the *C. elegans* C-terminal binding protein in the development of the nervous system [93]. In this chapter, I further characterized the role of CTBP-1 in controlling axonal development of the SMD motor neurons. Using isoform-specific mutant alleles generated using CRISPR-Cas9, I demonstrated the longer CTBP-1a isoform, but not the shorter CTBP-1b isoform, regulates dorsal SMD axon guidance, outgrowth, termination, and exploration behaviour. Based on these distinct functions for CTBP-1 isoforms, I investigated whether the THAP domain, present only in the CTBP-1a isoform, was involved in regulating SMDD axon guidance. My isoform-specific and structure-function rescue analysis revealed that the DNA-binding THAP domain is required for correct SMD development. Furthermore, I found that CTBP-1a functions both cell-autonomously and non-cell-autonomously to regulate SMDD axonal development.

CTBP-1 regulates SMDD axon guidance and termination

After outgrowth from the ventral side of the nerve ring, the SMDD axons extend along the dorsal sublateral cord during larval stages until adulthood [6, 25]. Such continuous outgrowth and guidance throughout larval stages contrasts from the majority of neurons in *C. elegans* that complete development during embryogenesis or early larval stages. Therefore, these SMDD axons may be controlled by distinct regulatory mechanisms. We previously identified a novel role for CTBP-1 in regulating SMDD axonal morphology [93]. In this study, we observed that *ctbp-1* hypomorphic mutants exhibit defective SMDD axonal morphology at the L4 stage, where the axons curled away from the dorsal sublateral cord [93]. To understand how CTBP-1a regulates SMDD axonal development, I performed detailed temporal analysis on SMDD axonal morphology during larval development and adulthood. I found that CTBP-1a regulates both the guidance and termination of SMDD axon outgrowth. When CTBP-1a is lost, the SMDD axons are misguided, curling away from the dorsal sublateral cord (Figure 3.5). These guidance defects first appear in late larval development (L4 stage), suggesting that early axon outgrowth is regulated independently from CTBP-1. Furthermore, the *ctbp-1a* guidance defects increased in severity and penetrance as the animals aged, suggesting that CTBP-1 functions primarily in later life to regulate SMDD axonal development. *ctbp-1a* mutant animals also display aberrant overgrowth, where axons overextend beyond their correct position. These SMDD overextension defects are first detectable earlier than the axon guidance defects (L3 vs L4 stage, respectively) (Figure 3.6). As the SMDD axons ultimately overextend beyond their correct termination position, I refer to these as axon termination defects. Interestingly, *ctbp-1a* mutants display termination defects irrespective of whether the axons were present in the

dorsal sublateral cord or were misguided away from this fascicle. This was the first evidence to suggest that CTBP-1-regulated SMDD axon extension occurs from within the SMDD neurons and not from the external environment. Using the *pctbp-1a::GFP* transgenic reporter, I also showed that CTBP-1a regulates SMDV axon guidance. The SMDV axons extend along the ventral sublateral cord [6]. When *ctbp-1a* was mutated, the SMDV axons displayed similar axon guidance defects to the SMDDs, where they curled away from the ventral sublateral cord (Figure 3.11). Although it was not quantified, I observed that the SMDV axons also displayed overextension defects. Taken together, these findings demonstrate that CTBP-1a functions to regulate the guidance and termination of the SMD motor neuron axons. In contrast, the *ctbp-1b* mutants displayed wild-type SMDD axon guidance and termination, demonstrating that the shorter CTBP-1b isoform does not regulate SMDD axonal development (Figure 3.8). These results suggested that domains present only in the CTBP-1a isoform control SMDD axonal development.

When does CTBP-1a regulate SMDD axonal development?

The results in this chapter demonstrated that CTBP-1a regulates SMDD axon extension in the later stages of larval development and adulthood. Interestingly, I observed that CTBP-1 is expressed in the SMDD neurons from early in embryogenesis through to adulthood (Figure 3.10). The SMDD axons first extend during embryogenesis to pioneer the nerve ring [11]. Although CTBP-1a is expressed during these embryonic stages, it does not appear to function in regulating early SMDD outgrowth, as all axons in *ctbp-1a* mutant animals extend along the dorsal sublateral cord, at least partially before guidance errors occur. Also, the SMDD axon guidance and termination defects of *ctbp-1a* mutants are only apparent later in development, but the timing of this regulation is unclear. As CTBP-1 is a transcriptional repressor, it is potentially regulating the expression of particular genes at distinct time points to ensure correct SMDD axonal development. To explore the timing of this regulation, we could knockdown *ctbp-1a* expression at different developmental stages using RNA interference or auxin-inducible degradation. Previously, unbiased RNA interference (RNAi) screens have identified many genes involved in axon guidance and axon regeneration [172, 173]. Knockdown of *ctbp-1* at different larval stages could reveal when *ctbp-1* is required and whether earlier expression is sufficient to regulate later stages of axonal development. Recently, the auxin-inducible degradation (AID) system that enables rapid target protein degradation was optimized for *C. elegans* [174]. AID could be used to analyse CTBP-1a function by degrading CTBP-1 at specific developmental stages. In addition, AID-mediated protein degradation is reversible, therefore the effect of loss of CTBP-1a could be analysed dynamically in short developmental time frames. Both of these techniques also allow tissue-specific knockdown, so depletion of

CTBP-1a in particular tissues could reveal both the timing and location of CTBP-1 function in order to regulate SMDD axonal development.

CTBP-1a acts cell-autonomously to regulate SMDD development

Using the *pctbp-1a::GFP* transcriptional reporter, I found that CTBP-1a is expressed in the SMDD neurons. This expression pattern suggested that CTBP-1a acts cell-autonomously to regulate SMDD axonal development. Consistent with this, complete rescue of *ctbp-1a* axon guidance defects occurred by driving *ctbp-1a* cDNA expression with the *ctbp-1a* promoter or *lad-2* promoters, which drive overlapping expression in the SMD neurons (Figure 3.10) [55]. Ideally, a cell-specific promoter would be used to drive CTBP-1a expression solely in the SMD neurons. To date, however, there are no reported SMD-specific promoters. The *lad-2* promoter is thus far the most specific for the SMD neurons, as it drives expression in only 5 classes of neurons [55]. The *pctbp-1a::GFP* marker I have reported in this chapter has limited expression in the nervous system, and the only axons that are visible are the four SMD axons (Figure 3.10). Deletions could be made in the *ctbp-1a* 5kb promoter construct (promoter deletion analysis) to potentially reveal specific promoter sequence that specifically drives SMD expression. However, the fact that we are able to rescue the *ctbp-1a* mutant SMDD developmental defects with two independent promoters that overlap in the SMDDs strongly supports a cell-autonomous function for CTBP-1a.

Interestingly, ectopic *ctbp-1a* expression from the surrounding hypodermal tissue was also able to partially rescue the SMDD axon guidance defects (Figure 3.10). The outgrowth of the SMDD axon in the dorsal sublateral tract is normally tightly constrained by the surrounding hypodermis and muscle cells (Figure 1.3). These results suggest that expressing CTBP-1a from the surrounding hypodermis can partially restore correct SMDD axon guidance. Whether CTBP-1a is normally expressed and regulates gene transcription in the hypodermis is currently unclear. The *ctbp-1a* promoter construct used for complete SMDD axon guidance rescue did not reveal detectable hypodermal expression, suggesting that SMDD axonal development does not require CTBP-1 regulation from this tissue (Figure 3.10). Previously, a translational reporter that drove expression of both CTBP-1 isoforms displayed low levels of hypodermal expression [89]. This reporter tagged both CTBP-1 isoforms at the C-terminus, and therefore the individual expression patterns of CTBP-1a and CTBP-1b are not able to be distinguished. It is therefore possible that only the CTBP-1b isoform is expressed in the hypodermis. If this is the case, and CTBP-1a is not usually expressed in the hypodermis, these rescue results suggest that ectopic CTBP-1a can function from nearby tissues to regulate downstream targets, and hence SMDD axonal development.

The CTBP-1a THAP domain is required for regulating SMDD axonal development

The isoform-specific mutations first revealed that the longer CTBP-1a isoform, but not the shorter CTBP-1b isoform, controls SMDD axonal development. The principal difference between these two isoforms is that CTBP-1a contains an additional N-terminal THAP domain (Figure 3.2). Proteins that contain THAP domains can act as transcriptional repressors by directly binding promoter sequences, and this requires a zinc-dependent C2CH motif [87]. I hypothesized that the CTBP-1a THAP domain may directly regulate gene transcription through this DNA-binding motif. Indeed, the structure-function rescue experiments revealed that mutation of cysteine residues in the THAP motif of CTBP-1a inhibited its ability to rescue *ctbp-1a* mutant SMDD axon guidance defects (Figure 3.15). These cysteine mutations were previously shown to remove the DNA-binding activity of the human THAP1 protein, but importantly these mutations did not cause THAP1 protein instability [87]. I further found that expressing the CTBP-1a THAP domain alone is sufficient to partially rescue SMDD defects of *ctbp-1a(tm5512)* animals (Figure 3.15). In contrast, mutating the PXDLS binding motif of CTBP-1a did not change the rescuing ability of CTBP-1a (Figure 3.15). Previously identified functions for CTBP-1 in transcriptional regulation required the PXDLS binding motif to bind corepressor proteins [65, 68]. My data instead suggests that the THAP domain of CTBP-1a can directly regulate transcription and hence axonal development.

CTBP-1a is the first example of a THAP-containing protein being involved in *C. elegans* neuronal development. Other *C. elegans* THAP-containing proteins have essential roles in tissue development. For example, it has long been known that the THAP transcriptional factor LIN-15B regulates vulval development [175]. Additionally, the THAP-containing GON-14 is a pleotropic regulator of larval development, controlling growth, gonadogenesis and vulval development [176]. Although other *C. elegans* THAP domains have not shown to regulate neuronal development, studies in mammalian models suggest that the role of THAP domains in controlling nervous system development may be conserved. Human THAP1 functions as a transcription factor that directly binds DNA to regulate cell-cycle and proliferation pathway genes [87, 177]. Several mutations in the THAP domain of THAP1 have been shown to cause DYT6 primary dystonia, a neurological disorder that leads to involuntary muscle contractions [178, 179]. Mutations in the THAP domain impair DNA binding function [179]. Thap1 null mice are embryonic lethal, therefore partial loss-of-function mouse models have been analysed [180, 181]. Heterozygous Thap1$^{+/-}$ mice display decreased numbers of cerebellar large projection neurons in the cerebellum and decreased striatal medium spiny neuron (MSN) neurite outgrowth [180, 182]. Similarly, mice with conditional Thap1 knockout in the nervous system display decreased dendritic branching in striatal MSNs [181]. Additionally, both Thap1

reduction-of-function mouse models display defective motor function [180, 181]. RNA-sequencing of Thap1$^{+/-}$ mutants revealed dysregulated genes involved in axonal guidance and synaptic plasticity [182].

Because THAP domains can directly bind DNA, CTBP-1a regulation of SMDD axonal development may be dependent on direct transcriptional regulation by the THAP domain. It is unknown what specific sequence the CTBP-1a THAP domain can bind to. The Nicholas lab previously published that the *C. elegans* CTBP-1 THAP could bind to the sequence recognized by human THAP1 using gel-shift assays [85]. However, later experiments found this to be non-sequence specific binding [88]. This is unsurprising as the consensus binding sites for THAP domains within and across different species reported so far are all unique [183]. The identification of THAP domain binding sites in the past have used a variety of methods, including SELEX (systematic evolution of ligands by exponential enrichment) and ChIP-seq (chromatin immunoprecipitation sequencing) [183]. To determine what DNA sequence CTBP-1a-THAP recognises, I would perform whole-genome ChIP-seq to identify the motif that CTBP-1a THAP directly binds to and identify putative target genes. ChIP-seq would also theoretically reveal motifs bound by the corepressor CTBP-1-containing complex, therefore a mutated-THAP control may allow us to distinguish between the DNA sequences bound by the canonical CTBP-1 corepressor complex and those bound by the THAP domain. Optimally, these ChIP-seq experiments would require the CTBP-1a isoform to be tagged at the endogenous locus. Unfortunately, my attempts to tag the individual CTBP-1 isoforms interfered with the protein function and will require further optimization, which I will discuss next.

Alternative methods for tagging CTBP-1

Because the CTBP-1a and CTBP-1b isoforms play distinct roles in SMDD development, we asked whether this was due to different spatial expression patterns. In order to understand which tissue CTBP-1a functions in to regulate SMDD axonal development, I first tagged the N-terminus of CTBP-1a and CTBP-1b with mCherry protein. Analysis of these tagged strains revealed that the resultant fusion proteins were nonfunctional, as these animals displayed SMDD axon guidance defects. The presence of the large mCherry tag at the endogenous locus could be interfering with protein folding or stability of CTBP-1a or could be directly preventing the putative DNA-binding of the N-terminal THAP domain. Taken together with the results demonstrating that the THAP domain is important for CTBP-1's role in SMDD development, it is perhaps not surprising that the N-terminal mCherry tag directly preceding the THAP domain made the CTBP-1a protein non-functional. Future experiments to determine the expression pattern of the individual isoforms could tag the N-terminus of CTBP-1a and CTBP-1b with

smaller tags, such as HA or FLAG, which may not disrupt the protein structure and function. These smaller tags could be used for immunostaining experiments to determine the expression pattern. In addition, if the small CTBP-1a N-terminal tag did not interfere, these strains could be used for the aforementioned ChIP-seq experiments to determine the binding sequence of the CTBP-1a THAP domain. However, these smaller tags may still disrupt the CTBP-1a THAP domain function due to their proximity with the N-terminus. The constructs used for rescuing SMDD axon defects in *ctbp-1a* mutant animals contained mCherry fused to the *ctbp-1a* cDNA C-terminus (Figure 3.13), demonstrating that the presence of a C-terminal mCherry tag did not cause the CTBP-1a protein to become nonfunctional. Therefore endogenous fluorescent tags on the C-terminus could be added using CRISPR-Cas9. Because this method would tag both isoforms at their shared C-terminus, one could subsequently mutate the transcriptional start site of *ctbp-1b*, so that this shorter isoform is unable to be transcribed. Repeating this, but instead mutating the *ctbp-1a* transcriptional start site, would allow for analysis of each isoform's expression.

CTBP-1a autoregulation

In the course of investigating the role of CTBP-1a in axonal development, I also found that CTBP-1a autoregulates its own expression. This is supported by two lines of evidence. Firstly, *ctbp-1a* mRNA is upregulated in *ctbp-1a* mutants (Figure 3.3). Conversely, the *ctbp-1b* transcript levels did not change in *ctbp-1a* mutants, demonstrating that the upregulation occurs specifically to compensate for the lost CTBP-1a isoform (Figure 3.3). Second, I observed increased *pctbp-a::GFP* levels in *ctbp-1a* mutants, indicating that the *ctbp-1a* promoter is being upregulated when CTBP-1a function is lost (Figure 3.12). These results lead to the conclusion that CTBP-1a levels are autoregulated at the transcriptional level. This autoregulation is possibly a conserved function for THAP family members. The human THAP1 transcription factor regulates its own expression by specifically binding to and repressing its own promoter [184]. Mutations in THAP1 caused higher THAP1 expression levels in neuronal human induced pluripotent stem cells, as quantified by qPCR [184]. Autoregulation of *Thap1* mRNA levels was also evident in Thap1 mouse models, where heterozygous Thap1$^{+/-}$ mice display upregulation of *Thap1* mRNA levels to compensate for the reduction of Thap1 expression [181]. This increase in expression when THAP1 is mutated is remarkably similar to the increased expression levels I observed when CTBP-1a is mutated.

Are the defective SMDD axons in *ctbp-1* mutants functional?

In this chapter, I observed that when CTBP-1a is lost, the SMD axons are misguided and aberrantly overextend into incorrect regions. This prompted the question of whether the SMDs are able to properly function as motor neurons when misplaced. *C. elegans* axons form *en passant* synapses, requiring close proximity to connect to their synaptic partners [6]. The SMDs are one of the five classes of motor neurons with axons that run in the sublateral cords to innervate body wall muscle cells [10]. Along the anterior region of the sublateral cords, acetylcholine is extensively released, suggesting that functioning synapses form between axons in the sublateral tract and the muscles [10]. When *ctbp-1a* is mutated, these axons are misplaced in different body regions, and could therefore be losing synaptic connections or forming ectopic synapses. When we first observed the mild axon curl defects in L4 stage *ctbp-1a* mutants, we investigated whether the axon could form synapses [93]. Indeed, the pre-synaptic marker RAB-3 localised and clustered to the misguided distal tip of the SMDD axon in L4 stage *ctbp-1a* mutant [93]. We were unable to analyse the RAB-3 pattern of expression in the portion of the SMDD axon that extended along the dorsal sublateral cord, since the marker was widely expressed in many neurons in/near this region [93]. Nonetheless, these results demonstrated that ectopic presynapses were forming on SMD axons that curl away from the dorsal sublateral cord. My findings demonstrate that the mild curl phenotype worsens as the animals age so that the axons are misplaced from their correct position, and may therefore form ectopic synapses with inappropriate partners. In addition, the mutant SMD neurons that overextend in the dorsal sublateral cord may inappropriately innervate more posterior muscle cells.

As the SMD neurons function as motor neurons, a possible assay to determine whether SMDs function appropriately when CTBP-1a is lost would be to analyse body movement/locomotion. In this chapter, I began investigating this using the exploration behavior assay, where I demonstrated that *ctbp-1a* mutants displayed decreased exploration behavior (Figure 3.16). *C. elegans* explore their environment with forward movement and occasional turns and reversals. These movements are regulated by sensory neurons, interneurons and motor neurons in response to different conditions, including the presence of food [13]. Significantly reduced exploration behaviour could be caused by changes in behaviour responses or general defects in locomotion [163]. As SMDD motor neurons function in key aspects of locomotion, including head bending and omega turn amplitude [12-14], I hypothesise that the decreased exploration behaviour of *ctbp-1a* mutants can be attributed, at least partially, to defective SMDD development. Exploration assays were performed on young adult animals, and at this stage, the majority of SMDD axons are misguided and/or overextended (Figure 3.5-3.6).

Previous studies of SMD function have focused on the effects of cell ablation [12-14]. Recently, Yeon *et al.* analysed the function of the SMDD and SMDV neurons individually, and observed that targeted SMDD ablation induces ventral circling locomotion while SMDV ablation induces dorsal circling locomotion [14]. They demonstrated that the SMD neurons steer forward locomotion, where SMDD and SMDV neurons regulate dorsal head movement and SMDV regulate ventral movement [14]. Interestingly, Yeon *et al.* further observed that *ctbp-1(ok498)* hypomorph mutants displayed a ventral circling phenotype similar to that observed when the SMDD cell bodies are ablated [14]. Yeon *et al.* attributed this movement phenotype to the defective SMDD axon morphology we previously reported [93]. My work, however, has demonstrated that both the SMDD and SMDV axons are defective when *ctbp-1a* is mutated. Thus, I speculate that whilst there are locomotion defects in *ctbp-1* mutants, locomotion defects would not be directed towards a particular orientation. My results in this chapter indicate that the posterior portion of the axon is misplaced when CTBP-1 regulation is lost, and therefore I predict that it is the synaptic connections to the body wall muscles that will be altered. Detailed analysis of the movement of the isoform-specific mutants could be performed to determine the effect of these misplaced axons.

4. Candidate screen to identify genes involved in CTBP-1-regulated SMDD development

4.1 Introduction

In the previous chapter, I demonstrated that the transcriptional repressor CTBP-1a regulates the development of the SMDD axons. Thus far, we have not identified any genes that act in the CTBP-1-regulated SMDD axonal development pathway. In this chapter, I performed epistasis experiments with putative CTBP-1 target genes, as well as genes with known neuronal roles, to determine if they are involved in SMDD axonal development.

4.2 Identifying putative CTBP-1 target genes through analysing microarray datasets

As CTBP-1 functions as a transcriptional repressor, I predict that downstream genes are upregulated when CTBP-1a is lost, causing defects in SMDD axon outgrowth. To identify these upregulated genes, I analysed two available microarray datasets performed on *ctbp-1* hypomorphic mutants compared to wild-type. Previously, Yang Shi's group published a genome-wide expression microarray comparing *ctbp-1(ok498)* mutant and wild-type populations [90]. The *ctbp-1(ok498)* allele used for this study is a 1629 bp in-frame deletion that results in a largely absent dehydrogenase-like domain [90]. The *ok498* allele truncates both CTBP-1a and CTBP-1b proteins, resulting in predicted proteins that are 457 and 336 amino acids long, respectively. We previously showed that *ctbp-1(ok498)* mutant animals display mild defective SMDD axons at the L4 stage [93]. The *ok498* microarray was performed on populations of wild-type and *ctbp-1(ok498)* mutant young adults. Out of 22000 genes represented on the microarray, 243 genes were changed by >2 fold, and 213 (90%) of these were upregulated [90].

In addition, the Nicholas lab performed a microarray comparing *ctbp-1(eg613)* mutant and wild-type populations (unpublished). The *eg613* mutation is a splice site mutation of G to A in the last nucleotide of *ctbp-1a* intron 9 [91]. It is predicted to generate a premature stop codon towards the end of the dehydrogenase-like domain, resulting in truncated CTBP-1a and CTBP-1b proteins of 387 and 266 amino acids, respectively [91]. We previously observed that *ctbp-1(eg613)* mutant animals also display mild levels of defective SMDD axons at the L4 stage [93]. Only 2 biological replicates of wild-type and *ctbp-1(eg613)* populations were analysed. This resulted in a microarray dataset with low significance power, with no differentially expressed genes able to be determined. Although these results cannot be verified statistically,

I asked if any of the >2 fold upregulated genes overlapped with the >2 fold upregulated genes in the published *ctbp-1(ok498)* microarray.

I processed the two microarray datasets to determine what genes were upregulated in both *ctbp-1* hypomorphic mutant backgrounds compared to wild-type. I found that 48 genes were upregulated in both microarrays, and I further narrowed down this list to 12 genes that have known expression in the nervous system and/or hypodermis (Figure 4.1). These tissues were of interest as I demonstrated in the last chapter that CTBP-1a can function from the SMDD neurons and the hypodermis to control SMDD axonal development. This expression pattern analysis was performed using the Wormmine tool that extracts expression patterns published on WormBase (http://intermine.wormbase.org/tools/wormmine/begin.do).

A

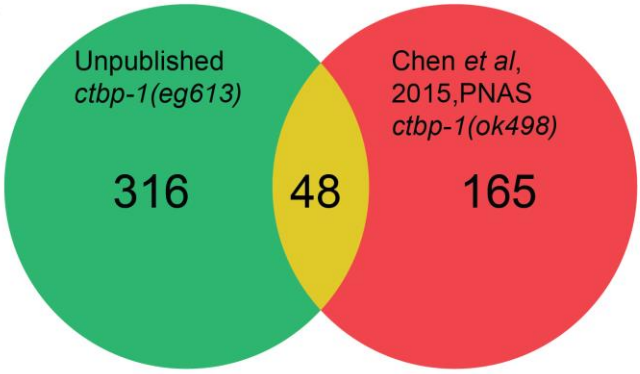

B

Sequence name	Gene name	Known expression
ZK377.1	*wrt-6*	neurons, hypodermis
ZK1290.8	*wrt-10*	hypodermis
Y47D7A.5	*grl-5*	hypodermis
Y65B4BR.6	*grl-16*	hypodermis
F28F8.2	*acs-2*	neurons, hypodermis
ZK75.1	*ins-4*	neurons
T05D4.4	*osm-7*	hypodermis
F57C12.1	*nas-38*	hypodermis
R09B5.9	*cnc-4*	hypodermis
F58H1.2		hypodermis
R12E2.7		hypodermis
C42D4.3		hypodermis

Hedgehog (Hh)-related genes

Figure 4.1 Upregulated genes identified in two microarray datasets.

(A) Venn diagram of 48 genes present in both independent datasets. (B) Genes with reported expression in neurons and/or hypodermis. Four *Hedgehog(Hh)*-related genes highlighted in yellow.

Of particular interest was the fact that 4 of the 12 overlapping upregulated genes expressed in the hypodermis and/or nervous system are *Hedgehog(Hh)*-related genes. *C. elegans Hh*-related genes share sequence similarity to *Drosophila* and vertebrate Hedgehog genes, which have known roles in neuronal development e.g. [23, 24]. Recently, a role for *Hh*-related genes in *C. elegans* neurodevelopment was identified [22]. Overexpression of the *Hh*-related genes *wrt-8* and *grl-16* during embryogenesis caused PVQ axon guidance defects [22].

4.3 SMDD defects caused by CTBP-1 mutations cannot be replicated with RNAi

RNA mediated interference (RNAi) is a technique that decreases gene expression by targeting mRNA molecules for destruction [185]. I aimed to use RNAi to determine the effect of knocking down candidate genes in a *ctbp-1a* mutant background on SMDD neuronal development. Before using this method for a screen of putative CTBP-1 target genes, I tested whether RNAi would replicate the *ctbp-1a* mutant SMDD phenotype. Because CTBP-1 can function cell-autonomously to regulate SMDD development (Chapter 1), it is important that knockdown occurs in both tissues. The *C. elegans* nervous system is naturally resistant to RNAi treatment, partially attributed to the absence of the transmembrane protein SID-1 in neuronal cells [186]. To achieve systemic knockdown, SID-1 is expressed pan-neuronally under the *unc-119* promoter (*uIs69* (*punc-119::sid-1*)) [186] (Figure 4.2). I crossed the *uIs69* transgene into wild-type and *ctbp-1a(tm5512)* mutant animals. I treated these animals with empty vector RNAi and assayed day 1 adults at 25°C. I also performed these RNAi assays on animals without the *uIs69* (*punc-119::sid-1)* transgene to determine the effect of RNAi knockdown in non-neuronal tissue. Unexpectedly, the *uIs69; ctbp-1a(tm5512)* mutant displayed increased SMDD defects relative to *ctbp-1a(tm5512)* animals when treated with empty vector (~80% and ~48%, respectively) (Figure 4.2B). There was also an increase in defective SMDD axons from wild-type to *uIs69* (0% to ~10%) (Figure 4.2B). Increased SMDD defects in *uIs69* transgenic animals also occurred at the L4 stage (2 biological replicates, data not shown). This suggests that the ectopic presence of the SID-1 channel is causing neuronal changes that exacerbate SMDD defects.

I also performed *ctbp-1* RNAi with the same conditions. The *ctbp-1* RNAi vector targets the last two exons of both isoforms, so is predicted to knockdown both CTBP-1a and CTBP-1b [158]. Knocking down *ctbp-1* in wild-type and *uIs69* backgrounds did not replicate SMDD defects seen with *ctbp-1a* mutants (Figure 4.2B). Therefore, this demonstrates that RNAi

knockdown of *ctbp-1,* either systemic or in non-neuronal tissues only, does not phenocopy SMDD axon guidance defects.

Taken together, these results suggest that neuronally-enhanced RNAi causes non-specific neuronal defects, and RNAi does not sufficiently knock-down *ctbp-1*. Therefore, it is not an appropriate technique to study the role of CTBP-1 or putative CTBP-1 target genes in neuronal development. Due to the inability to perform RNAi experiments, I performed all subsequent epistasis experiments by using mutant alleles that were publicly available or I made using CRISPR-Cas9.

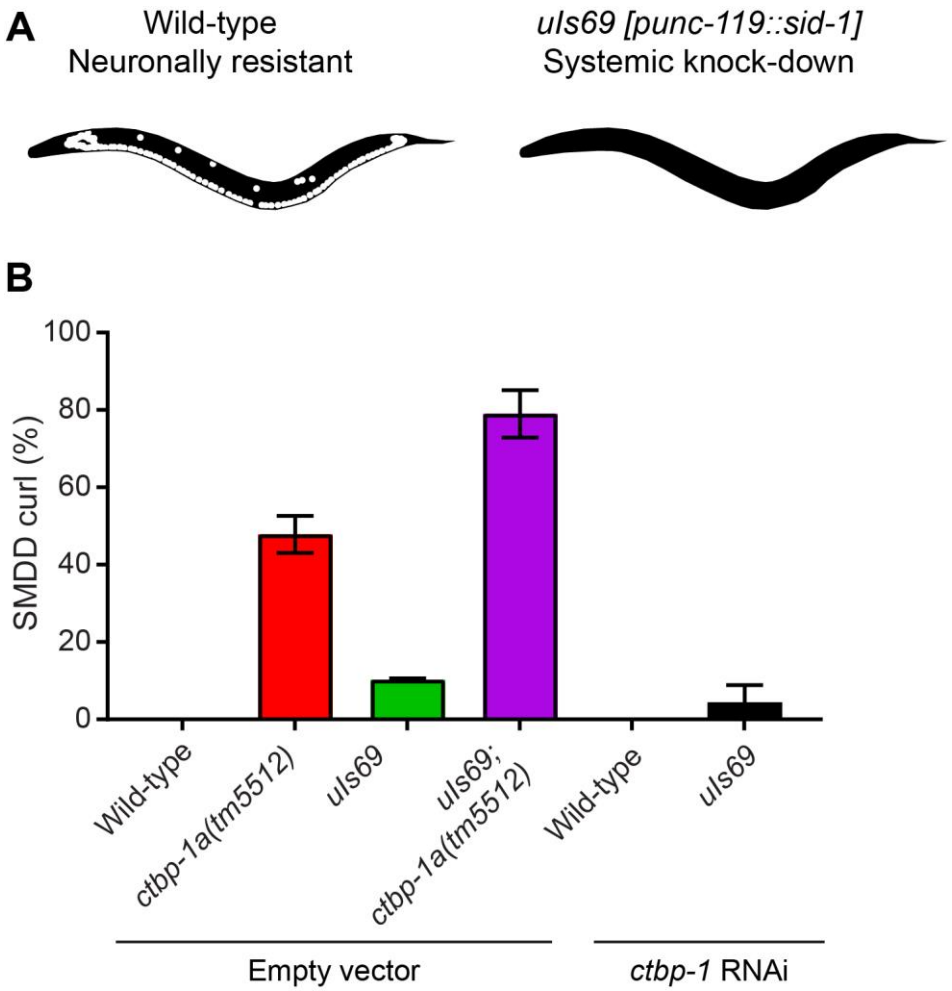

Figure 4.2 *ctbp-1* knockdown does not phenocopy *ctbp-1* mutations.
(A) Schematic of resistance of wild-type or *uIs69* transgenic worms to RNAi treatment, where black tissues have expected knockdown by RNAi treatment. (B) Quantification of SMDD curl (%) in wild-type, transgenic and mutant animals after RNAi treatment with empty or *ctbp-1* RNAi vectors. Day 1 of adulthood at 25°C, n>60 axons. Data presented as mean ± SD (bar) of 2 biological replicates (statistical tests were not performed).

4.4 CRISPR-Cas9-generated *wrt-6* and *wrt-10* mutants

Before beginning double mutant analysis, I assessed which genes had reduction-of-function or null alleles available. There were no published mutants available for *wrt-6* or *wrt-10* so I used CRISPR-Cas9 to generate random mutations.

The first gene I targeted using CRISPR-Cas9 was the *Hh*-related gene *wrt-6.* WRT-6 has one protein isoform that is 593 amino acids long [187]. I designed a sgRNA to target the first exon of *wrt-6* (Figure 4.3A). I injected wild-type animals with the sgRNA, Cas9 and co-injection marker, and generated three separate lines containing different large frameshift deletions spanning the PAM site (Figure 4.3B). The *aus41* deletion resulted in a premature stop codon whereas the *aus42* and *aus43* deletions resulted in amino acid changes for the majority of the protein (Figure 4.3B). It is likely that *wrt-6(aus41)* is a null allele due to the premature stop codon after 7 amino acids, so this allele was used for future assays.

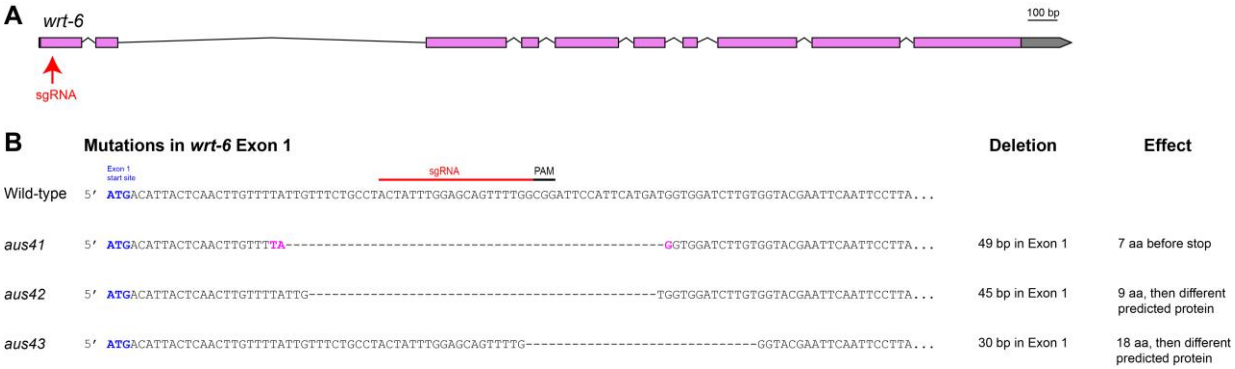

Figure 4.3 New *wrt-6* alleles generated by CRISPR-Cas9.
(A) Schematic of *wrt-6* gene locus, where the sgRNA (red arrow) targets the first exon. Exons (pink boxes), introns (solid lines) and untranslated regions (grey boxes) are indicated; 5' is on the left. (B) Mutations made in wild-type sequence of *wrt-6* exon 1. Dashes indicate deleted bases in mutant alleles: *aus41* is a 49 bp deletion, *aus42* is a 45 bp deletion and *aus43* is a 30 bp deletion. 5' is on the left, transcriptional start site indicated in blue.

The same process was designed for the *Hh*-related gene *wrt-10*. WRT-10 is expressed throughout all life stages in the hypodermis, and has one protein isoform that is 258 amino acids long [187, 188]. I designed a sgRNA to target the first *wrt-10* exon, and performed CRISPR-Cas9 on wild-type animals as described above (Figure 4.4A). This resulted in two separate deletion alleles (5 bp and 2 bp in *aus36* and *aus37* respectively). Both *wrt-6(aus36)* and *wrt-10(aus37)* alleles cause frameshifts and premature stop codons, and are predicted

null mutants based on the peptide length (Figure 4.4B). Both alleles were used for further analysis.

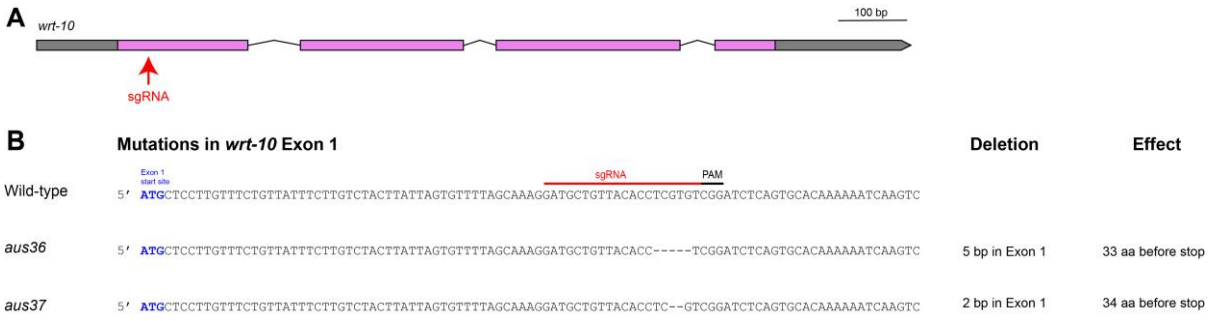

Figure 4.4 New *wrt-10* alleles generated by CRISPR-Cas9.
(A) Schematic of *wrt-10* gene locus, where the sgRNA (red arrow) targets the first exon. Exons (pink boxes), introns (solid lines) and untranslated regions (grey boxes) are indicated; 5' is on the left. (B) Mutations made in wild-type sequence of *wrt-10* exon 1. Dashes indicate deleted bases in mutant alleles: *aus36* is a 5 bp deletion and *aus37* is a 2 bp deletion. 5' is on the left, transcriptional start site indicated in blue.

These *wrt-6* and *wrt-10* mutant alleles were viable and displayed no gross morphological phenotypes. We have published details of these alleles in the microPublication article “New deletion alleles for *Caenorhabditis elegans* Hedgehog pathway-related genes *wrt-6* and *wrt-10*” [189]. These strains are now available to the worm community at the *Caenorhabditis* Genetics Center (CGC).

4.5 Candidate CTBP-1 target genes

During this project, I analysed 7 out of 12 candidate CTBP-1-target genes I identified through the microarray analysis. I analysed the SMDD axons of single and double mutants to determine whether these genes have a role in SMDD development, dependent or independent of CTBP-1. If the candidate genes are normally repressed by CTBP-1 in the context of SMDD axonal development, removing their function in a *ctbp-1* mutant background may restore wild-type SMDD axon development. Alternatively, if the phenotype worsened in double mutants, it means these genes are likely to function in parallel pathways to control SMDD axonal development.

4.5.1 WRT-6 and WRT-10

The first genes of interest were two members of the *C. elegans* Hedgehog-related (Hh-related) pathway: *wrt-6* and *wrt-10*. The *warthog* family member *wrt-6* encodes a predicted secreted signalling molecule that contains an N-terminal Wart domain and a C-terminal autoprocessing domain (Hint or Hog domain) [187, 190, 191]. *wrt-10* encodes another member of the *warthog* family and contains the Wart domain but lacks the Hog domain [187, 191]. Previously, RNAi knockdown of *wrt-6* and *wrt-10* revealed they function in multiple aspects of *C. elegans* development, including growth and movement [192]. However, no known neuronal roles for these Hh-related genes have been identified.

WRT-6 is expressed in hypodermal and neuronal sheath and socket cells [187]. WRT-10 is expressed throughout all life stages in the hypodermis [187, 188]. As detailed in section 4.3, I first generated putative null *wrt-6* and *wrt-10* mutants. I found that *wrt-6(aus41)* mutant animals displayed wild-type SMDD axons (Figure 4.5A). Furthermore, the *wrt-6(aus41); ctbp-1a(tm5512)* mutants did not enhance or reduce SMDD axon curl defects of *ctbp-1a(tm5512)* mutants (Figure 4.4A). The same trend was identified for *wrt-10*. The two *wrt-10* mutants, *wrt-10(aus36)* and *wrt-10(aus37),* displayed normal SMDD axon guidance (Figure 4.4B). Both of the double *wrt-10; ctbp-1a* mutants displayed the same penetrance of curly SMDD axons as the *ctbp-1a(tm5512)* mutants (Figure 4.4B). This demonstrates that neither *wrt-6* nor *wrt-10* are involved in SMDD development.

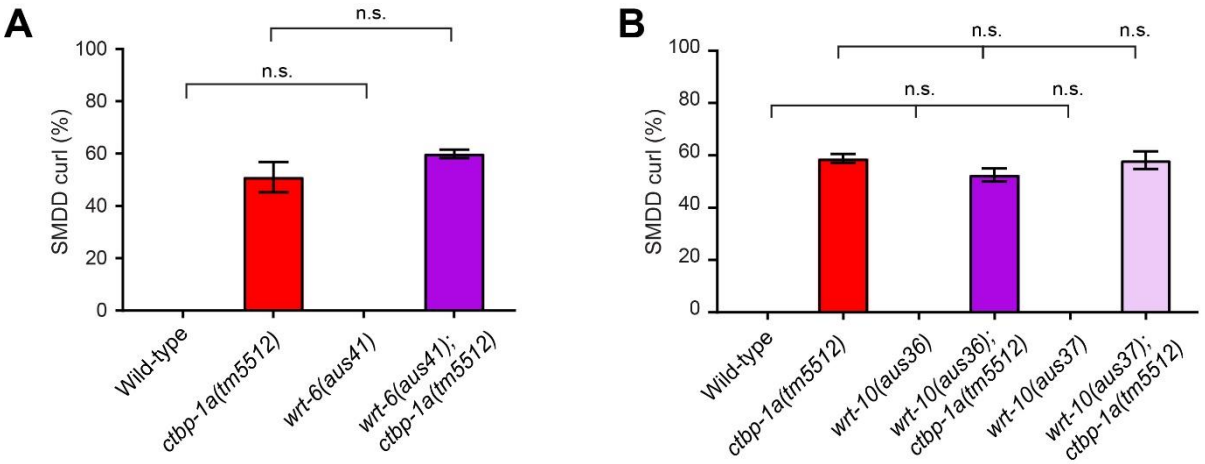

Figure 4.5 The *Hh*-related genes *wrt-6* and *wrt-10* are not involved in SMDD development.
(A-B) Quantification of SMDD curls (%) of *wrt-6* (A) and *wrt-10* (B) mutants, day 1 adults at 25°C. Data presented as mean ± SEM (bar) of 3 biological replicates, n>60 axons. n.s – not significant (one-way ANOVA with Tukey's correction).

4.5.2 GRL-5 and GRL-16

The next genes of interest were *grl-5* and *grl-16*. These genes are members of the *ground-like* (*grl*) family of Hedgehog-related genes. Recently, it was shown that overexpression of *grl-16* during embryogenesis caused PVQ axon guidance defects, where the axons cross over the ventral midline as they extend anteriorly [22]. These axon guidance defects also occurred after overexpression of another Hedgehog-related gene *wrt-8* [22]. This was the first study to identify a role for *Hh*-related signalling in *C. elegans* axon guidance, and suggests that *Hh*-related genes can act as novel axon guidance cues.

GRL-5 is expressed in the hypodermis and rectal epithelial cells [188]. Two mutant alleles were available for *grl-5*: *ok2700* and *ok2671*. The *ok2700* deletion is 365 bp deletion over the last two exons (Figure 4.6A, WormBase). The *ok2671* allele is a complex substitution where a G nucleotide substitutes a 623 bp deletion that covers the last two exons and 3'UTR (Figure 4.6, WormBase). Both mutations are predicted to remove the majority of the predicted GRL-5 protein. Both of the *grl-5* mutants displayed wild-type SMDD axons (Figure 4.6B-C). The double *grl-5; ctbp-1a* mutants did not significantly differ in defective SMDD axon curl penetrance from *ctbp-1a* mutants (Figure 4.6B-C). These data demonstrate that *grl-5* is not involved in SMDD development.

GRL-16 is predicted to be enriched in several tissues, including the hypodermis and nervous system (WormBase). There are no published expression patterns for *grl-16*, but preliminary results from Sharlynn Wu (Nicholas lab) indicated that *grl-16* was expressed in the hypodermis and rectal epithelial cells (Honours thesis [193]). This aligns with the hypodermal expression previously observed for many Hedgehog genes [187, 188]. Recently, single cell sequencing analysis reported that *grl-16* is highly expressed in the hypodermis and at a lower level in neurons [171]. There are 3 predicted *grl-16* isoforms, and the *ok2959* deletion removes 473 bp over the first intron and second exon shared between all isoforms (Figure 4.6D, WormBase). The *grl-16* mutant animals displayed wild-type SMDD axons (Figure 4.6E). The double *grl-16(ok2959); ctbp-1a(tm5512)* mutants did not enhance or reduce SMDD axon defects of *ctbp-1a(tm5512)* mutants (Figure 4.6E), demonstrating that *grl-16* does not play a role in SMDD axonal development.

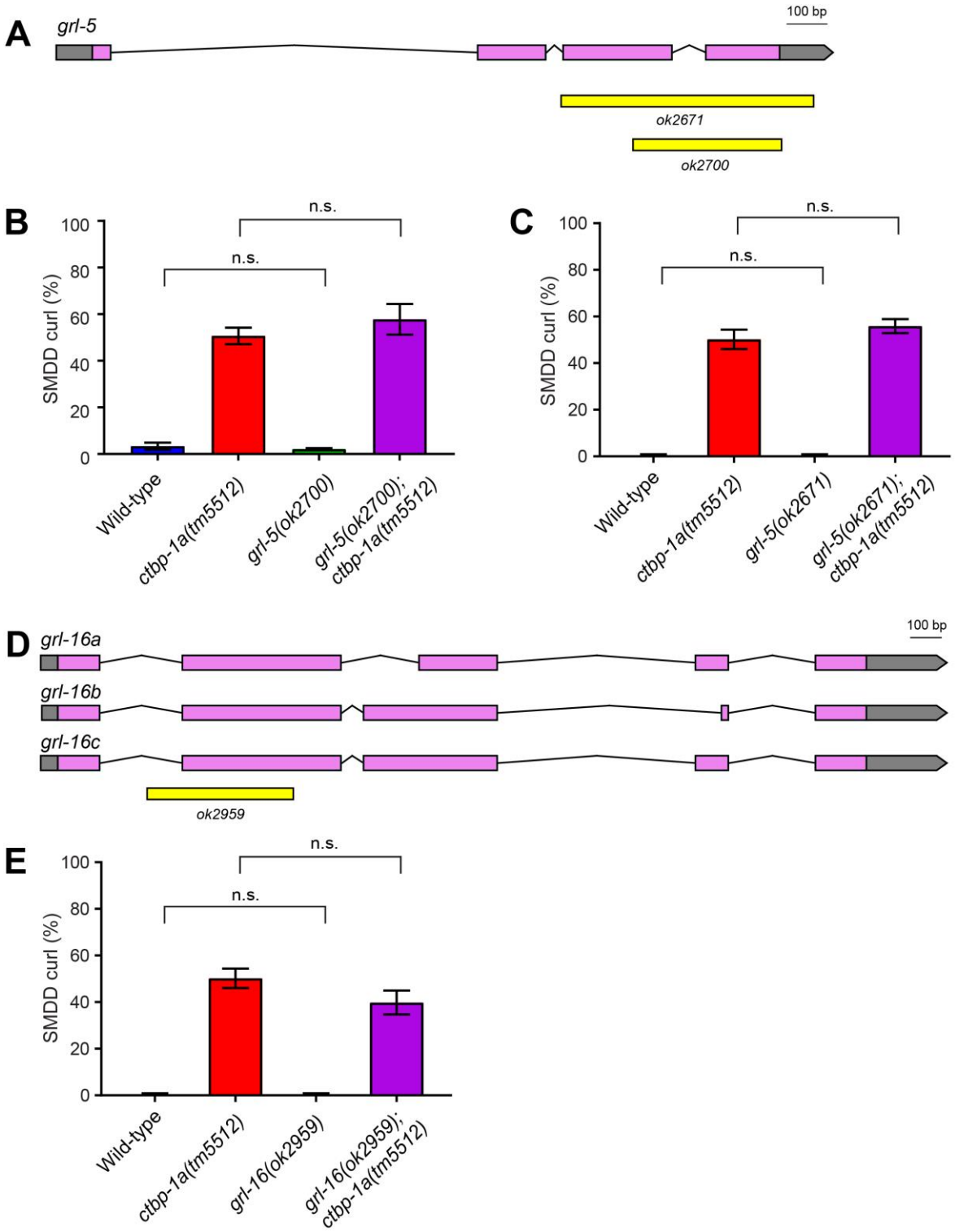

Figure 4.6 The *Hh*-related genes *grl-5* and *grl-16* are not involved in SMDD axonal development. (A) Schematic of *grl-5* genomic locus, with the position of the *ok2671* and *ok2700* deletions (yellow boxes). Exons (pink boxes), introns (solid lines) and untranslated regions (grey boxes) are indicated; 5' is on the left. Adapted from WormBase. (B-C) Quantification of SMDD curl phenotype (%) of *grl-5* mutants, day 1 adults at 25°C. Data presented as mean ± SEM (bar) of 3 biological replicates, n>60 axons. n.s – not significant (one-way ANOVA with Tukey's correction). (D) Schematic of *grl-16* gene

locus, with the position of the *ok2959* deletion (yellow box). *grl-16* has three isoforms, *a-c*. Exons (pink boxes), introns (solid lines) and untranslated regions (grey boxes) are indicated; 5' is on the left. Adapted from WormBase. (E) Quantification of SMDD curl phenotype (%) of *grl-16* mutants, day 1 adults at 25°C. Data presented as mean ± SEM (bar) of 3 biological replicates, n>60 axons. n.s – not significant (one-way ANOVA with Tukey's correction).

4.5.3 INS-4

INS-4 is one of 40 insulin-like peptides (ILPs) encoded in the *C. elegans* genome and is expressed throughout the larval stages and adulthood in many cell types, including the nervous system and hypodermis [194, 195]. INS-4 is secreted from sensory and motor neurons and acts as an agonist of the insulin-like growth factor receptor DAF-2 [196]. INS-4 acts redundantly with other ILPs to regulate dauer formation, L1 arrest and synaptic development [196-198].

The *ok3534* allele was publicly available but details of the exact mutation have not been published (pending curation on CGC and WormBase). I sequenced the *ins-4* genomic region of wild-type and *ins-4(ok3534)* mutant animals with Sanger sequencing and determined that *ok3534* is a 415 bp deletion over the start site and exon 1 (Figure 4.7A, Appendix Figure 8.3). The large deletion of the promoter and transcriptional start site leads me to predict *ok3534* is a null allele.

Mutating *ins-4* does not cause defective SMDD axons in day 1 adults (Figure 4.7B). The double *ins-4; ctbp-1a* mutant displayed a mild reduction in curly SMDD axon phenotype, relative to *ctbp-1*a mutants (~36% and ~50% respectively, $p<0.05$) (Figure 4.7B). This suggests that *ins-4* may play a role in CTBP-1-regulated SMDD development. I subsequently examined SMDD axons of L4 stage animals to see whether loss of *ins-4* activity in a *ctbp-1* mutant background would consistently rescue SMDD axons at different life stages. At the L4 stage, there was no significant reduction of curly SMDD axons between double *ins-4; ctbp-1a* and single *ctbp-1a* mutants (Figure 4.7C). These results suggest that *ins-4* may be involved in only the later stages of SMDD axon guidance. To investigate the adulthood defects further, I performed length analysis of SMDD axons of day 1 adult animals to see whether the length defect of *ctbp-1a* mutants was reduced in double *ins-4; ctbp-1a* mutants. As previously observed, *ctbp-1a* mutant animals have significantly increased SMDD axon length compared to wild-type animals (~200 µm and ~165 µm respectively, $p<0.0001$, Figure 4.7D). The average length of the double *ins-4; ctbp-1*a mutant was the same as the single *ctbp-1a* mutant (~220 µm for both, Figure 4.7D), suggesting that *ins-4* is not involved in regulating SMDD axon termination. These

inconsistent results mean that I cannot conclude that INS-4 is involved in regulating SMDD axonal development, but it may play a minor role.

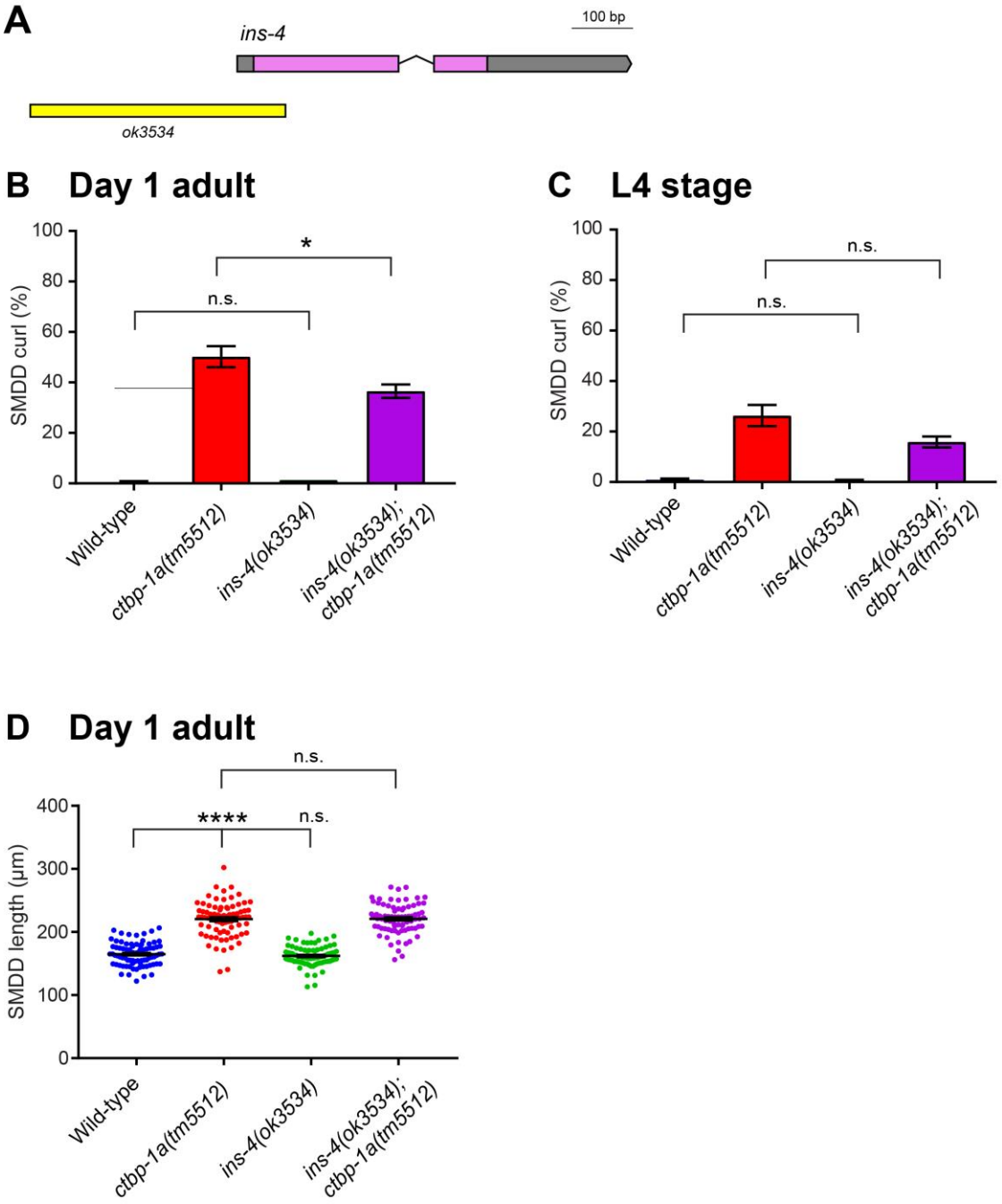

Figure 4.7 *ins-4* may be involved in late stages of SMDD axonal development.

(A) Schematic of *ins-4* genomic locus, with the position of the *ok3534* deletion (yellow box). Exons (pink boxes), introns (solid lines) and untranslated regions (grey boxes) are indicated; 5' is on the left. Adapted from WormBase. (B-C) Quantification of SMDD curl phenotype (%) of day 1 adult (B) and L4 stage animals at 25°C (C). Data presented as mean ± SEM (bar) of 3 biological replicates, n>100 axons. *p<0.05, n.s– not significant (one-way ANOVA with Tukey's correction).

(D) Length of SMDD axons of wild-type and mutant day 1 adult animals at 25°C. Data presented as individual axon lengths (points) with mean ± SEM (bar) of 2 pooled biological replicates, n>75 axons. ****p<0.0001, n.s – not significant (one-way ANOVA with Tukey's correction).

4.5.4 ACS-2

ACS-2 is an acyl-CoA synthetase that catalyses the conversion of fatty acids to Acyl-CoA, which is an essential step in fatty acid metabolism for energy production. Accordingly, ACS-2 plays an important role in metabolism, and RNAi inhibition of *acs-2* causes increased fat storage [199, 200]. ACS-2 localizes to mitochondria in many tissues, including hypodermis, muscle, intestine and neurons [199].

The *ok2457* mutation is a 1394 bp deletion that would remove the majority of the protein, including the translational start site (Figure 4.8A, WormBase). Due to the lack of most of the protein, including the translational start site, this is predicted to be a null allele. At day 1 of adulthood, *acs-2(ok2457)* mutants displayed normal SMDD axons (Figure 4.8B). The double *acs-2(ok2457); ctbp-1a(tm5512)* mutants did not enhance or reduce the defective SMDD axon penetrance of *ctbp-1a(tm5512)* mutant (Figure 4.8B), demonstrating that *acs-2* is not involved in CTBP-1 regulated SMDD axonal development.

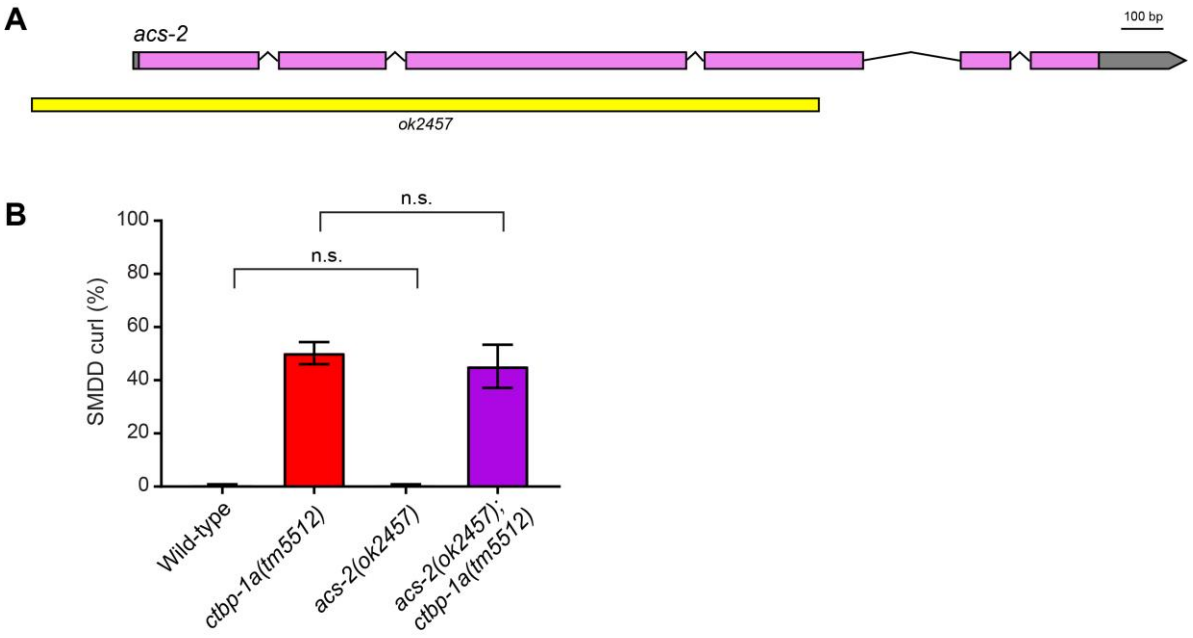

Figure 4.8 *acs-2* is not involved in SMDD axonal development.
(A) Schematic of *acs-2* genomic locus, with the position of the *ok2457* deletion (yellow box). Exons (pink boxes), introns (solid lines) and untranslated regions (grey boxes) are indicated; 5' is on the left. Adapted from WormBase. (B) Quantification of SMDD curl phenotype (%) of wild-type and mutant animals. Data

presented as mean ± SEM (bar) of 3 biological replicates, n>100 axons. **p<0.01, ***p<0.001, n.s – not significant (one-way ANOVA with Tukey's correction).

4.5.5 NAS-38

NAS-38 is one of 40 *C. elegans* astacin-like metalloproteases and is expressed in the hypodermis, seam cells and rectal epithelial cells [201, 202]. Inhibition of *nas-38* by RNAi leads to extension of lifespan [203]. NAS-38 was identified as a candidate synaptic remodelling gene through RNAi and suppressor screens, but no further studies have been performed [204].

The *ok3407* allele was not previously characterised, so I performed Sanger sequencing to determine the nature of the mutation (Appendix Figure 8.4). The wild-type *nas-38* transcript consists of 17 exons, and the NAS-38 protein is 745 amino acids long (WormBase). The *ok3407* mutation is a 378 bp deletion over the last 3 exons (exons 15-17), so it is possible that the mutated protein has residual function (Figure 4.9, Appendix Figure 8.4).

The SMDD assays performed for the other candidate genes could not be performed for single *nas-38* and double *nas-38; ctbp-1* mutants. The single and double *nas-38(ok3407)* mutants were sick and did not grow at the same rate as the wild-type and *ctbp-1a(tm5512)* controls at either 20°C or 25°C. I scored a population of ~40 animals once they reached the L4 stage and found that *nas-38(ok3407)* mutant animals displayed wild-type axons (0% defective SMDD axons). Double *nas-38; ctbp-1a(tm5512)* mutant animals displayed 32% defective SMDD axons, which does not differ from the average single *ctbp-1a(tm5512)* percentage at L4 stage. The lack of observable changes in SMDD defects meant that I did not pursue *nas-38* as a candidate gene any further.

Figure 4.9 Schematic of *nas-38* genomic locus.
Position of the *ok3407* deletion (yellow box). Exons (pink boxes), introns (solid lines) and untranslated regions (grey boxes) are indicated; 5' is on the left. Adapted from WormBase.

In summary, I analysed putative CTBP-1 target genes to determine if they function in CTBP-1a-regulated SMDD axon development. These seven genes, with varying predicted functions, were not involved in SMDD axon guidance. The results of the SMDD curl assays performed on the analysed genes is summarised in Table 4.1.

Table 4.1 Summary of the SMDD curl phenotype (%) of candidate CTBP-1-regulated genes. Alleles *aus36*, *aus37* and *aus41* generated in this project. 'Wild-type vs mutant' and '*ctbp-1a(tm5512)* vs double *ctbp-1a(tm5512)*; *mutant*' represents the p-value from a one-way ANOVA followed by Tukey's correction, *p<0.05, n.s – not significant. [1] See section 4.5.5 for details on *nas-38* scoring.

			Day 1 adult at 25°C, unless specified	
Gene	**Function**	**Mutant allele**	**Wild-type vs *mutant***	***ctbp-1a(tm5512)* vs double *ctbp-1a(tm5512); mutant***
grl-5	*hedgehog*-like protein	*ok2700*	n.s	n.s
		ok2671	n.s	n.s
grl-16	*hedgehog*-like protein	*ok2959*	n.s	n.s
acs-2	acyl-CoA synthetase	*ok2457*	n.s	n.s
wrt-6	*hedgehog*-like protein	*aus41*	n.s	n.s
wrt-10	*hedgehog*-like protein	*aus36*	n.s	n.s
		aus37	n.s	n.s
ins-4	insulin-like peptide	*ok3534*	n.s	n.s at L4 stage, * at day 1
nas-38	metalloprotease	*ok3407*	--- [1]	--- [1]

4.5.6 LIPS-7

Next, I was interested in whether genes that are already known to be regulated by CTBP-1 could be involved in SMDD axonal development. The only confirmed CTBP-1-regulated gene is the triacylglycerol (TAG) lipase *lips-7*. CTBP-1 regulates both lifespan and acute functional tolerance to ethanol through repression of *lips-7* expression [89-91]. Accordingly, when *ctbp-1* is mutated, *lips-7* expression is upregulated [89, 90]. CTBP-1 regulates *lips-7* expression through the NADH binding motif [89, 90]. LIPS-7 is expressed in multiple tissues, but is primarily expressed in the hypodermis [89].

The *lips-7(ok3110)* mutant allele is a 300 bp deletion which removes the last exon and part of the 3'UTR of both *lips-7* isoforms (Figure 4.10A) [161]. At L4 stage and day 1 of adulthood, *lips-7(ok3110)* mutant animals do not display SMDD defects (Figure 4.10B). The double *lips-7(ok3110); ctbp-1a(tm5512)* mutant animals display no significant change in penetrance from single *ctbp-1a(tm5512)* mutant animals at L4 (~18% for both) or day 1 (~54% and ~57%, respectively) (Figure 4.10B). This suggests that although *lips-7* transcription is regulated by CTBP-1, LIPS-7 does not play a role in the development of the SMDD axons.

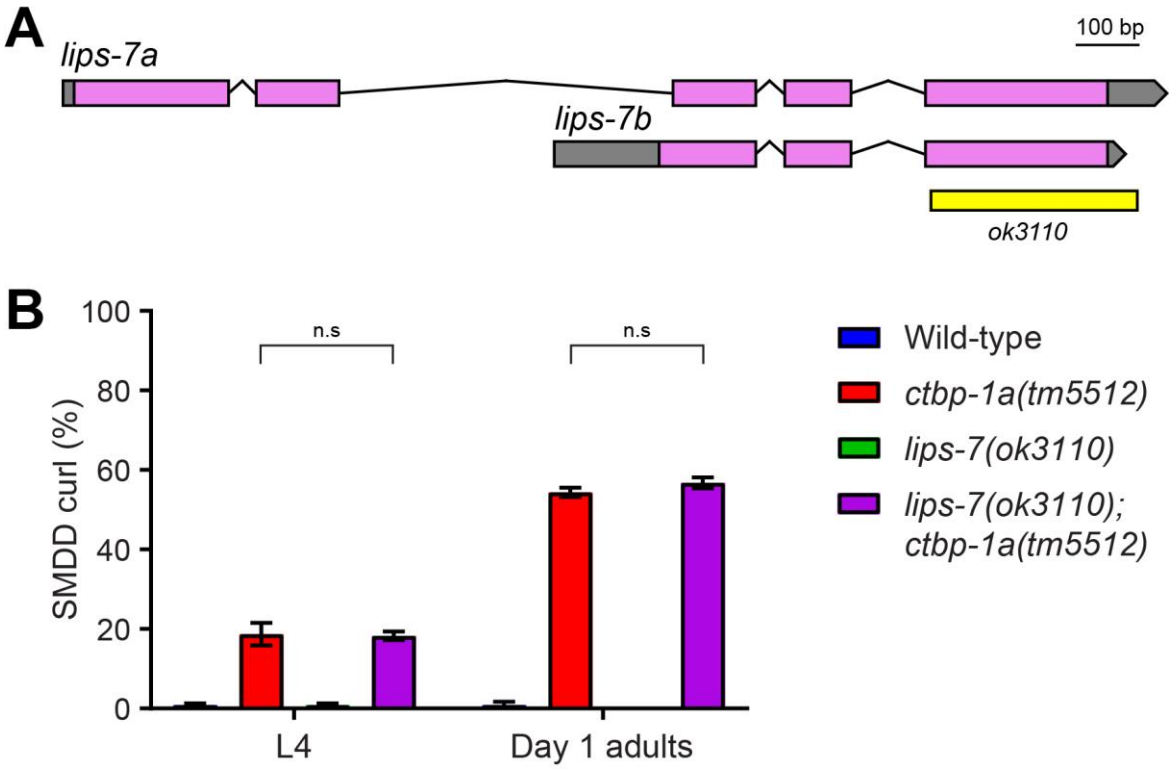

Figure 4.10 *lips-7* is not involved in SMDD development.

(A) Schematic of *lips-7* genomic locus, with the position of the *ok3110* deletion (yellow box). *lips-7* has two isoforms: *a-b*. Exons (pink boxes), introns (solid lines) and untranslated regions (grey boxes) are indicated; 5' is on the left. Adapted from WormBase. (B) Quantification of SMDD curl (%) of L4 stage and day 1 adult animals at 25°C, n>100 axons. Data presented as mean ± SEM (bar) of 3 biological replicates, n>100 axons. n.s – not significant (one-way ANOVA with Tukey's correction).

4.6 Candidate genes involved in neuronal development

I was also interested in whether genes with known roles in neuronal development were involved in SMDD development. I chose genes based on their known functions in axon guidance and termination, which is explained below for each gene, and performed epistasis experiments.

4.6.1 CWN-2

CWN-2 is one of five *C. elegans* Wnt ligands. CWN-2 is expressed mostly in the anterior half of the animal, including the pharynx, anterior body wall muscle cells and head neurons [44, 47, 205]. Specifically, *cwn-2* expression was visible in the SMD neurons [205]. Recently, *cwn-2*

was found to be the most highly expressed gene in the SMDD neurons in L4 stage animals through single-cell RNA-sequencing [206].

CWN-2 has known roles in longitudinal axon guidance. CWN-2 acts as a local attractive cue for posterior axon outgrowth of the RMED/V motor neurons [47]. RMED and RMEV motor neurons have axons that run along the dorsal and ventral cords, respectively, before terminating in the middle of the body [47]. In *cwn-2* mutant young adult animals, the RMED/V posterior axons fail to extend posteriorly and enter the longitudinal tracts [47]. This defect can be rescued by expressing *cwn-2* posterior to the nerve ring, demonstrating that CWN-2 expression is required at specific locations to attract RMED/V axon outgrowth [47].

At the L1 stage, *cwn-2* mutants also displayed incorrect outgrowth of axons that leave the nerve ring [205]. Using the *ceh-24::GFP* transgene that labels the SIA and SIB neurons, as well as two SMDs, Kennerdell *et al.* observed that axons navigated incorrectly anterior of the nerve ring [205]. They observed that the SIA and SIB sublateral motor neuron axons failed to exit the nerve ring or exited and extended into incorrect nerve cords [205]. Although this marker labels two SMD axons, Kennerdell *et al.* did not report a specific phenotype for the SMDD neurons [205]. This may be because the SMDD axons have not extended far beyond the nerve ring at this early larval stage and hence outgrowth defects would not be reliably detectable. Therefore, I aimed to investigate whether CWN-2 regulates SMDD axonal development by analysing animals at L4 stage and day 1 of adulthood, to ask if SMDD axons enter and extend along the dorsal sublateral cord.

CWN-2 is also required to regulate nerve ring placement [205]. In *cwn-2* mutant L1 stage animals, the nerve ring is shifted anteriorly. These defects can be rescued by ectopic expression from cells both anterior and posterior to the nerve ring, suggesting that the specific location of CWN-2 expression is not important [205]. The developmental timing of CWN-2 is important in this context, however, seen with heat-shock expression experiments [205]. The nerve ring defects are rescued only when CWN-2 is expressed at the comma stage of embryogenesis when the nerve ring is developing, and not when expressed after the comma stage [205]. This suggests that CWN-2 is important for the early stages of nerve ring development.

The *ok895* allele is a 905 bp deletion that removes the majority of the *cwn-2* exons, and is therefore a predicted null allele (WormBase, Figure 4.11A). This allele was used for the aforementioned studies that determined a role for CWN-2 in axon guidance [47, 205]. In the majority of *cwn-2(ok895)* mutants and double *cwn-2(ok895); ctbp-1a(tm5512)* mutants, the SMDD axons were not visible in the dorsal sublateral tract at either L4 stage or day 1 of

adulthood (Figure 4.11B, Table 4.2). The axons were visible in wild-type and *ctbp-1a(tm5512)* mutants, in previously observed ratios of straight/wild-type or curly/defective (Figure 4.11B, Table 4.2). The absence of SMDD axons in the dorsal sublateral cord in *cwn-2* mutants suggests that CWN-2 is involved early in SMDD development and that the axons either do not extend or extend in incorrect directions when *cwn-2* is lost. There were no visible axons within the dorsal or lateral cords. This suggests that if the SMDD axons are extending, they may be aberrantly growing along the VNC, where the axon growth would be obscured by other axons marked with the *pglr-1::GFP* marker. Alternatively, they may be extending anteriorly, which would also be obscured by the bright *pglr-1::GFP* marker that is expressed in multiple neuronal cell bodies and axons.

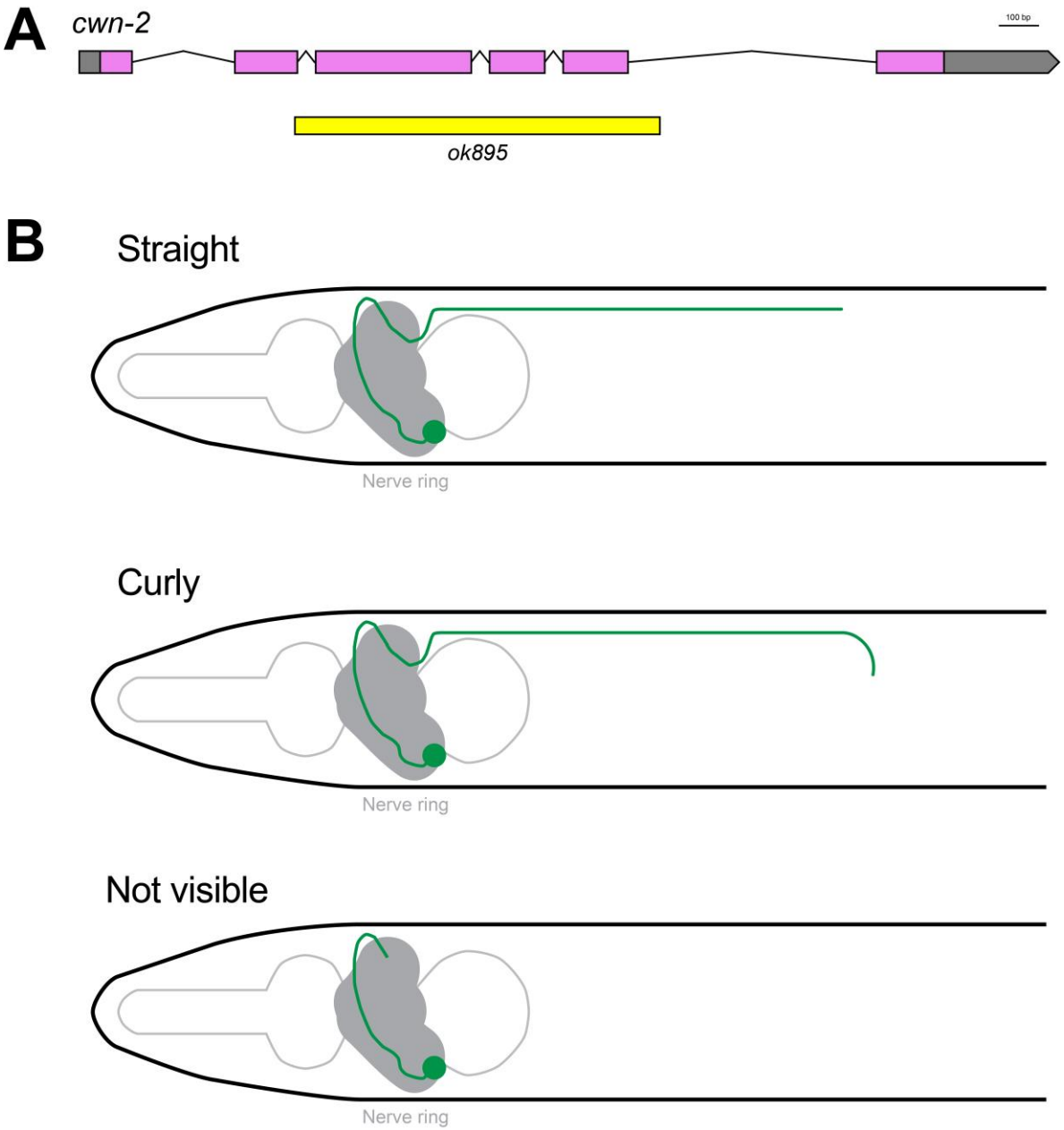

Figure 4.11 *cwn-2* mutants do not have visible SMDD axons along the dorsal sublateral cord. (A) Schematic of *cwn-2* genomic locus, with the position of the *ok895* deletion (yellow box). Exons (pink boxes), introns (solid lines) and untranslated regions (grey boxes) are indicated; 5' is on the left. Adapted from WormBase. (B) Schematic of SMDD axon phenotypes. 'Straight' axons extend along the dorsal sublateral cord, 'curly' axons curl off and leave the dorsal sublateral cord, and 'not visible' means axons are not entering or extending along the dorsal sublateral cord. SMDD neurons in green, pharynx in light grey. Table 4.2 *cwn-2* mutants do not have visible SMDD axons along the dorsal sublateral cord.

Quantification of SMDD axon morphology phenotype for wild-type and mutant animals. One replicate at 25°C, 34-40 animals at the L4 stage and day 1 of adulthood. Assay performed during Honours [207].

	L4 stage				Day 1 adults			
Genotype	Wild-type	*ctbp-1a*	*cwn-2*	*cwn-2; ctbp-1a*	Wild-type	*ctbp-1a*	*cwn-2*	*cwn-2; ctbp-1a*
Straight (%)	99	69	5	5	97	42	4	4
Curly (%)	0	30	3	3	1	55	0	3
Not visible (%)	1	1	92	93	2	3	96	97

4.6.2 RPM-1 and FSN-1

Next, I was interested in whether genes involved in axon termination would also be involved in regulating SMDD development. RPM-1 is an ubiquitin ligase closely related to the *Drosophila* presynaptic protein Highwire and the mammalian Myc binding protein Pam [208]. RPM-1 is involved in regulating axon termination and synaptic organisation [26, 208]. RPM-1 is widely expressed in the nervous system from embryogenesis until adulthood [26, 208]. In *rpm-1* mutants, mechanosensory and GABAergic motor neuron axons overextend past their termination points and can extend into incorrect body regions [26, 27]. I was interested in whether *rpm-1* also regulates SMDD axon outgrowth.

The *rpm-1(ju41)* allele is a G/A substitution that causes a premature stop codon after 3563 residues out of 3766 residues (Figure 4.12A, [208]). Although most of the protein is predicted to be translated, *ju41* acts as a strong loss-of-function mutation [208]. At the L4 stage and day 1 of adulthood, *rpm-1(ju41)* mutants displayed wild-type SMDD axons (Figure 4.12B). At the L4 stage, the double *rpm-1(ju41); ctbp-1a(tm5512*) mutant had reduced defective SMDD axons compared to *ctbp-1a(tm5512)* (~12% and ~20% respectively, $p<0.05$) (Figure 4.12B). This decrease was not seen, however, in adult animals, with the double mutants displaying ~53% defective SMDD axons compared to ~44% in *ctbp-1a* mutants (n.s) (Figure 4.12B). This inconsistent reduction in SMDD axon curl phenotype suggests that RPM-1 is not involved in SMDD axon guidance.

Because RPM-1 has been previously implicated in axon termination, I was interested to determine whether RPM-1 was also involved in SMDD axon termination. I performed SMDD axon length assays on day 1 adults. The length of the *rpm-1(ju41)* mutant SMDD axons did not significantly differ from wild-type animals (~162 and ~160 µm, respectively, Figure 4.12C), demonstrating that *rpm-1* does not play a role in SMDD axon termination. The double *rpm-1; ctbp-1a* mutant displayed a mild, yet significant, increase in axon length compared to the single *ctbp-1a* mutant (~222 and ~235 µm, respectively, Figure 4.12C). Overall, these results

demonstrate that RPM-1 is not involved in SMDD axonal development, and that CTBP-1 regulates axon outgrowth separately from RPM-1-directed axon termination.

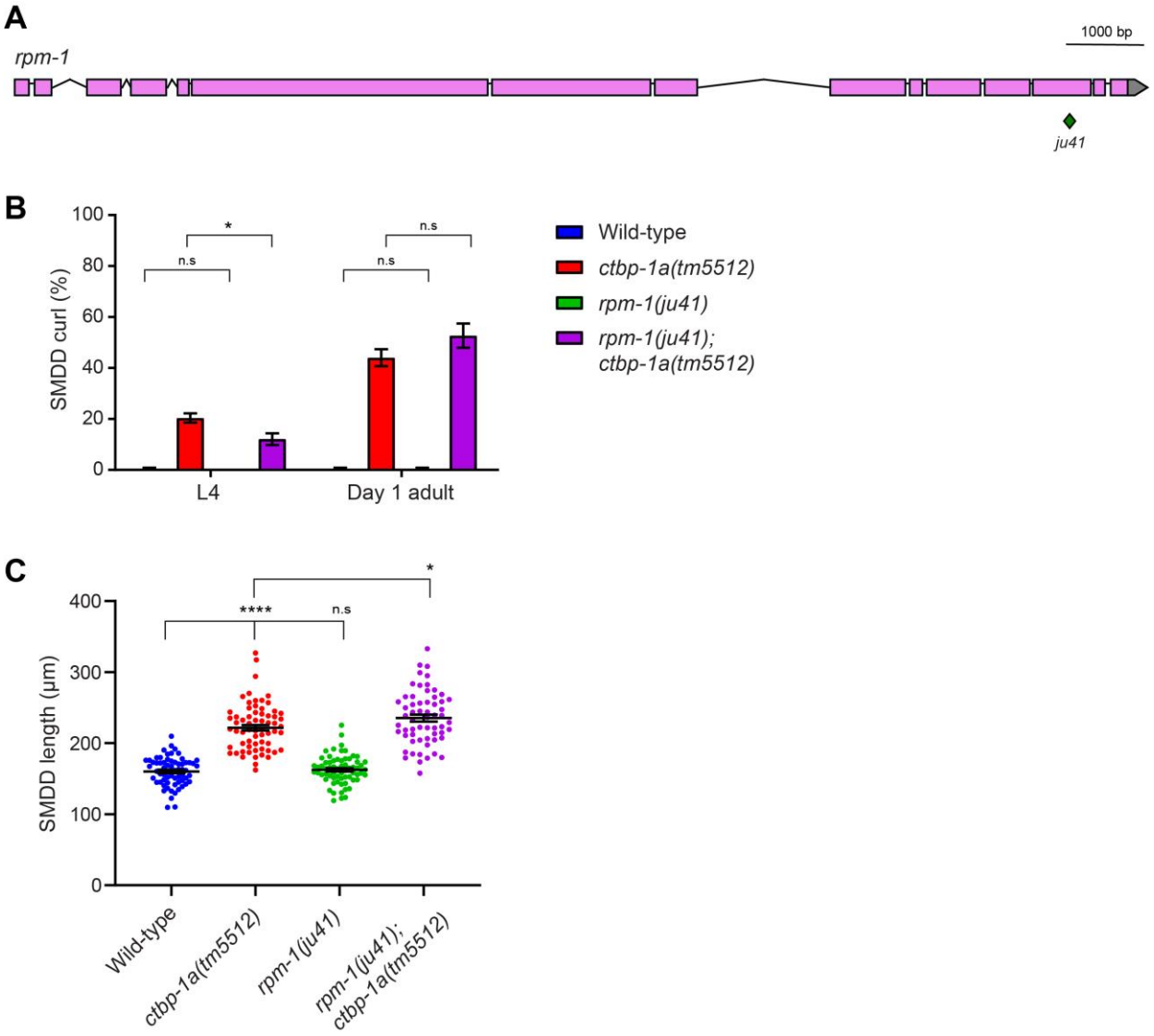

Figure 4.12 *rpm-1* is not involved in SMDD axonal development.
(A) Schematic of *rpm-1* genomic locus, with the position of the *ju41* substitution (green diamond). Exons (pink boxes), introns (solid lines) and untranslated regions (grey boxes) are indicated; 5' is on the left. Adapted from WormBase. (B) Quantification of SMDD curl phenotype (%) of L4 stage and day 1 adults at 25°C. Data presented as mean ± SEM (bar) of 3 biological replicates, n>100 axons. *p<0.05, n.s – not significant (one-way ANOVA with Tukey's correction). (C) Length of SMDD axons of wild-type and mutant day 1 adult animals at 25°C. Data presented as individual axon lengths (points) with mean ± SEM (bar) of 2 pooled biological replicates, n>60 axons. *p<0.05, ****p<0.0001, n.s – not significant (one-way ANOVA with Tukey's correction).

Another gene identified in the *rpm-1* axon termination pathway is *fsn-1*. FSN-1 is an F-box domain protein that is expressed throughout the nervous system [209]. FSN-1 and RPM-1

physically associate in a SCF (Skp, Cullin, F-box) ubiquitin-ligase complex [209]. *fsn-1* mutants display similar mechanosensory ALM and PLM axon termination defects as *rpm-1* mutants, where the anterior-directed axons overextend [210]. Genetic analysis indicates that RPM-1 and FSN-1 function in the same pathway to regulate axon termination [210]. The *fsn-1* mutant defects are not as severe as *rpm-1* mutants, however, as RPM-1 function is also mediated by the guanine nucleotide exchange factor GLO-4 [27, 210, 211].

The *gk429* null allele is a 1001 bp deletion over the translational start site (Figure 4.13A, WormBase). The *fsn-1(gk439)* mutants displayed wild-type SMDD axons (Figure 4.13B). In both L4 larvae and day 1 adults, double *fsn-1(gk439); ctbp-1a(tm5512)* and single *ctbp-1a(tm5512)* mutants displayed the same defective SMDD axon penetrance (Figure 4.13B). This demonstrates that *fsn-1* is not involved in SMDD development, and further supports that *rpm-1* is not involved in SMDD development.

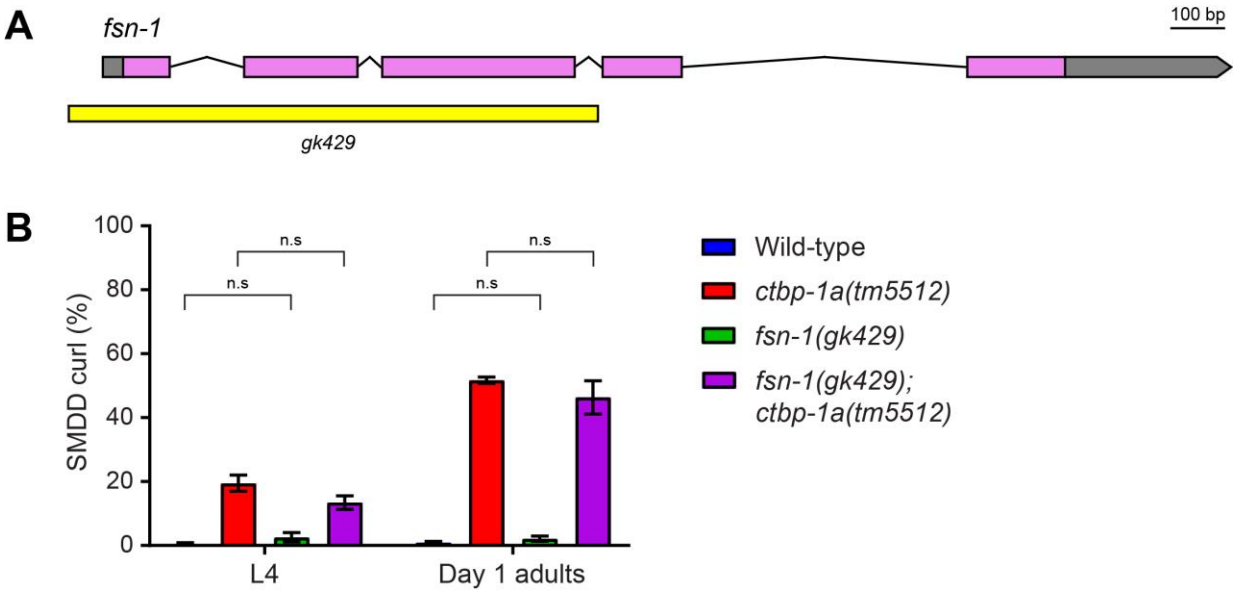

Figure 4.13 *fsn-1* is not involved in SMDD axonal development.
(A) Schematic of *fsn-1* genomic locus, with the position of the *gk429* deletion (yellow box). Exons (pink boxes), introns (solid lines) and untranslated regions (grey boxes) are indicated; 5' is on the left. Adapted from WormBase. (B) Quantification of SMDD curl phenotype (%) of L4 stage and day 1 adults at 25°C. Data presented as mean ± SEM (bar) of 3 biological replicates, n>100 axons. *p<0.05, n.s – not significant (one-way ANOVA with Tukey's correction).

4.6.3 AST-1

AST-1 is an ETS-domain transcription factor that is expressed in many neurons, including dopamergic DA and SMDD motor neurons [21, 212]. AST-1 is highly expressed in the SMDD

neurons at the L4 stage (ranked 93rd out of 180 genes expressed in single-cell RNA-sequencing data) [206]. AST-1 functions as a terminal selector gene for DA cell fate through activating the specific dopamine motif present in all members of the highly conserved dopamine pathway [212]. Consistent with this, loss of *ast-1* causes the failure of all DA neurons to terminally differentiate [212].

AST-1 regulates axon guidance of multiple classes of neurons. The *ast-1(rh300)* hypomorphic mutant displays axon guidance defects in the PDE sensory neurons [212]. Normally, the PDE axons extend together in the right VNC fascicle, but in *ast-1* mutants, one of the axons aberrantly enters the left fascicle [212]. AST-1 also regulates VNC interneuron axon guidance [21]. In *ast-1* mutants, there are two types of interneuron axon guidance defects: laterally growing axons and ventral midline crossing defects. Laterally growing axons occur when interneuron axons fail to reach the VNC and instead extend in variable lateral directions [21]. Also seen in *ast-1* mutants are ventral midline crossing defects, where axons that normally extend posteriorly along the VNC cross the ventral midline and extend along the incorrect axon tracts [21]. AST-1 functions in the same genetic pathway as UNC-6/Netrin and the UNC-40 receptor to regulate interneuron axon guidance [21]. Interestingly, the marker used for visualising interneuron axon guidance was the *pglr-1::GFP* marker I also use in this project, but they did not report any phenotypes for the SMDD neurons (either wild-type or mutant) [21]. Because of AST-1 expression in SMDD neurons and its known role in axon guidance, I was interested in whether AST-1 regulates SMDD development.

For analysing the SMDD axons, I was unable to use a null *ast-1* mutant because they arrest development and die as young larvae due to severe pharyngeal defects [21]. Instead, I used the *ast-1(rh300)* point mutation, which results in substitution of glycine to arginine in the DNA-binding ETS-domain (Figure 4.14A) [21]. This mutation causes axon guidance defects in *pglr-1::GFP* expressing neurons, but the penetrance was less severe than the null *hd92* mutant [21]. The *ast-1(rh300)* single mutants display wild-type SMDD axons at both L4 stage and day 1 of adulthood at 25°C (assay performed in Honours, [207]). At the L4 stage, the *ast-1(rh300); ctbp-1a(tm5512)* double mutant displays an increased penetrance from ~24% to ~60% ($p<0.0001$, Figure 4.14B). At day 1 of adulthood, however, the defective axon penetrance did not significantly increase (~60% to ~71%, Figure 4.14B). To determine if these results were replicable, I performed the assays on day 2 adults at 20°C. As previously demonstrated in Figure 3.4, the *ctbp-1a* mutants display similar SMDD curl penetrance at day 1 of adulthood at 25°C and day 2 of adulthood at 20°C (~60% in Figure 4.14B, ~65% in Figure 4.14C). The double *ast-1(rh300); ctbp-1a(tm5512)* mutants displayed increased defective SMDD axons in day 2 adults compared to *ctbp-1a(tm5512)* mutants (~65% to ~87%, $p<0.01$, Figure 4.14C).

This additive penetrance suggests that AST-1 functions in a parallel pathway to CTBP-1 to regulate SMDD development.

Interestingly, I observed that *ast-1(rh300)* single and double mutants displayed extra axons that sometimes entered and/or extended laterally along the dorsal or dorsal sublateral cords. This phenotype was previously described as an effect of defective VNC axon guidance [21], and did not confound the results as I was able to distinguish these lateral axons from SMDD axons based on their morphology and fluorescence intensity.

These results thus far suggest that AST-1 and CTBP-1 function in parallel pathways to control SMDD development. I wanted to confirm these results using another *ast-1* allele, *hd1*. The *hd1* allele also contains a point mutation, which results in an alanine to valine substitution in the ETS-domain (Figure 4.14A) [21]. Like *rh300*, *hd1* mutant animals exhibit axon guidance defects [21]. The available strain I used to cross into the *rhIs4* reporter and create *ast-1(hd1); ctbp-1a(tm5512)* double mutants also contained the *rol-6(e187)* mutation. *ast-1* and *rol-6* are located close to each other on chromosome II (~5 cM), and are unlikely to recombine through conventional crosses. This means that the single nucleotide change in the *hd1* allele can be followed during crosses by observing rolling homozygous *rol-6* mutants. The presence of the *rol-6* mutation, however, caused the animals to rotate on different angles when scored for SMDD axons. Although I was previously able to distinguish which axons were VNC, lateral or SMDD axons, the different angle of the animal made it difficult to follow the normal nerve cord positioning. Therefore, I could not score using the *rhIs4* reporter as axons in the VNC or other cords were obscuring the SMDD axons in *rol-6* mutant worms. Instead, I crossed *ast-1(hd1); rol-6(e187)* into the *pctbp-1a::GFP* reporter strain described in Chapter 3 to observe only SMDD and SMDV axons. I did not observe extra lateral growing axons in *ast-1* mutants using the *pctbp-1a::GFP* reporter, suggesting that the lateral defective axons are not CTBP-1-expressing neurons.

The *ast-1(hd1); rol-6(e187)* mutants displayed wild-type SMDD axons, demonstrating that the *Rol* phenotype does not cause SMDD defects (Figure 4.14D). SMDD axon defects in *ast-1(hd1); rol-6(e187); ctbp-1a* mutants increased compared to *ctbp-1a(tm5512)* animals (~41% to ~74%, $p<0.01$, Figure 4.14D). This enhanced penetrance was also observed in SMDV axons (~43% to ~67%, $p<0.01$) (Appendix Figure 8.5). These data confirm that AST-1 regulates SMDD development, but acts in a parallel pathway to CTBP-1.

Interestingly, reducing AST-1 function does not cause defective SMDD axons alone, and its role is only observable when CTBP-1a function is also removed. There is likely residual AST-

1 function using the *rh300* and *hd1* alleles. It is also possible that AST-1 acts redundantly with other protein(s) to regulate SMDD development that acts downstream of CTBP-1.

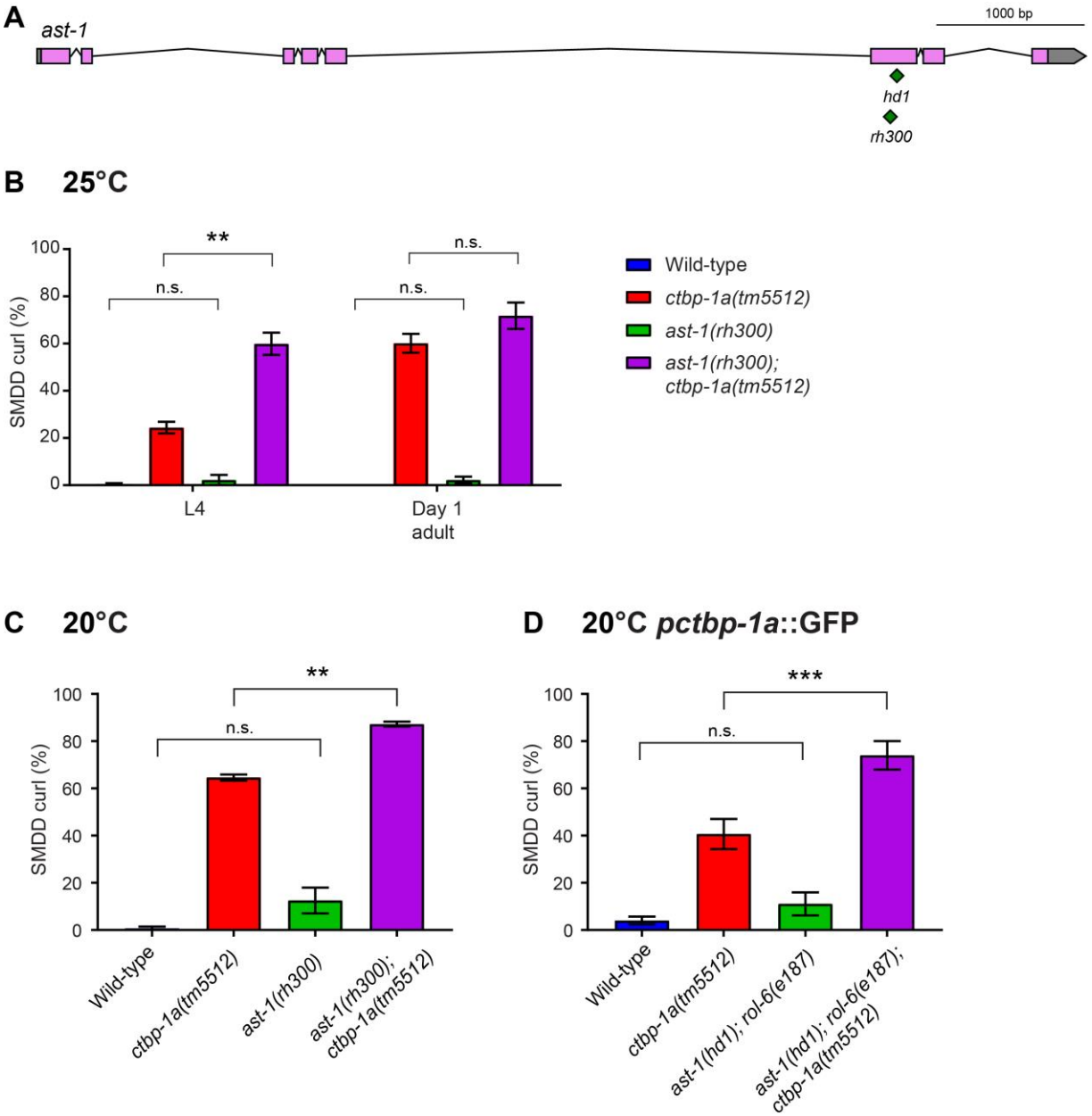

Figure 4.14 AST-1 acts in a parallel pathway to CTBP-1 to regulate SMDD axonal development. (A) Schematic of *ast-1* genomic locus, with the position of the *rh300 and hd1* substitutions (green diamonds). Exons (pink boxes), introns (solid lines) and untranslated regions (grey boxes) are indicated; 5' is on the left. Adapted from WormBase. (B) Quantification of SMDD curl phenotype (%) of *ast-1(rh300)* single and double mutants at L4 stage and day 1 adults at 25°C. (C) Quantification of SMDD curl phenotype (%) of *ast-1(rh300)* single and double mutants at day 2 of adulthood at 20°C. (C) Quantification of SMDD curl phenotype of *ast-1(hd1)* single and double mutants at day 2 of adulthood at 20°C. *pctbp-1a::GFP* generated in Chapter 3 used to score SMDD axons. (B-D) Data presented as

mean ± SEM (bar) of 3 biological replicates, n>100 axons. **p<0.01, ***p<0.001, n.s – not significant (one-way ANOVA with Tukey's correction).

4.7 Discussion

In this chapter, I aimed to identify genes that function in the same genetic pathway as CTBP-1a to control SMDD axonal development. I investigated the role of putative CTBP-1-target genes and genes with known roles in axonal development using single and double mutant epistasis experiments. I identified novel roles for the Wnt ligand CWN-2 and ETS-domain transcription factor AST-1 in SMDD development.

ctbp-1 RNAi does not replicate SMDD axonal defects

In this chapter, I wanted to perform an RNAi screen to identify genes that, when knocked down, would suppress the mutant SMDD axon phenotype of *ctbp-1a* mutants. As CTBP-1a functions cell- and cell-non-autonomously to regulate SMDD axonal development, I investigated whether RNAi knockdown would occur in the SMDD axons. RNAi is inefficient in the nervous system, therefore I introduced the *uIs69 (punc-119::sid-1)* transgene that ectopically expresses the SID-1 channel in the nervous system to enhance RNAi in neurons [186]. I performed *ctbp-1* RNAi knockdown in wild-type animals and animals harbouring the *uIs69* transgene, where knockdown should occur in non-neuronal tissues and systemically, respectively. In both backgrounds, animals treated with *ctbp-1* RNAi did not phenocopy the SMDD axon guidance defects of *ctbp-1a* mutants (Figure 4.2). These results suggest that *ctbp-1* was not sufficiently knocked down to produce a detectable phenotype. The animals were exposed to the RNAi vectors for 2 generations before assessing the SMDD axon morphology. To determine whether *ctbp-1* was being knocked down, we could perform qRT-PCR to determine whether *ctbp-1* transcript levels were reduced in the whole animal. Furthermore, it is possible that *ctbp-1* knockdown in the whole animal was occurring but RNAi is still inefficient in the SMDD neurons using this system. These data demonstrate that RNAi is not an appropriate method to analyse CTBP-1 function in SMDD axonal development.

A further caveat of this approach was that the presence of the *uIs69 (punc-119::sid-1)* transgene resulted in an increase in SMDD axon guidance defects (Figure 4.2). Previously, RNAi experiments performed in the *uIs69* background robustly phenocopied known neuronal gene mutants, including those involved in locomotion and touch sensitivity [186, 213]. The *sid-1*-expressing strains did not display defects in gross neuronal morphology or behaviour [186]. My results, however, suggest that ectopically expressing the SID-1 channel causes SMDD

defects. This is possibly caused by inappropriate silencing of genes that are important for SMDD axonal development. Alternatively, genetic mutations may be present in the *uIs69* strain background that were not lost through outcrossing and that cause SMDD developmental defects. Overall, due to the insufficient knockdown and effects of transgenes on SMDD development, I performed all further experiments using genetic mutants.

Putative CTBP-1 target genes are not involved in SMDD axonal development

To identify potential downstream targets of CTBP-1, I performed analysis on two available microarray datasets. As CTBP-1 functions as a transcriptional corepressor, I focused on genes that were upregulated in *ctbp-1* mutants in both of these datasets. I further narrowed the list of putative CTBP-1 target genes to those expressed in the nervous system and hypodermis, where CTBP-1 is expressed [89]. I analysed the single and double mutants for axon guidance defects, but was unable to identify any genes that regulate SMDD axonal development, dependent or independent of CTBP-1a. There are a few possible reasons that this microarray analysis did not reveal any genes controlling SMDD axonal development. First, the microarrays were performed on young adult animals. Earlier, I identified that *ctbp-1a* mutants display SMDD axon guidance and termination defects that begin in mid-late larval development. As the defects are first observed in larval development, the genes that control SMDD axonal development may be dysregulated at earlier stages and relevant upregulation may no longer be detected by the young adult stage. Second, these microarrays were performed on whole animals. In Chapter 3, I found that CTBP-1 can function cell-autonomously to control SMDD development (Figure 3.14), therefore this method may have hidden relevant tissue-specific changes in gene expression. Lastly, these microarrays were performed on hypomorphic mutants that are predicted to reduce the function of both CTBP-1 isoforms. As truncated CTBP-1a and CTBP-1b isoforms may still be expressed in these hypomorphic strains, the microarrays may not represent the transcriptional changes of complete loss of CTBP-1 function.

To identify genes that function downstream of CTBP-1a to control SMDD development, I would instead perform RNA-sequencing to allow the unbiased identification of dysregulated genes in *ctbp-1* mutant backgrounds. In Chapter 3, I earlier demonstrated that only the longer CTBP-1a isoform is involved in SMDD development. Isoform-specific and null *ctbp-1* mutations were not made until after the microarrays were performed (Chapter 3). I would perform RNA-seq on the isoform-specific and null mutants to potentially reveal differential transcript expression caused by loss of one or both CTBP-1 isoforms. In addition, these experiments could be performed at multiple developmental stages to identify upregulated genes during different stages of SMDD axon outgrowth. As CTBP-1 controls SMDD axonal development cell-

autonomously, ideally we could perform cell-specific RNA-seq to detect transcriptional changes in the SMDD neurons. Recently, significant advances have been made in cell-specific RNA-seq in *C. elegans* [171, 206]. Notably, the transcriptomes of the SMDD neurons of wild-type L4 stage animals were recently profiled [206]. Performing single-cell RNA-seq on *ctbp-1* isoform-specific mutants may reveal downstream targets of CTBP-1a for SMDD development.

Among the putative CTBP-1 target genes were four members of the *C. elegans* Hedgehog-related pathway. Hedgehog genes regulate neuronal development in mice and *Drosophila* [23, 24], but the roles of Hedgehog-like signalling in *C. elegans* is understudied. Recently, Riveiro *et al*. showed that overexpression of the secreted Hedgehog-related genes *grl-16* and *wrt-8* caused defective PVQ axon guidance, where axons cross the ventral midline as they extend from the head to the tail [22]. This was the first evidence for a conserved function for the Hedgehog-related pathway in *C. elegans* longitudinal axon guidance. As I identified multiple upregulated Hedgehog-related genes in *ctbp-1* mutants, including *grl-16*, I speculated that CTBP-1 may regulate Hedgehog-related signalling to control SMDD axon guidance. However, I found that loss of none of these genes (*wrt-6*, *wrt-10*, *grl-5* and *grl-16*) ameliorates the SMDD axon defects of *ctbp-1a* mutants (Figure 4.5-4.6). Furthermore, the single mutants of these genes do not display SMDD axon guidance defects. These data suggest that these Hedgehog-related genes do not function in SMDD axon guidance, and that CTBP-1a regulates other genes to control SMDD axonal development.

Although this microarray analysis did not elucidate any CTBP-1-target genes involved in SMDD development, it could potentially be used to elucidate target genes involved in other processes. CTBP-1 also has roles in lifespan, acute functional tolerance to ethanol and regulation of lipid metabolism [90, 91], and the upregulated genes present in the microarrays may be involved in these processes. For example, the metalloprotease NAS-38 has a known role in lifespan [203], and therefore may be regulated by CTBP-1 to regulate longevity.

New deletion alleles of *C. elegans* Hedgehog pathway-related genes

In the course of investigating the role of Hedgehog-related genes in SMDD axon guidance, I generated the first putative null mutant alleles for two members of the *C. elegans* Hedgehog-related pathway: *wrt-6* and *wrt-10*. These genes both encode predicted secreted signalling molecules [187, 190, 191]. I used CRISPR-Cas9 to generate premature stop codons in the first exon of each gene, therefore they are likely to be molecular nulls. Although I found these genes were not involved in SMDD axonal development, they may be useful for determining other roles for these conserved factors. Previously, RNAi knockdown experiments in the hypersensitive *rrf-3* mutant background revealed that *wrt-6* and *wrt-10* knockdown caused

pleiotropic phenotypes, namely impaired body growth, abnormal fluid-filled vacuoles in the hypodermis and intestine, and uncoordinated movement [192]. In addition, *wrt-6* inhibition caused defective cuticle molting during late larval development [192]. The *wrt-6* and *wrt-10* null mutants I generated exhibit no gross morphological phenotypes, but in-depth phenotypic examination is required to determine if these genes are involved in these, or other unidentified, developmental processes. These are the first reported deletion alleles generated for *wrt-6* and *wrt-10* and will therefore help reveal new insights into the functions of Hedgehog-related signalling. These alleles are now available at the *Caenorhabditis* Genetics Center (CGC) [189].

The Wnt ligand CWN-2 regulates SMDD development

In this chapter, I identified a novel role for the Wnt ligand CWN-2 in SMDD development. *cwn-2* mutants displayed a severe SMDD axon phenotype, where the axons did not visibly extend in the dorsal sublateral cord (Table 4.2). This phenotype is different to the defective SMDD axonal development observed when CTBP-1a is lost. In *ctbp-1* mutants, the SMDD axons always extend, at least partially, in the dorsal sublateral tract, demonstrating that the initial stages of outgrowth into the dorsal sublateral tract is not controlled by CTBP-1a. When *cwn-2* is lost, however, the SMDD axons do not visibly extend along the dorsal sublateral cord. The lack of visible SMDD axons in *cwn-2* mutants could be due to a failure of axon outgrowth from the cell body, or misguided axon growth towards incorrect nerve cords. Previously, CWN-2 was shown to act as an attractive cue for the axon outgrowth of the RMED/V GABAergic motor neurons [47]. In *cwn-2* mutants, the RMED/V neurons failed to initiate posterior axon outgrowth from the cell body in the nerve ring [47]. These defects can be rescued by expressing *cwn-2* in regions posterior to the nerve ring, suggesting that CWN-2 acts non-cell-autonomously to attract axon outgrowth [47]. Consistent with this hypothesis, ectopic *cwn-2* expression of anterior to the RMED cell bodies triggered aberrant anterior axon extension [47]. Therefore, in this context, CWN-2 acts as an attractive cue for initial axon outgrowth. Another study observed that *cwn-2* mutants displayed defective axon guidance of the SIA and SIB sublateral motor neurons [205]. These axons normally extend from the nerve ring posteriorly along the sublateral cords [6]. When *cwn-2* was lost, these axons aberrantly extended anteriorly towards the tip of the head or in different nerve cords [205]. Unlike the RMEV motor neurons described above, these axons do not fail to extend, but are instead misguided to incorrect body regions. Taken together, these studies demonstrate that CWN-2 can regulate distinct stages of axonal development in different contexts.

Thus far, I have been unable to distinguish between whether *cwn-2* mutant SMDD axons display abnormal outgrowth and/or guidance due to the presence of many other neurons in the

pglr-1::GFP marker. Instead, we could use the *pctbp-1a::GFP* transcriptional reporter (Chapter 3) to analyse the SMDD cell bodies and axons. Because the SMDs are visible from embryogenesis, we could track the SMDDs in *cwn-2* mutants to determine whether the axons fail to extend or aberrantly extend towards other body regions.

It would also be interesting to determine whether CWN-2 functions as an axon guidance cue for SMDD axonal development. Wnt ligands can act as both attractive and repulsive cues for *C. elegans* axon guidance. For example, CWN-2 functions as an attractant for RMED motor neuron axon outgrowth [47], whereas the Wnt ligands LIN-44 and EGL-20 function as repellents for D-type motor neuron axon termination [46]. CWN-2 is highly expressed in anterior tissues, including head neurons, pharynx and anterior muscle cells [44, 47, 205]. This anterior expression overlaps with the SMDD cell body and axon projection, therefore, it is possible that CWN-2 acts as an attractive cue for SMDD axon outgrowth and guidance. Interestingly, CWN-2 is highly expressed in the SMDD neurons in larval stages and adulthood [205, 206], suggesting that it may be required in the SMDD neurons to control axonal development. Resupplying *cwn-2* under various promoters in the *cwn-2* mutant could reveal the temporal and spatial nature of CWN-2 regulation of SMDD axonal development.

AST-1 and CTBP-1 function in parallel pathways for SMDD development

My findings demonstrate a novel role for the ETS-domain transcription factor AST-1 in SMDD development. Previously, AST-1 was shown to regulate longitudinal axon guidance of VNC interneurons and PDE sensory neurons [21, 212]. For VNC interneuron axon guidance, *ast-1* functions in the same genetic pathway as UNC-6/Netrin and the receptor UNC-40/DCC [21]. In this chapter, I found that loss of *ast-1* enhances the SMDD defects of *ctbp-1a* mutants. This additive penetrance of *ast-1; ctbp-1a* double mutants suggests that AST-1 and CTBP-1 function in parallel pathways for SMDD development.

Intriguingly, when *ast-1* alone is mutated, the SMDD axons are wild-type. Because null *ast-1* mutants display lethality during early larval development [21], I had to use the point mutation alleles *rh300* and *hd1*. These alleles both contain point mutations of highly conserved residues in the DNA-binding ETS domain [21]. The *ast-1* null and point mutant animals display the same penetrance of VNC midline crossing defects, suggesting that the point mutations act as molecular nulls in this context [21]. However, the null *hd2* mutants have a higher penetrance of aberrantly extending VNC axons, showing that in different contexts, these alleles likely have residual function [21]. Therefore, it is possible that the *ast-1* point mutants (*rh300* and *hd1*) I used to analyse SMDD axonal development are still able to bind to promoters to regulate gene transcription and therefore control correct SMDD axon guidance.

5. Transcriptional control of an L1CAM regulates SMDD axonal development

5.1 Introduction

L1 cell adhesion molecules (L1CAMs) are critical regulators of nervous system development maintenance and function [94]. A previous study found that the *C. elegans* L1CAM LAD-2 regulates the guidance of sublateral axons [25]. In this chapter, I investigated whether LAD-2 functions in the same pathway as CTBP-1a to regulate SMDD axonal development. In addition, I investigated the role of the other *C. elegans* L1CAM SAX-7 in SMDD axonal development.

5.2 LAD-2 and CTBP-1 regulate SMDD development in distinct pathways

LAD-2 is a *C. elegans* L1CAM that regulates axon guidance of multiple neurons that extend in sublateral cords [25]. In this context, LAD-2 functions as a non-canonical receptor for the ephrin EFN-4 and semaphorin MAB-20 [25, 41]. LAD-2 is expressed in 14 neurons, including the SMDD neurons [25]. Wang *et al.* reported *lad-2* mutants display SMD defects of aberrant ventral or dorsal turns and general wandering, but did not specify whether these were SMDD or SMDV. Based on the position of these axons on opposing sides of the ventral nerve cord, I speculate that these are SMDV axons (Figure 3A-B in [25]). As CTBP-1 regulates both SMDD and SMDV development (Chapter 3), I hypothesised that *lad-2* is also involved in SMDD axonal development, and may control SMDD development through the same genetic pathway as *ctbp-1a*.

The *lad-2* gene locus encodes two transcripts, which are translated into two protein isoforms: LAD-2L and LAD-2S (Figure 5.1) [25]. LAD-2L contains six Ig-like domains, a transmembrane region, five fibronectin type III (FNIII) domains and a short cytoplasmic tail (Figure 5.1). The LAD-2S contains only the first four and a partial fifth Ig-like domain, and is predicted to be secreted extracellularly (Figure 5.1) [25]. To determine the function of LAD-2 in SMDD development, I performed assays using null *lad-2(tm3056)* mutant animals. The *tm3056* allele is a 1064 bp out-of-frame deletion that is predicted to cause a premature stop codon after the second Ig-like domain of both LAD-2L and LAD-2S isoforms (WormBase) (Figure 5.1). The *tm3056* allele likely functions as a null allele. Accordingly, Wang *et al.* demonstrated there was no detectable LAD-2 staining in *lad-2(tm3056)* mutant animals using anti-LAD-2 antibodies that targeted the cytoplasmic tail of LAD-2L [25].

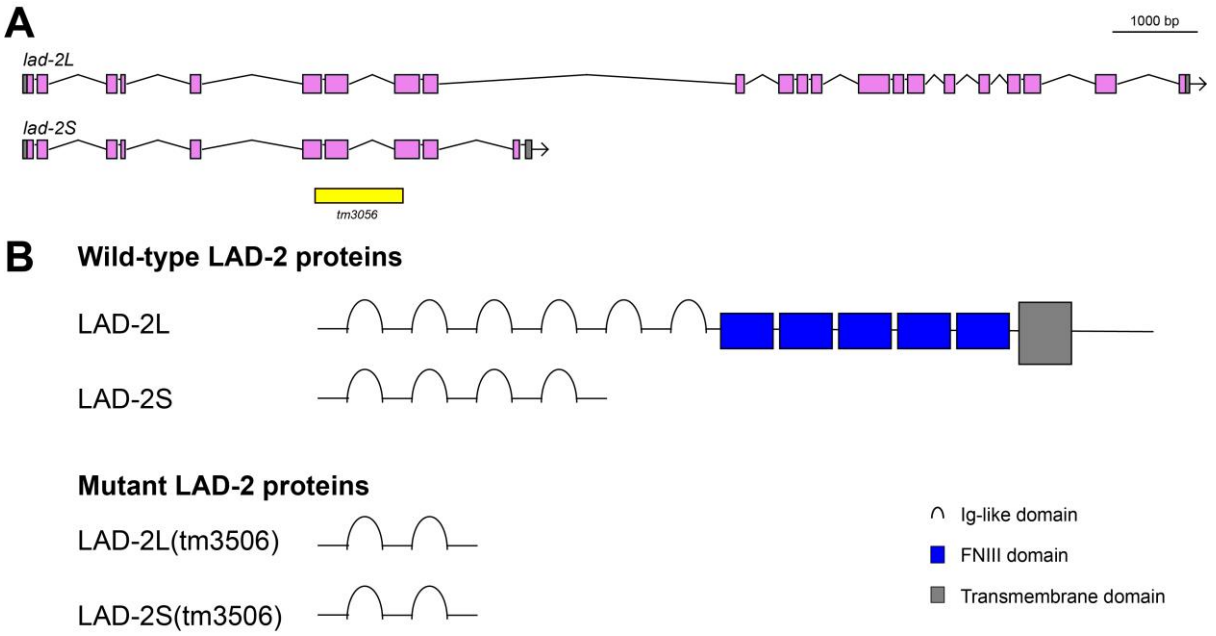

Figure 5.1 Wild-type and mutant *lad-2* alleles.
(A) Schematic of *lad-2* genomic locus, with the position of the *tm3056* deletion (yellow box). *lad-2* has two isoforms: *lad-2L* and *lad-2S*. Exons (pink boxes), introns (lines) and UTRs (grey box) are indicated; 5' is on the left. Adapted from WormBase. (B) Predicted domain structure of wild-type and mutant LAD-2 proteins. Key for the different domains is in the bottom-right corner, N-terminus is on the left.

I examined SMDD axon morphology of *lad-2(tm3056)* mutants and found they displayed qualitatively similar axon defects to *ctbp-1a(tm5512)* mutants, where the axons leave the dorsal sublateral tract (Figure 5.2A). The *lad-2(tm3056); ctbp-1a(tm5512)* double mutant also exhibited the same gross SMDD curl phenotype (Figure 5.2A). I quantified the SMDD curl phenotype and *lad-2(tm3056)* mutants displayed ~39% SMDD curls at the L4 stage and ~40% at day 1 of adulthood, therefore demonstrating that *lad-2* mutants do not display an increase in SMDD curl penetrance with age (Figure 5.2B). This contrasts to the increase in SMDD curl penetrance observed in *ctbp-1a* mutants (Figure 5.2B). Further, the SMDD curl penetrance of double *lad-2(tm3056); ctbp-1a(tm5512)* mutants is additive when compared to either the single mutant, suggesting that these factors regulate SMDD axon extension in parallel pathways (Figure 5.2B).

Interestingly, I observed ~40% curly SMDD axons in *lad-2(tm3056)* mutants, whilst Chen *et al.* observed ~55% defective SMD axon migration [25]. For scoring SMD axon morphology, we both used the same *pglr-1::GFP* (*rhIs4*) reporter marker, but based on their representative confocal micrographs, Chen *et al.* appear to have rolled the animals to score the SMDV axons [25]. This difference in defective axon penetrance further suggests that Chen *et al.* scored SMDV axon defects. It is also possible that they were scoring both SMDD and SMDV axons,

and/or we have different parameters of scoring for axons that leave the dorsal sublateral cord. Further experiments should be performed using the *pctbp-1a::GFP* marker, in which only the 4 SMD axons are visible, to determine the effect of removing *lad-2* on all 4 SMD neurons.

Because *lad-2* mutants display SMDD guidance defects, where they curl away from the dorsal sublateral cord, I hypothesised the axons may also display defective termination. I examined the SMDD axon length of *lad-2* single and double mutants. The *lad-2(tm3056)* mutant displays the same axon length as wild-type animals at both L4 stage and day 1 of adulthood (L4: ~99 µm and ~106 µm, respectively, day 1: ~156 µm and ~162 µm, respectively (Figure 5.2C). The *lad-2(tm3056); ctbp-1a(tm5512)* double mutant exhibits SMDD axon lengths that do not significantly differ from the *ctbp-1*a mutant alone, at both developmental stages (Figure 5.2C).

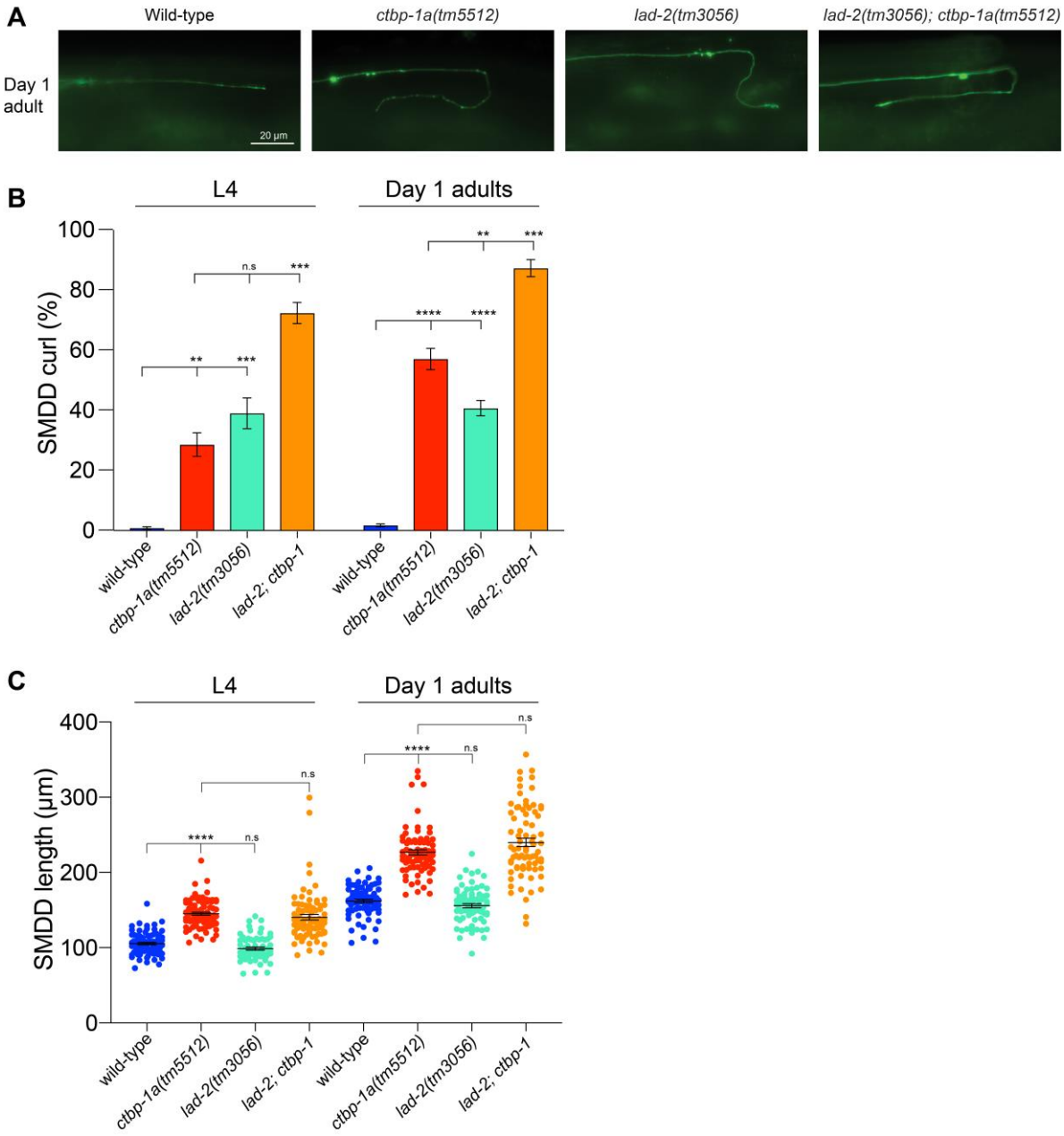

Figure 5.2 LAD-2 and CTBP-1 regulate SMDD axonal development in distinct genetic pathways. (A) Representative fluorescence micrographs of SMDD axonal morphology in day 1 adults at 25°C. Scale bar= 20 µm. (B) Quantification of the SMDD curl phenotype (%) of wild-type and mutant animals at the L4 stage and day 1 of adulthood at 25°C. Data presented as mean ± SEM (bar) of 3 biological replicates, n>100 axons. **p<0.01, ***p<0.001, ****p<0.0001, n.s – not significant (one-way ANOVA with Tukey's correction). (C) Quantification of SMDD length (µm) of wild-type and mutant animals at the L4 stage and day 1 of adulthood at 25°C. Data presented as mean ± SEM (bar) of 2 pooled biological replicates, n=67-82 axons. ****p<0.0001, n.s – not significant (one-way ANOVA with Tukey's correction).

Because ~40% of *lad-2* mutant SMDD axons display the curl phenotype (Figure 5.2B), I also examined the SMDD axon length of curly or straight axons to determine if there was any

significant difference in axon length. There was no significant difference in the *lad-2* mutant SMDD axon length whether they were straight/wild-type or curly/defective at either L4 stage or day 1 of adulthood (Appendix Figure 8.6). These results demonstrate that although *lad-2* mutant animals display defects in axon guidance, termination of axon growth occurs normally. The termination of *lad-2* mutant axons occurs even when these axons are outside the dorsal sublateral fascicle i.e. curled away from the dorsal sublateral cord.

Overall, these data demonstrate that LAD-2 and CTBP-1a regulate SMDD development in parallel genetic pathways. Similar to the *ctbp-1a* mutant phenotype, *lad-2* mutant axons are misguided away from the dorsal sublateral cord. However, *lad-2* mutant SMDD axons grow the correct length, whether they extend within the sublateral cord or in an inappropriate environment outside the cord. In contrast, the *ctbp-1a* mutant SMDD axons over-extend whether they remain in the dorsal sublateral tract or are misguided. This further supports the hypothesis that the overextension phenotype of *ctbp-1a* mutant axons are not dependent on their environment.

5.3 CTBP-1 does not regulate development of other *lad-2*-expressing sublateral axons

The SMD neurons extend axons in the sublateral nerve cords adjacent to axons of the SDQL/R and PLN neurons (Figure 5.3A) [6]. Interestingly, the L1CAM LAD-2 regulates axonal development of the SDQL, SDQR and PLN sublateral neurons [25]. These cholinergic sensory/interneurons are all born post-embryonically in the L1 stage and extend axons longitudinally within the sublateral cords [8, 214]. To determine whether CTBP-1 is also involved in the guidance of other sublateral axons, I performed single and double mutant assays analysing individual axonal trajectories.

The SDQL/R neurons are non-symmetric sensory/interneurons. The SDQ cell bodies are positioned far from each other, but both the SDQR and SMDDR axons extend in close proximity in the dorsal sublateral cord (Figure 5.3A). The SDQR cell body is located in the anterior body region and its axon extends anteriorly towards the nerve ring in the dorsal sublateral cord [6]. It was previously demonstrated that *lad-2* mutants display defective SDQR axon guidance, where its axon leaves the dorsal sublateral cord and extend ventrally towards and along the VNC [25]. I analysed whether *ctbp-1a* and *lad-2* single and double mutants displayed defects in this sublateral axon. I scored the SDQR axons as defective if it left the dorsal sublateral cord and extended ventrally. The *lad-2(tm3056)* mutants displayed ~78% defective SDQR axons, which was significantly higher than wild-type animals (wild-type: ~12%,

Figure 5.3B). The *ctbp-1a(tm5512)* mutants did not display significantly higher SDQR axon phenotype than wild-type (~25% and ~12%, respectively, Figure 5.3B). Further, the *lad-2; ctbp-1a* double mutant SDQR defect penetrance was not significantly different from the single *lad-2* mutant (~83% and ~77%, respectively, Figure 5.3B). Overall, these data demonstrate that CTBP-1a does not regulate SDQR axonal development.

I also analysed SDQL axon projections in *ctbp-1a* mutants. The SDQL cell body is situated in the anterior part of the body and the axons extend anteriorly, initially along the lateral axon tract before turning dorsally and extending along the anteriorly along the dorsal sublateral tract [6]. In *lad-2* mutants, the SDQL axon extends ventrally towards and subsequently along the VNC, instead of turning dorsally to enter the dorsal sublateral tract [25]. I scored for SDQL defects, which I defined as any SDQL axon that extended ventrally at any stage of axon extension. The *lad-2(tm3056)* mutants exhibited ~82% defective SDQL phenotype (Figure 5.3C). This was significantly higher than the wild-type and *ctbp-1a(tm5512)* mutant populations (~22% and ~34%, respectively, Figure 5.3C). The double *lad-2; ctbp-1a* mutant did not significantly differ in penetrance from the *lad-2(tm3056)* mutant (~84% and ~82%, respectively, (Figure 5.3C). Therefore, these data demonstrate that CTBP-1a also does not regulate SDQL axon guidance.

The final sublateral axons that displays guidance defects in *lad-2* mutants are the PLN sensory/ interneurons. The PLN cell bodies are located in the tail of the animal and the axons extend anteriorly along the ventral cord until the midbody, where they extend along the ventral sublateral cord until they terminate in the nerve ring [6]. The PLN axon is in close proximity with the SMDV axon in the ventral sublateral cord (Figure 5.3A). It was previously shown that *lad-2* mutants display defective PLN axon guidance where PLN axons initially extend anteriorly then curl away and extend posteriorly back towards the tail [25]. I scored PLN axons as defective if they aberrantly extended posteriorly, and found that *lad-2(tm3056)* mutants displayed ~45% defective PLN axons (Figure 5.3D). The *ctbp-1a(tm5512)* mutants displayed the same low levels of defective PLN axons as wild-type animals (~8% and 12%, respectively, Figure 5.3D). The PLN defects of double *lad-2; ctbp-1a* mutants did not significantly differ from the single *lad-2* mutants (~43% and ~45%, respectively, Figure 5.3D). These data demonstrate that CTBP-1a does not function in the LAD-2-regulated PLN guidance pathway.

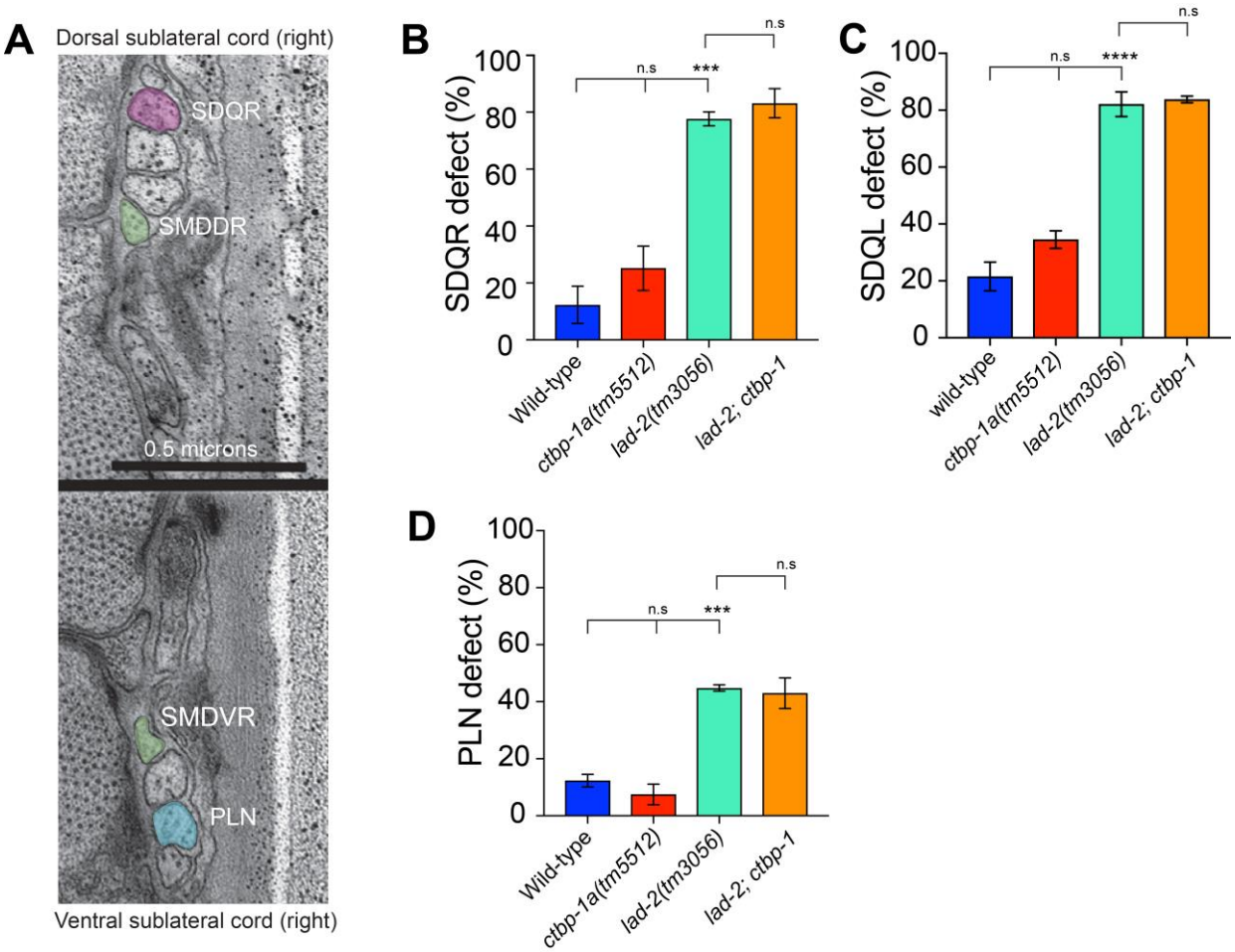

Figure 5.3 *ctbp-1a* mutant animals do not display defects in other sublateral cord axons.
(A) SDQR axons (pink) and PLN axons (blue) extend along the right sublateral cords with the SMDD and SMDV axons (green). Electron microscopy images supplied by David Hall, Albert Einstein College of Medicine. Scale bar= 0.5 µm. (B-D) Quantification of SDQR (B), SDQL (C) and PLN (D) defects (%). Day 1 adults grown at 25°C. Data presented as mean ± SEM (bar) of 3 biological replicates, n>100 axons. n.s – not significant (one-way ANOVA with Tukey's correction).

Taken together, these results demonstrate that CTBP-1a does not function in the LAD-2-mediated axon guidance pathway. The SQDL, SDQR and PLN all extend axons within the sublateral tracts, but in *ctbp-1a* mutants, these axons display wild-type morphology. This suggests that there is no gross morphological defect in the hypodermal tissue or muscle that adversely affect the development of the sublateral cords in *ctbp-1a* mutants. This strengthens my earlier evidence that CTBP-1 functions cell-autonomously to regulate SMD development, as other neurons in the sublateral cords are not affected. In contrast, loss of LAD-2 causes defects in the axon guidance of multiple axons that extend in the sublateral cords, suggesting that loss of this L1CAM may cause structural defects of the sublateral cords, causing the axons to be misguided.

5.4 SAX-7 is involved in CTBP-1-regulated SMDD development

Due to the critical importance of the L1CAM LAD-2 for SMDD development, I hypothesized that the other *C. elegans* L1CAM ortholog SAX-7 may also play a role in SMDD axonal development. SAX-7 is widely expressed in the nervous system and hypodermis, and has many reported roles in neuronal cell body and axon maintenance [142-144]. The *sax-7* locus encodes two alternatively spliced transcripts: *sax-7L* and *sax-7S*. These encode two protein isoforms: the longer SAX-7L and shorter SAX-7S. SAX-7L contains six Ig-like domains, five fibronectin-III (FNIII) domains and the cytoplasmic tail that contains ankyrin, FERM and PDZ binding sequences [142]. The shorter SAX-7S lacks the first two Ig-like domains (Figure 5.4B) [142].

To determine the effect of SAX-7 loss, I used four different mutants that affect either or both long or short SAX-7 isoforms: *ot820, nj48, nj53* and *eq1*. The *sax-7*S-specific allele *ot820* is a 8 bp deletion, 15 bp from the *sax-7*S start codon, that causes a premature stop codon after 49 amino acids [215]. The *sax-7*L-specific allele *nj53* is a 724 bp deletion over the start site and first 2 exons of *sax-7*L [141]. As well as isoform-specific mutants, there are also two predicted null or loss-of-function alleles: *eq1* and *nj48*. The *eq1* mutation is a 2020 bp deletion over the fifth FNIII repeat to 3'UTR [147]. *nj48* is a 568 bp deletion over *sax-7*L exon 5 and *sax-7*S exons 1 and 2 [141]. Because the deletion covers introns and exons, it is unclear how it affects the spliced protein. In an earlier study, SAX-7S and SAX-7L protein bands were not detectable in *sax-7(nj48)* mutants, suggesting that this allele is a null [141]. However, in a later study, positive SAX-7 immunostaining was detected in the *sax-7(nj48)* mutant background [146]. Although these results suggest that *sax-7(nj48)* does not remove all SAX-7 activity, it affects both isoforms.

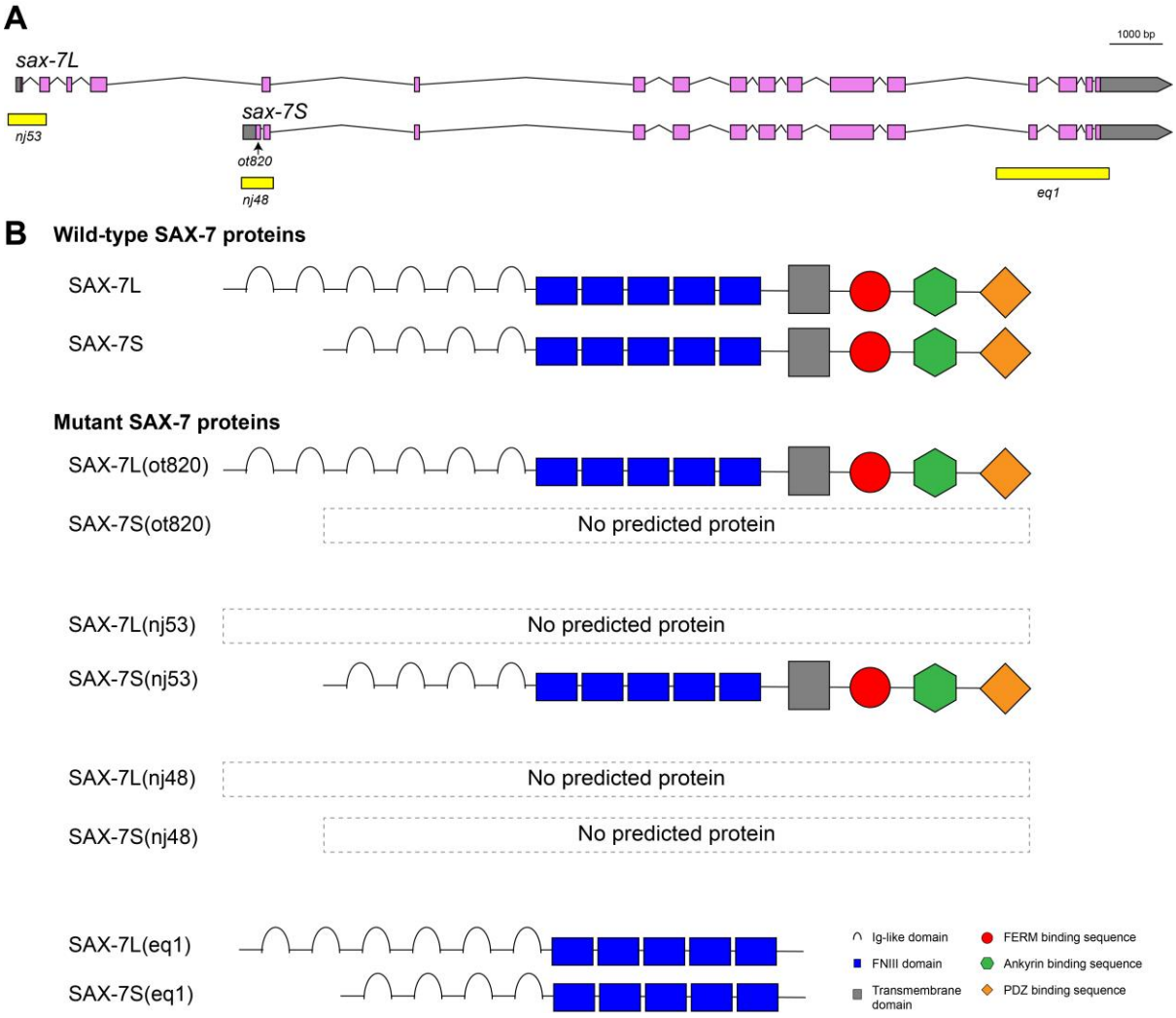

Figure 5.4 Wild-type and mutant *sax-7* alleles.

(A) Schematic of *sax-7* genomic locus, with the position of the *nj53, ot820, nj48* and *eq1* deletions (yellow boxes and arrow). *sax-7* has two isoforms: *sax-7L* and *sax-7S*. Exons (pink boxes), introns (lines) and UTRs (grey box) are indicated; 5' is on the left. Adapted from WormBase. (B) Predicted domain structure of wild-type and mutant SAX-7 proteins. Key for domains in the bottom-right corner, N-terminus is on the left.

To analyse whether SAX-7 is involved in SMDD axonal development, I performed SMDD assays on *sax-7* and *ctbp-1a* single and double mutants. Some *sax-7* mutant strains were sick at 25°C, therefore I performed the assays on Day 2 adults at 20°C. The *sax-7* mutant strains displayed wild-type axons (0-3% SMDD curls for all *sax-7* single mutants, Figure 5.5A). This demonstrates that SMDD development is not dependent on SAX-7. Strikingly, however, in *sax-7(eq1); ctbp-1a(tm5512)* mutants, the SMDD curl phenotype caused by the *ctbp-1a(tm5512)* mutation was suppressed (~20% down from ~55%, Figure 5.5A). This significant amelioration of the SMDD curl phenotype was confirmed using the *nj48* allele (~29%, Figure 5.5A).

I next analysed isoform-specific mutants to determine if one or both of the SAX-7 isoforms are involved in SMDD development (Figure 5.4). In the *sax-7S(ot820); ctbp-1a(tm5512)* mutant I observed significantly reduced SMDD curl phenotype compared to *ctbp-1a(tm5512)* mutants (~31% and ~55%, respectively) (Figure 5.5A). However, this significant decrease in SMDD curl phenotype did not occur in *sax-7L(nj53); ctbp-1a(tm5512)* mutants (~61%, Figure 5.5A). This indicates that loss of *sax-7S*, but not *sax-7L*, suppresses the *ctbp-1a(tm5512)* SMDD curl phenotype.

The *sax-7S(ot820)* mutant did not display any gross developmental or morphological phenotypes at 25°C, therefore I examined the SMDD axons at specific developmental stages at 25°C for consistency with previous SMDD curl assays in chapters 3 and 4. The *sax-7S(ot820); ctbp-1a* mutant consistently suppressed the *ctbp-1a* mutant curl phenotype at both the L4 stage and day 1 of adulthood at 25°C: at the L4 stage, the curl phenotype reduced from ~25% to ~9%, and at day 1 stage, the curl phenotype reduced from ~58% to ~22% (Figure 5.5B). Interestingly, there is incomplete or partial reduction of defective SMDD axons in *sax-7S(ot820); ctbp-1a(tm5512)* animals, suggesting that dysregulation of other molecules may also cause SMDD axon defects in *ctbp-1a* mutant animals.

Because loss of *sax-7S* suppresses the *ctbp-1a* mutant curl phenotype, I hypothesised that it may also suppress the *ctbp-1a* length phenotype. I therefore performed length assays on the *sax-7S* single and double mutants at both the L4 stage and day 1 of adulthood. At L4 stage there was no significant difference between the length of the *ctbp-1a* mutant and *sax-7S; ctbp-1a* mutant (~140 µm and ~139 µm, respectively, Figure 5.5C). At day 1 of adulthood, there was a mild reduction in length in the double mutant (~232 µm compared to *ctbp-1a* mutant ~249 µm, Figure 5.5C). Although there was a mild suppression of the double mutant at day 1 of adulthood, the *sax-7S; ctbp-1a* double mutant exhibited significantly increased SMDD axon length compared to wild-type at both developmental stages (Figure 5.5C). Overall, these results demonstrate that *sax-7S* does not suppress the *ctbp-1a* mutant overgrowth defect. This suggests that the molecular mechanism(s) through which CTBP-1a controls SMDD guidance and termination are distinct.

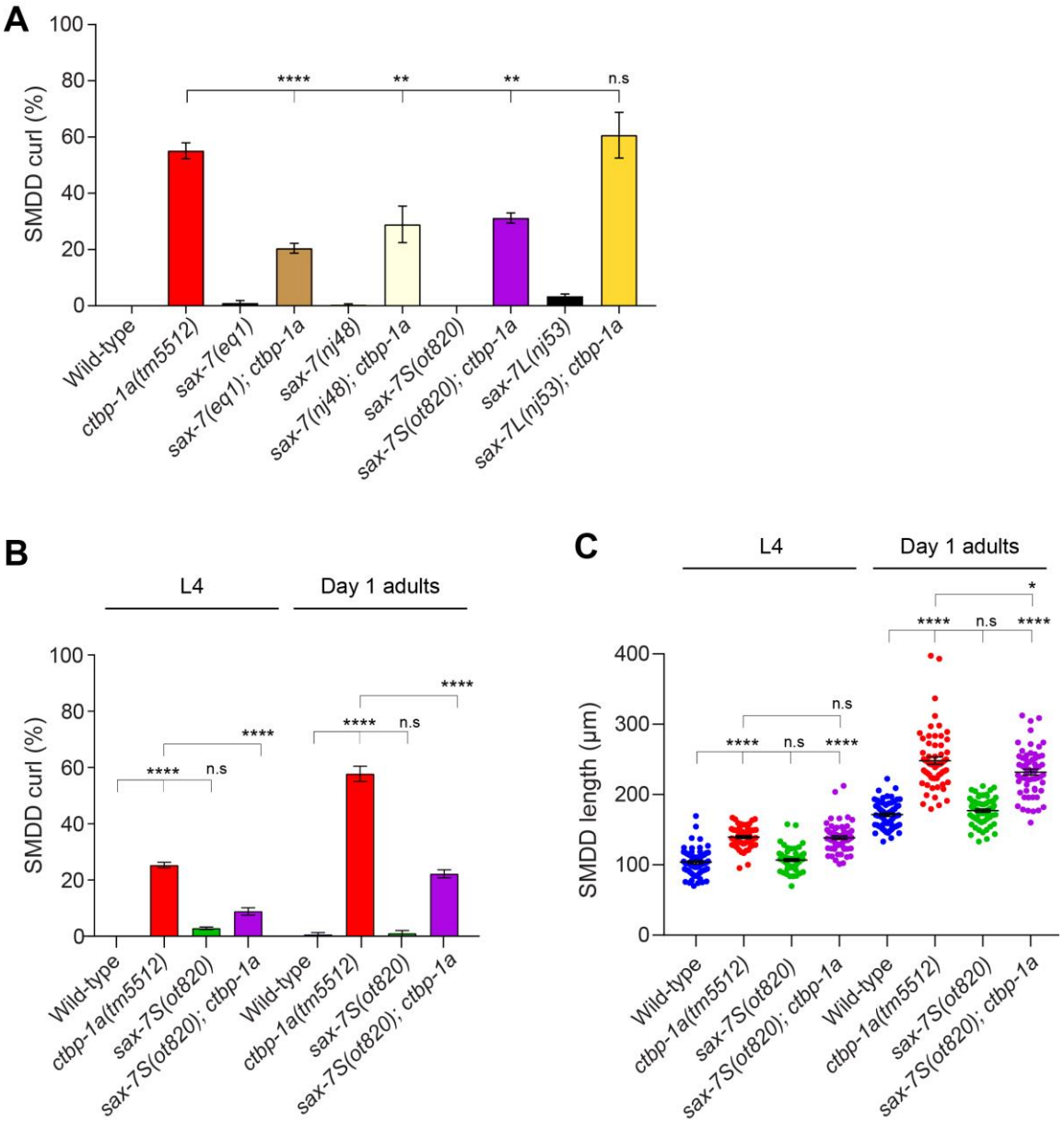

Figure 5.5 *ctbp-1a* mutant SMDD axon guidance defects are dependent on SAX-7S.

(A) Quantification of the SMDD curl phenotype (%) of wild-type and mutant animals at day 2 of adulthood at 20°C. Data presented as mean ± SEM (bar) of 3 biological replicates, n>100 axons. **p<0.01, ***p<0.001, ****p<0.001, n.s – not significant (one-way ANOVA with Tukey's correction). (B) Quantification of the SMDD curl phenotype (%) of wild-type and mutant animals at L4 stage and day 1 of adulthood at 25°C. Data presented as mean ± SEM (bar) of 3 biological replicates, n>100 axons. ****p<0.001, n.s – not significant (one-way ANOVA with Tukey's correction). (C) Quantification of SMDD length (µm) of wild-type and mutant animals at the L4 stage and day 1 of adulthood at 25°C. Data presented as mean ± SEM (bar) of 2 pooled biological replicates, n= 60-64 axons. *p<0.01, ****p<0.0001, n.s – not significant (one-way ANOVA with Tukey's correction).

5.5 SAX-7 is not involved in LAD-2 mediated axon guidance

I next asked whether removal of *sax-7* specifically reduced the *ctbp-1a* mutant phenotype, or can also non-specifically reduce the SMDD axon defects of *lad-2* mutants. I performed SMDD curl assays on L1CAM and CTBP-1a double and triple mutants. The double *lad-2(tm3056); sax-7(eq1)* null mutant SMDD curl penetrance was not significantly different from the *lad-2(tm3056)* mutant (~45% and ~38%, respectively, Figure 5.6). This confirmed previously published results, where Wang *et al.* determined that *sax-7* does not participate in *lad-2*-related axon guidance [25]. The triple *lad-2; sax-7; ctbp-1a* mutant curl phenotype (~68%) was significantly reduced compared to the double *lad-2; ctbp-1a* mutant (~92%), but this was not reduced to *lad-2* mutant levels (~38%, Figure 5.6). These results reinforce my hypothesis that *sax-7S* is specifically involved in CTBP-1-regulated axonal development and not in all SMDD developmental processes.

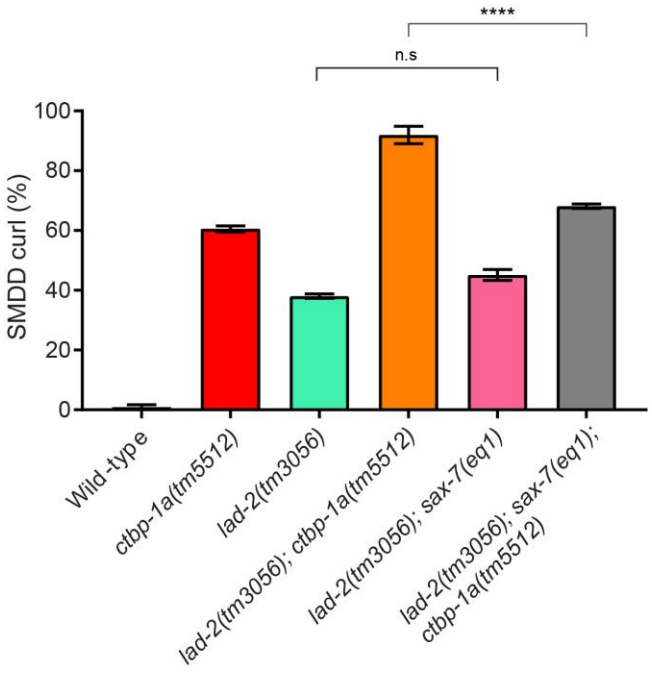

Figure 5.6 SAX-7 is not involved in LAD-2-mediated axon guidance.
Quantification of the SMDD curl phenotype (%) of wild-type and mutant animals at day 2 of adulthood at 20°C. Data presented as mean ± SEM (bar) of 3 biological replicates, n>100 axons. n.s – not significant (one-way ANOVA with Tukey's correction).

5.6 CTBP-1a regulates expression of *sax-7S*

The genetic evidence presented thus far suggests that increased *sax-7S* expression in the absence of CTBP-1a causes the SMDD curl phenotype. To examine whether CTBP-1a regulates *sax-7S* expression, I performed qRT-PCR on RNA samples extracted from wild-type and *ctbp-1a(tm5512)* mutant animals at the L4 larval stage or in mixed populations (Figure 5.7). I found that the expression level of *sax-7S*, but not *sax-7L*, is increased in the *ctbp-1a(tm5512)* mutant at the L4 stage compared to wild-type (Figure 5.7A). The expression of the *sax-7S* transcript increased ~2 fold when *ctbp-1a* was mutated (Figure 5.7A). This increase in *sax-7S* expression did not also occur in mixed stage populations (Figure 5.7B). Together, these data suggest that CTBP-1a represses *sax-7S* expression at particular developmental stages to enable correct SMDD axonal development.

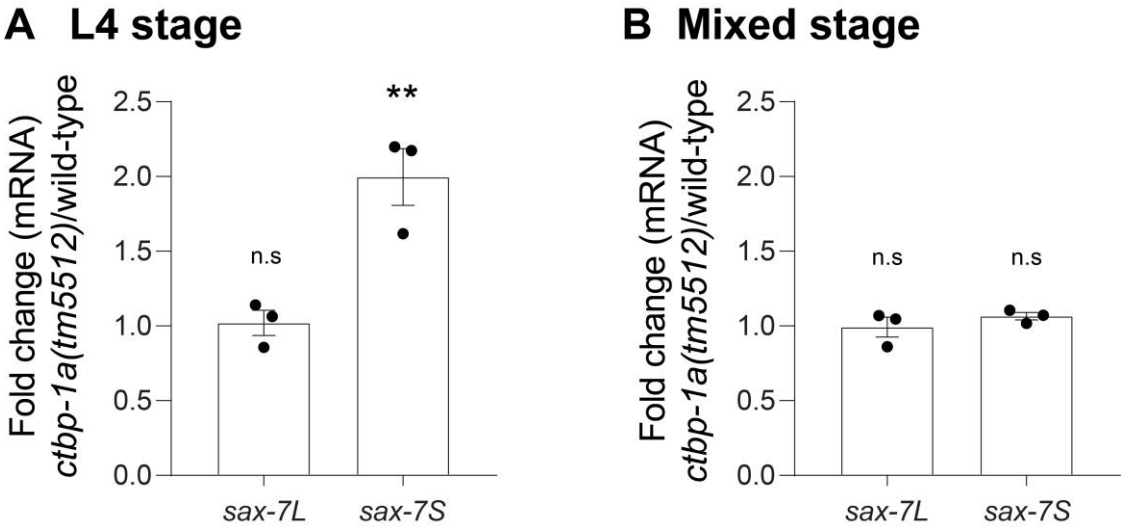

Figure 5.7 SAX-7S is upregulated in *ctbp-1a(tm5512)* L4 stage mutant animals.
qRT-PCR data showing the expression level of *sax-7S* and *sax-7L* transcripts in *ctbp-1a(tm5512)* mutants relative to wild-type at the L4 stage (A) or mixed stage populations (B). Data presented as 3 biological replicates (points) with mean ± SEM (bar). Statistical significance was determined relative to the corresponding transcript in wild-type animals, **p<0.01, n.s– not significant (one-way ANOVA with Dunnett's multiple comparisons test).

5.7 SAX-7S overexpression causes SMDD defects

As upregulation of *sax-7S* in *ctbp-1a* mutant animals causes SMDD axonal defects, I predicted that inappropriate overexpression of SAX-7S in wild-type animals would also cause SMDD axon defects. To test this, I transgenically overexpressed *sax-7S* cDNA under the 5kb *ctbp-1a*

promoter in wild-type animals (Figure 5.8B). This caused a mild SMDD curl phenotype in three independent transgenic lines (~14-17% curly, Figure 5.8B). Interestingly, the SMDD axons were often not visible in animals overexpressing *sax-7S* cDNA (~35-58% not visible, Figure 5.8B). The presence of many cell bodies and axons in the bright *glr-1::GFP* marker means that I could not determine whether these axons were extending from the cell body or in which direction they were aberrantly extending. In comparison, ~4% of axons were not visible in the wild-type animals (Figure 5.8B). This suggests that overexpressing *sax-7S* using the *ctbp-1a* promoter causes a neomorphic phenotype, where the SMDD axons do not extend in the dorsal sublateral cord. I earlier observed this phenotype in Wnt ligand *cwn-2* mutants (4.6.1), and hypothesized that these 'not visible' neurons either do not exit the nerve ring or extend in incorrect areas of the body that are obscured by other neurons expressed in the *pglr-1::GFP* (*rhIs4*) reporter (Figure 5.8A). These results suggest that overexpressing the L1CAM SAX-7 leads to severe defects in SMDD development, where the axons underextend or aberrantly extend in incorrect cords.

I next transgenically overexpressed *sax-7S* under the tissue-specific neuronal *lad-2* or hypodermal *dpy-7* promoters. Overexpressing *sax-7S* cDNA in the SMDD neurons using the *lad-2* promoter did not cause significant SMDD axon curls compared to wild-type (~2-5% curly, Figure 5.8C). However, these *lad-2* promoter driven *sax-7s* overexpression lines exhibited ~32-46% axons that were not visible in the dorsal sublateral cord (4 transgenic lines, Figure 5.8C). In contrast, overexpressing *sax-7S* cDNA in the hypodermis under the *dpy-7* promoter did not cause a detectable effect on SMDD development (2 transgenic lines, Figure 5.8D). The *pdpy-7::sax-7s* overexpression lines displayed straight axons, with no significant increase in either curly or non-visible axons compared to wild-type (Figure 5.8D).

Taken together, these results demonstrate that overexpressing *sax-7S* in the SMDD neurons causes severe defects in SMDD development, where the SMDD axons fail to extend or extend aberrantly. This suggests that correct regulation of SAX-7S expression by CTBP-1a is crucial for correct development of the SMDD neurons.

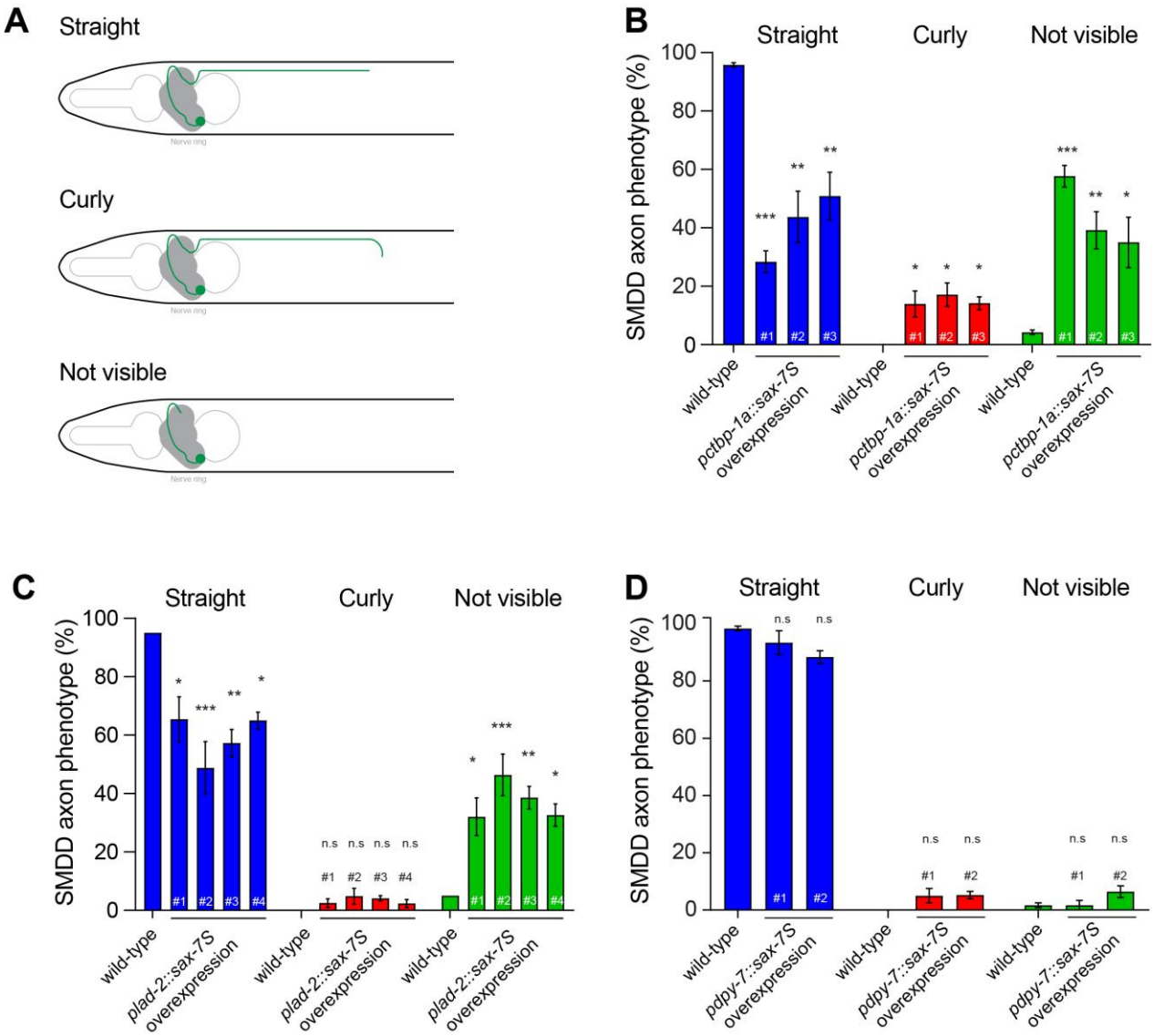

Figure 5.8 *sax-7S* overexpression in neurons causes neomorphic SMDD defects.

(A) Schematic of SMDD axon phenotypes. 'Straight' axons extend along the dorsal sublateral cord, 'curly' axons curl off and leave the dorsal sublateral cord, and 'not visible' means axons are not entering or extending along the dorsal sublateral cord. SMDD neurons in green, pharynx in light grey. (B-D) Quantification of SMDD axon phenotype (%) of *sax-7S* overexpression in neurons (*pctbp-1a::sax-7S* lines 1-3, B, and *plad-2::sax-7S* lines 1-4, C) and hypodermis (*pdpy-7::sax-7S* lines 1-2, D). (B-D) Data presented as mean ± SEM (bar) of 3 biological replicates, n>50 animals. *p<0.05, **p<0.05, ***p<0.001, n.s – not significant (one-way ANOVA with Tukey's correction).

5.8 Inappropriate interaction between the L1CAMs SAX-7 and LAD-2 in the SMDD neurons

The results presented so far indicate that ectopic expression of the L1CAM SAX-7 in the SMDD neurons causes a severe detrimental effect on SMDD development. Because LAD-2 is required for SMDD axon guidance, I predicted that the neomorphic phenotype caused by *sax-7* overexpression in the SMDD neurons could be due to an inappropriate interaction between the two *C. elegans* L1CAMs. To test this hypothesis, I crossed the *lad-2(tm3056)* mutation into one of the *plad-2::sax-7* overexpression lines (*rpEx1891*; line 1 in Figure 5.8C). Removing *lad-2* from this *sax-7S* overexpression line significantly decreased the 'not visible' axon phenotype (Figure 5.9), which shows that the SMDD defects caused by *sax-7S* overexpression is dependent on LAD-2. This suggests that SAX-7S inappropriately interacts with LAD-2 to engender a neomorphic effect on SMDD development.

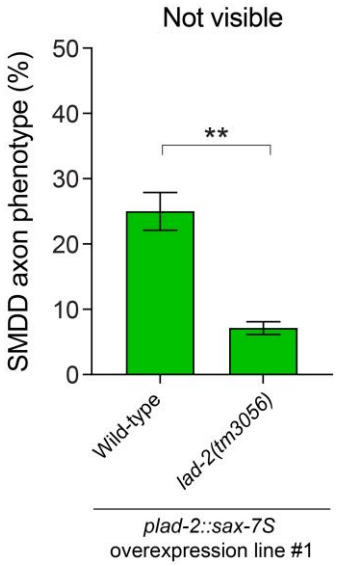

Figure 5.9 Loss of *lad-2* reduces the neomorphic SMDD axon phenotype caused by *sax-7S* overexpression.

Quantification of not visible SMDD axon phenotype (%) of wild-type and *lad-2* mutant *sax-7S* overexpression line 1 (*rpEx1891*). Data presented as mean ± SEM (bar) of 3 biological replicates, n>50 animals. **p<0.05 (unpaired t-test).

5.9 Discussion

In this chapter, I found that CTBP-1 controls SMDD development by repressing expression of the L1CAM SAX-7. Repression of SAX-7 is critical for SMDD development as SAX-7 overexpression causes a severe detrimental effect on SMDD outgrowth. I further presented evidence that the L1CAM LAD-2 acts in a parallel pathway to CTBP-1 and SAX-7 in controlling SMDD development. Therefore, the two *C. elegans* L1CAMs have distinct functions in regulating the development of the SMDD neurons.

LAD-2 regulates SMDD axonal development in a parallel pathway to CTBP-1

Previously, it was found that the L1CAM LAD-2 regulates the guidance of sublateral axons through acting as a non-canonical receptor for semaphorin and ephrin signalling [25, 41]. In this chapter, I have shown that CTBP-1a and LAD-2 act in parallel pathways to regulate SMDD axonal development. This was first evident with the *lad-2* and *ctbp-1a* mutant SMDD axon phenotypes. The *lad-2* mutant SMDD curl phenotype did not increase between the L4 stage and day 1 of adulthood (Figure 5.2). This contrasts to the *ctbp-1a* mutant phenotype, where the SMDD axon guidance defect increases in severity and penetrance over time (Figure 3.5 and Figure 5.2). Wang *et al.* previously reported that axon guidance defects were first visible at the L1 stage, suggesting that axons are being misguided early on as they extend along the sublateral cord [25]. In this project, I found that *ctbp-1a* mutants only begin displaying SMDD axon guidance defects, where the axons curl away from the dorsal sublateral cord, from the L4 stage. Therefore, LAD-2 functions earlier than CTBP-1 to regulate early SMDD axon outgrowth.

LAD-2 and CTBP-1 also regulate different steps of axonal development. The *lad-2* mutant SMDD axons display defects in axon guidance, but do not display defects in axon termination (Figure 5.2). The *lad-2* mutant axons were misguided away from the sublateral cord but terminated at the correct length, irrespective of whether or not they curled away from the sublateral cord, demonstrating that *lad-2* is only involved in guiding SMDD axon outgrowth. In contrast, I earlier found that *ctbp-1a* mutant SMDD axons are both misguided and aberrantly overextend (Chapter 3), indicating that CTBP-1 controls the guidance and termination of the SMDD axons.

In addition to regulating SMDD axonal development, LAD-2 regulates the outgrowth of other sublateral axons [25]. These axons are all cholinergic neurons that extend (or continue to extend) post-embryonically along the sublateral cords, leading the authors to speculate that LAD-2 is required to ensure that these late-extending axons grow correctly and do not merge

with the main nerve cords [25]. In contrast, CTBP-1a does not regulate the development of these other sublateral axons (Figure 5.3). Therefore, LAD-2 regulates the guidance of additional sublateral axons that are not regulated by CTBP-1.

In the previous studies that identified a role for LAD-2 in axon guidance, it was not determined whether LAD-2 functions cell-autonomously. Wang *et al.* transgenically rescued the SMD, PLN and SDQ axon guidance defects with a genomic *lad-2* construct [25]. They did not, however, rescue these defects with cell- or tissue-specific promoters. Recently, single-cell RNA-sequencing confirmed that *lad-2* is highly expressed in the nervous system, but also revealed that *lad-2* is expressed at a lower level in muscle cells in L2 stage animals [171]. Taken together with the results that LAD-2 regulates the guidance of multiple neurons in the sublateral cords, this raises the possibility that LAD-2 may function non-cell-autonomously to direct sublateral axon extension. To determine if LAD-2 regulation of SMDD axonal development is cell-autonomous, we could transgenically express *lad-2* cDNA driven by the *ctbp-1a* promoter to see if this rescues the SMDD axon guidance defects of *lad-2* null mutants.

CTBP-1a represses the L1CAM SAX-7 to allow correct axonal development

In this chapter, I also investigated the role of the L1CAM SAX-7 in SMDD axonal development. Previous studies have shown that SAX-7 functions to maintain neuronal architecture once neurons have finished developing [141, 145, 146]. In the context of SMDD axonal development, loss of *sax-7* alone does not cause any detectable phenotype (Figure 5.5). However, I found that removal of the SAX-7 short isoform but not the long isoform suppresses the SMDD curl phenotype of *ctbp-1a* mutant animals (Figure 5.5). This genetic evidence suggested that CTBP-1a normally represses the function of the SAX-7S isoform. Consistent with this, in a *ctbp-1a* mutant, *sax-7S* expression is upregulated when CTBP-1a is lost (Figure 5.7). These results led us to hypothesise that ectopic overexpression of SAX-7S would cause defects in SMDD axonal development. I observed that transgenic overexpression of SAX-7S in the SMDD neurons caused a dramatic SMDD axon phenotype, where the axons did not visibly extend in the dorsal sublateral cord. In contrast, overexpressing *sax-7S* in the hypodermis did not cause this neomorphic phenotype. This suggests that precise spatial regulation of SAX-7S by CTBP-1a is required for SMDD axonal development.

Both of the SMDD promoters (*ctbp-1a* and *lad-2*) ectopically drive *sax-7S* expression in the SMDD neurons from early in embryogenesis through to adulthood (Chapter 3 and [25], respectively). Thus far, I have been unable to determine whether the *sax-7* overexpression SMDD axons are failing in axon outgrowth or extending aberrantly in other nerve cords. To determine whether/where these axons are extending, we could overexpress *sax-7S* cDNA in

animals expressing the *pctbp-1a::GFP* reporter. As I discussed in Chapter 4 regarding the *cwn-2* mutant phenotype (Section 4.7), this would allow the tracking of SMDD axon outgrowth as only the SMDD axons are visible.

Parallel regulation of SMDD axonal development by the two *C. elegans* L1CAMs

The SMDD axon phenotype caused *sax-7S* overexpression led me to hypothesise that SMDD axonal development was severely impacted by an inappropriate interaction between LAD-2 and misexpressed SAX-7. Consistent with this, removing *lad-2* from the *sax-7* overexpression background reduced the neomorphic SMDD axon phenotype (Figure 5.9). These results indicate that when SAX-7 is misexpressed in the SMDD neurons, it inappropriately interacts with the other L1CAM LAD-2 to cause defects in SMDD axonal development. It would be interesting to determine what domains of SAX-7S are essential for this neomorphic phenotype. Like mammalian L1CAMs, SAX-7 is composed of extracellular Ig-like and FNIII domains and an intracellular domain that contains ankyrin, FERM and PDZ binding motifs [142]. In future studies, we could individually delete these domains in the *sax-7S* overexpression constructs to observe the effect on SMDD axonal development. This analysis may reveal the SAX-7 domains that are interacting with LAD-2 to disrupt SMDD axon outgrowth.

Based on these results, I hypothesise that SAX-7 is not meant to be expressed in the SMDD neurons to allow LAD-2-mediated axon guidance. SAX-7 is widely expressed in the nervous system and hypodermis, and the identity of all individual SAX-7-expressing neurons has not been determined [142-144]. To determine if SAX-7 is normally expressed in wild-type animals in the SMDD neurons, we should first analyse the endogenous expression pattern of SAX-7 during different developmental stages. To identify the SMDD axons, we could co-express a fluorescent marker driven by the *pctbp-1a* promoter that would label the SMDD cell bodies and axons. Next, we could introduce the *ctbp-1a* mutation into these animals to determine whether SAX-7 is misexpressed in the SMDD neurons when CTBP-1a is lost. As I identified that CTBP-1 regulates the expression of the SAX-7S isoform only, this expression analysis would ideally be performed with SAX-7S-specific reporters.

In summary, I have shown that the transcriptional repressor CTBP-1a is required to repress SAX-7 in the SMDD neurons so that LAD-2 can direct SMDD axon outgrowth and guidance along the dorsal sublateral cord (Figure 5.10). These results reveal that correct temporal and spatial regulation of L1CAM expression is required for the development of the SMDD axons.

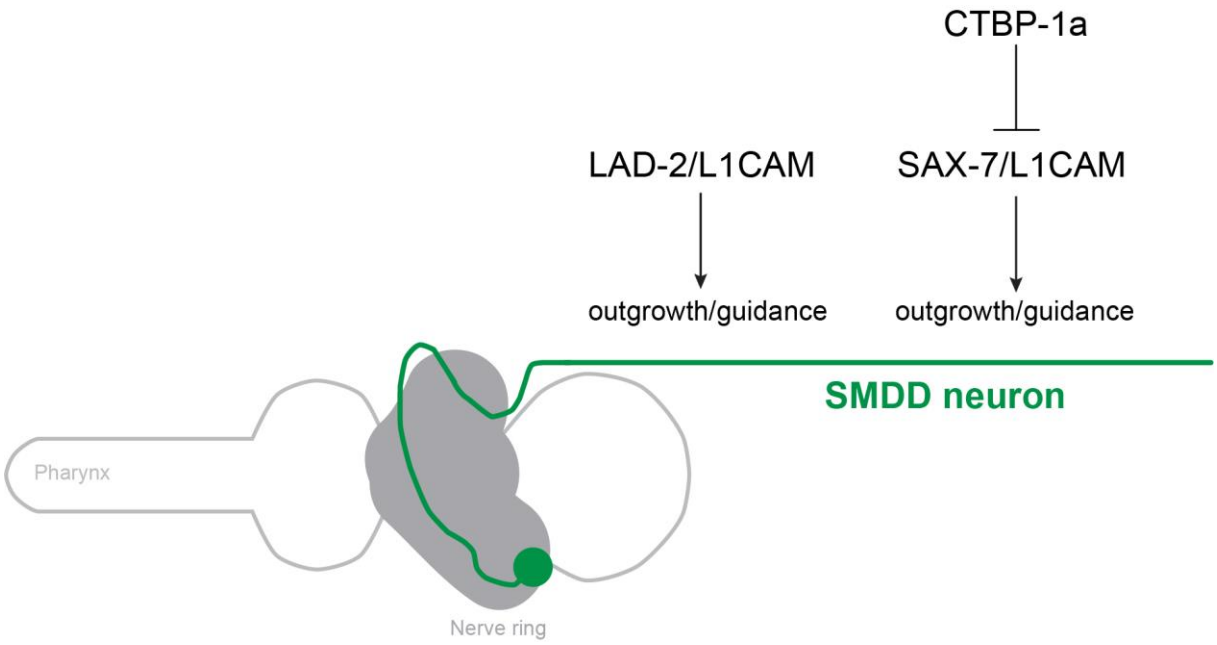

Figure 5.10 Regulation of SMDD axonal development by the L1CAMs LAD-2 and SAX-7.
CTBP-1a represses SAX-7 expression to allow correct axon guidance and outgrowth. In a parallel genetic pathway, LAD-2 regulates SMDD axon guidance. Anterior is left, ventral is down.

Regulation of L1CAMs by THAP-containing proteins is potentially conserved

In this chapter, I found that the THAP-containing CTBP-1a represses the L1CAM SAX-7 to allow correct SMDD axonal development. Studies in mammalian models suggest that regulation of L1CAMs by THAP-containing proteins may be conserved. RNA-sequencing analysis of Thap1 mutant mouse models revealed that L1 family members are dysregulated when Thap1 levels are reduced: in a conditional Thap1 knockout mouse model, L1CAM is differentially expressed [181], and heterozygous Thap1$^{+/-}$ mice exhibit significantly upregulated expression of the L1 family members Neurofascin and CHL1 in the striatum [182]. These transcriptional changes have not been confirmed. However, ChIP-sequencing data available on ENCODE indicate that human THAP1 can interact with the L1CAM locus (ENCSR000BNN) [216, 217]. Therefore, THAP1 may directly regulate expression of L1CAM in mammals.

6. Conclusion

6.1 Thesis summary

The main aim of this thesis was to gain insight into the role of the *C. elegans* transcriptional repressor CTBP-1 in axonal development. My results reveal that CTBP-1a is required for axonal development of the SMDD motor neurons. Instead of terminating their outgrowth as animals reach adulthood, the SMDD axons of animals lacking CTBP-1a continue to extend. In addition to regulating axon outgrowth, CTBP-1a is also required to maintain the SMDDs within the sublateral nerve cord. CTBP-1a regulates SMDD axon guidance by repressing the expression of the L1CAM SAX-7. This regulation is important, as dysregulation of SAX-7 causes severe defects in SMDD axon development. In a parallel pathway, the other *C. elegans* L1CAM LAD-2 regulates SMDD axon guidance. Collectively, my research has revealed that the correct expression of two L1CAMs is crucial for controlling SMDD development. I have shown that faithful SMDD development requires the repression of SAX-7 by CTBP-1a, which I hypothesize to be important for LAD-2 to perform its normal function.

6.2 Novel role for CTBP-1a THAP domain

C-terminal binding proteins regulate neuronal development in mammals and invertebrates [75, 77, 78, 81-83]. Consistent with this, we recently identified the first role for *C. elegans* CTBP-1 in neuronal development [93]. Specifically, we found that *C. elegans ctbp-1* hypomorphic mutants displayed defective axonal morphology of the SMDD motor neurons [93]. To further understand the function of CTBP-1 in SMDD axonal development, I analysed the development of these axons during larval development and adulthood and found that CTBP-1 controls axon termination from the L3 stage and axon guidance from the L4 stage (Chapter 3). Because of the known role of CtBPs as transcriptional corepressors, I predicted that *C. elegans* CTBP-1 regulates SMDD axonal development through binding corepressor proteins that harbour a PXDLS motif. In humans, it was recently found that the ability of CtBP1 to bind corepressor proteins is vital for correct neurodevelopment [77-79]. A pathogenic mutation in the CtBP1 PXDLS-binding cleft was reported in multiple patients with neurodevelopmental disabilities [77-79]. This mutation disrupted association with known members of the CtBP corepressor complex and resulted in altered regulation of genes involved in multiple cellular pathways, including brain development [79]. In *C. elegans*, CTBP-1a contains a conserved PXDLS-binding cleft, which is important for interactions with members of the corepressor complex [65, 68]. However, I found that the PXDLS-binding cleft is dispensable for CTBP-1-mediated SMDD axonal development. Using isoform-specific mutations and transgenic rescue analysis I

revealed that the THAP domain of CTBP-1a is required and sufficient for regulation of SMDD development. Overall, these results suggest that the intrinsic DNA-binding capacity of the CTBP-1a THAP domain, and not interactions with corepressor proteins, is critical for the function of CTBP-1a in controlling SMDD development.

The DNA-binding THAP domain is present in nematode CtBPs but is not present in mammalian CtBP family members [68], therefore it would be interesting to determine what function the THAP domain performs in *C. elegans* CTBP-1a. Over 100 distinct THAP proteins have been identified across diverse species, but the majority of these have not been characterized [87]. Many of the studied THAP proteins function in transcriptional regulation. For example, THAP1 and THAP11/Ronin can both activate and repress transcriptional targets [218, 219]. THAP domains function as sequence-specific DNA-binding motifs [86, 87], therefore the CTBP-1a THAP domain may directly bind DNA to repress gene transcription. However, THAP domains have also been found to bind other proteins [220]. The THAP domain of human THAP7 recruits corepressor proteins, including HDAC3, to repress transcription [220]. Therefore, the CTBP-1a THAP domain may interact with proteins to form a corepressor complex. As CTBP-1 can repress gene expression by binding proteins with the PXDLS motif [68], this raises the possibility that the THAP domain provides an additional mechanism to form corepressor complexes. Further investigation is required to determine the function of CTBP-1a THAP domain. We could perform ChIP-seq to identify the promoters that CTBP-1a binds, which may reveal novel THAP binding sites. In addition, we could perform pull-down of CTBP-1a followed by mass spectrometry analysis to identify proteins in the CTBP-1a-containing complex.

6.3 Proposed model for SMDD development

In the course of this study, I have identified multiple factors that are involved in the development of the SMDD axons. Taking all of these results together, I propose a model for SMDD axonal development (Figure 6.1). After being born in early embryogenesis, SMDD neurons extend axons from the ventral side of the body through the nerve ring [4, 6, 11]. This early axon outgrowth is regulated by the Wnt molecule CWN-2. During larval stages, the L1CAM LAD-2 controls SMDD axon guidance along the dorsal sublateral cord. In a parallel pathway, CTBP-1a represses the expression of the L1CAM SAX-7 to allow correct axon outgrowth. The expression of L1CAMs is tightly regulated to shape axon outgrowth and guidance decisions. In addition, CTBP-1a controls the late stages of SMDD axon termination through unidentified mechanisms (Figure 6.1).

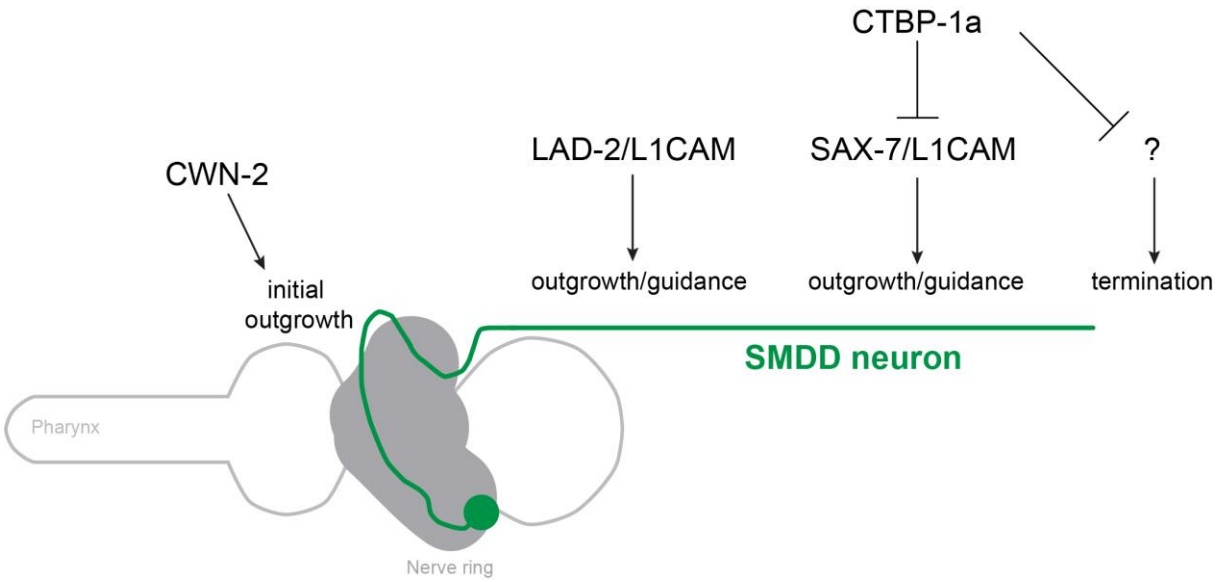

Figure 6.1 Model for SMDD axonal development.

The Wnt ligand CWN-2 regulates initial SMDD axon outgrowth from the nerve ring. The L1CAM LAD-2 regulates the outgrowth and guidance along the dorsal sublateral tract. In a parallel genetic pathway, the corepressor CTBP-1a represses the expression of the L1CAM SAX-7 to allow correct axon guidance. In addition, CTBP-1 controls axon termination through regulating unidentified genes. Anterior is left, ventral is down.

In Chapter 5, I found that overexpression of SAX-7 in the SMDD neurons caused a neomorphic phenotype, where the SMDD neurons fail to outgrow and/or enter inappropriate nerve cords. This phenotype is dependent on LAD-2 expression and is remarkably similar to loss of the Wnt ligand CWN-2. Therefore, it is possible that the interaction between the two L1CAMs causes sequestration or inhibition of the Wnt CWN-2. Thus far, *C. elegans* L1CAMs have not been implicated in regulation of Wnt signalling. However, it was recently found that human L1/L1CAM regulates canonical Wnt signalling [221]. In addition, it was previously shown that the *C. elegans* immunoglobulin superfamily member CAM-1 sequesters Wnt ligands to regulate vulval development [222]. Therefore, inappropriate expression of SAX-7 in the SMDD neurons may interact with LAD-2 and sequester CWN-2. CWN-2 is highly expressed in the SMDD neurons at the L4 stage when they undergo axon extension [205, 206]. In future studies, I will examine whether the aberrant L1CAM interaction causes Wnt sequestration by overexpressing CWN-2 in the *sax-7S* overexpression lines. If overexpression of CWN-2 ameliorated the neomorphic 'not visible' SMDD phenotype, this could reveal that inappropriate expression of SAX-7 with LAD-2 in the SMDD neurons acts as a sink for Wnt signalling. Furthermore, it would be interesting to use fluorescent expression markers to determine whether *cwn-2* expression changes when SAX-7S is overexpressed.

Alternatively, the interaction between the two L1CAMs could result in aberrant signalling during SMDD axonal development. Thus far, no overlapping roles or interaction between SAX-7 and LAD-2 have been identified [153]. Both LAD-2 and SAX-7 contain conserved extracellular Ig-like and FNIII domains, but LAD-2 contains a divergent cytoplasmic tail that contains no known motifs such as the ankyrin-binding motif present in SAX-7 and vertebrate L1CAMs [25]. The extracellular domains of SAX-7 mediate cell adhesion by homophilic and heterophilic interactions [141, 145]. In addition, the intracellular domains of SAX-7 interact with the actin cytoskeletal components UNC-44/ankyrin and STN-2/γ-syntrophin [146]. Therefore, the expression of SAX-7 with LAD-2 in the SMDD neurons may cause inappropriate adhesion and/or protein interactions. To test this possibility, we could express the individual SAX-7S domains (Ig-like, FNIII and intracellular domains) in wild-type animals and examine SMDD development. As suggested in the previous discussion (section 5.9), analysis of the effect of these constructs on SMDD axonal development may reveal the SAX-7S domains that cause severe defects in SMDD outgrowth.

In Chapter 4, I found that the ETS-domain transcription factor AST-1 functions in a parallel pathway to CTBP-1a to regulate SMDD axonal development. AST-1 is an essential transcription factor for *C. elegans* early larval development, and null mutants could not be used because of lethality [21]. Future analysis of AST-1 function in SMDD development could be performed by depleting AST-1 protein at different larval stages and adulthood using auxin-inducible degradation [174]. If AST-1 does not also have essential roles in these later developmental stages, degrading AST-1 could reveal whether complete loss of function causes defects in SMDD axon guidance. As I have also identified that LAD-2 functions in a parallel pathway to CTBP-1a, it would be interesting to investigate whether AST-1 functions in the same genetic pathway as LAD-2.

6.4 SMDD function

Because the SMDD neurons function as motor neurons, it would be interesting to determine whether mutations causing defects in SMDD axon outgrowth, guidance and/or termination affect motor function. In Chapter 3, I observed that *ctbp-1a* mutants display decreased exploration behaviour, suggesting that defective SMDD morphology may contribute to defective body movement. However, CTBP-1a is expressed in multiple neurons and could potentially regulate the development or function of other neurons in addition to the SMDs. We previously found that there are no gross defects in neuronal morphology in *ctbp-1a* mutants [93]. In Chapter 5, I found there was no defects in SDQ and PLN sensory axon development, indicating that loss of CTBP-1a does not cause general defects in axons that extend along the

sublateral cords. However, we have not analysed the development of all neurons either directly or indirectly controlling locomotion. Therefore, it is possible that defective exploration behaviour I observed in *ctbp-1a* mutants are not directly related to loss of SMD function. To determine if exploration behaviour defects were due to defective SMDD neurons, we could express *ctbp-1a* in just the SMDD neurons and see the effect on exploration behaviour. Thus far, no SMDD-specific promoters have been identified. However, recently Taylor *et al.* reported the gene expression profile of individual *C. elegans* neuron classes, including SMDD, at the L4 stage [206]. Analysing genes that are exclusively expressed in the SMDD neurons will potentially reveal a cell-specific promoter that can be used for transgenic rescue experiments.

The other members of the SMDD axonal development pathway, LAD-2, SAX-7 and CWN-2, all regulate the development or maintenance of multiple classes of neurons [25, 47, 145]. For example, *cwn-2* mutants also display defects in RMED/V motor neuron axon outgrowth [47]. Therefore, examining the locomotion of these pleiotropic mutant animals would not reveal the direct effect of aberrant SMD axonal development. Instead, future studies could focus on the synaptic output of SMDD axons. As all of these mutants display SMDD axons that do not extend in the sublateral cord, leave this tract and/or overextend in the cord, I hypothesise that the SMDD axons will not form functional synapses or will inappropriately synapse onto incorrect targets. All studies thus far have focussed on the role of SMD neurons in regulating head and neck bending [12-14], but have not studied the axons that extend along the sublateral cords. The sublateral axons have been understudied because they extend through body regions that were not completely imaged by electron microscopy until recently [10]. Recent analysis as part of the publication of the *C. elegans* adult connectome revealed that the 5 classes of sublateral motor neurons (including SMDs) synapse to muscle cells and release the neurotransmitter acetycholine [10]. However, the muscle cell targets of individual sublateral axons at different life stages have not been determined. Future studies to understand the function and muscle cell targets of SMDD axons in wild-type and mutant animals may help reveal the impact of aberrant SMDD axonal development.

6.5 SMDD axon termination

After outgrowth and extension along specific nerve cords, *C. elegans* axons typically terminate at reproducible positions. In this study, I found that CTBP-1a regulates SMDD axon guidance and termination. To my knowledge, this is the first identified factor involved in SMDD axon termination. Given that CTBP-1a is a transcriptional corepressor, it likely functions as a transcriptional regulator of genes involved in axon termination. I found that CTBP-1a controls SMDD axon guidance by repressing the L1CAM SAX-7. However, I found that loss of *sax-7S*

does not suppress the *ctbp-1a* overextension/termination defects (Chapter 5), which indicates that CTBP-1a mediates SMDD axon termination independently of SAX-7. To determine the pathway that CTBP-1 functions in to regulate SMDD axon termination, we could analyse known genes that regulate axon termination. Previously, several studies found that the ubiquitin ligase RPM-1 regulates termination of mechanosensory and GABAergic motor neuron axons [26, 27]. However, I found that *rpm-1* is not involved in SMDD axon termination (Chapter 4).

Additional regulators of *C. elegans* axon termination have been identified. Wnts act as instructive cues along the anterior-posterior axis for axon guidance and termination [46, 47]. The Wnts LIN-44 and EGL-20 are secreted from the tail to repel the DD6 motor neuron axon growth along the dorsal cord [46]. In Chapter 4, I found that the Wnt ligand CWN-2 plays an important role in SMDD axon outgrowth, and therefore Wnt signalling may play a key role in multiple steps of SMDD axon development. Interestingly, CtBP regulates Wnt signalling in vertebrates and invertebrates [223, 224]. For example, *Drosophila* CtBP (dCtBP) both represses and activates Wnt gene expression [224]. In addition, ephrin signalling regulates axon termination of multiple classes of neurons. Mutations of the ephrin receptor *vab-1* cause axon overextension phenotypes of both the PLM mechanosensory neurons and DVB motor neurons [40]. The PLM and DVB axons extend and terminate in different nerve cords [6], suggesting that ephrin signalling mediates the termination of axons in different environments. Therefore, CTBP-1a may function in the same pathway as known regulators of axon termination, including Wnts and ephrins. We could investigate whether these factors influence SMDD axon termination and perform epistasis experiments. Alternatively, we could perform a modifier screen on *ctbp-1a* mutants to identify mutations that either enhance or suppress the *ctbp-1a* termination phenotype [225]. This modifier screen could identify genes that function in the same genetic pathway as *ctbp-1a.* In addition, it could reveal genes that function in parallel pathways for SMDD termination. As we currently do not know any other regulators of SMDD axon termination, this unbiased screen could expand our understanding of *C. elegans* axon development.

6.6 Final remarks

In this thesis, I have characterised the roles of multiple factors that control *C. elegans* axonal development. The Wnt ligand CWN-2 is required for early SMDD axon outgrowth. At later developmental stages, CTBP-1a mediates the guidance of the SMDD axons along the sublateral cord by repressing the expression of the L1CAM SAX-7. In a parallel pathway, the L1CAM LAD-2 is required to regulate axon guidance. These conserved factors all play key

roles in nervous system development in mammalian model systems, and these findings may represent a conserved mechanism for regulation of brain development. Further investigations using the SMDD axons as a model system will provide insight into the mechanisms of longitudinal axonal development.

7. References

1. **Brenner S**. The genetics of Caenorhabditis elegans. *Genetics* 1974;77(1):71-94.
2. **Altun ZF, Hall DH**. *Introduction*. WormAtlas 2009.
3. **Herndon LA, Wolkow CA, Driscoll M, Hall DH**. *Introduction to Aging in C. elegans.* WormAtlas 2018.
4. **Sulston JE, Schierenberg E, White JG, Thomson JN**. The embryonic cell lineage of the nematode Caenorhabditis elegans. *Developmental biology* 1983;100(1):64-119.
5. **Varshney LR, Chen BL, Paniagua E, Hall DH, Chklovskii DB**. Structural properties of the Caenorhabditis elegans neuronal network. *PLoS Comput Biol* 2011;7(2):e1001066.
6. **White JG, Southgate E, Thomson JN, Brenner S**. The structure of the nervous system of the nematode Caenorhabditis elegans. *Philosophical transactions of the Royal Society of London Series B, Biological sciences* 1986;314(1165):1-340.
7. **Altun ZF, Hall DH**. *Nervous system, general description*. WormAtlas 2011.
8. **Sulston JE, Horvitz HR**. Post-embryonic cell lineages of the nematode, Caenorhabditis elegans. *Developmental biology* 1977;56(1):110-156.
9. **Albeg A, Smith CJ, Chatzigeorgiou M, Feitelson DG, Hall DH et al.** C. elegans multi-dendritic sensory neurons: morphology and function. *Mol Cell Neurosci* 2011;46(1):308-317.
10. **Cook SJ, Jarrell TA, Brittin CA, Wang Y, Bloniarz AE et al.** Whole-animal connectomes of both Caenorhabditis elegans sexes. *Nature* 2019;571(7763):63-71.
11. **Rapti G, Li C, Shan A, Lu Y, Shaham S**. Glia initiate brain assembly through noncanonical Chimaerin-Furin axon guidance in C. elegans. *Nature Neuroscience* 2017;20(10):1350-1360.
12. **Shen Y, Wen Q, Liu H, Zhong C, Qin Y et al.** An extrasynaptic GABAergic signal modulates a pattern of forward movement in Caenorhabditis elegans. *eLife* 2016;5.
13. **Gray JM, Hill JJ, Bargmann CI**. A circuit for navigation in Caenorhabditis elegans. *Proc Natl Acad Sci U S A* 2005;102(9):3184-3191.
14. **Yeon J, Kim J, Kim DY, Kim H, Kim J et al.** A sensory-motor neuron type mediates proprioceptive coordination of steering in C. elegans via two TRPC channels. *PLoS biology* 2018;16(6):e2004929.
15. **Durbin RM**. *Studies on the development and organisation of the nervous system of C. elegans*. Doctor of Philosophy Thesis, University of Cambridge; 1987.
16. **Chisholm AD, Hutter H, Jin Y, Wadsworth WG**. The Genetics of Axon Guidance and Axon Regeneration in Caenorhabditis elegans. *Genetics* 2016;204(3):849-882.
17. **Wadsworth WG, Bhatt H, Hedgecock EM**. Neuroglia and pioneer neurons express UNC-6 to provide global and local netrin cues for guiding migrations in C. elegans. *Neuron* 1996;16(1):35-46.
18. **Wadsworth WG, Hedgecock EM**. Hierarchical guidance cues in the developing nervous system of C. elegans. *BioEssays : news and reviews in molecular, cellular and developmental biology* 1996;18(5):355-362.
19. **Hao JC, Yu TW, Fujisawa K, Culotti JG, Gengyo-Ando K et al.** C. elegans slit acts in midline, dorsal-ventral, and anterior-posterior guidance via the SAX-3/Robo receptor. *Neuron* 2001;32(1):25-38.
20. **Hutter H**. Formation of longitudinal axon pathways in Caenorhabditis elegans. *Semin Cell Dev Biol* 2019;85:60-70.

21. **Schmid C, Schwarz V, Hutter H**. AST-1, a novel ETS-box transcription factor, controls axon guidance and pharynx development in C. elegans. *Developmental biology* 2006;293(2):403-413.
22. **Riveiro AR, Mariani L, Malmberg E, Amendola PG, Peltonen J et al.** JMJD-1.2/PHF8 controls axon guidance by regulating Hedgehog-like signaling. *Development* 2017.
23. **Bossing T, Brand AH**. Determination of cell fate along the anteroposterior axis of the Drosophila ventral midline. *Development* 2006;133(6):1001-1012.
24. **Charron F, Stein E, Jeong J, McMahon AP, Tessier-Lavigne M**. The morphogen Sonic hedgehog is an axonal chemoattractant that collaborates with Netrin-1 in midline axon guidance. *Cell* 2003;113(1):11-23.
25. **Wang X, Zhang W, Cheever T, Schwarz V, Opperman K et al.** The C. elegans L1CAM homologue LAD-2 functions as a coreceptor in MAB-20/Sema2 mediated axon guidance. *The Journal of cell biology* 2008;180(1):233-246.
26. **Schaefer AM, Hadwiger GD, Nonet ML**. rpm-1, a conserved neuronal gene that regulates targeting and synaptogenesis in C. elegans. *Neuron* 2000;26(2):345-356.
27. **Opperman KJ, Grill B**. RPM-1 is localized to distinct subcellular compartments and regulates axon length in GABAergic motor neurons. *Neural Dev* 2014;9.
28. **Li H, Kulkarni G, Wadsworth WG**. RPM-1, a Caenorhabditis elegans protein that functions in presynaptic differentiation, negatively regulates axon outgrowth by controlling SAX-3/robo and UNC-5/UNC5 activity. *The Journal of neuroscience : the official journal of the Society for Neuroscience* 2008;28(14):3595-3603.
29. **Najarro EH, Wong L, Zhen M, Carpio EP, Goncharov A et al.** Caenorhabditis elegans flamingo cadherin fmi-1 regulates GABAergic neuronal development. *The Journal of neuroscience : the official journal of the Society for Neuroscience* 2012;32(12):4196-4211.
30. **Huarcaya Najarro E, Ackley BD**. C. elegans fmi-1/flamingo and Wnt pathway components interact genetically to control the anteroposterior neurite growth of the VD GABAergic neurons. *Developmental biology* 2013;377(1):224-235.
31. **Steimel A, Wong L, Najarro EH, Ackley BD, Garriga G et al.** The Flamingo ortholog FMI-1 controls pioneer-dependent navigation of follower axons in C. elegans. *Development* 2010;137(21):3663-3673.
32. **Kruger RP, Aurandt J, Guan KL**. Semaphorins command cells to move. *Nat Rev Mol Cell Biol* 2005;6(10):789-800.
33. **Ginzburg VE, Roy PJ, Culotti JG**. Semaphorin 1a and semaphorin 1b are required for correct epidermal cell positioning and adhesion during morphogenesis in C. elegans. *Development* 2002;129(9):2065-2078.
34. **Huot J**. Ephrin signaling in axon guidance. *Prog Neuropsychopharmacol Biol Psychiatry* 2004;28(5):813-818.
35. **Egea J, Klein R**. Bidirectional Eph-ephrin signaling during axon guidance. *Trends in cell biology* 2007;17(5):230-238.
36. **Miller MA, Chin-Sang ID**. Eph receptor signaling in C. elegans. *WormBook* 2012:1-17.
37. **Zallen JA, Kirch SA, Bargmann CI**. Genes required for axon pathfinding and extension in the C. elegans nerve ring. *Development* 1999;126(16):3679-3692.
38. **Boulin T, Pocock R, Hobert O**. A novel Eph receptor-interacting IgSF protein provides C. elegans motoneurons with midline guidepost function. *Current biology : CB* 2006;16(19):1871-1883.

39. **Pocock R, Hobert O**. Oxygen levels affect axon guidance and neuronal migration in Caenorhabditis elegans. *Nature neuroscience* 2008;11(8):894-900.
40. **Mohamed AM, Chin-Sang ID**. Characterization of loss-of-function and gain-of-function Eph receptor tyrosine kinase signaling in C. elegans axon targeting and cell migration. *Developmental biology* 2006;290(1):164-176.
41. **Dong B, Moseley-Alldredge M, Schwieterman AA, Donelson CJ, McMurry JL et al.** EFN-4 functions in LAD-2-mediated axon guidance in Caenorhabditis elegans. *Development* 2016;143(7):1182-1191.
42. **Schwieterman AA, Steves AN, Yee V, Donelson CJ, Bentley MR et al.** The Caenorhabditis elegans Ephrin EFN-4 Functions Non-cell Autonomously with Heparan Sulfate Proteoglycans to Promote Axon Outgrowth and Branching. *Genetics* 2016;202(2):639-660.
43. **Ackley BD**. Wnt-signaling and planar cell polarity genes regulate axon guidance along the anteroposterior axis in C. elegans. *Developmental neurobiology* 2014;74(8):781-796.
44. **Harterink M, Kim DH, Middelkoop TC, Doan TD, van Oudenaarden A et al.** Neuroblast migration along the anteroposterior axis of C. elegans is controlled by opposing gradients of Wnts and a secreted Frizzled-related protein. *Development* 2011;138(14):2915-2924.
45. **Pan CL, Howell JE, Clark SG, Hilliard M, Cordes S et al.** Multiple Wnts and frizzled receptors regulate anteriorly directed cell and growth cone migrations in Caenorhabditis elegans. *Dev Cell* 2006;10(3):367-377.
46. **Maro GS, Klassen MP, Shen K**. A beta-catenin-dependent Wnt pathway mediates anteroposterior axon guidance in C. elegans motor neurons. *PloS one* 2009;4(3):e4690.
47. **Song S, Zhang B, Sun H, Li X, Xiang Y et al.** A Wnt-Frz/Ror-Dsh pathway regulates neurite outgrowth in Caenorhabditis elegans. *PLoS genetics* 2010;6(8).
48. **Hilliard MA, Bargmann CI**. Wnt signals and frizzled activity orient anterior-posterior axon outgrowth in C. elegans. *Dev Cell* 2006;10(3):379-390.
49. **Prasad BC, Clark SG**. Wnt signaling establishes anteroposterior neuronal polarity and requires retromer in C. elegans. *Development* 2006;133(9):1757-1766.
50. **Bulow HE, Boulin T, Hobert O**. Differential functions of the C. elegans FGF receptor in axon outgrowth and maintenance of axon position. *Neuron* 2004;42(3):367-374.
51. **Benard CY, Boyanov A, Hall DH, Hobert O**. DIG-1, a novel giant protein, non-autonomously mediates maintenance of nervous system architecture. *Development* 2006;133(17):3329-3340.
52. **Benard C, Tjoe N, Boulin T, Recio J, Hobert O**. The small, secreted immunoglobulin protein ZIG-3 maintains axon position in Caenorhabditis elegans. *Genetics* 2009;183(3):917-927.
53. **DeVore DL, Horvitz HR, Stern MJ**. An FGF receptor signaling pathway is required for the normal cell migrations of the sex myoblasts in C. elegans hermaphrodites. *Cell* 1995;83(4):611-620.
54. **Burket CT, Higgins CE, Hull LC, Berninsone PM, Ryder EF**. The C. elegans gene dig-1 encodes a giant member of the immunoglobulin superfamily that promotes fasciculation of neuronal processes. *Developmental biology* 2006;299(1):193-205.
55. **Aurelio O, Hall DH, Hobert O**. Immunoglobulin-domain proteins required for maintenance of ventral nerve cord organization. *Science* 2002;295(5555):686-690.

56. **Aurelio O, Boulin T, Hobert O**. Identification of spatial and temporal cues that regulate postembryonic expression of axon maintenance factors in the C. elegans ventral nerve cord. *Development* 2003;130(3):599-610.
57. **Benard CY, Blanchette C, Recio J, Hobert O**. The secreted immunoglobulin domain proteins ZIG-5 and ZIG-8 cooperate with L1CAM/SAX-7 to maintain nervous system integrity. *PLoS genetics* 2012;8(7):e1002819.
58. **Turner J, Crossley M**. The CtBP family: enigmatic and enzymatic transcriptional co-repressors. *BioEssays : news and reviews in molecular, cellular and developmental biology* 2001;23(8):683-690.
59. **Shi Y, Sawada J, Sui G, Affar el B, Whetstine JR et al.** Coordinated histone modifications mediated by a CtBP co-repressor complex. *Nature* 2003;422(6933):735-738.
60. **Kuppuswamy M, Vijayalingam S, Zhao LJ, Zhou Y, Subramanian T et al.** Role of the PLDLS-binding cleft region of CtBP1 in recruitment of core and auxiliary components of the corepressor complex. *Molecular and cellular biology* 2008;28(1):269-281.
61. **Chinnadurai G**. CtBP, an unconventional transcriptional corepressor in development and oncogenesis. *Molecular cell* 2002;9(2):213-224.
62. **Dcona MM, Morris BL, Ellis KC, Grossman SR**. CtBP- an emerging oncogene and novel small molecule drug target: Advances in the understanding of its oncogenic action and identification of therapeutic inhibitors. *Cancer Biol Ther* 2017;18(6):379-391.
63. **Stankiewicz TR, Gray JJ, Winter AN, Linseman DA**. C-terminal binding proteins: central players in development and disease. *Biomol Concepts* 2014;5(6):489-511.
64. **Fjeld CC, Birdsong WT, Goodman RH**. Differential binding of NAD+ and NADH allows the transcriptional corepressor carboxyl-terminal binding protein to serve as a metabolic sensor. *Proc Natl Acad Sci U S A* 2003;100(16):9202-9207.
65. **Nardini M, Spano S, Cericola C, Pesce A, Massaro A et al.** CtBP/BARS: a dual-function protein involved in transcription co-repression and Golgi membrane fission. *The EMBO journal* 2003;22(12):3122-3130.
66. **Kumar V, Carlson JE, Ohgi KA, Edwards TA, Rose DW et al.** Transcription corepressor CtBP is an NAD(+)-regulated dehydrogenase. *Molecular cell* 2002;10(4):857-869.
67. **Balasubramanian P, Zhao LJ, Chinnadurai G**. Nicotinamide adenine dinucleotide stimulates oligomerization, interaction with adenovirus E1A and an intrinsic dehydrogenase activity of CtBP. *FEBS Lett* 2003;537(1-3):157-160.
68. **Nicholas HR, Lowry JA, Wu T, Crossley M**. The Caenorhabditis elegans protein CTBP-1 defines a new group of THAP domain-containing CtBP corepressors. *Journal of molecular biology* 2008;375(1):1-11.
69. **Quinlan KG, Verger A, Kwok A, Lee SH, Perdomo J et al.** Role of the C-terminal binding protein PXDLS motif binding cleft in protein interactions and transcriptional repression. *Molecular and cellular biology* 2006;26(21):8202-8213.
70. **Nardini M, Svergun D, Konarev PV, Spano S, Fasano M et al.** The C-terminal domain of the transcriptional corepressor CtBP is intrinsically unstructured. *Protein science : a publication of the Protein Society* 2006;15(5):1042-1050.
71. **Lin X, Sun B, Liang M, Liang YY, Gast A et al.** Opposed regulation of corepressor CtBP by SUMOylation and PDZ binding. *Molecular cell* 2003;11(5):1389-1396.

72. **Kagey MH, Melhuish TA, Wotton D**. The polycomb protein Pc2 is a SUMO E3. *Cell* 2003;113(1):127-137.
73. **Zhang Q, Yoshimatsu Y, Hildebrand J, Frisch SM, Goodman RH**. Homeodomain interacting protein kinase 2 promotes apoptosis by downregulating the transcriptional corepressor CtBP. *Cell* 2003;115(2):177-186.
74. **Wang SY, Iordanov M, Zhang Q**. c-Jun NH2-terminal kinase promotes apoptosis by down-regulating the transcriptional co-repressor CtBP. *The Journal of biological chemistry* 2006;281(46):34810-34815.
75. **Hildebrand JD, Soriano P**. Overlapping and unique roles for C-terminal binding protein 1 (CtBP1) and CtBP2 during mouse development. *Molecular and cellular biology* 2002;22(15):5296-5307.
76. **Hubler D, Rankovic M, Richter K, Lazarevic V, Altrock WD et al.** Differential spatial expression and subcellular localization of CtBP family members in rodent brain. *PloS one* 2012;7(6):e39710.
77. **Beck DB, Cho MT, Millan F, Yates C, Hannibal M et al.** A recurrent de novo CTBP1 mutation is associated with developmental delay, hypotonia, ataxia, and tooth enamel defects. *Neurogenetics* 2016;17(3):173-178.
78. **Sommerville EW, Alston CL, Pyle A, He L, Falkous G et al.** De novo CTBP1 variant is associated with decreased mitochondrial respiratory chain activities. *Neurol Genet* 2017;3(5):e187.
79. **Beck DB, Subramanian T, Vijayalingam S, Ezekiel UR, Donkervoort S et al.** A pathogenic CtBP1 missense mutation causes altered cofactor binding and transcriptional activity. *Neurogenetics* 2019;20(3):129-143.
80. **Nibu Y, Zhang H, Bajor E, Barolo S, Small S et al.** dCtBP mediates transcriptional repression by Knirps, Kruppel and Snail in the Drosophila embryo. *The EMBO journal* 1998;17(23):7009-7020.
81. **Poortinga G, Watanabe M, Parkhurst SM**. Drosophila CtBP: a Hairy-interacting protein required for embryonic segmentation and hairy-mediated transcriptional repression. *The EMBO journal* 1998;17(7):2067-2078.
82. **Biryukova I, Heitzler P**. Drosophila C-terminal binding protein, dCtBP is required for sensory organ prepattern and sharpens proneural transcriptional activity of the GATA factor Pnr. *Developmental biology* 2008;323(1):64-75.
83. **Stern MD, Aihara H, Roccaro GA, Cheung L, Zhang H et al.** CtBP is required for proper development of peripheral nervous system in Drosophila. *Mechanisms of development* 2009;126(1-2):68-79.
84. **Hoang CQ, Burnett ME, Curtiss J**. Drosophila CtBP regulates proliferation and differentiation of eye precursors and complexes with Eyeless, Dachshund, Dan, and Danr during eye and antennal development. *Developmental dynamics : an official publication of the American Association of Anatomists* 2010;239(9):2367-2385.
85. **Liew CK, Crossley M, Mackay JP, Nicholas HR**. Solution structure of the THAP domain from Caenorhabditis elegans C-terminal binding protein (CtBP). *Journal of molecular biology* 2007;366(2):382-390.
86. **Roussigne M, Kossida S, Lavigne AC, Clouaire T, Ecochard V et al.** The THAP domain: a novel protein motif with similarity to the DNA-binding domain of P element transposase. *Trends Biochem Sci* 2003;28(2):66-69.
87. **Clouaire T, Roussigne M, Ecochard V, Mathe C, Amalric F et al.** The THAP domain of THAP1 is a large C2CH module with zinc-dependent sequence-specific DNA-binding activity. *Proc Natl Acad Sci U S A* 2005;102(19):6907-6912.

88. **Bessiere D, Lacroix C, Campagne S, Ecochard V, Guillet V et al.** Structure-function analysis of the THAP zinc finger of THAP1, a large C2CH DNA-binding module linked to Rb/E2F pathways. *The Journal of biological chemistry* 2008;283(7):4352-4363.
89. **Reid A, Yucel D, Wood M, Llamosas E, Kant S et al.** The transcriptional repressor CTBP-1 functions in the nervous system of Caenorhabditis elegans to regulate lifespan. *Experimental gerontology* 2014;60:153-165.
90. **Chen S, Whetstine JR, Ghosh S, Hanover JA, Gali RR et al.** The conserved NAD(H)-dependent corepressor CTBP-1 regulates Caenorhabditis elegans life span. *P Natl Acad Sci USA* 2009;106(5):1496-1501.
91. **Bettinger JC, Leung K, Bolling MH, Goldsmith AD, Davies AG**. Lipid environment modulates the development of acute tolerance to ethanol in Caenorhabditis elegans. *PloS one* 2012;7(5):e35192.
92. **Davies AG, Bettinger JC, Thiele TR, Judy ME, McIntire SL**. Natural variation in the npr-1 gene modifies ethanol responses of wild strains of C. elegans. *Neuron* 2004;42(5):731-743.
93. **Reid A, Sherry TJ, Yucel D, Llamosas E, Nicholas HR**. The C-terminal binding protein (CTBP-1) regulates dorsal SMD axonal morphology in Caenorhabditis elegans. *Neuroscience* 2015;311:216-230.
94. **Nagaraj K, Mualla R, Hortsch M**. The L1 family of cell adhesion molecules: a sickening number of mutations and protein functions. *Adv Neurobiol* 2014;8:195-229.
95. **Schafer MK, Frotscher M**. Role of L1CAM for axon sprouting and branching. *Cell Tissue Res* 2012;349(1):39-48.
96. **Garver TD, Ren Q, Tuvia S, Bennett V**. Tyrosine phosphorylation at a site highly conserved in the L1 family of cell adhesion molecules abolishes ankyrin binding and increases lateral mobility of neurofascin. *Journal of Cell Biology* 1997;137(3):703-714.
97. **Volkmer H, Hassel B, Wolff JM, Frank R, Rathjen FG**. Structure of the axonal surface recognition molecule neurofascin and its relationship to a neural subgroup of the immunoglobulin superfamily. *The Journal of cell biology* 1992;118(1):149-161.
98. **Stumpel C, Vos YJ**. L1 Syndrome. In: Adam MP, Ardinger HH, Pagon RA, Wallace SE, Bean LJH et al. (editors). *GeneReviews((R))*. Seattle (WA) 2015.
99. **Vos YJ, Hofstra RM**. An updated and upgraded L1CAM mutation database. *Hum Mutat* 2010;31(1):E1102-1109.
100. **Vos YJ, de Walle HE, Bos KK, Stegeman JA, Ten Berge AM et al.** Genotype-phenotype correlations in L1 syndrome: a guide for genetic counselling and mutation analysis. *J Med Genet* 2010;47(3):169-175.
101. **Weller S, Gartner J**. Genetic and clinical aspects of X-linked hydrocephalus (L1 disease): Mutations in the L1CAM gene. *Hum Mutat* 2001;18(1):1-12.
102. **Yamasaki M, Thompson P, Lemmon V**. CRASH syndrome: mutations in L1CAM correlate with severity of the disease. *Neuropediatrics* 1997;28(3):175-178.
103. **Cohen NR, Taylor JS, Scott LB, Guillery RW, Soriano P et al.** Errors in corticospinal axon guidance in mice lacking the neural cell adhesion molecule L1. *Current biology : CB* 1998;8(1):26-33.
104. **Demyanenko GP, Tsai AY, Maness PF**. Abnormalities in neuronal process extension, hippocampal development, and the ventricular system of L1 knockout mice. *The Journal of neuroscience : the official journal of the Society for Neuroscience* 1999;19(12):4907-4920.

105. **Rolf B, Kutsche M, Bartsch U**. Severe hydrocephalus in L1-deficient mice. *Brain Res* 2001;891(1-2):247-252.
106. **Fransen E, D'Hooge R, Van Camp G, Verhoye M, Sijbers J et al.** L1 knockout mice show dilated ventricles, vermis hypoplasia and impaired exploration patterns. *Human molecular genetics* 1998;7(6):999-1009.
107. **Dahme M, Bartsch U, Martini R, Anliker B, Schachner M et al.** Disruption of the mouse L1 gene leads to malformations of the nervous system. *Nature Genetics* 1997;17(3):346-349.
108. **Tapanes-Castillo A, Weaver EJ, Smith RP, Kamei Y, Caspary T et al.** A modifier locus on chromosome 5 contributes to L1 cell adhesion molecule X-linked hydrocephalus in mice. *Neurogenetics* 2010;11(1):53-71.
109. **Demyanenko GP, Schachner M, Anton E, Schmid R, Feng G et al.** Close homolog of L1 modulates area-specific neuronal positioning and dendrite orientation in the cerebral cortex. *Neuron* 2004;44(3):423-437.
110. **Montag-Sallaz M, Schachner M, Montag D**. Misguided axonal projections, neural cell adhesion molecule 180 mRNA upregulation, and altered behavior in mice deficient for the close homolog of L1. *Molecular and cellular biology* 2002;22(22):7967-7981.
111. **Heyden A, Angenstein F, Sallaz M, Seidenbecher C, Montag D**. Abnormal axonal guidance and brain anatomy in mouse mutants for the cell recognition molecules close homolog of L1 and NgCAM-related cell adhesion molecule. *Neuroscience* 2008;155(1):221-233.
112. **Sakurai K, Migita O, Toru M, Arinami T**. An association between a missense polymorphism in the close homologue of L1 (CHL1, CALL) gene and schizophrenia. *Mol Psychiatry* 2002;7(4):412-415.
113. **Chen QY, Chen Q, Feng GY, Lindpaintner K, Chen Y et al.** Case-control association study of the close homologue of L1 (CHL1) gene and schizophrenia in the Chinese population. *Schizophr Res* 2005;73(2-3):269-274.
114. **Ren J, Zhao T, Xu Y, Ye H**. Interaction between DISC1 and CHL1 in regulation of neurite outgrowth. *Brain Res* 2016;1648(Pt A):290-297.
115. **Bonora E, Lamb JA, Barnby G, Sykes N, Moberly T et al.** Mutation screening and association analysis of six candidate genes for autism on chromosome 7q. *Eur J Hum Genet* 2005;13(2):198-207.
116. **Marui T, Funatogawa I, Koishi S, Yamamoto K, Matsumoto H et al.** Association of the neuronal cell adhesion molecule (NRCAM) gene variants with autism. *Int J Neuropsychopharmacol* 2009;12(1):1-10.
117. **Pillai AM, Thaxton C, Pribisko AL, Cheng JG, Dupree JL et al.** Spatiotemporal ablation of myelinating glia-specific neurofascin (Nfasc NF155) in mice reveals gradual loss of paranodal axoglial junctions and concomitant disorganization of axonal domains. *J Neurosci Res* 2009;87(8):1773-1793.
118. **Sherman DL, Tait S, Melrose S, Johnson R, Zonta B et al.** Neurofascins are required to establish axonal domains for saltatory conduction. *Neuron* 2005;48(5):737-742.
119. **Zonta B, Tait S, Melrose S, Anderson H, Harroch S et al.** Glial and neuronal isoforms of Neurofascin have distinct roles in the assembly of nodes of Ranvier in the central nervous system. *The Journal of cell biology* 2008;181(7):1169-1177.
120. **Zhang A, Desmazieres A, Zonta B, Melrose S, Campbell G et al.** Neurofascin 140 is an embryonic neuronal neurofascin isoform that promotes the assembly of the node of Ranvier. *The Journal of neuroscience : the official journal of the Society for Neuroscience* 2015;35(5):2246-2254.

121. **Smigiel R, Sherman DL, Rydzanicz M, Walczak A, Mikolajkow D et al.** Homozygous mutation in the Neurofascin gene affecting the glial isoform of Neurofascin causes severe neurodevelopment disorder with hypotonia, amimia and areflexia. *Human molecular genetics* 2018;27(21):3669-3674.
122. **Monfrini E, Straniero L, Bonato S, Monzio Compagnoni G, Bordoni A et al.** Neurofascin (NFASC) gene mutation causes autosomal recessive ataxia with demyelinating neuropathy. *Parkinsonism Relat Disord* 2019.
123. **Anazi S, Maddirevula S, Salpietro V, Asi YT, Alsahli S et al.** Expanding the genetic heterogeneity of intellectual disability. *Hum Genet* 2017;136(11-12):1419-1429.
124. **Sakurai T, Lustig M, Babiarz J, Furley AJ, Tait S et al.** Overlapping functions of the cell adhesion molecules Nr-CAM and L1 in cerebellar granule cell development. *The Journal of cell biology* 2001;154(6):1259-1273.
125. **Castellani V, Chedotal A, Schachner M, Faivre-Sarrailh C, Rougon G**. Analysis of the L1-deficient mouse phenotype reveals cross-talk between Sema3A and L1 signaling pathways in axonal guidance. *Neuron* 2000;27(2):237-249.
126. **Falk J, Bechara A, Fiore R, Nawabi H, Zhou H et al.** Dual functional activity of semaphorin 3B is required for positioning the anterior commissure. *Neuron* 2005;48(1):63-75.
127. **Wright AG, Demyanenko GP, Powell A, Schachner M, Enriquez-Barreto L et al.** Close homolog of L1 and neuropilin 1 mediate guidance of thalamocortical axons at the ventral telencephalon. *The Journal of neuroscience : the official journal of the Society for Neuroscience* 2007;27(50):13667-13679.
128. **Bieber AJ, Snow PM, Hortsch M, Patel NH, Jacobs JR et al.** Drosophila neuroglian: a member of the immunoglobulin superfamily with extensive homology to the vertebrate neural adhesion molecule L1. *Cell* 1989;59(3):447-460.
129. **Dubreuil RR, MacVicar G, Dissanayake S, Liu CH, Homer D et al.** Neuroglian-mediated cell adhesion induces assembly of the membrane skeleton at cell contact sites. *Journal of Cell Biology* 1996;133(3):647-655.
130. **Bouley M, Tian MZ, Paisley K, Shen YC, Malhotra JD et al.** The L1-type cell adhesion molecule neuroglian influences the stability of neural ankyrin in the Drosophila embryo but not its axonal localization. *The Journal of neuroscience : the official journal of the Society for Neuroscience* 2000;20(12):4515-4523.
131. **Hortsch M, Bieber AJ, Patel NH, Goodman CS**. Differential splicing generates a nervous system-specific form of Drosophila neuroglian. *Neuron* 1990;4(5):697-709.
132. **Hall SG, Bieber AJ**. Mutations in the Drosophila neuroglian cell adhesion molecule affect motor neuron pathfinding and peripheral nervous system patterning. *Journal of neurobiology* 1997;32(3):325-340.
133. **Garcia-Alonso L, Romani S, Jimenez F**. The EGF and FGF receptors mediate neuroglian function to control growth cone decisions during sensory axon guidance in Drosophila. *Neuron* 2000;28(3):741-752.
134. **Kristiansen LV, Velasquez E, Romani S, Baars S, Berezin V et al.** Genetic analysis of an overlapping functional requirement for L1- and NCAM-type proteins during sensory axon guidance in Drosophila. *Mol Cell Neurosci* 2005;28(1):141-152.
135. **Chen W, Hing H**. The L1-CAM, Neuroglian, functions in glial cells for Drosophila antennal lobe development. *Developmental neurobiology* 2008;68(8):1029-1045.

136. **Martin V, Mrkusich E, Steinel MC, Rice J, Merritt DJ et al.** The L1-type cell adhesion molecule Neuroglian is necessary for maintenance of sensory axon advance in the Drosophila embryo. *Neural Dev* 2008;3:10.
137. **Goossens T, Kang YY, Wuytens G, Zimmermann P, Callaerts-Vegh Z et al.** The Drosophila L1CAM homolog Neuroglian signals through distinct pathways to control different aspects of mushroom body axon development. *Development* 2011;138(8):1595-1605.
138. **Enneking EM, Kudumala SR, Moreno E, Stephan R, Boerner J et al.** Transsynaptic coordination of synaptic growth, function, and stability by the L1-type CAM Neuroglian. *PLoS biology* 2013;11(4):e1001537.
139. **Zhang H, Wang Y, Wong JJ, Lim KL, Liou YC et al.** Endocytic pathways downregulate the L1-type cell adhesion molecule neuroglian to promote dendrite pruning in Drosophila. *Dev Cell* 2014;30(4):463-478.
140. **Godenschwege TA, Murphey RK**. Genetic interaction of Neuroglian and Semaphorin1a during guidance and synapse formation. *J Neurogenet* 2009;23(1-2):147-155.
141. **Sasakura H, Inada H, Kuhara A, Fusaoka E, Takemoto D et al.** Maintenance of neuronal positions in organized ganglia by SAX-7, a Caenorhabditis elegans homologue of L1. *The EMBO journal* 2005;24(7):1477-1488.
142. **Chen L, Ong B, Bennett V**. LAD-1, the Caenorhabditis elegans L1CAM homologue, participates in embryonic and gonadal morphogenesis and is a substrate for fibroblast growth factor receptor pathway-dependent phosphotyrosine-based signaling. *The Journal of cell biology* 2001;154(4):841-855.
143. **Dong X, Liu OW, Howell AS, Shen K**. An extracellular adhesion molecule complex patterns dendritic branching and morphogenesis. *Cell* 2013;155(2):296-307.
144. **Salzberg Y, Diaz-Balzac CA, Ramirez-Suarez NJ, Attreed M, Tecle E et al.** Skin-derived cues control arborization of sensory dendrites in Caenorhabditis elegans. *Cell* 2013;155(2):308-320.
145. **Pocock R, Benard CY, Shapiro L, Hobert O**. Functional dissection of the C. elegans cell adhesion molecule SAX-7, a homologue of human L1. *Mol Cell Neurosci* 2008;37(1):56-68.
146. **Zhou S, Opperman K, Wang X, Chen L**. unc-44 Ankyrin and stn-2 gamma-syntrophin regulate sax-7 L1CAM function in maintaining neuronal positioning in Caenorhabditis elegans. *Genetics* 2008;180(3):1429-1443.
147. **Wang X, Kweon J, Larson S, Chen L**. A role for the C. elegans L1CAM homologue lad-1/sax-7 in maintaining tissue attachment. *Developmental biology* 2005;284(2):273-291.
148. **Liang X, Dong X, Moerman DG, Shen K, Wang X**. Sarcomeres Pattern Proprioceptive Sensory Dendritic Endings through UNC-52/Perlecan in C. elegans. *Dev Cell* 2015;33(4):388-400.
149. **Diaz-Balzac CA, Lazaro-Pena MI, Ramos-Ortiz GA, Bulow HE**. The Adhesion Molecule KAL-1/anosmin-1 Regulates Neurite Branching through a SAX-7/L1CAM-EGL-15/FGFR Receptor Complex. *Cell Rep* 2015;11(9):1377-1384.
150. **Opperman K, Moseley-Alldredge M, Yochem J, Bell L, Kanayinkal T et al.** A novel nondevelopmental role of the sax-7/L1CAM cell adhesion molecule in synaptic regulation in Caenorhabditis elegans. *Genetics* 2015;199(2):497-509.
151. **Axang C, Rauthan M, Hall DH, Pilon M**. The twisted pharynx phenotype in C. elegans. *BMC Dev Biol* 2007;7:61.
152. **Grana TM, Cox EA, Lynch AM, Hardin J**. SAX-7/L1CAM and HMR-1/cadherin function redundantly in blastomere compaction and non-muscle myosin

accumulation during Caenorhabditis elegans gastrulation. *Developmental biology* 2010;344(2):731-744.
153. **Chen LH, Zhou S**. "CRASH"ing With the Worm: Insights Into L1CAM Functions and Mechanisms. *Dev Dynam* 2010;239(5):1490-1501.
154. **Chen C, Fenk LA, de Bono M**. Efficient genome editing in Caenorhabditis elegans by CRISPR-targeted homologous recombination. *Nucleic acids research* 2013;41(20):e193.
155. **Norris AD, Kim HM, Colaiacovo MP, Calarco JA**. Efficient Genome Editing in Caenorhabditis elegans with a Toolkit of Dual-Marker Selection Cassettes. *Genetics* 2015;201(2):449-458.
156. **Frokjaer-Jensen C, Davis MW, Hopkins CE, Newman BJ, Thummel JM et al.** Single-copy insertion of transgenes in Caenorhabditis elegans. *Nat Genet* 2008;40(11):1375-1383.
157. **Miyabayashi T, Palfreyman MT, Sluder AE, Slack F, Sengupta P**. Expression and function of members of a divergent nuclear receptor family in Caenorhabditis elegans. *Developmental biology* 1999;215(2):314-331.
158. **Rual JF, Ceron J, Koreth J, Hao T, Nicot AS et al.** Toward improving Caenorhabditis elegans phenome mapping with an ORFeome-based RNAi library. *Genome research* 2004;14(10B):2162-2168.
159. **Schindelin J, Arganda-Carreras I, Frise E, Kaynig V, Longair M et al.** Fiji: an open-source platform for biological-image analysis. *Nature methods* 2012;9(7):676-682.
160. **Yu C, Zhang Y, Yao S, Wei Y**. A PCR based protocol for detecting indel mutations induced by TALENs and CRISPR/Cas9 in zebrafish. *PloS one* 2014;9(6):e98282.
161. **Reid A**. *The carboxyl-terminal binding protein-1 (CTBP-1) can function in the nervous system to regulate longevity, gene expression and axon guidance*. PhD Thesis, The University of Sydney; 2015.
162. **Kamath RS, Martinez-Campos M, Zipperlen P, Fraser AG, Ahringer J**. Effectiveness of specific RNA-mediated interference through ingested double-stranded RNA in Caenorhabditis elegans. *Genome biology* 2001;2(1).
163. **Flavell SW, Pokala N, Macosko EZ, Albrecht DR, Larsch J et al.** Serotonin and the neuropeptide PDF initiate and extend opposing behavioral states in C. elegans. *Cell* 2013;154(5):1023-1035.
164. **Yucel D**. *Investigations into the function and regulation of the C-terminal binding protein (CTBP-1) in C. elegans*. University of Sydney; 2012.
165. **Ran FA, Hsu PD, Wright J, Agarwala V, Scott DA et al.** Genome engineering using the CRISPR-Cas9 system. *Nat Protoc* 2013;8(11):2281-2308.
166. **Calarco JA, Friedland AE**. Creating Genome Modifications in C. elegans Using the CRISPR/Cas9 System. *Methods in molecular biology* 2015;1327:59-74.
167. **Friedland AE, Tzur YB, Esvelt KM, Colaiacovo MP, Church GM et al.** Heritable genome editing in C. elegans via a CRISPR-Cas9 system. *Nature methods* 2013;10(8):741-743.
168. **Chorev M, Carmel L**. The function of introns. *Front Genet* 2012;3:55.
169. **Stein LD, Bao Z, Blasiar D, Blumenthal T, Brent MR et al.** The genome sequence of Caenorhabditis briggsae: a platform for comparative genomics. *PLoS biology* 2003;1(2):E45.
170. **Kabat JL, Barberan-Soler S, McKenna P, Clawson H, Farrer T et al.** Intronic alternative splicing regulators identified by comparative genomics in nematodes. *PLoS Comput Biol* 2006;2(7):e86.

171. **Cao J, Packer JS, Ramani V, Cusanovich DA, Huynh C et al.** Comprehensive single-cell transcriptional profiling of a multicellular organism. *Science* 2017;357(6352):661-667.
172. **Schmitz C, Kinge P, Hutter H**. Axon guidance genes identified in a large-scale RNAi screen using the RNAi-hypersensitive Caenorhabditis elegans strain nre-1(hd20) lin-15b(hd126). *Proc Natl Acad Sci U S A* 2007;104(3):834-839.
173. **Nix P, Hammarlund M, Hauth L, Lachnit M, Jorgensen EM et al.** Axon regeneration genes identified by RNAi screening in C. elegans. *The Journal of neuroscience : the official journal of the Society for Neuroscience* 2014;34(2):629-645.
174. **Zhang L, Ward JD, Cheng Z, Dernburg AF**. The auxin-inducible degradation (AID) system enables versatile conditional protein depletion in C. elegans. *Development* 2015;142(24):4374-4384.
175. **Huang LS, Tzou P, Sternberg PW**. The lin-15 locus encodes two negative regulators of Caenorhabditis elegans vulval development. *Mol Biol Cell* 1994;5(4):395-411.
176. **Chesney MA, Kidd AR, 3rd, Kimble J**. gon-14 functions with class B and class C synthetic multivulva genes to control larval growth in Caenorhabditis elegans. *Genetics* 2006;172(2):915-928.
177. **Cayrol C, Lacroix C, Mathe C, Ecochard V, Ceribelli M et al.** The THAP-zinc finger protein THAP1 regulates endothelial cell proliferation through modulation of pRB/E2F cell-cycle target genes. *Blood* 2007;109(2):584-594.
178. **Bressman SB, Raymond D, Fuchs T, Heiman GA, Ozelius LJ et al.** Mutations in THAP1 (DYT6) in early-onset dystonia: a genetic screening study. *Lancet Neurol* 2009;8(5):441-446.
179. **Fuchs T, Gavarini S, Saunders-Pullman R, Raymond D, Ehrlich ME et al.** Mutations in the THAP1 gene are responsible for DYT6 primary torsion dystonia. *Nat Genet* 2009;41(3):286-288.
180. **Ruiz M, Perez-Garcia G, Ortiz-Virumbrales M, Meneret A, Morant A et al.** Abnormalities of motor function, transcription and cerebellar structure in mouse models of THAP1 dystonia. *Human molecular genetics* 2015;24(25):7159-7170.
181. **Frederick NM, Shah PV, Didonna A, Langley MR, Kanthasamy AG et al.** Loss of the dystonia gene Thap1 leads to transcriptional deficits that converge on common pathogenic pathways in dystonic syndromes. *Human molecular genetics* 2019;28(8):1343-1356.
182. **Zakirova Z, Fanutza T, Bonet J, Readhead B, Zhang W et al.** Mutations in THAP1/DYT6 reveal that diverse dystonia genes disrupt similar neuronal pathways and functions. *PLoS genetics* 2018;14(1):e1007169.
183. **Gervais V, Campagne S, Durand J, Muller I, Milon A**. NMR studies of a new family of DNA binding proteins: the THAP proteins. *J Biomol NMR* 2013;56(1):3-15.
184. **Erogullari A, Hollstein R, Seibler P, Braunholz D, Koschmidder E et al.** THAP1, the gene mutated in DYT6 dystonia, autoregulates its own expression. *Biochim Biophys Acta* 2014;1839(11):1196-1204.
185. **Conte D, Jr., MacNeil LT, Walhout AJ, Mello CC**. RNA Interference in Caenorhabditis elegans. *Curr Protoc Mol Biol* 2015;109:26 23 21-30.
186. **Calixto A, Chelur D, Topalidou I, Chen X, Chalfie M**. Enhanced neuronal RNAi in C. elegans using SID-1. *Nature methods* 2010;7(7):554-559.
187. **Aspock G, Kagoshima H, Niklaus G, Burglin TR**. Caenorhabditis elegans has scores of hedgehog-related genes: sequence and expression analysis. *Genome research* 1999;9(10):909-923.

188. **Hao L, Johnsen R, Lauter G, Baillie D, Burglin TR**. Comprehensive analysis of gene expression patterns of hedgehog-related genes. *BMC genomics* 2006;7:280.
189. **Sherry TN, HR; Pocock, R**. New deletion alleles for Caenorhabditis elegans Hedgehog pathway-related genes wrt-6 and wrt-10. *microPublication Biology* 2019.
190. **Burglin TR**. Evolution of hedgehog and hedgehog-related genes, their origin from Hog proteins in ancestral eukaryotes and discovery of a novel Hint motif. *BMC genomics* 2008;9:127.
191. **Burglin TR**. Warthog and groundhog, novel families related to hedgehog. *Current biology : CB* 1996;6(9):1047-1050.
192. **Zugasti O, Rajan J, Kuwabara PE**. The function and expansion of the Patched- and Hedgehog-related homologs in C. elegans. *Genome research* 2005;15(10):1402-1410.
193. **Wu S**. *Characterising the roles of Hedgehog-related genes in neuronal development in Caenorhabditis elegans*. Honours Thesis, The University of Sydney; 2017.
194. **Ritter AD, Shen Y, Fuxman Bass J, Jeyaraj S, Deplancke B et al.** Complex expression dynamics and robustness in C. elegans insulin networks. *Genome research* 2013;23(6):954-965.
195. **Pierce SB, Costa M, Wisotzkey R, Devadhar S, Homburger SA et al.** Regulation of DAF-2 receptor signaling by human insulin and ins-1, a member of the unusually large and diverse C. elegans insulin gene family. *Genes Dev* 2001;15(6):672-686.
196. **Hung WL, Wang Y, Chitturi J, Zhen M**. A Caenorhabditis elegans developmental decision requires insulin signaling-mediated neuron-intestine communication. *Development* 2014;141(8):1767-1779.
197. **Chen Y, Baugh LR**. Ins-4 and daf-28 function redundantly to regulate C. elegans L1 arrest. *Developmental biology* 2014;394(2):314-326.
198. **Hung WL, Hwang C, Gao S, Liao EH, Chitturi J et al.** Attenuation of insulin signalling contributes to FSN-1-mediated regulation of synapse development. *The EMBO journal* 2013;32(12):1745-1760.
199. **Van Gilst MR, Hadjivassiliou H, Jolly A, Yamamoto KR**. Nuclear hormone receptor NHR-49 controls fat consumption and fatty acid composition in C. elegans. *PLoS biology* 2005;3(2):e53.
200. **Ashrafi K, Chang FY, Watts JL, Fraser AG, Kamath RS et al.** Genome-wide RNAi analysis of Caenorhabditis elegans fat regulatory genes. *Nature* 2003;421(6920):268-272.
201. **Hunt-Newbury R, Viveiros R, Johnsen R, Mah A, Anastas D et al.** High-throughput in vivo analysis of gene expression in Caenorhabditis elegans. *PLoS biology* 2007;5(9):e237.
202. **Mohrlen F, Hutter H, Zwilling R**. The astacin protein family in Caenorhabditis elegans. *Eur J Biochem* 2003;270(24):4909-4920.
203. **Hamilton B, Dong Y, Shindo M, Liu W, Odell I et al.** A systematic RNAi screen for longevity genes in C. elegans. *Genes Dev* 2005;19(13):1544-1555.
204. **Petersen SC, Watson JD, Richmond JE, Sarov M, Walthall WW et al.** A transcriptional program promotes remodeling of GABAergic synapses in Caenorhabditis elegans. *The Journal of neuroscience : the official journal of the Society for Neuroscience* 2011;31(43):15362-15375.
205. **Kennerdell JR, Fetter RD, Bargmann CI**. Wnt-Ror signaling to SIA and SIB neurons directs anterior axon guidance and nerve ring placement in C. elegans. *Development* 2009;136(22):3801-3810.

206. **Taylor SR, Santpere G, Reilly M, Glenwinke L, Poff A et al.** Expression profiling of the mature C. elegans nervous system by single-cell RNA-Sequencing. *BioRxiv* 2019.
207. **Sherry TJ**. *Investigating the Role of CTBP-1 in Neuronal Development in Caenorhabditis elegans*. Honours Thesis, The University of Sydney; 2015.
208. **Zhen M, Huang X, Bamber B, Jin Y**. Regulation of presynaptic terminal organization by C. elegans RPM-1, a putative guanine nucleotide exchanger with a RING-H2 finger domain. *Neuron* 2000;26(2):331-343.
209. **Liao EH, Hung W, Abrams B, Zhen M**. An SCF-like ubiquitin ligase complex that controls presynaptic differentiation. *Nature* 2004;430(6997):345-350.
210. **Grill B, Bienvenut WV, Brown HM, Ackley BD, Quadroni M et al.** C. elegans RPM-1 regulates axon termination and synaptogenesis through the Rab GEF GLO-4 and the Rab GTPase GLO-1. *Neuron* 2007;55(4):587-601.
211. **Tulgren ED, Turgeon SM, Opperman KJ, Grill B**. The Nesprin Family Member ANC-1 Regulates Synapse Formation and Axon Termination by Functioning in a Pathway with RPM-1 and beta-Catenin. *PLoS genetics* 2014;10(7).
212. **Flames N, Hobert O**. Gene regulatory logic of dopamine neuron differentiation. *Nature* 2009;458(7240):885-889.
213. **Yu H, Aleman-Meza B, Gharib S, Labocha MK, Cronin CJ et al.** Systematic profiling of Caenorhabditis elegans locomotive behaviors reveals additional components in G-protein Galphaq signaling. *Proc Natl Acad Sci U S A* 2013;110(29):11940-11945.
214. **Pereira L, Kratsios P, Serrano-Saiz E, Sheftel H, Mayo AE et al.** A cellular and regulatory map of the cholinergic nervous system of C. elegans. *eLife* 2015;4.
215. **Rahe D, Carrera, I., Cosmanescu, F., & Hobert, O.** An isoform-specific allele of the *sax-7* locus. *microPublication Biology* 2019.
216. **Dunham I, Kundaje A, Aldred SF, Collins PJ, Davis C et al.** An integrated encyclopedia of DNA elements in the human genome. *Nature* 2012;489(7414):57-74.
217. **Davis CA, Hitz BC, Sloan CA, Chan ET, Davidson JM et al.** The Encyclopedia of DNA elements (ENCODE): data portal update. *Nucleic acids research* 2018;46(D1):D794-D801.
218. **Aguilo F, Zakirova Z, Nolan K, Wagner R, Sharma R et al.** THAP1: Role in Mouse Embryonic Stem Cell Survival and Differentiation. *Stem Cell Rep* 2017;9(1):92-107.
219. **Dejosez M, Levine SS, Frampton GM, Whyte WA, Stratton SA et al.** Ronin/Hcf-1 binds to a hyperconserved enhancer element and regulates genes involved in the growth of embryonic stem cells. *Genes Dev* 2010;24(14):1479-1484.
220. **Macfarlan T, Kutney S, Altman B, Montross R, Yu J et al.** Human THAP7 is a chromatin-associated, histone tail-binding protein that represses transcription via recruitment of HDAC3 and nuclear hormone receptor corepressor. *The Journal of biological chemistry* 2005;280(8):7346-7358.
221. **Shkurnikov MY, Knyazev EN, Wicklein D, Schumacher U, Samatov TR et al.** Role of L1CAM in the Regulation of the Canonical Wnt Pathway and Class I MAGE Genes. *Bull Exp Biol Med* 2016;160(6):807-810.
222. **Green JL, Inoue T, Sternberg PW**. The C. elegans ROR receptor tyrosine kinase, CAM-1, non-autonomously inhibits the Wnt pathway. *Development* 2007;134(22):4053-4062.
223. **Hamada F, Bienz M**. The APC tumor suppressor binds to C-terminal binding protein to divert nuclear beta-catenin from TCF. *Dev Cell* 2004;7(5):677-685.

224. **Fang M, Li J, Blauwkamp T, Bhambhani C, Campbell N et al.** C-terminal-binding protein directly activates and represses Wnt transcriptional targets in Drosophila. *The EMBO journal* 2006;25(12):2735-2745.
225. **Jorgensen EM, Mango SE**. The art and design of genetic screens: Caenorhabditis elegans. *Nat Rev Genet* 2002;3(5):356-369.

8. Appendices

8.1 Appendix Figures

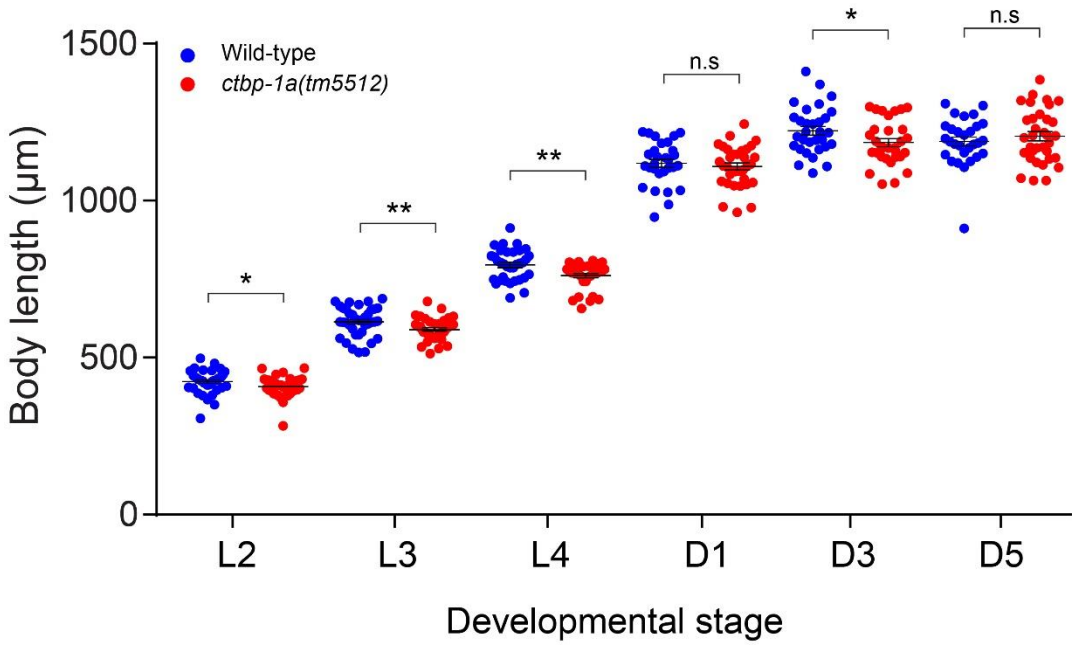

Appendix Figure 8.1 Body length of wild-type and *ctbp-1a(tm5512)* mutant animals at defined larval and adulthood stages.

Data presented as individual body lengths in µm (points) with mean ± SEM (bar) of 2 pooled biological replicates, n= 29-42 animals. *p<0.05, **p<0.01, n.s – not significant (unpaired t-test for each developmental stage). All performed at 25°C.

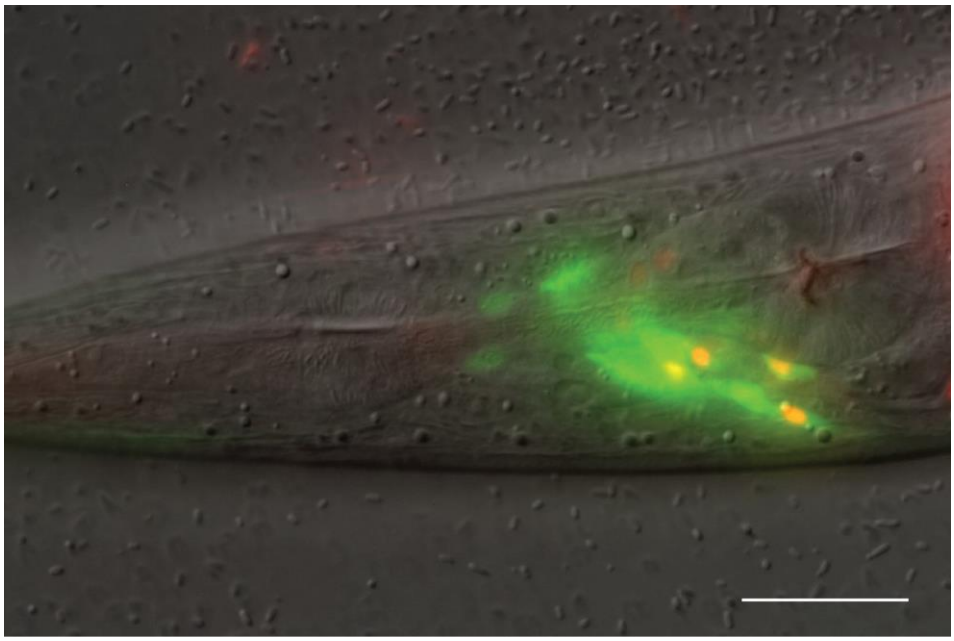

Appendix Figure 8.2 mCherry is visible in neurons in rescue lines.
Representative image of *pctbp-1a::ctbp-1a cDNA::mCherry* (*rpEx1812*). Colocalisation (yellow) with *glr-1* expressing neurons (*pglr-1::GFP* (*rhIs4*)). Anterior is to the left, ventral is down. Scale bar= 20 µm.

***ins-4(ok3534)* 415 bp deletion**

5′ ttcatgactaatttttaattcctgtgttgttcctgatctagtttatttattatttcacatgattttaaagaaatgtcttaaggaatatattccaatgtct
ttttccattgctctcgaaatgaaaagtctttttccctatatgtctctccatgcgcttgccccgcccaatccctttaacgttcgtggcgcttgacgcatca
gtcatattttcttctttttttgaacggataaaaaggcggagcgttttcaacaaaattgatgtgacctccagatgaactccgcccatctgataagtataaa
aagatgaatattaaatctatcaatcacttcaatttcaagctcttcaaaaagattgttaattttcataatttttcagaagtttttcaaaagctccaagaga
ATGTTTTCATTCTTTACATATTTCCTTCTCTCCGCACTTCTTCTCTCCGCTTCATGTCGACAACCTTCCATGGACACCAGCAAAGCCGATCGTATTCTAC
GAGAGATCGAAATGGAAACAGAACTCGAAAATCAACTCTCCCGAGCACGACGAGTCCCAGCTGGAGAGGTTCGTGCCTGTGGAAGACGACTTCTTCTCTT
TGTCTGGTCAACCTGTGGAGAACCATGCACGCCACgtacgtttaatgctaaaaatttttttaaaaaaccttaatctgaatttattatttttcagAAGAGGA
CATGGACATTGCCACAGTTTGCTGCACAACACAGTGCACTCCATCATATATAAAACAAGCTTGCTGCCCAGAAAAGTAAaaacagtcgtccaacaagcca

Exon 1
Exon 2
Deletion

Appendix Figure 8.3 Characterisation of *ok3534* deletion in *ins-4* gene locus.
415 bp deletion (underlined) over 5' UTR and start of exon 1. 5' UTR and introns in lowercase, exons in uppercase and highlighted in individual colours; key at bottom left. Identified with Sanger sequencing using primers outside the deletion area.

***nas-38(ok3407)* 378 bp deletion**

5′ ACTTCCTCCTATCAATTCGTTAGCTGGAGTTCTACCATCTACACAAGCTCCAGATATTATCAATAGTGTATTAGgtacggcggctttattcagacaaagt
ttattattgggtctagcagtcactatgaacttacgagtgtttgtgaccgtgtatctacagttacggtaagagttatccagtaaatactataaattgtagg
aacggatcctgattctatctgtagagacacaattaagaaacagaaacaaaatgtgtaaattatggctaaattatggtgaagcaaatgttttcagAATGCG
GCTGTGGAGCTTGGTCTGAATGGCAAGGTGAATGCTCCCAGCAGTGTGGCGGATGCGGTCATCGACTGAGGAAGCGAGAGTGCAAAAAAGAAGCTTGCAG
gtttggaaattaaatgtcacatttatgtctatcaataacattttgtagAAAAGAAGAAAAACGCCCATGCAACTTCTCAGCATGCCCCGACGGCACTAAC
TTCCTAATCAACAATGCTGAATTCCATATTCTTTGGAGAGGGTGTTGTGTTGGGTTGTTCAGgtattatattttcaataaacaaatttcaaaatagctta
tcttagATCCGGAGATCAATGCTCCGCCCTGGAAACTGAATCGAACCCATTCTTCAAAATTATCAACAGCCTGCTGAACATTCAAGATGCTAAGAACAAT
GATACGTTAATAGCAAAAAGAATGATGCGAGGAGAACACTAAtgtatttatttgttataatgtcaactatgtatatgtgttataatttgtcagaaactct

Exon 14 Exon 16 Deletion
Exon 15 Exon 17

Appendix Figure 8.4 Characterisation of *ok3407* deletion in *nas-38* gene locus.
378 bp deletion (underlined) over introns and exons. 5' UTR and introns in lowercase, exons in uppercase and highlighted in individual colours; key at bottom left. Identified with Sanger sequencing using primers outside the deletion area.

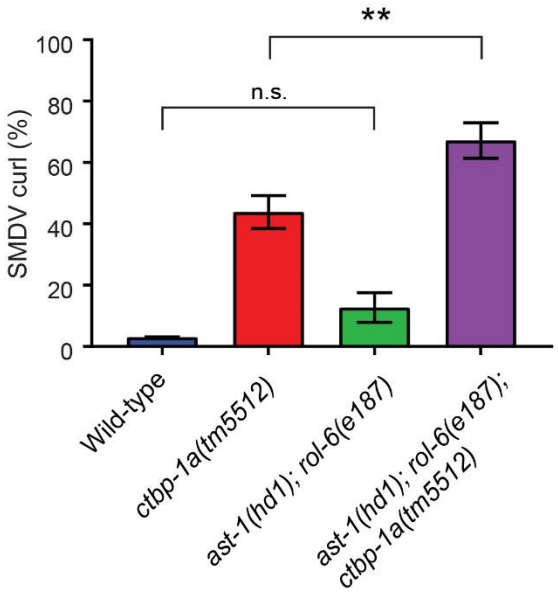

Appendix Figure 8.5 AST-1 acts in a parallel pathway to CTBP-1 to regulate SMDV development.
Quantification of SMDV curl phenotype of *ast-1(hd1)* single and double mutants at day 2 of adulthood at 20°C. *pctbp-1a::GFP* generated in Chapter 3 used to score SMDV axons. Data presented as mean ± SEM (bar) of 3 biological replicates, n>100 axons. **p<0.01, n.s – not significant (one-way ANOVA with Tukey's correction).

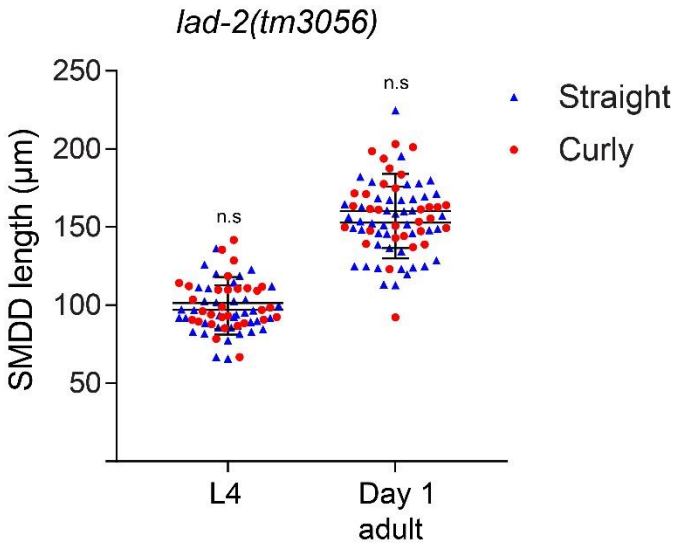

Appendix Figure 8.6 *lad-2* mutant SMDD axon length does not differ whether the axons are straight/wild-type or curly/defective.

Quantification of SMDD length (in µm) of straight (blue triangle) and curly (red circle) axons in *ctbp-1a(tm5512)* mutant animals. Data presented as individual axon lengths (straight: blue triangle, curly: red dot) with mean ± SD (bar) of 2 biological replicates, n>60 axons. n.s – not significant (unpaired t-test for each developmental stage).

8.2 List of oligonucleotides used in this study

Appendix Table 8.1 Oligonucleotides for genotyping *C. elegans* strains and detecting CRISPR-Cas9 mutations.

Name	Sequence (5′ to 3′)
1082	TGCAATGCTAAACTGAGTCGC
1083	GGACACTGGTCTTCCACAGG
1084	TATAGGTGAAGCCCGTTGCG
1236	AAGGGGTACGGTAGCAGGAT
1237	CGCAGAGCCCAAGTACTCAA
1238	TTTGAACGACCCGGGAGATG
1250	GACAGAACCCGAAGAAGGCA
1251	AGCCATGTAACTTCAAGGGGG
1252	ACAAGATTCCATCCCCATGATTGA
1325	CAGGTGTTAAATGAAGCTGTGG
1326	TCGAAATTTTTGAACCGTCATG
1327	CAAGCGTTTCCTGAATCGAAG
1328	GCCAATGGTACTAAACCGACG
1330	GCGCCTATTTCATCCAGAAG
1351	GACTGCTAGGAGCTATTGCAAG
1354	TCGGGGTTACTGAAGTGGAC
1355	TTTTGGAGGCAGCTCAATC
1427	CTAGACGATTCCTCCGTAATCG
1428	ATCGGGATGAACATTCTCAAC
1429	ATATCCCAACGGATTGCTAGC
1535	CACACCAACACACGTAAGGG
1536	GTAGTATTTCTCAGTGTCTGTCCC
1537	GTTCTCACCACCCTTCACAATC
1538	CCGGTACCGACTTGGAACTA
1539	AGAAAGCTGGGTCGTGAGAC
1540	TGCTCCAACATTCACCGCTG
1541	GATTGTTTGAAAGCGAAGCACG
1542	CCAGCCCAACCTAAGCCTAA
1543	AAAGCCAGAACCAACCACTG
1544	ACTCAATGGCAAAAGATGCC
1546	TGTATCGGAGGTGCCGGAAG
1547	GGAGTGGTGCGAATCTGACT
1558	GCAACAATCGGTCCGTCCAC
1559	GATGCTGTTACACCTCGTGT

Name	Sequence (5′ to 3′)
1560	GGTTTCAGCACGGCAAGAAG
1655	GCGGATTCCATTCATGATGG
1656	GAGCCACTTACAGTCCAAGG
TS31	AAGGAGGCGTTACCCATGAG
TS32	ATGAAGGTTGTGGTATTCGGTG
TS40	ATCCAACGTGCTTCCTCATG
TS42	GAAACATGGACGGCAGGAACG
TS43	TGCCTCTGCTCCAAATTCTG
TS45	CGGCTTCACAGTCTCCCATTC
TS46	CAGAATGATGCGACTCGGGAAG
TS73	GTCTACCACTACCGTCATTCC
TS74	ATTTGCACTTGTCCACGATGAG
TS142	TGGGGTTACGAGAGACGATGG
TS143	GATGTTCTCGGCTGTACATGTG
TS181	TGGAAGATCAGAGTCTTGATGG
TS182	TTCTTCAGGATTGAACTGCGAG

Appendix Table 8.2 Oligonucleotides for sgRNA construction.

Target	Name	Sequence (5′ to 3′)
sgRNA universal R primer	AA149	AAACATTTAGATTTGCAATTCAATTA
ctbp-1 sgRNA 1 exon 1b	1320	GCCAATGGTACTAAACCGACGGTTTTAGAGCTAGAAATAGCAAG
ctbp-1 sgRNA 2 exon 4b	1319	GGTGTTAAATGAAGCTGTGGGTTTTAGAGCTAGAAATAGCAAG
wrt-10 sgRNA	1552	GATGCTGTTACACCTCGTGTGTTTTAGAGCTAGAAATAGCAAG
wrt-6 sgRNA	1551	GCGGATTCCATTCATGATGGGTTTTAGAGCTAGAAATAGCAAG

Appendix Table 8.3 Oligonucleotides for constructing homology arms for tagging CTBP-1b.

Direction	Name	Sequence (5′ to 3′)
Upstream	1342	AACGACGGCCAGTGAATTCACTAGTCAGCGGAAAAGAAGAAGAGTGG
	1343	CTTCACCCTTTGAGACCATACTAGTTGCTATCAGCTGATAACGAAGG
Downstream	1344	TGGATGAATTGTATAAGGCGGCCGCCATGGGTGGCGAAGCCAATGG
	1345	ATGATTACGCCAAGCTTGCGGCCGCGGGTGGGGCATACTGTATCAGC

Appendix Table 8.4 Oligonucleotides for mutagenesis.

Name	Sequence (5′ to 3′)
1363	AACCGACGGGCTCGCAAAAGC
1364	TAGTACCATTGGCTTCGC
TS148	CATTTGATATGGTGAGCAAGGGCGAGG
TS149	TCACCATATCAAATGATGGAGTTGATG
TS150	CTGGATTTCCGAACGCTAAATTTCGCTCTCGGTATCGTGG
TS151	CGTTCGGAAATCCAGCAGTCGTCGGCATTTTTTCTACCG
TS152	AACAGTTGAGTTTTGCGATGCCCAGTCG
TS153	CAAAACTCAACTGTTGCAACGTCTTTCAG

Appendix Table 8.5 Oligonucleotides for Sanger sequencing.

Name	Sequence (5′ to 3′)
1222	AGTCGACTGGGCATCGCAAA
1309	GGAGTAGTCGTTCTGTTTACAC
1329	CCCGGTCATCATTTCATTTC
1330	GCGCCTATTTCATCCAGAAG
1353	CAATTTCTCGAAGCCAGTGTG
1368	GCTTCCGACAAGTGTCCGC
1369	GTTTCCGCTTTTGCGACC
1380	TGTCGGAAGCTCGGAAGC
1381	GCTTCTAAATGCGCATAGTGG
1382	GCTGTCAAAGTTGAACAATGAG
1386	CGCCCCATTATTGAGTAGGA
AA86	GCCAGGAGCGTACAATGTTA
AA89	AGTTTTGCGGTTTGTGTTCC
pPD49.26 F	CAAAGGACCCAAAGGTATGTTTCG
pPD49.26 R	AGAGTAATTGGACTTAGAAGTCAGAGG
pPD95.75 F	ATGACCATGATTACGCCAAGC
pPD95.75 R	TTCCGTATGTTGCATCACC
pPD95.75 mCherry	TCGAACTCGTGGCCGTTCACG
pPD49.26 F	CAAAGGACCCAAAGGTATGTTTCG

Appendix Table 8.6 Oligonucleotides for cloning expression and rescue constructs.

Name	Sequence (5′ to 3′)
TS1	GAAATGAAATAAGCTTAAGCTTAATGCAAATACAGTAGAAA
TS2	CCGGGGATCCTCTAGATGCGGGTTCGTCACAGAA
TS100	GCATTCGTAGAATTCCAACTGAGCG
TS101	TTTTTTCTACCGGTACCCTCCAAGG
TS102	TACCGGTAGAAAAAAATGGGGTTACGAGAGACGATGG
TS103	GAATTCTACGAATGCCTAGACAAACGTCGACGTTGATCC
TS122	ATGGTGAGCAAGGGCGAGG
TS123	TTTTTCTACCGGTACCCTCCAAGG
TS124	GTACCGGTAGAAAAAATGCCGACGACTTGTGGATTTC
TS125	GCCCTTGCTCACCATTGTGGCCAATGGTTGCTC
TS126	GTACCGGTAGAAAAAATGGGTGGCGAAGCCAATG
TS128	CGACTCTAGAGGATCCAAGCTTAATGCAAATACAGTAGAAA
TS129	CCAATCCCGGGGATCCTGCGGGTTCGTCACAGAA
TS130	CGACTCTAGAGGATCACGGGAAGGGGCATAATGT
TS131	CCAATCCCGGGGATCTGTTGGAAAAATCCAAAAAAAAAGT
TS136	CATCTAGAGGATCCCCGGGA
TS137	AAGCTTATTTCATTTCCAAGTTGTT
TS138	AAATGAAATAAGCTTACGGGAAGGGGCATAATGT
TS139	GGGATCCTCTAGATGTGTTGGAAAAATCCAAAAAAAAAGT
TS140	CGACTCTAGAGGATCCAAGCTTCCACGATTTCTCGC
TS141	CCAATCCCGGGGATCCCTCTAGAGTCGACCTGCAGTTGC

Appendix Table 8.7 Oligonucleotides used for qRT-PCR.

Target	Name	Sequence (5′ to 3′)
ctbp-1a	965	CCGTCAGGTGACAGTCCATC
	937	TCATCCTTGTGCTCGTCATAC
ctbp-1b	938	CCGTCAGGTGACAGTCCATC
	939	AAGTCACGAAAACTCCGGCT
Y45F10D.4	1548	AAGCGTCGGAACAGGAATC
	1549	TTTTTCCGTTATCGTCGACTC
sax-7S	TS107	CTACTGTTCCTTGTGTCGGA
	TS108	GTTGGAGGCATTTGTTGCA
sax-7L	TS109	GCCACATATCATCAGGCAG
	TS110	CGGTATCTGCATTCTTATCGT
pmp-3	pmp-qPCR_F	TGCTTGATAATCCAGATCAACG
	pmp-qPCR_R	TTGGAGCTAGAAGATCATTGGA